UNIVERSITÀ
POLITECNICA
DELLE MARCHE

Research Doctorate in

Life and Environmental Sciences

Curriculum

Civil and Environmental Protection

Cycle XXXIIº

Eastern Mediterranean Sea palaeoceanography at the time of sapropel S1 deposition

PhD-Student:

Rubén Amezcua Buendía

Supervisor:

Prof. Alessandra Negri

Co-supervisors:

Prof. Claudia Diamantini,

Prof. Domenico Potena

Dr. Gianluca Marino

Rubén Amezcua Buendía
Department of Life and Environmental Sciences
Faculty of Science
Laboratory of Stratigraphy, Sedimentology and Paleoecology
Polytechnic University of Marche
Ancona, Italy
Via Brecce Bianche, 60131 Ancona
r.amezcua@pm.univpm.it

Supervisor:

Prof. Alessandra Negri

Co-supervisor:

Prof. Claudia Diamantini

Prof. Domenico Potena

Dr. Gianluca Marino

The research described in this thesis was carried out at the Department of Life and Environmental Sciences and at the Department of Information Engineering, Polytechnic University of Marche, Via Brecce Bianche, 60131 Ancona, Italy.

Table of contents

a mi familia

General introduction

In an era of complex and rapid environmental change, the scientific community is making a great effort in understanding and predicting nature's dynamic (Dietze et al., 2018; Eyring et al., 2016; Rineau et al., 2019). This has increased availability of information about the Earth's surface, atmosphere, and ocean that can be used to understand our Earth system as a whole (Yang et al., 2019), and resolve unprecedented challenges as such climate change and global warming (Faghmous & Kumar, 2014; Manogaran & Lopez, 2018; Peri & Sasahara, 2019) or increasing intensity and frequency of ecological disasters and reduction of its impacts (Pollard et al., 2018; Yu et al., 2018, 2019). Also, several efforts have been made to improve traditional database tools according to the growing complexity and volume of data (Kepner et al., 2014; Kezunovic et al., 2013), which has led to an increase of the databases existing. To address the challenges of this continuous growth, it is necessary to apply sophisticated analytical methods to extract actionable insight from these datasets. As a result, we need to address the applicability for Big Data Analytics (BDA) techniques to help collect, correlate, and analyze the large volume of data more quickly and thoroughly than ever before. BDA or Data Analytics (DA) techniques are used to capture, store, transfer, analyze, and visualize enormous amounts of structured and unstructured data (LaValle et al., 2011). Among the massive volume of data, the data processing is fundamental to eliminate redundant, inconsistent, and noisy data (Bhattacharyya & Ivanova, 2017) in order to obtain heterogeneous data. According to Dobre & Xhafa (2014), every day the world produces around 2.5 quintillion bytes of data, with 90% of these data generated in the world being unstructured. This preprocessing consumes around 50–80% of the entire time for data analytics (Kempler & Mathews, 2017). Besides the volume of data, the wide range of disciplines in the Earth Sciences and the associated research methods and tools have collectively led to a considerable heterogeneity of the data (Ma et al., 2015). As a consequence, the data that comes from heterogeneous data sources (e.g., PANGAEA, Janus, NOAA), which contain different models of data representation (e.g., XML, JSON, relational tables) and present different ways to obtain the data (e.g., APIs, search forms, CVS downloads), must be organized and normalized (standardized) to obtain a proper and more efficient use of BDA techniques. After data processing, the main focus of DA is to reveal hidden patterns and unknown correlations from a large volume of

heterogeneous data (Yang et al., 2019). All this makes the use of BDA in Earth Sciences a challenge, and at the same time, a great opportunity for scientific advance.

In Earth Science, several digital platforms such as PANGAEA, Neotoma, Janus, or NOAA provide a large amount of dataset about the climate past. However, few studies (Alberico et al., 2017; Emile-Geay et al., 2017) have used these novel techniques in order to reconstruct past climates. In an era where climate change remains one of the major international environmental challenges, improve the knowledge of past climates can aid our understanding of future climate change. According to the most recent studies (NOAA, 2019; IPPC, 2019), the ocean and land warming is directly correlated to the sea-level rise, which is also observed in the Mediterranean Sea (Marcos et al., 2016). Previous investigations on the future sea-level rise across the Mediterranean Sea (Marcos & Tsimplis, 2008; Tsimplis et al., 2008; Carillo et al., 2012; Jordà & Gomis, 2013) have focused on the effects of water density variations, which influence on the Mediterranean Sea circulation, but the results obtained showed greater discrepancies. In this context, a period with similar characteristics (seawater warming and sea-level rise) occurred during the Last Glacial Maximum-Holocene that led to deposition of the most recent sapropel (S1). It is noteworthy that these climate conditions (seawater warming and sea-level rise) will not lead to future sapropel deposition, because it is controlled by orbital forcing (Rossignol-Strick, 1983, 1985), but a deeper and more comprehensive understanding of the modes of operation of the Mediterranean Sea as a whole during these periods of climate changes can be obtained. Since the first study about the sapropels and their origin (Kullenberg, 1952), a large amount of data has been published, some of which have been organized, standardized, related, and stored in the database *BEyOND*. This large volume of data gives a unique opportunity to study the sapropel problem and the Mediterranean Sea as a whole through DA techniques.

The Mediterranean Sea

Climatology and oceanography

The Mediterranean Sea is constituted of two basins (western and eastern Mediterranean) connected by the Strait of Sicily. All processes (e.g., rates of evaporation, salinity, runoff, precipitation...) that occur within the Mediterranean Sea are controlled by the balance of the flow through the Straits of Gibraltar (Béthoux, 1979; Carter, 1956) and Sicily (Giorgi & Lionello, 2008) which spells great differences between western and eastern Mediterranean Sea. The climatology of the Mediterranean depends on the subtropical atmospheric systems since it resides at the transition zone between the high- to mid-latitude. The climate varies between mild, wet winters and hot, dry summers (Eshel, 2002).

The general circulation in the Mediterranean Sea is composed of three principal and interacting spatial scales: basin scale, sub-basin scale (e. g. Adriatic, Levantine, Alboran) and mesoscale (Robinson et al., 2001). Indeed, other forcing mechanisms as surface wind and thermohaline circulation play a key role in this circulation (POEM Group, 1992). Three principal water masses divide the Mediterranean Sea: surface water mass (SWM; 0-200 m), intermediate water mass (IWM; 200-600 m) and, deep water mass (DWM; >600 m). The water mass best-know in the eastern Mediterranean Sea is the Levantine Intermediate Water (LIW). Its formation is located in Cyprus- Rhodes area (Rohling et al., 2015) where, in winter, strong, cold and dry winds occur over the eastern Mediterranean (Özsoy, 1981). From their region of formation, the LIW flows westwards between 150-600 m, changing its salinity and temperature. A part enters in the Adriatic and Aegean Sea and contribute to precondition Eastern Mediterranean Deep Water formation (EMDW), and the major part flows along the Ionian Sea to Strait of Sicily. The Mediterranean Sea is a region with several deep water formation sites: (1) the Adriatic Sea and (2) the Aegean Sea (eastern Mediterranean Deep Waters, EMDW) and, (3) the Gulf of Lions (western Mediterranean Deep Waters, WMDW).

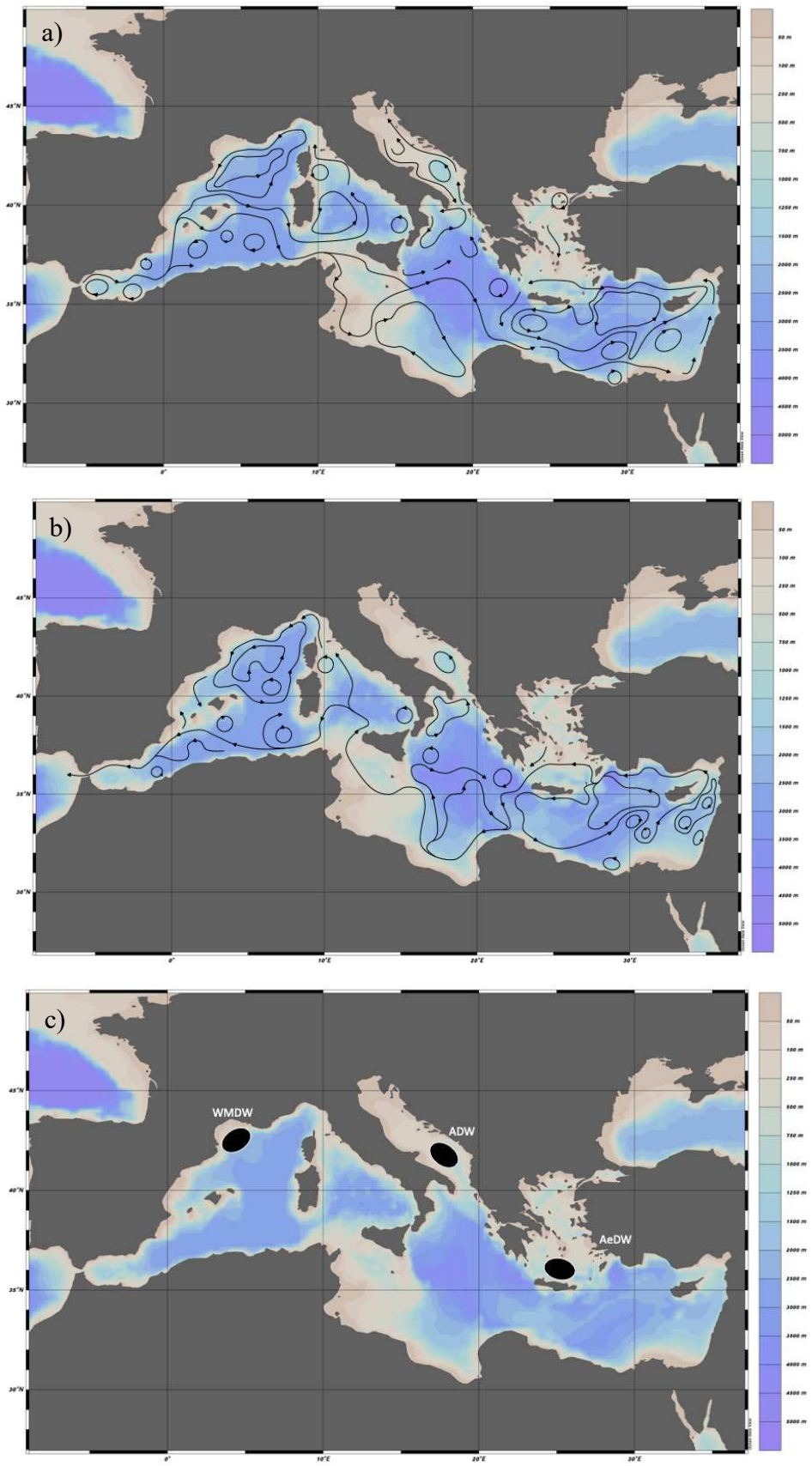

Fig. 1. Maps of Mediterranean Sea circulation based on Pinardi et al., 2015. a) Sea surface circulation schematic. b) Circulation pattern of the intermediate waters. c) Sites of deep water formation. Maps generated with Ocean Data View.

Sapropel

The sapropel origin is still matter of discussion, centered on the (1) close relationships between sapropels and fluctuations of the Earth's orbital parameters (Hilgen, 1991; Lourens et al., 1996; Rossignol-Strick, 1983, 1985; Ziegler et al., 2010) and (2) the hydrographic (Cita et al., 1977; Kidd et al., 1978; Kullenberg, 1952; Murat & Got, 1987; Myers et al., 1998; Rohling, 1991, 1994; Ryan & Cita, 1977; Vergnaud-Grazzini et al., 1977), biogeochemical and ecological changes (Calvert, 1983; De Lange et al., 2008; Gallego-Torres et al., 2011; Kemp et al., 1999; Negri & Giunta, 2001; Principato et al., 2003; Sachs & Repeta, 1999; Sarmiento et al., 1988) which led to sapropel deposition.

Over the last decade numerous multi-proxy studies (Azrieli-Tal et al., 2014; Bout-Roumazeilles et al., 2013; Filippidi et al., 2019; Hennekam et al., 2014; Mojtahid et al., 2015; Tachikawa et al., 2015; Tesi et al., 2017; Van Helmond et al., 2015; Zwiep et al., 2018) have provided more knowledge about sapropel deposition but the debate about its origin is still open.

Dissertation structure

This thesis is organized in three chapters, of which one has already been published (Amezcua-Buendía et al., 2019) and two are in preparation for submission:

Chapter 1 describes the design and implementation of the database *BEyOND* (Big paleo OceaN Data) and assesses the potential use of DA in the sapropel study. *BEyOND* contains a large amount of paleodata record of the Mediterranean Sea past 20.000 years history including the sapropel (S1). *BEyOND* manages effectively the cores from different regions or water depths, obtaining a result (relative to a determined proxy in the S1 interval) that assembles all cores used. These results could be expressed according to the region or water depths, among others, showing evidence on the differences or similarities existing among them due to local o global forcings. The correlations of the different cores are obtained through SQL queries.

Chapter 2 investigates the timing of the most recent sapropel (S1) deposition. The results based on geochemical and micropaleontological data suggest the sapropel S1 a synchronous event (10.1-6.5 cal. ka BP) in the whole eastern Mediterranean Sea. From these finding derives a fundamental improvement of the database *BEyOND* operability as it is allowed to correlate data based on age.

Chapter 3 presents the results obtained for the study of sapropel S1 through DA techniques. During the S1 deposition, when the water column is stratified and the water circulation in the whole eastern Mediterranean Sea is reduced, our results show that cold events at 9.5, 8.5 (related to 8.2 ka event), and 7.5 cal. ka BP that reactivated intermediate/deep waters formation, causing the (partial)interruption of S1 and the productivity variation. In addition, the core depth has been observed as the main driver causing the different TOC accumulation in the sub-basins, that is related to enhanced preservation.

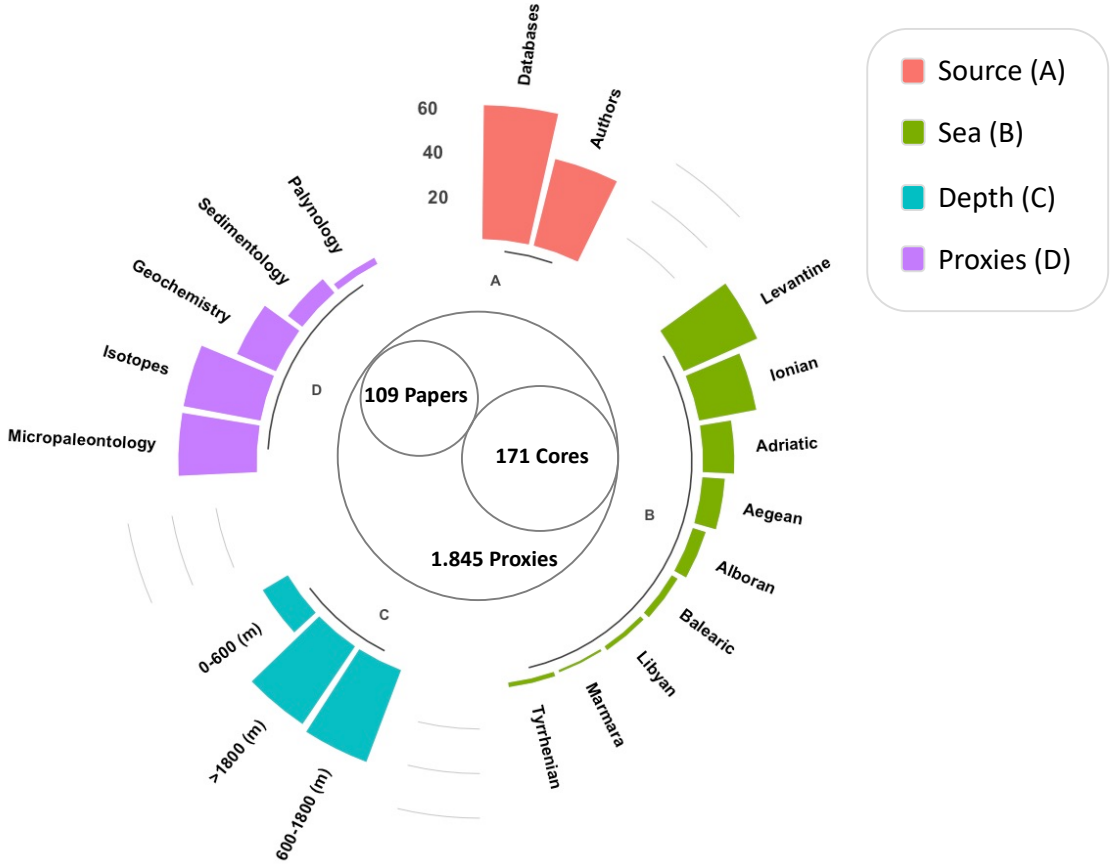

Fig. 2. Barplot describing the data on *BEyOND*

References:

Alberico, I., Giliberti, I., Insinga, D. D., Petrosino, P., Vallefuoco, M., Lirer, F., ... & Marsella, E. (2017). Marine sediment cores database for the Mediterranean Basin: a tool for past climatic and environmental studies. Open Geosciences, 9(1), 221-239. https://doi.org/10.1515/geo-2017-0019

Ariztegui, D., Asioli, A., Lowe, J. J., Trincardi, F., Vigliotti, L., Tamburini, F., ... & Van der Kaars, S. (2000). Palaeoclimate and the formation of sapropel S1: inferences from Late Quaternary lacustrine and marine sequences in the central Mediterranean region. *Palaeogeography, Palaeoclimatology, Palaeoecology*, 158(3–4), 215–240. https://doi.org/10.1016/S0031-0182(00)00051-1

Béthoux, J.P. (1979). Budgets of the Mediterranean Sea. Their dependence on the local climate and on the characteristics of the Atlantic waters. *Oceanol. Acta*, 2(2), 157-163.

Bhattacharyya, S., & Ivanova, D. (2017). Scientific computing and big data analytics: Application in climate science. *Distributed computing in big data analytics* (pp. 95-106). Springer, Cham. https://doi.org/10.1007/978-3-319-59834-5_6

Bout-Roumazeilles, V., Combourieu-Nebout, N., Desprat, S., Siani, G., Turon, J. L., & Essallami, L. (2013). Tracking atmospheric and riverine terrigenous supplies variability during the last glacial and the Holocene in central Mediterranean. *Climate of the Past*, 9(3), 1065-1087. https://doi.org/10.5194/cp-9-1065-2013

Calvert, S. E. (1983). Geochemistry of Pleistocene sapropels and associated sediments from the Eastern Mediterranean. *Oceanologica Acta*, 6(3), 255-267.

Carillo, A., Sannino, G., Artale, V., Ruti, P. M., Calmanti, S., & Dell'Aquila, A. (2012). Steric sea level rise over the Mediterranean Sea: present climate and scenario simulations. *Climate dynamics*, 39(9-10), 2167-2184. http://doi.org/10.1007/s00382-012-1369-1

Carter, D. B. (1956). The water balance of the Mediterranean and Black Seas. Centerton, N.J: Drexel Institute of Technology, Laboratory of Climatology. 9, 127-174.

Cita, M. B., Vergnaud-Grazzini, C., Robert, C., Chamley, H., Ciaranfi, N., & d'Onofrio, S. (1977). Paleoclimatic record of a long deep sea core from the eastern Mediterranean. *Quaternary Research*, 8(2), 205-235. https://doi.org/10.1016/0033-5894(77)90046-1

Dietze, M. C., Fox, A., Beck-Johnson, L. M., Betancourt, J. L., Hooten, M. B., Jarnevich, C. S., ... & Loescher, H. W. (2018). Iterative near-term ecological forecasting: Needs, opportunities, and challenges. *Proceedings of the National Academy of Sciences*, 115(7), 1424-1432. https://doi.org/10.1073/pnas.1710231115

Dobre, C., & Xhafa, F. (2014). Intelligent services for big data science. *Future generation computer systems*, 37, 267-281. https://doi.org/10.1016/j.future.2013.07.014

Emile-Geay, J., McKay, N. P., Kaufman, D. S., Von Gunten, L., Wang, J., Anchukaitis, K. J., et al. (2017). A global multiproxy database for temperature reconstructions of the Common Era. *Scientific Data*, 4, 170088. https://doi.org/10.1038/sdata.2017.88

Eshel, G. (2002). Mediterranean climates. *Israel Journal of Earth Sciences*, 51, 157-168. https://doi.org/10.1560/DMG1-06P2-908U-WDYY

Eyring, V., Bony, S., Meehl, G. A., Senior, C. A., Stevens, B., Stouffer, R. J., & Taylor, K. E. (2016). Overview of the Coupled Model Intercomparison Project Phase 6 (CMIP6) experimental design and organization. *Geoscientific Model Development*, 9(5), 1937-1958. https://doi.org/10.5194/gmd-9-1937-2016

Faghmous, J. H., & Kumar, V. (2014). A big data guide to understanding climate change: The case for theory-guided data science. *Big data*, 2(3), 155-163. https://doi.org/10.1089/big.2014.0026

Filippidi, A., & De Lange, G. J. (2019). Eastern Mediterranean Deep Water Formation During Sapropel S1: A Reconstruction Using Geochemical Records Along a Bathymetric Transect in the Adriatic Outflow Region. *Paleoceanography and Paleoclimatology,* 34(3), 409-429. https://doi.org/10.1029/2018PA003459

Gallego-Torres, D., Martinez-Ruiz, F., Meyers, P. A., Paytan, A., Jimenez-Espejo, F. J., & Ortega-Huertas, M. (2011). Productivity patterns and N-fixation associated with Pliocene-Holocene sapropels: Paleoceanographic and paleoecological significance. *Biogeosciences*, 8(2), 415–431. http://doi.org/10.5194/bg-8-415-2011

Giorgi, F., & Lionello, P. (2008). Climate change projections for the Mediterranean region. *Global and Planetary Change*, 63(2), 90–104. http://doi.org/10.1016/j.gloplacha.2007.09.005

Hennekam, R., Jilbert, T., Schnetger, B., & de Lange, G. J. (2014). Solar forcing of Nile discharge and sapropel S1 formation in the early to middle Holocene eastern Mediterranean. *Paleoceanography*, 29(5), 343-356. https://doi.org/10.1002/2013PA002553

Hilgen, F. J. (1991). Astronomical calibration of Gauss to Matuyama sapropels in the Mediterranean and implication for the Geomagnetic Polarity Time Scale. *Earth and Planetary Science Letters,* 104(2-4), 226-244. http://doi.org/10.1016/0012-821X(91)90206-W

IPCC. (2019). Summary for Policymakers. In: IPCC Special Report on the Ocean and Cryosphere in a Changing Climate [H.- O. Pörtner, D.C. Roberts, V. Masson-Delmotte, P. Zhai, M. Tignor, E. Poloczanska, K. Mintenbeck, M. Nicolai, A. Okem, J. Petzold, B. Rama, N. Weyer (eds.)]. In press.

Jordà, G., & Gomis, D. (2013). On the interpretation of the steric and mass components of sea level variability: The case of the Mediterranean basin. *Journal of Geophysical Research: Oceans*, 118(2), 953-963. https://doi.org/10.1002/jgrc.20060

Kemp, A. E. S., Pearce, R. B., Koizumi, I., Pike, J., & Rance, S. J. (1999). The role of mat-forming diatoms in the formation of Mediterranean sapropels. *Nature,* 398(6722), 57. http://doi.org/10.1038/18001

Kempler, S., & Mathews, T. (2017). Earth science data analytics: Definitions, techniques and skills. *Data Science Journal*, 16. http://doi.org/10.5334/dsj-2017-006

Kepner, J., Gadepally, V., Michaleas, P., Schear, N., Varia, M., Yerukhimovich, A., & Cunningham, R. K. (2014). Computing on masked data: a high performance method for improving big data veracity. *High Performance Extreme Computing Conference* (HPEC) (pp. 1-6). IEEE. https://doi.org/10.1109/HPEC.2014.7040946

Kezunovic, M., Xie, L., & Grijalva, S. (2013). The role of big data in improving power system operation and protection. *IREP Symposium Bulk Power System Dynamics and Control-IX Optimization, Security and Control of the Emerging Power Grid* (pp. 1-9). IEEE. https://doi.org/10.1109/IREP.2013.6629368

Kidd, R.B., Cita, M.B., & Ryan, W.B.F. (1978). Stratigraphy of eastern Mediterranean sapropel sequences recovered during Leg 42A and their paleoenvironmental significance. Initial Rep. Deep Sea Drill. Proj. 42A, 421–443. https://doi.org/10.2973/dsdp.proc.42-1.113-1.1978

Kullenberg, B. (1952). On the salinity of the water contained in marine sediments. *Medd. Oceanogr. Inst. Göteb*. 21, 1–38.

LaValle, S., Lesser, E., Shockley, R., Hopkins, M. S., & Kruschwitz, N. (2011). Big data, analytics and the path from insights to value. *MIT sloan management review,* 52(2), 21-32.

Lourens, L. J., Antonarakou, A., Hilgen, F. J., Van Hoof, A. A. M., Vergnaud-Grazzini, C., & Zachariasse, W. J. (1996). Evaluation of the Plio-Pleistocene astronomical timescale. *Paleoceanography*, 11(4), 391-413. http://doi.org/10.1029/96PA01125

Ma, Y., Wu, H., Wang, L., Huang, B., Ranjan, R., Zomaya, A., & Jie, W. (2015). Remote sensing big data computing: Challenges and opportunities. *Future Generation Computer Systems*, 51, 47-60. https://doi.org/10.1016/j.future.2014.10.029

Manogaran, G., & Lopez, D. (2018). Spatial cumulative sum algorithm with big data analytics for climate change detection. *Computers & Electrical Engineering*, 65, 207-221. https://doi.org/10.1016/j.compeleceng.2017.04.006

Marcos, M., Jorda, G., & Cozannet, G. L. (2016). Sub-chapter 2.2.1. Sea level rise and its impacts on the Mediterranean. In Moatti, J., & Thiébault, S. (Eds.), The Mediterranean region under climate change: A scientific update. IRD Éditions. https://doi.org/10.4000/books.irdeditions.23454

Marcos, M., & Tsimplis, M. N. (2007). Forcing of coastal sea level rise patterns in the North Atlantic and the Mediterranean Sea. *Geophysical Research Letters*, 34(18). https://doi.org/10.1029/2007GL030641

Mojtahid, M., Manceau, R., Schiebel, R., Hennekam, R., & de Lange, G. J. (2015). Thirteen thousand years of southeastern Mediterranean climate variability inferred from an integrative planktic foraminiferal-based approach. *Paleoceanography,* 30(4), 402-422. https://doi.org/10.1002/2014PA002705

Murat, A., & Got, H. (1987). Middle and Late Quaternary depositional sequences and cycles in the eastern Mediterranean. *Sedimentology*, 34(5), 885-899. https://doi.org/10.1111/j.1365-3091.1987.tb00810.x

Myers, P.G., Haines, K., Rohling, E.J., (1998). Modelling the paleo-circulation of the Mediterranean: The last glacial maximum and the Holocene with emphasis on the formation of sapropel S1. *Paleoceanography*, 13, 586–606. https://doi.org/10.1029/98PA02736

Negri, A., & Giunta, S. (2001). Calcareous nannofossil paleoecology in the sapropel S1 of the Eastern Ionian sea: Paleoceanographic implications. *Palaeogeography, Palaeoclimatology, Palaeoecology*, 169(1–2), 101–112. https://doi.org/10.1016/S0031-0182(01)00219-X

NOAA. (2019). National Centers for Environmental Information, State of the Climate: Global Climate Report for May 2019, published online June 2019.

Özsoy, E. (1981). On the atmospheric factors affecting the Levantine Sea (No. 25). European Centre for Medium Range Weather Forecasts.

Pinardi, N., Zavatarelli, M., Adani, M., Coppini, G., Fratianni, C., Oddo, P., et al. (2015). Mediterranean Sea large-scale low-frequency ocean variability and water mass formation rates from 1987 to 2007: A retrospective analysis. *Progress in Oceanography*, 132, 318–332. http://doi.org/10.1016/j.pocean.2013.11.003

POEM group. (1992). General circulation of the eastern Mediterranean Sea. *Earth Sci. Rev.* 32, 285–308.

Peri, G., & Sasahara, A. (2019). The impact of global warming on rural-urban migrations: evidence from global big data (No. 25728). *National Bureau of Economic Research*. https://doi.org/10.3386/w25728

Pollard, J. A., Spencer, T., & Jude, S. (2018). Big Data Approaches for coastal flood risk assessment and emergency response. *Wiley Interdisciplinary Reviews: Climate Change*, 9(5), e543. https://doi.org/10.1002/wcc.543

Principato, M. S., Giunta, S., Corselli, C., & Negri, A. (2003). Late Pleistocene-Holocene planktonic assemblages in three box-cores from the Mediterranean Ridge area (west-southwest of Crete): Palaeoecological and palaeoceanographic reconstruction of sapropel S1 interval. *Palaeogeography, Palaeoclimatology, Palaeoecology*, 190, 61–77. https://doi.org/10.1016/S0031-0182(02)00599-0

Rineau, F., Malina, R., Beenaerts, N., Arnauts, N., Bardgett, R. D., Berg, M. P., ... & De Boeck, H. J. (2019). Towards more predictive and interdisciplinary climate change ecosystem experiments. *Nature climate change*, 9, 809–816. https://doi.org/10.1038/s41558-019-0609-3

Robinson, A. R., Leslie, W. G., Theocharis, A., & Lascaratos, A. (2001). Mediterranean Sea Circulation. *Encyclopedia of Ocean Sciences(Second Edition)* (pp. 710–725). https://doi.org/10.1016/B978-012374473-9.00376-3.

Rohling, E. J. (1994). Review and new aspects concerning the formation of eastern Mediterranean sapropels. *Marine Geology*, 122(1–2), 1–28. https://doi.org/10.1016/0025-3227(94)90202-X

Rohling, E. J., & Hilgen, F. J. (1991). The eastern Mediterranean climate at times of sapropel formation: a review. *Journal of Geosciences/Geologie en Mijnbouw*.

Rohling, E. J., Marino, G., & Grant, K. M. (2015). Mediterranean climate and oceanography, and the periodic development of anoxic events (sapropels). *Earth-Science Reviews*, 143, 62-97. https://doi.org/10.1016/j.earscirev.2015.01.008

Rossignol-Strick, M. (1983). African monsoons, an immediate climate response to orbital insolation. *Nature*, 304(5921), 46-49.

Rossignol-Strick, M. (1985). Mediterranean Quaternary sapropels, an immediate response of the African monsoon to variation of insolation. *Palaeogeography, palaeoclimatology, palaeoecology*, 49(3-4), 237-263. https://doi.org/10.1016/0031-0182(85)90056-2

Ryan, W. B., & Cita, M. B. (1977). Ignorance concerning episodes of ocean-wide stagnation. *Developments in Sedimentology*, 23, 197-215. https://doi.org/10.1016/S0070-4571(08)70558-2

Sachs, J. P., & Repeta, D. J. (1999). Oligotrophy and nitrogen fixation during eastern Mediterranean sapropel events. *Science*, 286(5449), 2485-2488. https://doi.org/10.1126/science.286.5449.2485

Sarmiento, J. L., Herbert, T., & Toggweiler, J. R. (1988). Mediterranean nutrient balance and episodes of anoxia. *Global Biogeochemical Cycles*, 2(4), 427-444. https://doi.org/10.1029/GB002i004p00427

Tachikawa, K., Vidal, L. A., Cornuault, M., Garcia, M., Pothin, A., Sonzogni, C., ... & Revel, M. (2015). Eastern Mediterranean Sea circulation inferred from the conditions of S1 sapropel deposition. *Climate of the Past*, 11(6), 855–867. https://doi.org/10.5194/cp-11-855-2015

Tesi, T., Asioli, A., Minisini, D., Maselli, V., Dalla Valle, G., Gamberi, F., ... & Trincardi, F. (2017). Large-scale response of the Eastern Mediterranean thermohaline circulation to African monsoon intensification during sapropel S1 formation. *Quaternary Science Reviews*, 159, 139–154. https://doi.org/10.1016/j.quascirev.2017.01.020

Tsimplis, M. N., Marcos, M., & Somot, S. (2008). 21st century Mediterranean sea level rise: steric and atmospheric pressure contributions from a regional model. *Global and Planetary Change*, 63(2-3), 105-111. https://doi.org/10.1016/j.gloplacha.2007.09.006

Van Helmond, N. A., Hennekam, R., Donders, T. H., Bunnik, F. P., de Lange, G. J., Brinkhuis, H., & Sangiorgi, F. (2015). Marine productivity leads organic matter preservation in sapropel S1: palynological evidence from a core east of the Nile River outflow. *Quaternary Science Reviews*, 108, 130-138. https://doi.org/10.1016/j.quascirev.2015.05.031

Vergnaud-Grazzini, C., Ryan, W. B., & Cita, M. B. (1977). Stable isotopic fractionation, climate change and episodic stagnation in the eastern Mediterranean during the late Quaternary. *Marine Micropaleontology*, 2, 353-370. https://doi.org/10.1016/0377-8398(77)90017-2

Yang, C., Yu, M., Li, Y., Hu, F., Jiang, Y., Liu, Q., ... & Gu, J. (2019). Big Earth data analytics: A survey. *Big Earth Data*, 3(2), 83-107. https://doi.org/10.1080/20964471.2019.1611175

Yu, M., Huang, Q., Qin, H., Scheele, C., & Yang, C. (2019). Deep learning for real-time social media text classification for situation awareness–Using Hurricanes Sandy, Harvey, and Irma as case studies. *International Journal of Digital Earth*, 12(11), 1230-1247. https://doi.org/10.1080/17538947.2019.1574316

Yu, M., Yang, C., & Li, Y. (2018). Big data in natural disaster management: a review. *Geosciences*, 8(5), 165. https://doi.org/10.3390/geosciences8050165

Ziegler, M., Tuenter, E., & Lourens, L. J. (2010). The precession phase of the boreal summer monsoon as viewed from the eastern Mediterranean (ODP Site 968). *Quaternary Science Reviews,* 29(11-12), 1481-1490. https://doi.org/10.1016/j.quascirev.2010.03.011

Zwiep, K. L., Hennekam, R., Donders, T. H., van Helmond, N. A. G. M., de Lange, G. J., & Sangiorgi, F. (2018). Marine productivity, water column processes and seafloor anoxia in relation to Nile discharge during sapropels S1 and S3. *Quaternary Science Reviews,* 200, 178-190. https://doi.org/10.1016/j.quascirev.2018.08.026

Chapter 1

BEyOND, a new tool for sapropel S1 studies in the Mediterranean Sea

R. Amezcua-Buendía[1], C. Diamantini[2], D. Potena[2], A. Negri[1]

[1] *Department of Life and Environmental Sciences. Polytechnic University of Marche. Via Brecce Bianche, 60131 Ancona, Italy*

[2] *Department of Information Engineering. Polytechnic University of Marche. Via Brecce Bianche, 60131 Ancona, Italy*

Published in *Alpine and Mediterranean Quaternary*, vol. 32, no. 2, p. 167-184

Abstract

Science advances and, with it, the storage of large amounts of data. The need to use this data efficiently, quickly and safely is possible thanks to the Big Data Analytics (BDA) that allows us to store and relate data in order to obtain new knowledge. In this paper we present and explain how we constructed the new database, "*BEyOND*", that provides a wide variety of organized and standardized paleoproxies relative to the past 20.000 years of Mediterranean Sea history. *BEyOND* makes available to all researchers the possibility to extract and analyze data. We focused on a specific interval of time corresponding to the deposition of the most recent sapropel (S1) and the potential uses offered by the tool. *BEyOND* contains 126 sediment cores data from 79 scientific papers and a total of 1.678 different proxy related data that have been categorized in: geochemistry, isotopes, pollen, sediment grain size, coccolithophore, dinoflagellate and foraminifera.

Our work highlights the development of a new methodology to correlate data, including the cases where data regarding the precise age control for each core was missing.

It highlights as well the potential of using data analytics to extract hidden patterns and new knowledge also in the field of paleoceanography.

1. Introduction

The science of earth and environment has matured through two major phases and it is entering a third one. In the first phase, which ended two decades ago, science was oriented and focused on developing knowledge in geology, atmospheric chemistry, oceanography, ecosystems, and other fields of the Earth system. In the 1980s, the scientific community began to investigate these disciplines as interacting elements of a single system. In this second phase, we started to understand complex phenomena such as climate change, which links concepts from atmospheric and oceanic science, biology, and human behavior. In the emerging third phase, knowledge developed primarily for the purpose of scientific understanding, is being completed with the new knowledge created through data science and applications that allow us to acquire, manage, and make available data that helps us to take action and practical decisions (Dozier & Gail, 2009).

Nowadays, one of the most challenging tasks in Earth science is the possibility to use the vast amount of literature data by means of the new technology often referred to as the simple word "BIG DATA". Big Data Analytics (BDA) allows to explore huge volumes of data, coming from heterogeneous data sources, in order to extract novel, useful and human understandable knowledge. To this end, BDA refers to methodologies coming from several research areas, like machine learning, data mining, statistics, artificial intelligence and database (Gandomi & Haider, 2015). The amount of data available nowadays is really huge and as by IBM, 90% of the data have been added in the last 2 years (IBM Marketing Cloud, 2017). Most scientific disciplines could be described as small data, or even data poor. Therefore, in these fields most of the experiments or studies are based on few data points. Many disciplines in geological sciences like palaeoceanography, paleoclimatology fall among them. However, although each single study is based on relatively few data, the whole set of studies potentially offers a considerable amount of data, provided that we are able to collect and correlate them. BDA technologies can provide us the toolsets to integrate these different data sources, organize them in a database, that supports data analysis.

In the last years many data have been stored and made accessible in several fields of research, including natural hazards (e.g., EM-DAT https://www.emdat.be/), chemistry (e.g., ChemSpider http://www.chemspider.com/), biology (e.g., GenBank https://www.ncbi.nlm.nih.gov/genbank/); as for the paleo studies domain, several databases are under construction and implementation and among them, the best known

are PANGAEA (https://www.pangaea.de/), NOAA (https://www.ncdc.noaa.gov/data-access/paleoclimatology-data/datasets), IODP (http://www-odp.tamu.edu/database/) and, NEOTOMA (https://www.neotomadb.org/).

The PANGAEA database contains data (geochemistry, isotopes, pollen, sedimentology, stratigraphy, microfossils) georeferenced in time and space regarding all the fields that comprise environmental sciences. The Janus database (IODP) stores and retrieves data collected on the drill ship JOIDES Resolution, while National Centers for Environmental Information (NCEI), that it is the world's largest provider of weather and climate data, provides the data to NOAA. Finally, NEOTOMA database is focused on the paleo data from the Pliocene to the Quaternary. This variety of databases potentially gives many benefits to researchers but implies the presence of some obstacles too. The availability of a wide variety and quantity of data provides researchers with new possibilities to compare and correlate their data, potentially without the need to perform new measurements. In addition, more accuracy is provided because of the possibility to choose, among many data, those that appear to be more meaningful for a given type of research. Nevertheless, there are several difficulties related to the heterogeneity of data sources (e.g., structured and related data in a database or unstructured data provided in the form of publication), the model of the data representation (e.g., XML, JSON, relational tables…), the forms of access (e.g., APIs, search forms, CVS downloads…), and the structure of the data (e.g., It is frequent that studies dealing with the same proxy, express the results in different units). This hinders the ability to correlate data and, therefore, the comparison of results. Looking towards the future it is hence critical that the scientific community becomes aware of the necessity to create standards that ensure a universal data format (McKay & Emile-Geay, 2016) that would increase the quality of the results and decrease the time of reworking them. According to Bell (2009) we are at a stage of development that is analogous to when the printing press was invented, and The Jim Gray's fourth paradigm, data intensive computing, is in an initial phase but cannot be neglected. Data analysis covers a whole range of activities throughout the workflow pipeline, including the use of databases (versus a collection of flat files that a database can access), analysis and modelling, and then data visualization. Jim Gray's recipe for designing a database for a given discipline is that it must be able to answer the 20 key questions that the scientist wants to ask. Gray called this new paradigm "*eScience*" and characterized it as "*IT meets scientists*". Whether you're a

scientist or a technologist, this new data-intensive science is fascinating stuff (McFedries, 2011).

The most important problem when using a BDA approach in disciplines that use not only areal data, but sediment core data, is the need to uniform data and to refer it to events in time. This additional data type consists in the result of accumulation during time and therefore represents a record of processes occurring through time.

Project 418 is an ESSO-managed pilot project which addresses some of EarthCube's core activities envisioned for the EarthCube Cyberinfrastructure (Lingerfelt et al., 2018). These activities include Resource Registration, Data Discovery, and Data Access. Project 418 will serve as a pilot for the beginning point for these tasks, provide a foundation for future initiatives, as well as become a core component linking data facilities of EarthCube funded projects.

EarthCube supported LinkedEarth (Khider et al., 2018) project. It is a further development helping manifest a better future by creating an online platform that (1) enables the curation of a publicly-accessible database by paleoclimate experts themselves, and (2) fosters the development of community data standards, including an ontology. In turn, these developments enable cutting-edge data-analytic tools to be built and applied to a wider array of datasets than ever possible before, supporting more rigorous assessments of the magnitude and rates of pre-industrial climate change. More information at the LinkedEarth's site http://linked.earth show that there is a growing community sharing a key objective: the development of a community standard for paleoclimate data and metadata.

The LinkedEarth cyberinfrastructure also supported the development of the Past Global Changes past 2,000 years project (PAGES2k). In this contest, Emile-Geay et al. (2017) used a community-sourced database (PAGES2k temperature database) including a wide variety of proxies, like marine sediments, lake sediments, glacier ice or trees with the goal to reconstruct the global temperature of the Common Era.

Finally, Alberico et al. (2017), created the WDB-Paleo database that contains paleoclimatic proxies data of marine sediment core with the objective of studying the past climatic and environmental conditions of Mediterranean Sea.

The aim of the present paper is to describe the database *BEyOND* (Big palEo OceaN Data), that we have ideated and implemented using paleodata record of the last 20.000 years.

Method:

In order to design the database, we first defined our research questions as:

1. is it possible to correlate data at the minimum level of granularity (namely at sub-sample level), provided that sample range is heterogeneous in different studies?
2. is it possible to correlate proxies at different aggregation levels (e.g., cores from different areas, cores at different depths, proxies of the same core from different papers)?
3. is it possible to support an exploratory data analysis for Sapropel S1?

As a second step, we analyzed different sources, namely research papers and existing databases, to identify available data, their structure and format.

On the basis of collected requirements, *BEyOND* has been built following state-of-the-art design methodology, starting from a conceptual design.

Finally, the database has been populated by extracting, transforming and loading subsets of data from existing databases and, when needed, manually inserting those data published in research papers only. The databases will be described in Section 2.1.

To manage the different data that derive from different sources and standards, we used Data Analytics (DA). Ridge (2014) defines DA as any activity that involves applying analytical processes to data by using computer systems for the purpose of deriving insight from that data. DA allows us to explore huge amounts of data with the purpose of extracting new patterns or information that is comprehensible for further study. The objective of this work is to provide researchers, with *BEyOND*, a database which integrates heterogeneous paleo-data from several sources and allows researchers to extract, correlate and aggregate data through the standard database query language SQL.

2. Database Design

The database design is the data organization according to a database model, which determines its logical structure, that is, the manner in which data can be stored, organized and manipulated. To design our database, it was fundamental to know the data characteristics to be inserted and the goal to achieve with it. Yet, how databases are designed is another fundamental information. *BEyOND* mainly provides data of the Mediterranean Sea past 20.000 years history, but our study is focused on a specific interval of time corresponding to the deposition of the most recent sapropel (S1). Sapropels were defined by Kidd et al. (1978) as sharply-defined, dark-colored

sedimentary layers with a C_{org} content >2 wt.% and a thickness >1 cm. The sapropel origin is still matter of discussion, centered on the (1) close relationships between sapropels and fluctuations of the Earth's orbital parameters (Hilgen, 1991; Lourens et al., 1996; Ziegler et al., 2010) and (2) the hydrographic (Myers et al., 1998; Rohling, 1991, 1994), biogeochemical and ecological changes (Gallego-Torres et al., 2011; Kemp et al., 1999; Negri & Giunta, 2001; Principato et al., 2003; Sachs & Repeta, 1999; Sarmiento et al., 1988) which led to sapropel deposition.

Over the last decade numerous studies (Azrieli-Tal et al., 2014; Bout-Roumazeilles et al., 2013; Hennekam et al., 2014; Incarbona et al., 2011; Mojtahid et al., 2015; Tesi et al., 2017; Triantaphyllou, 2014) provided more knowledge about sapropel deposition but the debate about its origin is still open. In fact, the scientific struggle between those invoking simple anoxia of the Mediterranean Sea (Cita et al., 1977; Olausson, 1961; Rossignol-Strick, 1983, 1985; Ryan, 1972; Thunell, 1979; Thunell et al., 1977) and those invoking increased export productivity causing anoxia (Calvert & Price, 1983; Pedersen & Calvert, 1990) is still unsolved, even if some papers point to a combination of effects (Martinez-Ruiz et al., 2000; Myers et al., 1998; Rohling et al., 2015; Stratford et al., 2000).

2.1. Data sources

The starting point for the design of *BEyOND* is the study of other already existing databases, and of the literature.

The databases used are:

- PANGAEA: it is one of the biggest digital data libraries for the earth system science and it has provided us with a large amount of data. All the data derive from marine sediment cores that are georeferenced in space (with latitude, longitude and depth below sea) and in time (geological age). PANGAEA provides a web interface for initial data search and different formats for data download.
- NOAA (National Oceanic and Atmospheric Administration): it contains current and historical data focused on the conditions of the oceans and atmosphere. The access of the data can be through traditional access methods as web-based or FTP (File Transfer Protocol) and they mainly provide the data in ".txt" or ".xls" format.
- Janus database: ODP (Ocean Drilling Program) and IODP (International Ocean Discovery Program) data are stored in the same database, Janus. This database is based on a relational data model and contains marine geoscience data collected

onboard the drillship *JOIDES Resolution*. Data can be visualized through the Janus Web site and downloaded in ".txt" format.

- Global Pollen Database (GPD): it contains data of fossil and modern pollen records from natural archives where data are hosted by NOAA. Databases such as North American Pollen Databases (NAPD) or European Pollen Database (EPD) have been the precursors of this database.
- Neotoma Paleoecology Database: it is a multiproxy paleoecological database that covers the Pliocene-Quaternary, including modern microfossil samples, and that works like a centralized database with virtual constituent databases (NAPD, EPD, FAUNMAP) and which is implemented through Microsoft SQL Server. Data is accessible from Neotoma Explorer, an interactive web application for searching and downloading data in ".txt" format.

Of the above databases, we focused our analysis on the portion of data describing marine sediment cores.

As for the literature analysis, we started searching digital libraries for the following keywords: "sapropel", "anoxia", "Holocene", "Mediterranean Sea" and "productivity".

2.2. Categories of data

BEyOND has been organized around cores, which are geolocated and numbered in order to be identifiable. Cores are divided into samples (portion of the core between two discrete depth values) where several proxy measurements have been made in each sample.

The proxies inserted in the database are considered as a function of the category (e.g., geochemistry, sedimentology, isotopes…), but also of the method of analysis and measurement unit of the proxy itself.

In this regard, the first step has been the categorization of data in geochemistry, isotopes, sedimentology (sediment grain size and composition), palynology and micropaleontology (coccolithophore, dinoflagellate and foraminifera). Fig. 1 shows the distribution of proxies in the different cores that have been taken into account.

Some proxies, especially in geochemistry, show an issues related to the analytical method: in fact, different methods can be used for the analysis (e.g., barium has been obtained by Inductively Coupled Plasma - Atomic Emission Spectroscopy (ICP-AES), Inductively Coupled Plasma - Mass Spectrometry (ICP-MS) or X-Ray Fluorescence

(XRF). Another problem is the measurement unit of some proxies: in fact, even when the methodology is the same, results can be expressed in different units (e.g., Aluminum can be expressed in mg/kg or as a percentage of total weight).

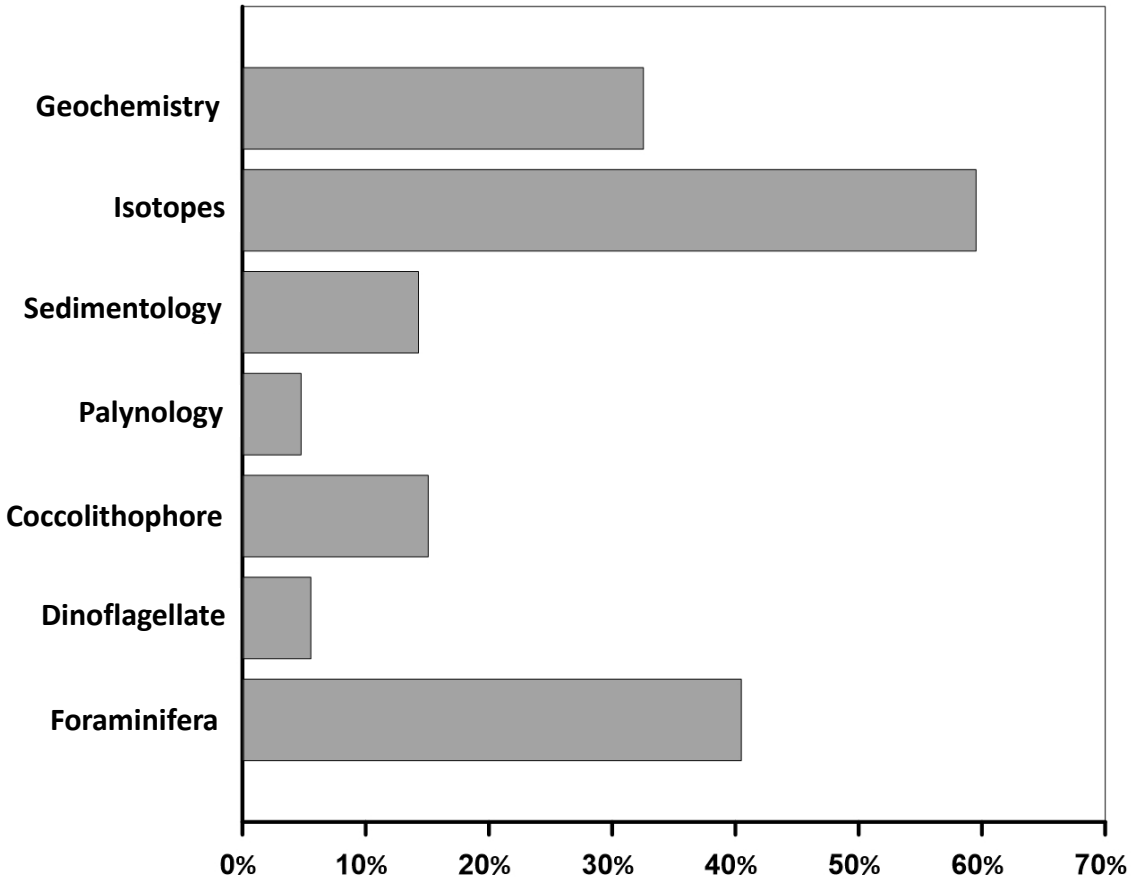

Fig. 1. Percentage of cores in *BEyOND*, associated with the different proxies in the Mediterranean Sea.

Geochemistry:

In general, the geochemical proxies are very useful in the study of palaeoceanography and paleoclimate. In fact, the chemical composition of the marine sediment provides information about past climates, ocean circulation, sea-floor conditions and changes in the sediment over time (Calvert & Pedersen, 2007). Trace elements provide clues about the aeolian or river input to marine sediments (Frigola et al., 2008; Jimenez-Espejo et al., 2007) while other elements such as Barium, Aluminum and Phosphorus allow to reconstruct marine paleoproductivity (Martinez-Ruiz et al., 2015; Möbius et al., 2010). Redox-sensitive elements are used to recognize bottom water conditions (Martinez-Ruiz et al., 2000; Tachikawa et al., 2015; Tesi et al., 2017; Tribovillard et al., 2006). Fig. 2A shows the position of cores providing geochemical data.

A total of 41 cores are located in deep environment of the Mediterranean Sea. Fig. 2B shows how we categorized the geochemical data according mainly to the measurement methods (ICP-AES, ICP-MS, AAS, XRF, AAS-XRF and CHN Analyzer) and the unit (mg/kg and percentage) in which the proxy data have been expressed.

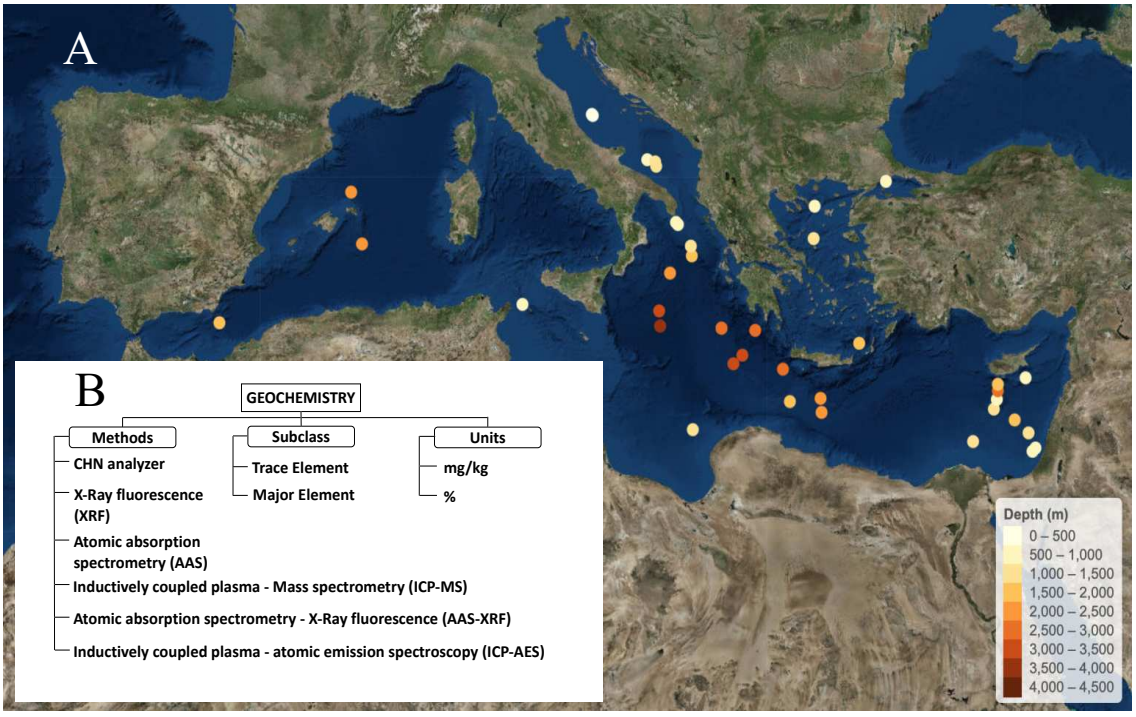

Fig. 2. (A) Core associated with geochemistry data. (B) Diagram showing the geochemistry proxies classification used for the Database *BEyOND*.

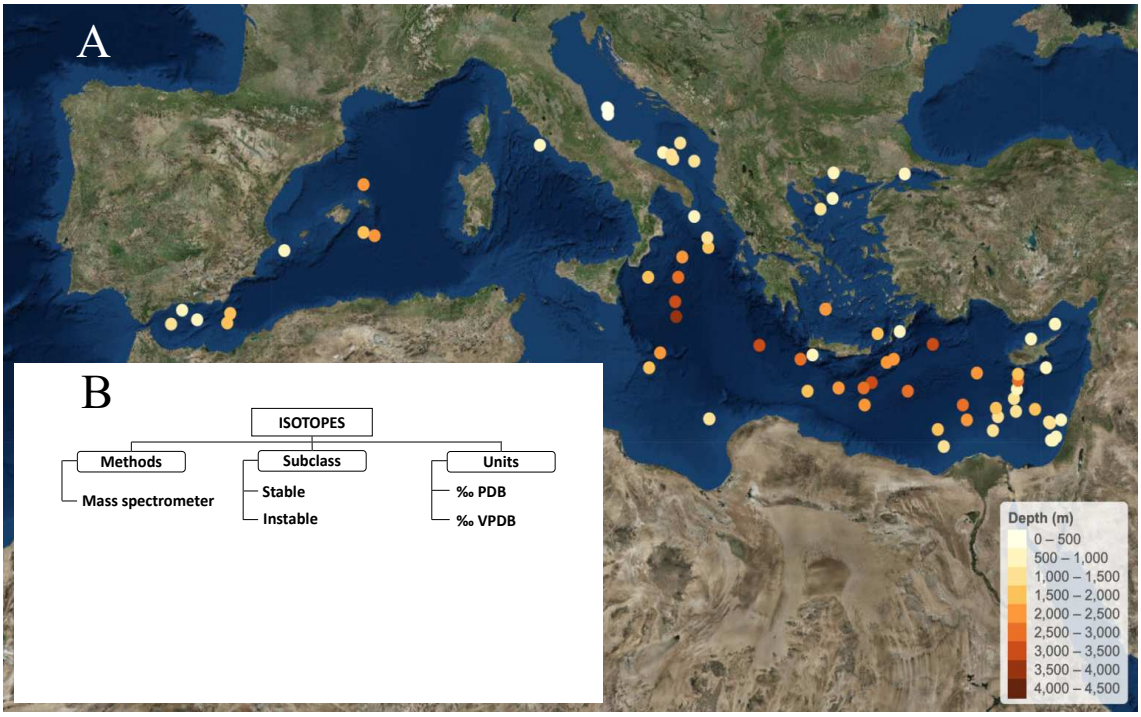

Fig. 3. (A) Core associated with stable Isotopes data. (B) Diagram showing the stable isotope proxies classification used for the Database *BEyOND*.

Isotopes:

Stable oxygen and carbon isotope records of benthic and planktonic foraminifera are a powerful tool for palaeoceanography and paleoclimate studies. The $\delta^{18}O$ signal shows fluctuations of global ice volume (Grazzini & Pierre, 1991; Jimenez-Espejo et al., 2008), changes in sea salinity (Fontugne et al., 1989) and the freshwater input (Dubois-Dauphin et al., 2017). The $\delta^{13}C$ signal provides information about deep water properties and its circulation, organic matter fluxes and carbon cycling of the oceans (Mackensen et al., 2001; Sarnthein et al., 1994; Woodruff & Savin, 1985; Zahn et al., 1986). Fig. 3A describes the position of the 75 cores providing isotopes data and Fig. 3B the categorization of the data that have been measured by a single method (mass spectrometer) and expressed in two different units (‰ PDB and ‰VPDB).

Sediment grain size and composition:

Sedimentology helps to comprehend the systems that control paleoclimatic and palaeohydrological changes. The clay mineral study contributes to understanding processes related to oceanic circulation, wind directions, precipitations just like the dynamics river inputs (Ehrmann et al., 2007, 2016). In addition, the grain size distribution, which is conditioned by physical processes, helps to know the transport processes and source areas (Bout-Roumazeilles et al., 2013; Ehrmann et al., 2007). Fig. 4A shows the positions of the 18 cores associated with the grain size and composition of the sediments, while in Fig. 4B the methods utilized for these cores (Laser diffraction, CLS, XRF and XRD) and the measurement units (μm and percentage) are reported.

Palynology:

Pollen records in marine sediments provide accurate information on paleovegetation, palaeohydrology and paleoclimate on a local and global level. Pollen is studied in order to reconstruct changes in temperature and precipitation occurred in the past (Kotthoff et al., 2008; Langgut et al., 2011) but is also used to investigate processes such as productivity (Hennekam et al., 2015). As is evident from Fig. 5A, however very few data (only 6 cores) are available for the investigated interval. Fig. 5B shows the only methodology used for palynology, that correspond to quantitative analysis (counts of pollen grains) (Parker & Arnold, 1999), and the unit of measurement (pollen grain).

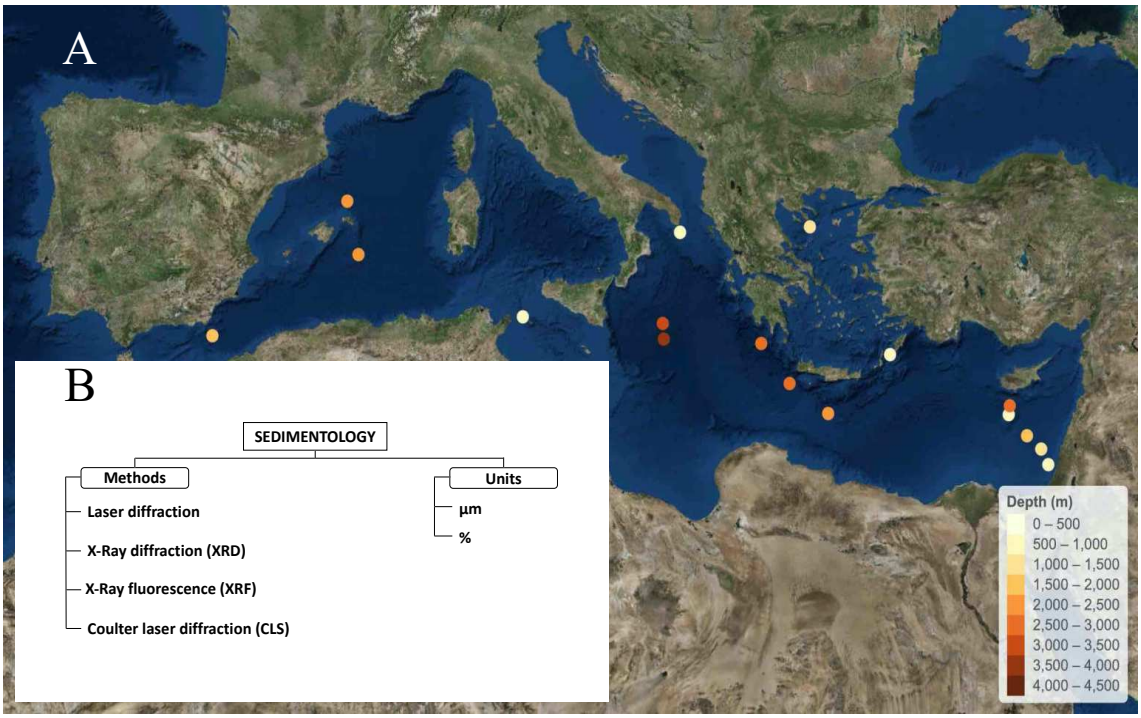

Fig. 4. (A) Core associated with Sedimentology data. (B) Diagram showing the sedimentology classification used for the Database *BEyOND*.

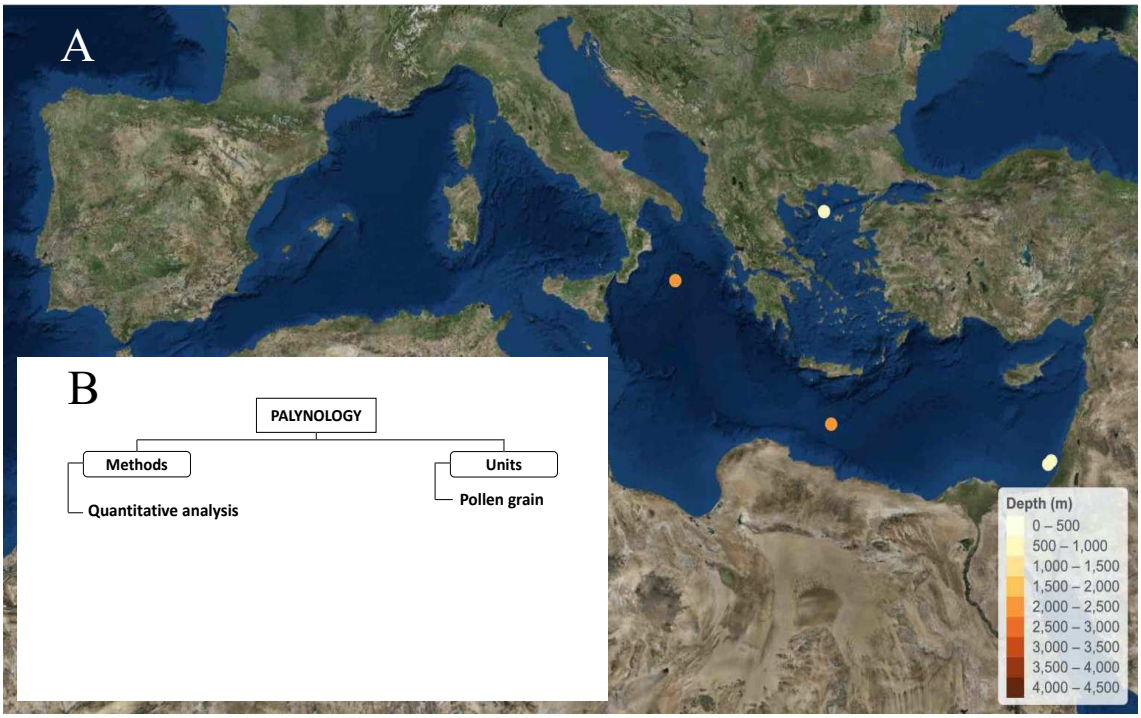

Fig. 5. (A) Core associated with Palynology data. (B) Diagram showing the palynology proxies classification used for the Database *BEyOND*.

Coccolithophores:

Coccolithophores are planktonic microalgae living in almost all oceanic areas. According to the specialists, changes in coccolith abundances permits to assess primary production fluctuations and, based on these, water column modifications (Negri & Giunta, 2001; Principato et al., 2003). Furthermore, a relation between reworked specimens eroded from continental sediment brought to the ocean by the river runoff is hypothesized by Negri et al., 1999 which evidence increased river discharge during sapropel deposition. Finally, the presence or absence of selected species allows the recognition of oligotrophic or eutrophic environments (Crudeli et al., 2006). Fig. 6A shows the location of the cores (19) reporting coccolithophore data. Fig. 6B shows the methodology of analysis used in coccolithophore studies, that is quantitative on smear slide (Bown & Young, 1998), whose values are expressed in number of coccolithophore counted or percentage.

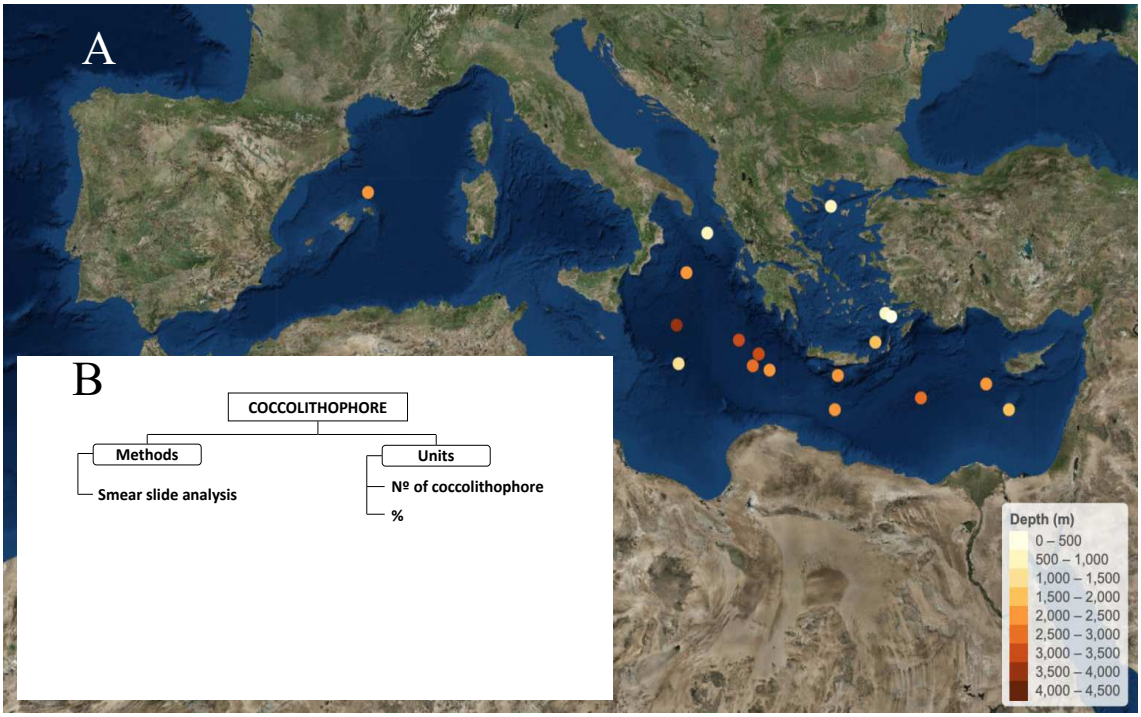

Fig. 6. (A) Core associated with Coccolithophore data. (B) Diagram showing the coccolithophore proxies classification used for the Database *BEyOND*.

Dinoflagellate:

Dinoflagellates are a group of unicellular protists that can be identified using the light microscope, and are (usually) recognized by their golden-brown plastids, assimilative cell with indented waist, distinctive swimming patterns, and relatively large

nucleus that contains visible chromosomes (Carty & Parrow, 2015). Resting Cyst association is closely related with parameters such as temperature, salinity and nutrient concentration (Meier et al., 2002, 2004). Also, they can give information about oxidation fronts, productivity and bottom oxygen conditions, and through this, on bottom water circulation (Zonneveld et al., 2001). Dinoflagellate data are scarce as shown Fig. 7A (7 cores). Fig. 7B displays the only method (quantitative analysis) and unit of measurement (Cyst) inserted in database.

Foraminifera:

Foraminifera are single-celled amoeboid protist comprising the order Foraminiferida (or Foraminifera of supergroup Rhizaria), characterized by reticulating pseudopods and typically a shell. They may be planktonic or benthic, are mainly marine and are found in all marine environments.

The study of foraminifera contributes to knowledge of several processes in palaeoceanography, paleoclimate, paleoproductivity and palaeohydrology. The abundance, assemblage and size of planktonic foraminifera are the result of increased or decreased productivity due to hydrological conditions (e.g., water column stratification, turbidity, salinity), climate (e.g., river input, temperature) (Mojtahid et al., 2015; Principato et al., 2003; Tesi et al., 2017; Triantaphyllou et al., 2010). Benthic foraminifera are indicators of the deep water conditions as oxygen content in the interstitial and bottom water as well as the food supply and availability (Abu-Zied et al., 2008; Gupta et al., 2008; Kuhnt et al., 2007; Schmiedl et al., 1998). The locations of the 51 cores that have studied the foraminifera data are presented in Fig. 8A. In addition, Fig. 8B shows the two subclasses (planktonic or benthonic). In both subclasses foraminifera are measured by "quantitative analysis" and expressed in three different measurement units (number of foraminifers, percentage or number of foraminifers/gr).

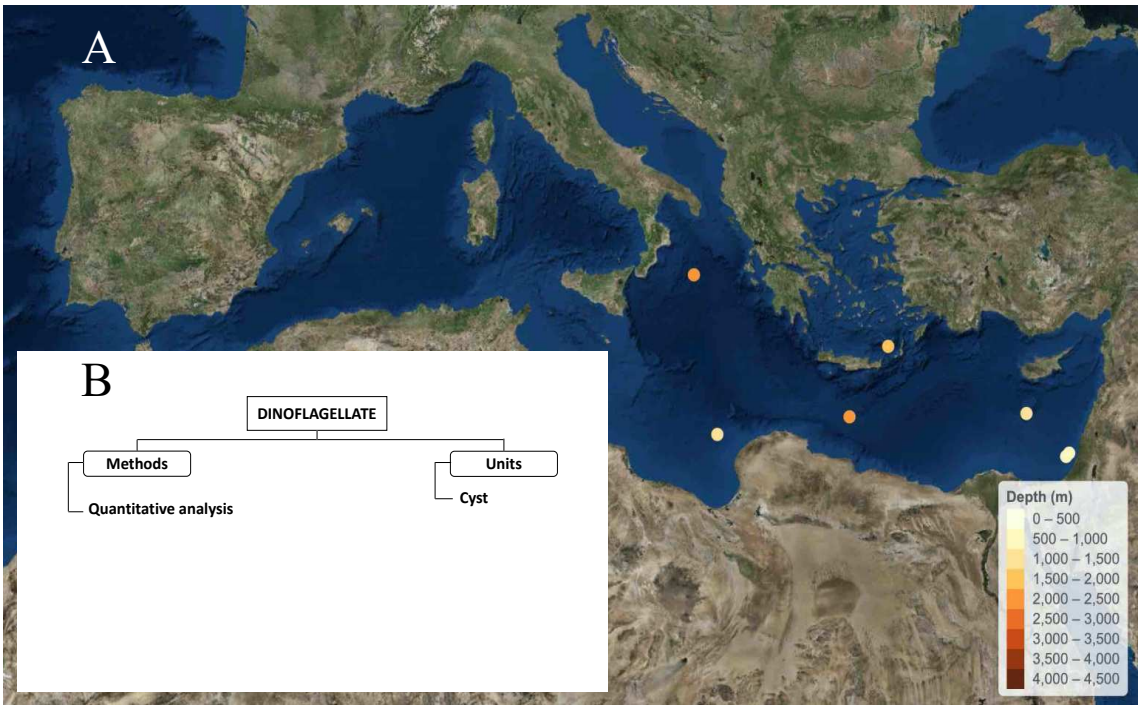

Fig. 7. (A) Core associated with Dinoflagellate data. (B) Diagram showing the dinoflagellate proxies classification used for the Database *BEyOND*.

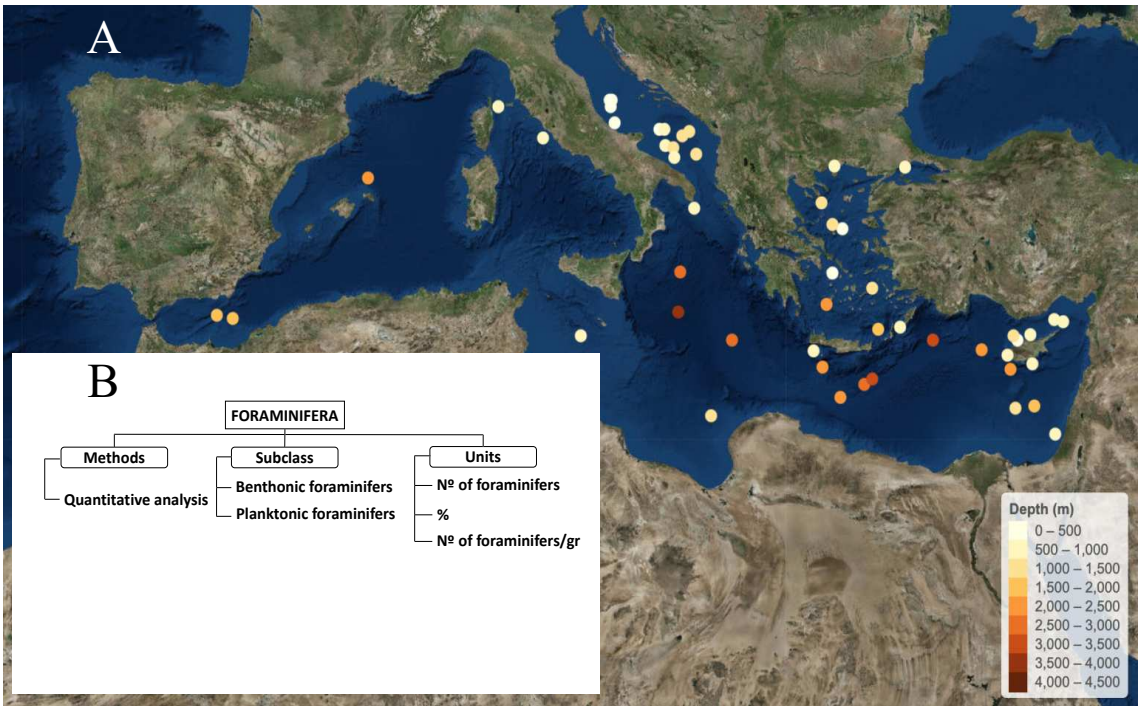

Fig. 8. (A) Core associated with Foraminifera data. (B) Diagram showing the foraminifera proxies classification used for the Database *BEyOND*.

2.3. Design Methodology

The conceptual modelling is a very important phase in designing a quality database (Elmasri & Navathe, 2010). It provides an abstract representation of the application domain, focusing on the description of the major concepts involved and of their relationships, without being misled by database implementation details.

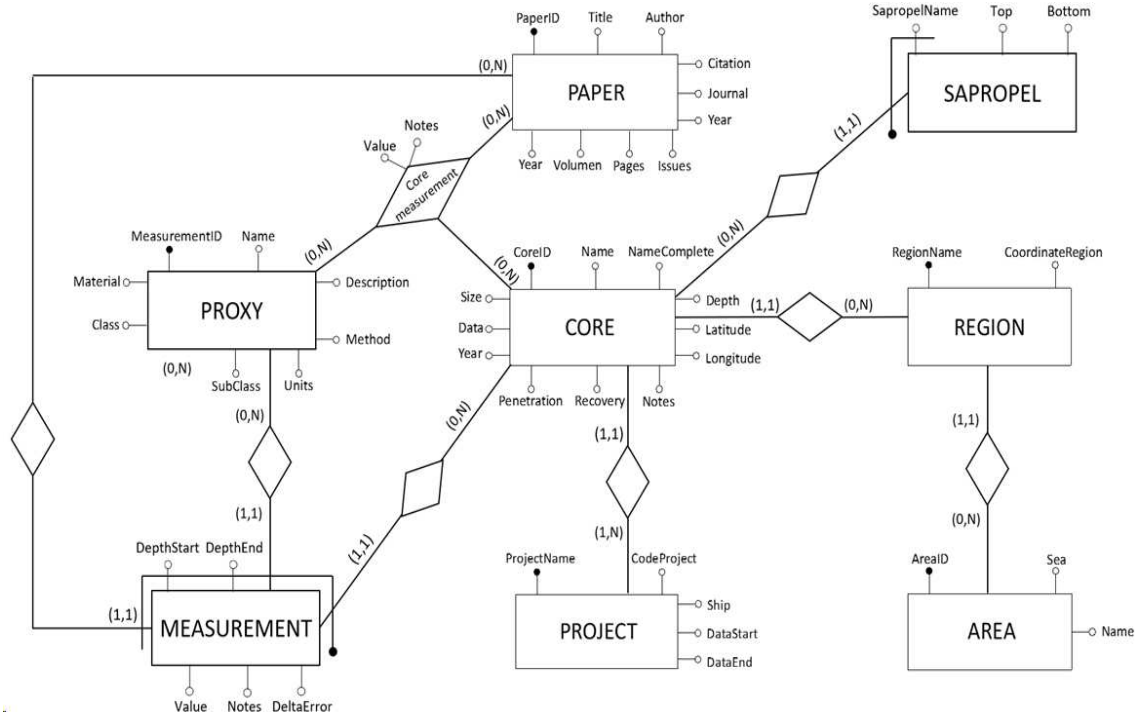

Fig. 9. E-R Schema of *BEyOND*.

In particular, Fig. 9 shows the conceptual schema of the *BEyOND* database expressed in the Entity-Relationship (E-R) model. In the E-R graphical notation, rectangles represent entities, while diamonds represent relationships between entities. Entities are conceptual abstractions of a class of real world objects, which in turn are named instances (or occurrences) of the entity (e.g., the entity "core" has the real cores as instances). Instances of relationship are n-ples of entity instances that are someway related to each other (e.g., an instance of "core measurement" is a triple whose components are a particular measure or proxy, the particular core where the proxy has been taken, and the particular paper where the measurement has been published). Circles associated to entities or relationships represent attributes, e.g., relevant characteristics we want to record about them (e.g., a core is described by its name, latitude and longitude, the date of sampling, etc.). Finally, the black circle in each entity represents the identifier, e.g., an attribute whose value uniquely characterizes each entity occurrence (e.g., the

CoreID). In general, an identifier can be defined through a set of attributes. In some cases, an identifier can not be built using only attributes of the entity, but has to include identifiers of other entities that are linked through relationships. This latter is the case of the entity "measurement", which represents the value of a given proxy measured between two depth values of a given core, as reported in a specific research paper. Hence, the identifier of "measurement" is formed by two internal attributes representing the start and the end depth of the sample (DepthStart and DepthEnd respectively) and the identifiers of "paper", "proxy" and "core" entities respectively. In turn, an instance of "core" is characterized by both the investigation "project" in which the core has been collected, and the geographical "region" it belongs to. Each region is part of an "area", namely a given sea and zone (e.g., the Ionian Sea in the Eastern Mediterranean area).

It is worth noting that the concept of "measurement" is central in the *BEyOND* schema, since it represents the finest measurement we can store in the database. Using relationships, we have defined between "measurement" and other entities, we are able to extract information which is not explicitly stored in the database. For instance, we are able to derive proxies values for a "virtual core", namely the aggregation of all cores in a given region or area. Furthermore, proxies values can be aggregated on the basis of the core on which they were measured, the category of proxy, and so on. Moreover, we can also compare and correlate measurements related to the same sample but reported in different papers, and to the same sapropel but in different cores. Examples of application of analysis enabled by *BEyOND* are described in Section 3.

We like to note that the conceptual methodology adopted allows to obtain a compact, normalized, non-redundant schema that still maintains the same expressive capacity and information richness of existing databases. As an example, the problem of the variable "age": pre-existing databases can only correlate data where the age variable has been calculated, while in *BEyOND* we can insert data with and without the age variable because we use a different method to correlate them (see section 3).

2.4. Implementation

BEyOND has been implemented using the relational model. The adopted database management system is MySQL. The schema reported in Fig. 10 has been obtained from the E-R schema of Fig. 9 by following the rules for E-R to relational schema translation.

The database *BEyOND* is publicly available at http://beyond.dii.univpm.it/. It is focused on paleoclimatology and palaeoceanography studies where all data have been

obtained from marine sediment cores. Whenever possible, we extracted and transformed data coming from other existing databases (see Section 2.1) and loaded them in *BEyOND*. Other data have been manually inserted starting from published papers, sometimes directly asking the authors to provide excel files.

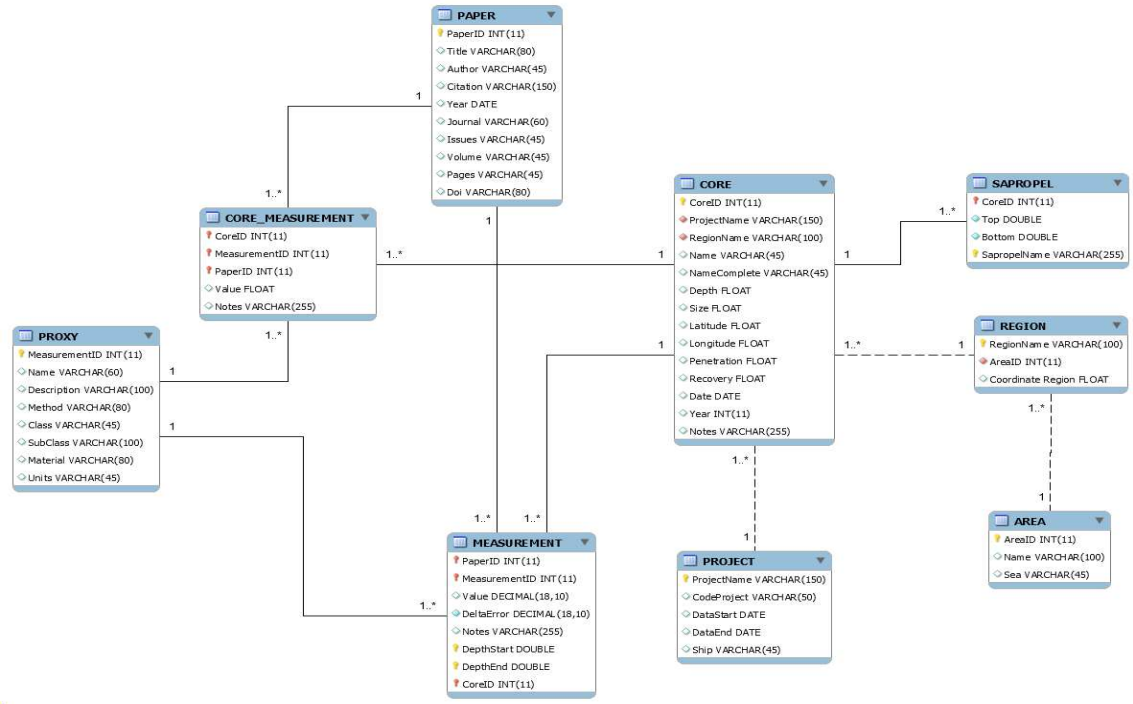

Fig. 10. The relational schema of *BEyOND*. The key symbols are a primary key, while attributes with a red symbol are foreign keys.

Currently, we have inserted data from:

- 79 papers;
- 126 cores (see Fig. 11);
- 1.678 different proxy related data that correspond to all the different ways found in literature used to express the same proxy. See Table 1 that clarifies this concept: e.g., the Aluminum element is classified into 10 different ways because authors calculated and expressed the proxy with different methods and units);
- 283.135 proxy measurements.

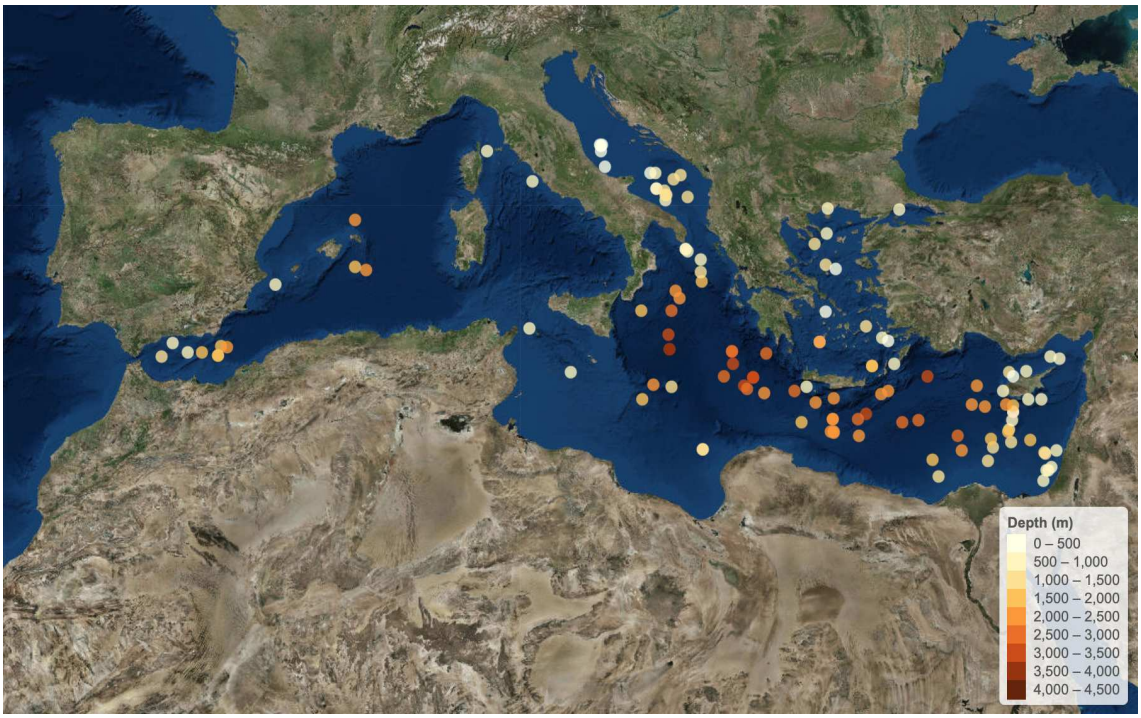

Fig. 11. Map of the Mediterranean Sea with the locations and depths of cores used in *BEyOND*.

Name	Description	Method	Class	SubClass	Material	Units
Al	Aluminum	Energy dispersive polarization X-ray fluorescence spectrometer (EDP-XRF)	Geochemistry	Major Element		mg/kg
Al	Aluminum	Atomic absorption spectrometry (AAS)	Geochemistry	Major Element		%
Al	Aluminum	Atomic absorption spectrometry (AAS)	Geochemistry	Major Element		mg/kg
Al	Aluminum	Atomic absorption spectrometry - X-Ray fluorescence (AAS-XRF)	Geochemistry	Major Element		%
Al	Aluminum	Inductively coupled plasma - atomic emission spectroscopy (ICP-AES)	Geochemistry	Major Element		%
Al	Aluminum	Inductively coupled plasma - atomic emission spectroscopy (ICP-AES)	Geochemistry	Major Element		mg/kg
Al	Aluminum	Inductively coupled plasma - Mass spectrometry (ICP-MS)	Geochemistry	Major Element		mg/kg
Al	Aluminum	X-Ray fluorescence (XRF)	Geochemistry	Major Element		counts
Al	Aluminum	X-Ray fluorescence (XRF)	Geochemistry	Major Element		mg/kg
Al	Aluminum	X-Ray fluorescence (XRF-Mo tube)	Geochemistry	Major Element		%

Table 1. Example of the different ways to express the aluminum proxy in *BEyOND*.

The reasons for the creation of a new database are: (1) most of the data are available in repositories, like PANGAEA or NOAA, where data can be downloaded as tab-delimited texts but no functionality is provided to query the repository nor to combine data coming from different sources; (2) in literature, all databases are organized according to core-age where all the data are expressed in function to age. In *BEyOND*, age is represented as any other proxy, through the concept of "measurement" (see section 2.3),

allowing us a greater flexibility. Indeed, we are able to store proxies' values of a (sample of a) core even if the age is not provided.

3. Applications

To demonstrate the impact of *BEyOND*, in this section we show a set of possible applications to the reconstruction of a combined stack relative to a proxy in the S1 interval, supported by advanced analyses based on a rich set of integrated data.

In fact, to explain processes across a certain area during a certain interval of time we cannot focus on a single field of research (e.g., geochemistry) but we must relate different studies in order to complement and strengthen different discoveries. For this reason, it is of basic importance that every researcher can access and use the data, but also contribute populating the database with his/her data.

Furthermore, the creation of the database, allows us to use data analytics, to access and analyze data with the purpose of gaining and discovering useful patterns and trends in large data sets (Lussier & Hendon, 2016). We have managed to correlate cores located at different depths, presenting different thicknesses, that is to say, different sedimentation rates across the Mediterranean Sea. These correlations have been carried out by SQL queries. We have standardized the depth values of the cores on the basis of the depth values of the sapropel lithology using the following formulas:

$$Standardized\ Start = \frac{DepthStart - TopS1}{BottomS1 - TopS1}$$

$$Standardized\ End = \frac{DepthEnd - TopS1}{BottomS1 - TopS1}$$

Where DepthStart is the top part of the sample (usually of centimetric thickness) analyzed measured starting from the top of the core. Analogously, DepthEnd is the base of the sample analyzed. TopS1 is the top of the sapropel, while BottomS1 is its base.

CoreID	DepthStart (m)	DepthEnd (m)	Proxy Value	Top S1 (m)	Bottom S1 (m)	Standardized Start (m)	Standardized End (m)
1	0,01	0,015	1	0,015	0,035	-0,25	0
1	0,02	0,025	2	0,015	0,035	0,25	0,5
1	0,04	0,045	0,5	0,015	0,035	1,25	1,5
2	0	0,005	0,5	0,005	0,02	-0,33	0
2	0,01	0,015	2,5	0,005	0,02	0,33	0,66
2	0,025	0,03	0,7	0,005	0,02	1,33	1,66
3	0,01	0,02	0,5	0,025	0,045	-0,75	-0,25
3	0,03	0,04	2	0,025	0,045	0,25	0,75
3	0,05	0,06	0,5	0,025	0,045	1,25	1,75

Table 2. Example of averaging depth data: CoreID is the number identifying the core (1;2;3). DepthStart and DepthEnd are the beginning and the end of the measured sample starting from the core-top. Proxy Value is the value obtained in the measured sample for a particular proxy (e. g., TOC). Top S1 and Bottom S1 are the sapropel interval top and base depth respectively. Standardized Start and Standardized End are the new depths obtained with the formulas reported in text.

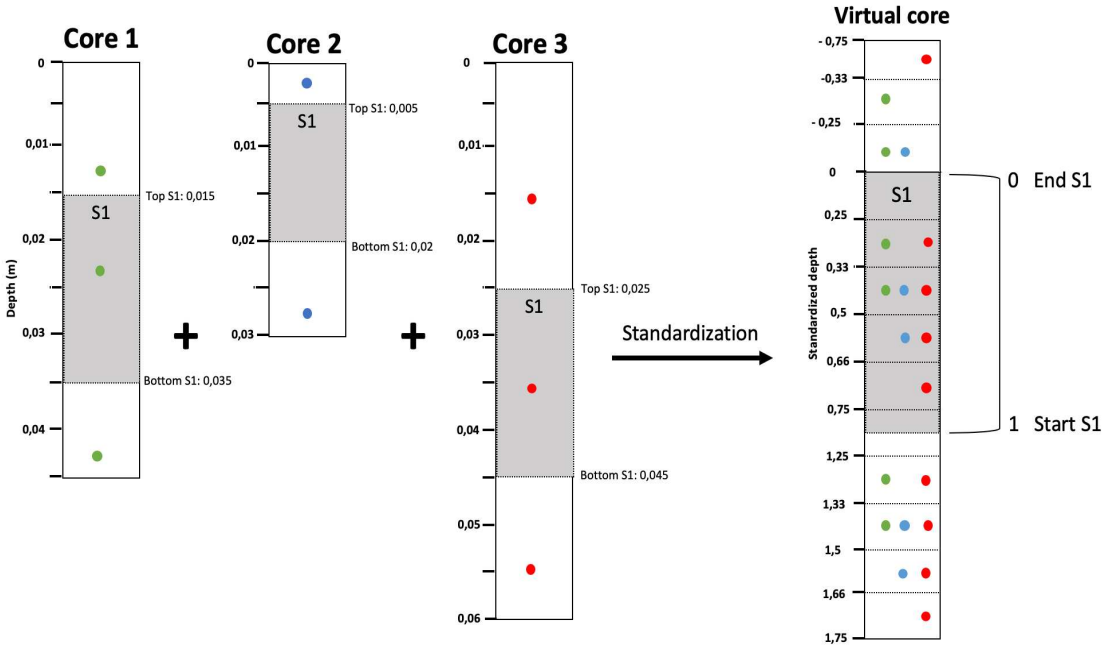

Fig. 12. Standardization of 3 exemplified cores. The intervals S1 are at different depths and the sedimentation rate is different in every core. The green, blue and red dots are the points measured in the cores. Start S1 and End S1 correspond to the sapropel base and top respectively.

Table 2 shows the new depths (Standardized Start and Standardized End) obtained with the use of these formulas. Then, the proxy values were averaged in the same standardized depth range.

Let C1 and C2 be two different cores, let $Bottom_1S_1$ and Top_1S_1 be the bottom and the top depths measured for S1 of the core Ci;

Let V1(x,y) and V2(x,y) be two functions returning the values of the same proxy measured between depths "x" and "y" on C1 and C2 respectively;
Let D1 and D2 be the sets of samples depths of C1 and C2 respectively, and let "m" and "p" be the cardinality of D1 and D2 respectively;

$$\forall\, d_i \in D1, dn_{1i} = \frac{d_i - Top_1S_1}{Bottom_1S_1 - Top_1S_1}\ ;\ D1n = \{dn_{11}, dn_{12}, \dots, dn_{1m}\}$$

$$\forall\, d_i \in D2, dn_{2i} = \frac{d_i - Top_2S_1}{Bottom_2S_1 - Top_2S_1}\ ;\ D2n = \{dn_{21}, dn_{22}, \dots, dn_{2p}\}$$

$$\forall\, d_k \in (D1_n \cup D2_n)$$

$$V'(d_k, d_{k+1}) = average\ \left(V1\left(dn_{1i}, dn_{1j}\right) + V2\left(dn_{2h}, dn_{2l}\right)\right),$$

$$s.t.\ (d_k \geq dn_{1i} \wedge d_{k+1} \leq dn_{1j}) \wedge (d_k \geq dn_{2h} \wedge d_{k+1} \leq dn_{2l})$$

The function V'(x,y) represents the average values of the proxy measured at normalized depths. As for C1 and C2, we can see V'(x,y) as the function returning values of the considered proxy in the interval [x,y] of a "virtual core" computed as average of C1 and C2 (see Fig. 12). Here, the value 1 identifies the beginning of sapropel and the value 0 corresponds to the top of it (as indicated by the different authors and therefore it is based on different methods such as color, micropaleontology, geochemistry, etc.). It is noteworthy that this way the ages of the base and the top of the sapropel are not important, because the query provides a stack, combining all the different sapropel thicknesses found in the database. This allows to compare the trend recorded in the different proxies regardless of age as illustrated in the following examples.

To demonstrate the effectiveness of different cores correlation for the sapropel interval, we carried out some analysis with *BEyOND*. Firstly, we evaluated the correspondence between age and Standardized depth. Fig. 13 considers 37586 age values, of which 22916 in the standardized interval [0,1], from 20 cores. It is evident that the sapropel (S1) interval show a linear trend where r=0.92. Hence, a direct correlation between age and standardized depth is observed.

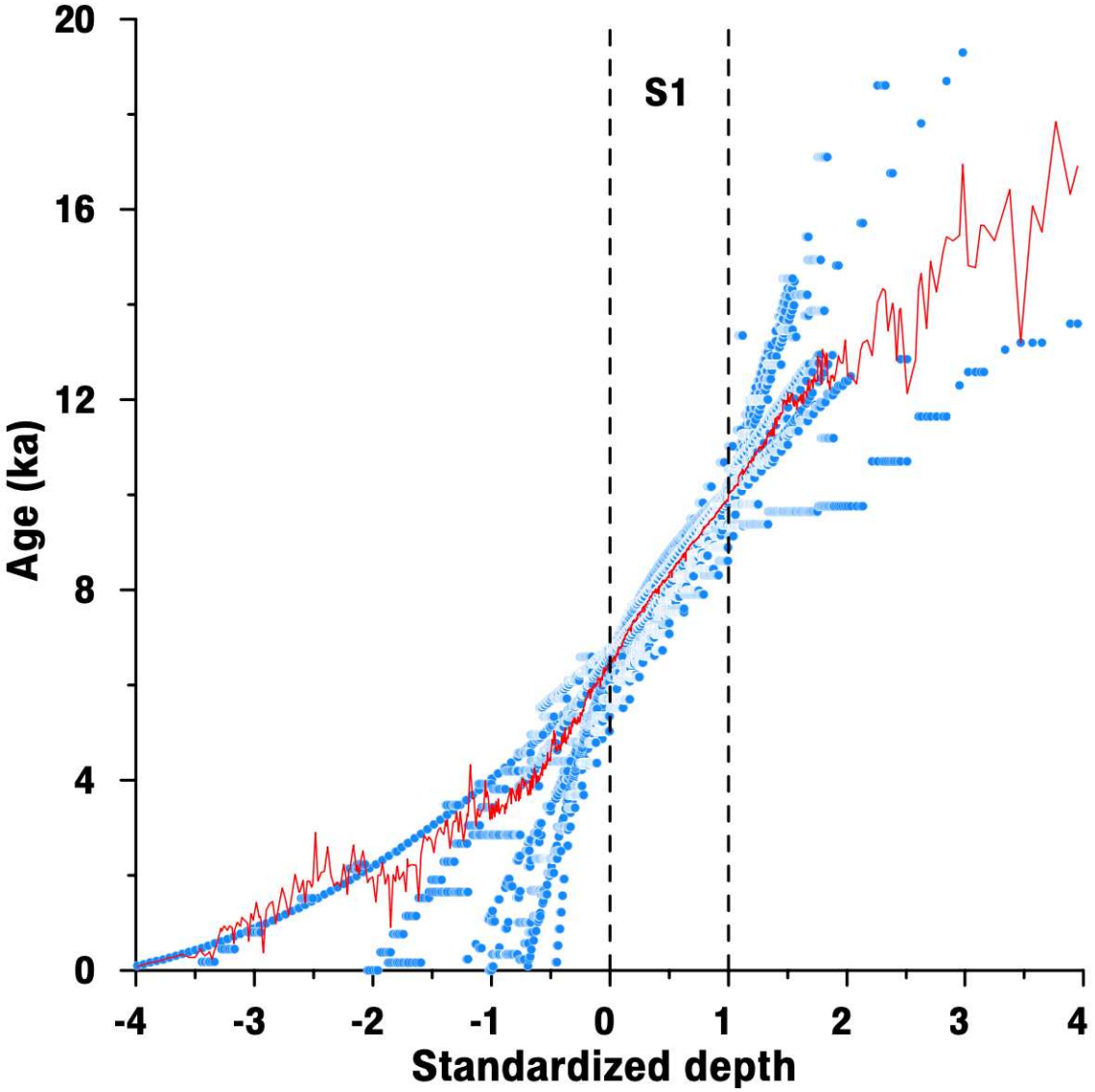

Fig. 13. Age vs Standardized depth. (a) Blue dots correspond to Eastern Mediterranean Sea cores different ages obtained for the sapropel interval. (b) The red line shows the average age for these cores. Vertical dashed black lines represent sapropel interval (S1) where the beginning of sapropel is 1 and the top is 0 standardized depth.

Then we evaluated the correspondence between TOC, Age and Standardized depth. Fig. 14 shows the perfect trend overlay between TOC vs Age and TOC vs Standardized depth in the sapropel interval, thus supporting the effectiveness of our correlation method.

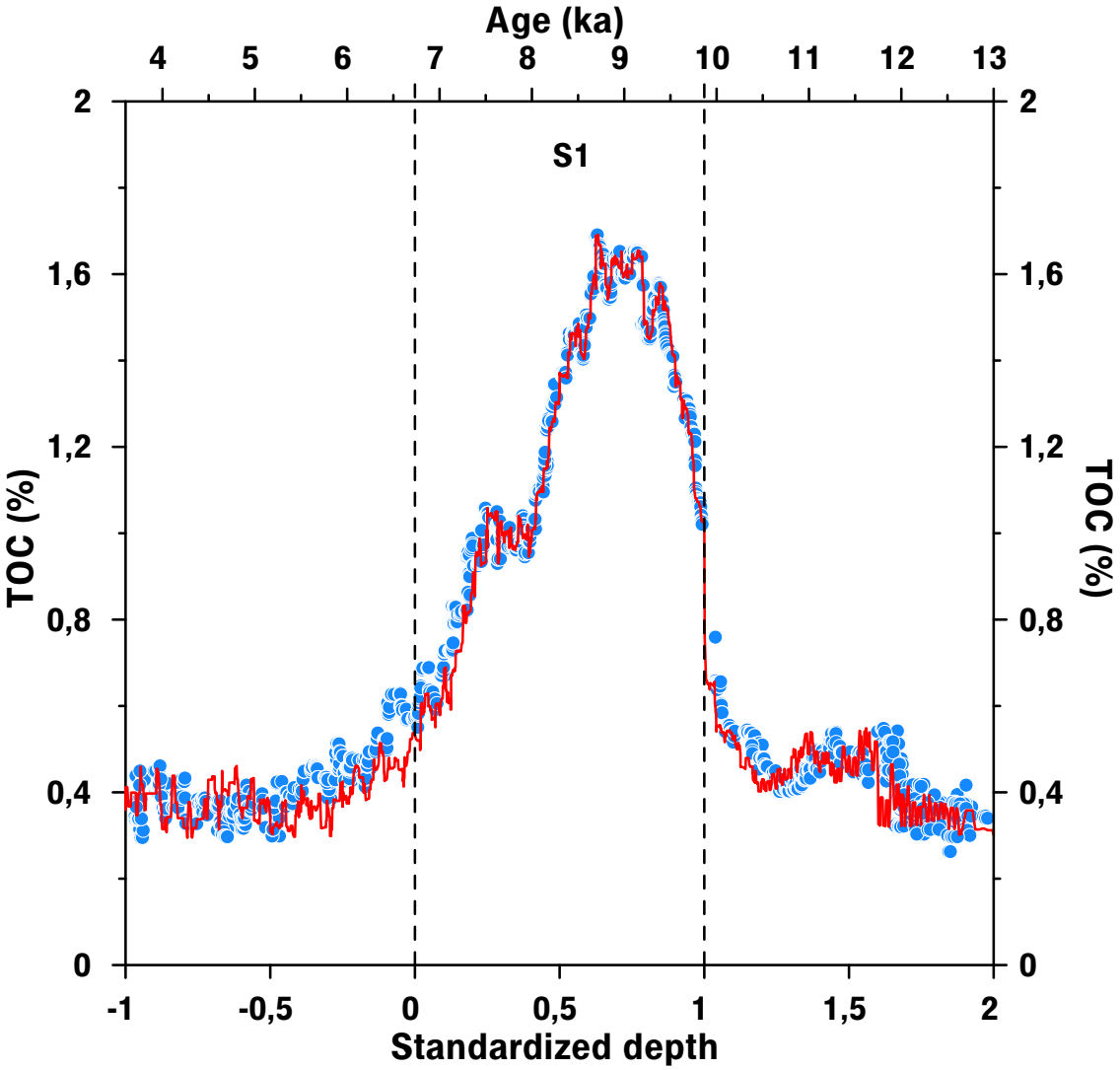

Fig. 14. TOC trend in the Eastern Mediterranean Sea. (a) Blue dots show TOC vs Age. (b) Red line shows TOC vs Standardized depth. Vertical dashed black lines represent sapropel interval (S1) where the beginning of sapropel is 1 and the top is 0 standardized depth.

As for data visualization Fig 1.15 shows the TOC (Total Organic Carbon) trend in 24 cores across the eastern Mediterranean Sea. As it is obvious the difference between inside and outside the sapropel interval is evident. Moreover, it must be underlined that these values are the result of the averages calculated among all the cores of the Eastern Mediterranean Sea. For this reason, the plot shows high standard deviations indicating that the data points are spread out over a wide range of values. Despite all this, a TOC drop around "0,5 standardized depth" corresponding to the sapropel interruption (Abu-Zied et al., 2008; Casford et al., 2003; de Rijk et al., 1999; Hennekam et al., 2014; Myers & Rohling, 2000; Rohling et al., 1997) is evident. Instead not all the studies cores show this interruption clearly.

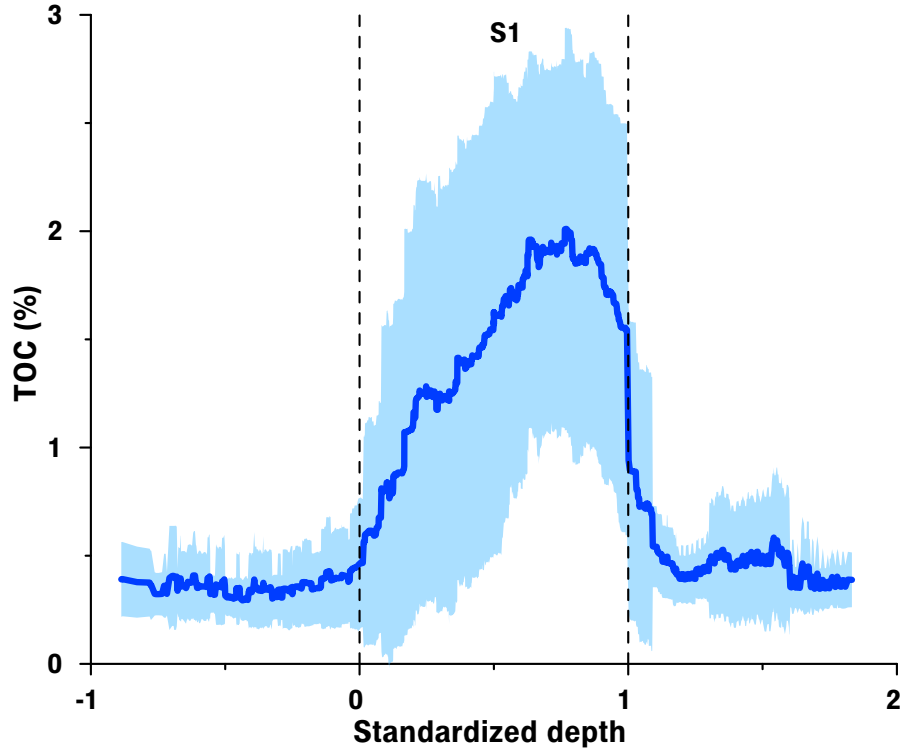

Fig. 15. TOC trend across the Eastern Mediterranean Sea. The blue line shows the TOC value. The blue-shadow indicate the standard deviation of TOC. Vertical dashed black lines represent sapropel interval (S1) where the beginning of sapropel is 1 and the top is 0 standardized depth.

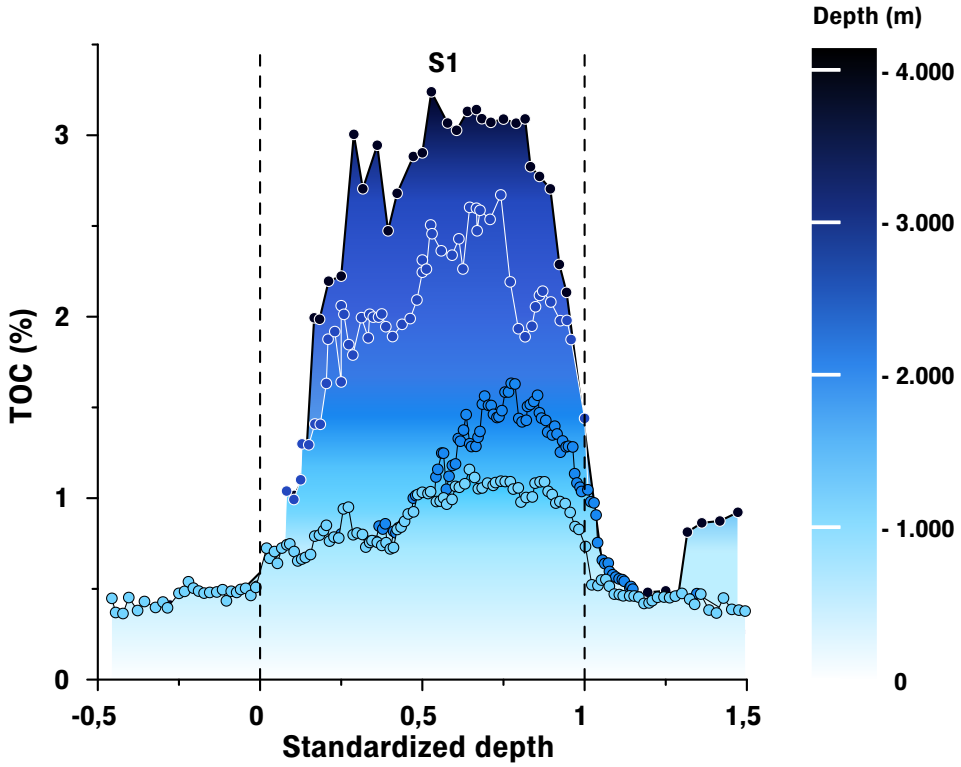

Fig. 16. TOC trend across the Eastern Mediterranean Sea based on the core depth. The cores are grouped as: 0-1000 m (light blue), 1000-2000 m (blue), 2000-3000m (dark blue) and >3000 m (black). Vertical dashed black lines represent sapropel interval (S1) where the beginning of sapropel is 1 and the top is 0 standardized depth.

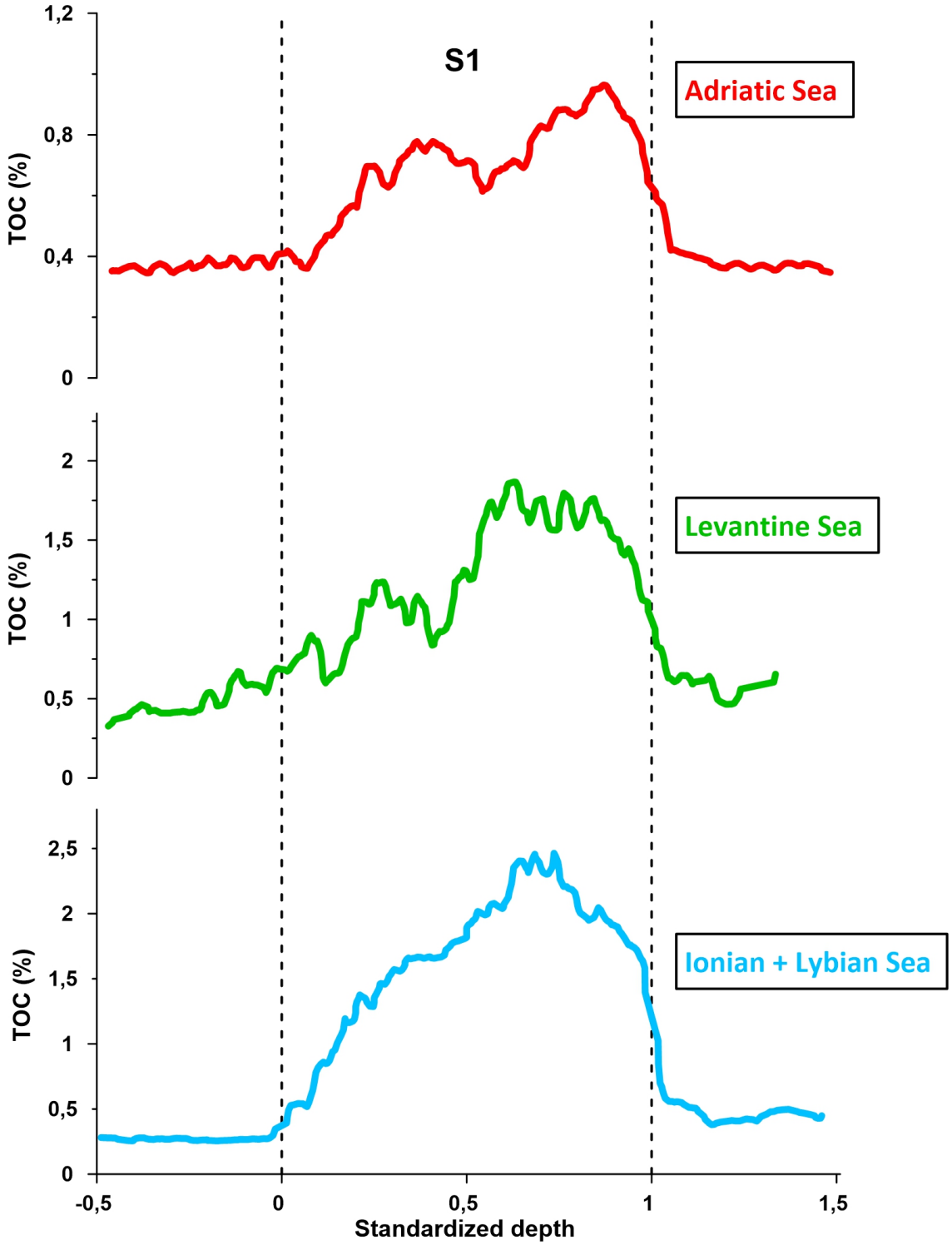

Fig. 17. TOC trend across the eastern Mediterranean Sea based on the area from where the cores have been sampled. The cores are grouped in three regions: Adriatic Sea (red), Levantine Sea (green), Ionian and Libyan Seas (blue). Vertical dashed black lines represent sapropel interval (S1) where the beginning of sapropel is 1 and the top is 0 standardized depth.

Another example of output is the TOC trend, based on the core depth of the cores in the Eastern Mediterranean Sea (Fig. 16). Cores are shown in four depth interval: 1) 0-1000 m, 2) 1000-2000 m, 3) 2000-3000 m and 4) deeper than 3000 m. Fig. 16 evidences the clear TOC% characterizing each depth range. Obviously, this great variation is reflected in the high standard deviation shown in Fig. 15.

The TOC plotted for different Mediterranean Sea areas is shown in Fig. 17. In this case, the three regions: Adriatic (Adriatic Sea), Levantine (Levantine Sea) and Ionian-Libyan (Ionian and Libyan Sea) clearly show different TOC behaviors. A clear bipartition is recorded in the Adriatic Sea, on the contrary, this is less clear in the Levantine and absent in the Ionian-Libyan Sea.

What we obtained is new when compared to previous works (Alberico et al., 2017; Emile-Geay et al., 2017). In fact, these databases only use records where the "age" is known, rejecting the records missing this variable. Instead, our database permit to manage core correlation in different region, at different depth and showing different sedimentation rates, using depth below sea floor (dbsf) and depths in the sapropel interval. Furthermore, our methodology does not suffer of unknown variable (Age) limiting the correlation of the cores. However, some issues still need to be addressed. In fact, as the aggregate results yield a mean value in the interval studied, then some events like the bottom ventilation or the burn-down interval evidenced by short lived spikes may result smoothed and the original lithological extension of the sapropel as indicated in Löwermark et al., (2006) may be less clear. On the other hand, the advantage to obtain a stack aggregating all the data across the Mediterranean allows a wider view and permit to appreciate large scale trends.

4. Conclusive remarks and future work

Paleoceanographic studies are always based on selected sites where researchers perform analyses rarely muti-proxies based, more frequently based on selected a one (e.g., micropaleontology or geochemistry). BDA potentially allow to reverse the approach exploiting already published data to be considered and combined all together.

BEyOND, based on a collection of data from existing databases (PANGAEA, NOAA, Neotoma…) and on data compiled from the literature, the database:

- provides a wide variety of organized and standardized paleoproxies relative to the past 20.000 years. This organization allows to correlate data, to extract hidden patterns and new knowledge.
- enables the analysis of the results in different ways, that is, geographic area or basin depth, allowing to visualize the different proxies trends as a whole.
- provides a great flexibility in the introduction of new proxies as *BEyOND* is organized around the "measurement" entity.
- allows the possibility to bypass the age variable (not always considered when data are published) and the possibility to correlate cores even when the age is not known. This is the most innovative feature proposed in this paper.

Our work highlights the advantages and difficulties in the use of new technologies (database, data analytics...) to exploit (paleo) environmental data to reconstruct the dynamics behind the past climate and oceanography related changes. With our results, we show the high potential of using data analytics. Yet, the new technology tools such as machine learning, data mining, artificial intelligence will increase their importance for future "paleo" studies. However, before this will happen, we strengthen the need for data standardization as it is the main issue when working with a huge data volumes. We therefore encourage the scientific community to take this challenge in order to improve the exchange and usability of this methodology.

BEyOND is open accessible to all researchers to extract data. As a long term objective, it will be implemented in order to add new data in a way that favors the exchange of knowledge as other databases do (e.g., PANGAEA or NOAA). Furthermore, an important achievement will be friendly database where advanced analyses do not need informatic skills. In this regard, we have already developed user-friendly graphical interfaces and services to perform the above described operations. New functionalities of exploratory analysis will be created in the next future. The output of this will be significantly increment in the data volume thanks to the whole contribution of the scientific community contribution. The rich set of integrated data then will be further exploited by the adopting of Data Mining techniques, which in the future will allow through automatic or semi-automatic methods the extraction of useful information from large amounts of data, and its scientific use.

References:

Abu-Zied, R. H., Rohling, E. J., Jorissen, F. J., Fontanier, C., Casford, J. S. L., & Cooke, S. (2008). Benthic foraminiferal response to changes in bottom-water oxygenation and organic carbon flux in the eastern Mediterranean during LGM to Recent times. *Marine Micropaleontology*, 67(1–2), 46–68. https://doi.org/10.1016/j.marmicro.2007.08.006

Alberico, I., Giliberti, I., Insinga, D. D., Petrosino, P., Vallefuoco, M., Lirer, F., Bonomo, S., Cascella, A., Anzalone, E., Barra, R., Marsella, E., & Ferraro, L. (2017). Marine sediment cores database for the Mediterranean Basin: A tool for past climatic and environmental studies. *Open Geosciences*, 9(1), 221–239. https://doi.org/10.1515/geo-2017-0019

Azrieli-Tal, I., Matthews, A., Bar-Matthews, M., Almogi-Labin, A., Vance, D., Archer, C., & Teutsch, N. (2014). Evidence from molybdenum and iron isotopes and molybdenum-uranium covariation for sulphidic bottom waters during Eastern Mediterranean sapropel S1 formation. *Earth and Planetary Science Letters*, 393, 231-242. https://doi.org/10.1016/j.epsl.2014.02.054

Bell, G. (2009) - Foreword. The Fourth Paradigm: Data-Intensive Scientific Discovery, xi-xv.

Bout-Roumazeilles, V., Combourieu-Nebout, N., Desprat, S., Siani, G., Turon, J. L., & Essallami, L. (2013). Tracking atmospheric and riverine terrigenous supplies variability during the last glacial and the Holocene in central Mediterranean. *Climate of the Past*, 9(3), 1065-1087. https://doi.org/10.5194/cp-9-1065-2013

Bown, P. R., & Young, J. R. (1998). Calcareous Nannofossil Biostratigraphy. In: Bown, P.R. (Ed.), Calcareous Nannofossil Biostratigraphy. Chapman and Hall, London, 132–199.

Calvert, S. E., & Pedersen, T. F. (2007). Chapter Fourteen Elemental Proxies for Palaeoclimatic and Palaeoceanographic Variability in Marine Sediments: Interpretation and Application. *Developments in Marine Geology*, 1, 567–644. https://doi.org/10.1016/S1572-5480(07)01019-6

Calvert S.E., & Price N.B. (1983) Geochemistry of Namibian Shelf Sediments. In: Suess E., Thiede J. (eds) *Coastal Upwelling Its Sediment Record*. NATO Conference Series (IV Marine Sciences), vol 10B. Springer, Boston, MA. https://doi.org/10.1007/978-1-4615-6651-9_17

Carty, S., Parrow, M. W. (2015). Dinoflagellates. *Freshwater Algae of North America*, pp. 773–807, https://doi.org/10.1016/B978-0-12-385876-4.00017-7

Casford, J. S. L., Rohling, E. J., Abu-Zied, R. H., Fontanier, C., Jorissen, F. J., Leng, M. J., et al. (2003). A dynamic concept for eastern Mediterranean circulation and oxygenation during sapropel formation. *Palaeogeography, Palaeoclimatology, Palaeoecology*, 190,103-119. https://doi.org/10.1016/S0031-0182(02)00601-6

Cita, M. B., Vergnaud-Grazzini, C., Robert, C., Chamley, H., Ciaranfi, N., & d'Onofrio, S. (1977). Paleoclimatic record of a long deep sea core from the eastern Mediterranean. *Quaternary Research*, 8(2), 205-235. https://doi.org/10.1016/0033-5894(77)90046-1

Crudeli, D., Young, J. R., Erba, E., Geisen, M., Ziveri, P., de Lange, G. J., & Slomp, C. P. (2006). Fossil record of holococcoliths and selected hetero-holococcolith associations from the Mediterranean (Holocene-late Pleistocene): Evaluation of carbonate diagenesis and palaeoecological-palaeocenographic implications. *Palaeogeography, Palaeoclimatology, Palaeoecology*, 237(2–4), 191–212. https://doi.org/10.1016/j.palaeo.2005.11.022

De Rijk, S., Hayes, A., & Rohling, E. J. (1999). Eastern Mediterranean sapropel S1 interruption: an expression of the onset of climatic deterioration around 7 ka BP. *Marine Geology*, 153(1-4), 337-343. https://doi.org/10.1016/S0025-3227(98)00075-9

Dozier, J., & Gail, W. B. (2009). The fourth paradigm: data intensive scientific discovery. The emerging science of environmental applications. *Microsoft Research*, Redmond, 13-19.

Dubois-Dauphin, Q., Montagna, P., Siani, G., Douville, E., Wienberg, C., Hebbeln, D., ... & Pons-Branchu, E. (2017). Hydrological variations of the intermediate water masses of the western Mediterranean Sea during the past 20 ka inferred from neodymium isotopic composition in foraminifera and cold-water corals. *Climate of the Past*, 13(1), 17–37. https://doi.org/10.5194/cp-13-17-2017

Ehrmann, W., Schmiedl, G., Hamann, Y., Kuhnt, T., Hemleben, C., & Siebel, W. (2007). Clay minerals in late glacial and Holocene sediments of the northern and southern Aegean Sea. *Palaeogeography, Palaeoclimatology, Palaeoecology,* 249(1–2), 36–57. https://doi.org/10.1016/j.palaeo.2007.01.004

Ehrmann, W., Schmiedl, G., Seidel, M., Krüger, S., & Schulz, H. (2016). A distal 140kyr sediment record of Nile discharge and East African monsoon variability. *Climate of the Past*, 12(3), 713–727. https://doi.org/10.5194/cp-12-713-2016

Elmasri, R., & Navathe, S. B. (2010). Fundamentals of Database Systems, sixth Edition. Pearson.

Emile-Geay, J., McKay, N. P., Kaufman, D. S., Von Gunten, L., Wang, J., Anchukaitis, K. J., ... & Henley, B. J. (2017). A global multiproxy database for temperature reconstructions of the Common Era. *Scientific Data*, 4, 170088. https://doi.org/10.1038/sdata.2017.88

Fontugne, M. R., Paterne, M., Calvert, S. E., Murat, A., Guichard, F., & Arnold, M. (1989). Adriatic deep water formation during the Holocene: Implication for the reoxygenation of the deep eastern Mediterranean Sea. *Paleoceanography,* 4(2), 199-206. https://doi.org/10.1029/PA004i002p00199

Frigola, J., Moreno, A., Cacho, I., Canals, M., Sierro, F. J., Flores, J. A., & Grimalt, J. O. (2008). Evidence of abrupt changes in Western Mediterranean Deep Water circulation during the last 50 kyr: A high-resolution marine record from the Balearic Sea. *Quaternary International,* 181(1), 88–104. https://doi.org/10.1016/j.quaint.2007.06.016

Gallego-Torres, D., Martinez-Ruiz, F., Meyers, P. A., Paytan, A., Jimenez-Espejo, F. J., & Ortega-Huertas, M. (2011). Productivity patterns and N-fixation associated with Pliocene-Holocene sapropels: Paleoceanographic and paleoecological significance. *Biogeosciences*, 8(2), 415–431. https://doi.org/10.5194/bg-8-415-2011

Gandomi, A., & Haider, M. (2015). Beyond the hype: Big data concepts, methods, and analytics. *International Journal of Information Management*, 35(2), 137-144. https://doi.org/10.1016/j.ijinfomgt.2014.10.007

Grazzini, C. V., & Pierre, C. (1991). High Fertility in the Alboran Sea Since the last Glacial Maximum. *Paleoceanography*, 6(4), 519–536. https://doi.org/10.1029/91PA00501

Gupta, A. K., Das, M., Clemens, S. C., & Mukherjee, B. (2008). Benthic foraminiferal faunal and isotopic changes as recorded in Holocene sediments of the northwest Indian Ocean. *Paleoceanography*, 23(2). https://doi.org/10.1029/2007PA001546

Hennekam, R., Jilbert, T., Schnetger, B., & de Lange, G. J. (2014). Solar forcing of Nile discharge and sapropel S1 formation in the early to middle Holocene eastern Mediterranean. *Paleoceanography*, 29(5), 343-356. https://doi.org/10.1002/2013PA002553

Hennekam, R., Donders, T. H., Zwiep, K., & de Lange, G. J. (2015). Integral view of Holocene precipitation and vegetation changes in the Nile catchment area as inferred from its delta sediments. *Quaternary Science Reviews*, 130, 189–199. https://doi.org/10.1016/j.quascirev.2015.05.031

Hilgen, F. J. (1991). Astronomical calibration of Gauss to Matuyama sapropels in the Mediterranean and implication for the Geomagnetic Polarity Time Scale. *Earth and*

Planetary Science Letters, 104(2-4), 226-244. https://doi.org/10.1016/0012-821X(91)90206-W

IBM Marketing Cloud (2017). 10 Key Marketing Trends for 2017 and Ideas for exceeding customer expectations. Available at: https://www-01.ibm.com/common/ssi/cgibin/ssialias?htmlfid=WRL12345USEN.

Incarbona, A., Ziveri, P., Sabatino, N., Manta, D. S., & Sprovieri, M. (2011). Conflicting coccolithophore and geochemical evidence for productivity levels in the Eastern Mediterranean sapropel S1. *Marine Micropaleontology,* 81(3-4), 131-143. https://doi.org/10.1016/j.marmicro.2011.09.003

Jimenez-Espejo, F. J., Martinez-Ruiz, F., Rogerson, M., González-Donoso, J. M., Romero, O. E., Linares, D., ... & Perez Claros, J. A. (2008). Detrital input, productivity fluctuations, and water mass circulation in the westernmost Mediterranean Sea since the Last Glacial Maximum. *Geochemistry, Geophysics, Geosystem*s, 9(11). https://doi.org/10.1029/2008GC002096

Jimenez-Espejo, F. J., Martinez-Ruiz, F., Sakamoto, T., Iijima, K., Gallego-Torres, D., & Harada, N. (2007). Paleoenvironmental changes in the western Mediterranean since the last glacial maximum: High resolution multiproxy record from the Algero-Balearic basin. *Palaeogeography, Palaeoclimatology, Palaeoecology,* 246(2–4), 292–306. https://doi.org/10.1016/j.palaeo.2006.10.005

Kemp, A. E. S., Pearce, R. B., Koizumi, I., Pike, J., & Rance, S. J. (1999). The role of mat-forming diatoms in the formation of Mediterranean sapropels. *Nature,* 398(6722), 57. https://doi.org/10.1038/18001

Khider, D., Emile-Geay, J., McKay, N. P., Gil, Y., Garijo, D., Ratnakar, V., ... & Bunn, A. (2019). PaCTS 1.0: a crowdsourced reporting standard for paleoclimate data. *Paleoceanography and paleoclimatology*, 34(10), 1570-1596. https://doi.org/10.1029/2019PA003632

Kidd, R. B., Cita, M. B., & Ryan, W. B. F. (1978). Stratigraphy of eastern Mediterranean sapropel sequences recovered during DSDP Leg 42A and their paleoenvironmental significance. *Initial Reports of the Deep Sea Drilling Project*, 42 (Pt. 1). https://doi.org/10.2973/dsdp.proc.42-1.113-1.1978

Kotthoff, U., Pross, J., Müller, U. C., Peyron, O., Schmiedl, G., Schulz, H., & Bordon, A. (2008). Climate dynamics in the borderlands of the Aegean Sea during formation of sapropel S1 deduced from a marine pollen record. *Quaternary Science Reviews*, 27(7–8), 832–845. https://doi.org/10.1016/j.quascirev.2007.12.001

Kuhnt, T., Schmiedl, G., Ehrmann, W., Hamann, Y., & Hemleben, C. (2007). Deep-sea ecosystem variability of the Aegean Sea during the past 22 kyr as revealed by Benthic Foraminifera. *Marine Micropaleontology*, 64(3–4), 141–162. https://doi.org/10.1016/j.marmicro.2007.04.003

Langgut, D., Almogi-Labin, A., Bar-Matthews, M., & Weinstein-Evron, M. (2011). Vegetation and climate changes in the South Eastern Mediterranean during the Last Glacial-Interglacial cycle (86 ka): New marine pollen record. *Quaternary Science Reviews*, 30(27–28), 3960–3972. https://doi.org/10.1016/j.quascirev.2011.10.016

Lingerfelt, E., Fils, D., & Shepherd, A. (2018). Project 418: A Funded Project of the EarthCube Science Support Office. *AGUFM*, 2018, IN31B-22.

Lourens, L. J., Antonarakou, A., Hilgen, F. J., Van Hoof, A. A. M., Vergnaud-Grazzini, C., & Zachariasse, W. J. (1996). Evaluation of the Plio-Pleistocene astronomical timescale. *Paleoceanography*, 11(4), 391-413. https://doi.org/10.1029/96PA01125

Löwemark, L., Lin, Y., Chen, H. F., Yang, T. N., Beier, C., Werner, F., ... & Kao, S. J. (2006). Sapropel burn-down and ichnological response to late Quaternary sapropel formation in two ~ 400 ky records from the eastern Mediterranean Sea. *Palaeogeography, Palaeoclimatology, Palaeoecology,* 239(3-4), 406-425. https://doi.org/10.1016/j.palaeo.2006.02.013

Lussier, R. N., & Hendon, J. R. (2016) - Fundamentals of Human Resource Management: Functions, Applications, Skill Development, (1st ed.). SAGE Publications, Los Angeles.

Mackensen, A., Rudolph, M., & Kuhn, G. (2001). Late pleistocene deep-water circulation in the subantarctic eastern Atlantic. *Global and Planetary Change,* 30(3-4), 197-229. https://doi.org/10.1016/S0921-8181(01)00102-3

Martinez-Ruiz, F., Kastner, M., Paytan, A., Ortega-Huertas, M., & Bernasconi, S. M. (2000). Geochemical evidence for enhanced productivity during S1 sapropel deposition in the eastern Mediterranean. *Paleoceanography*, 15(2), 200–209. https://doi.org/10.1029/1999PA000419

Martinez-Ruiz, F., Kastner, M., Gallego-Torres, D., Rodrigo-Gámiz, M., Nieto-Moreno, V., & Ortega-Huertas, M. (2015). Paleoclimate and paleoceanography over the past 20,000yr in the Mediterranean Sea Basins as indicated by sediment elemental proxies. *Quaternary Science Reviews*, 107, 25–46. https://doi.org/10.1016/j.quascirev.2014.09.018

McFedries, P. (2011) - The Coming Data Deluge, IEEE Spectrum, 48(2), 19-19, https://doi.org/10.1109/MSPEC.2011.5693066

McKay, N. P., & Emile-Geay, J. (2016). Technical note: The Linked Paleo Data framework - A common tongue for paleoclimatology. *Climate of the Past*, 12(4), 1093–1100. https://doi.org/10.5194/cp-12-1093-2016

Meier, K. J. S., Janofske, D., & Willems, H. (2002) - New calcareous dinoflagellates (Calciodinelloideae) from the Mediterranean Sea. Journal of Phycology, 38(3), 602-615, https://doi.org/10.1046/j.1529-8817.2002.t01-1-01191.x

Meier, K. J. S., Zonneveld, K. A. F., Kasten, S., & Willems, H. (2004). Different nutrient sources forcing increased productivity during eastern Mediterranean S1 sapropel formation as reflected by calcareous dinoflagellate cysts. *Paleoceanography*, 19(1), 1–12. https://doi.org/10.1029/2003PA000895

Möbius, J., Lahajnar, N., & Emeis, K. C. (2010). Diagenetic control of nitrogen isotope ratios in Holocene sapropels and recent sediments from the Eastern Mediterranean Sea. *Biogeosciences*, 7(11), 3901–3914. https://doi.org/10.5194/bg-7-3901-2010

Mojtahid, M., Manceau, R., Schiebel, R., Hennekam, R., & de Lange, G. J. (2015). Thirteen thousand years of southeastern Mediterranean climate variability inferred from an integrative planktic foraminiferal-based approach. *Paleoceanography,* 30(4), 402-422. https://doi.org/10.1002/2014PA002705

Myers, P. G., & Rohling, E. J. (2000). Modeling a 200-Yr interruption of the Holocene Sapropel S1. *Quaternary Research*, 53(1), 98-104. https://doi.org/10.1006/qres.1999.2100

Myers, P. G., Haines, K., & Rohling, E. J. (1998). Modeling the paleocirculation of the Mediterranean: The last glacial maximum and the Holocene with emphasis on the formation of sapropel S1. *Paleoceanography*, 13(6), 586-606. https://doi.org/10.1029/98PA02736

Negri, A., & Giunta, S. (2001). Calcareous nannofossil paleoecology in the sapropel S1 of the Eastern Ionian sea: Paleoceanographic implications. *Palaeogeography, Palaeoclimatology, Palaeoecology*, 169(1–2), 101–112. https://doi.org/10.1016/S0031-0182(01)00219-X

Negri, A., Giunta, S., Hilgen, F., Krijgsman, W., & Vai, G. B. (1999). Calcareous nannofossil biostratigraphy of the M. del Casino section (northern Apennines, Italy) and

paleoceanographic conditions at times of Late Miocene sapropel formation. *Marine Micropaleontology*, 36(1), 13-30. https://doi.org/10.1016/S0377-8398(98)00024-3

Olausson, E. (1961). Studies of deep sea cores. Rep, swed. Deep Sea Exped., 1947-1948, 8 (4), 353-391.

Parker, W. C., & Arnold, A. J. (1999). Quantitative methods of data analysis in foraminiferal ecology. *Modern Foraminifera*, 5, 71–89. Springer, Dordrecht. https://doi.org/10.1007/0-306-48104-9_5

Pedersen, T. F., & Calvert, S. E. (1990). Anoxia vs. productivity: what controls the formation of organic- carbon-rich sediments and sedimentary rocks?. *American Association of Petroleum Geologists Bulletin*, 74(4), 454–466. https://doi.org/10.1306/0C9B232B-1710-11D7-8645000102C1865D

Principato, M. S., Giunta, S., Corselli, C., & Negri, A. (2003). Late Pleistocene-Holocene planktonic assemblages in three box-cores from the Mediterranean Ridge area (west-southwest of Crete): Palaeoecological and palaeoceanographic reconstruction of sapropel S1 interval. *Palaeogeography, Palaeoclimatology, Palaeoecology*, 190, 61–77. https://doi.org/10.1016/S0031-0182(02)00599-0

Ridge, E. (2014). Guerrilla Analytics: A Practical Approach to Working with Data. Morgan Kaufmann.

Rohling, E. J. (1991). Shoaling of the Eastern Mediterranean Pycnocline due to reduction of excess evaporation: Implications for sapropel formation. *Paleoceanography*, 6(6), 747-753. https://doi.org/10.1029/91PA02455

Rohling, E. J. (1994). Review and new aspects concerning the formation of eastern Mediterranean sapropels. *Marine Geology*, 122(1–2), 1–28. https://doi.org/10.1016/0025-3227(94)90202-X

Rohling, E. J., Jorissen, F. J., & de Stigter, H. C. (1997). 200 Year interruption of Holocene sapropel formation in the Adriatic Sea. *Journal of Micropalaeontology,* 16(2), 97-108. https://doi.org/10.1144/jm.16.2.97

Rohling, E. J., Marino, G., & Grant, K. M. (2015). Mediterranean climate and oceanography, and the periodic development of anoxic events (sapropels). *Earth-Science Reviews*, 143, 62-97. https://doi.org/10.1016/j.earscirev.2015.01.008

Rossignol-Strick, M. (1983). African monsoons, an immediate climate response to orbital insolation. *Nature*, 304(5921), 46. https://doi.org/10.1038/304046a0

Rossignol-Strick, M. (1985). Mediterranean Quaternary sapropels, an immediate response of the African monsoon to variation of insolation. *Palaeogeography, Palaeoclimatology, Palaeoecology*, 49(3–4), 237–263. https://doi.org/10.1016/0031-0182(85)90056-2

Ryan, W. B. F. (1972) - Stratigraphy of late Quaternary sediments in the eastern Mediterranean. In: Stanley, D. J., Ed., The Mediterranean Sea: a natural sedimentation laboratory: 149-169. Stroudsburg, Pa.: Dowden, Hutchinson and Ross.

Sachs, J. P., & Repeta, D. J. (1999). Oligotrophy and nitrogen fixation during eastern Mediterranean sapropel events. *Science*, 286(5449), 2485-2488. https://doi.org/10.1126/science.286.5449.2485

Sarmiento, J. L., Herbert, T., Toggweiler, J. R. (1988) - Mediterranean nutrient balance and episodes of anoxia. Global Biogeochemical Cycles, 2(4), 427-444. https://doi.org/10.1029/GB002i004p00427

Sarnthein, M., Winn, K., Jung, S. J., Duplessy, J. C., Labeyrie, L., Erlenkeuser, H., & Ganssen, G. (1994). Changes in east Atlantic deepwater circulation over the last 30,000 years: Eight time slice reconstructions. *Paleoceanography*, 9(2), 209-267. https://doi.org/10.1029/93PA03301

Schmiedl, G., Hemleben, C., Keller, J., & Segl, M. (1998) - Impact of climatic changes on the benthic foraminiferal fauna in the Ionian Sea during the last 330,000 years. Paleoceanography, 13(5), 447-458. https://doi.org/10.1029/98PA01864

Stratford, K., Williams, R. G., & Myers, P. G. (2000). Impact of the circulation on sapropel formation in the eastern Mediterranean. Global Biogeochemical Cycles, 14(2), 683-695. https://doi.org/10.1029/1999GB001157

Tachikawa, K., Vidal, L., Cornuault, M., Garcia, M., Pothin, A., Sonzogni, C., et al. (2015). Eastern Mediterranean Sea circulation inferred from the conditions of S1 sapropel deposition. *Climate of the Past*, 11(6), 855–867. https://doi.org/10.5194/cp-11-855-2015

Tesi, T., Asioli, A., Minisini, D., Maselli, V., Dalla Valle, G., Gamberi, F., et al. (2017). Large-scale response of the Eastern Mediterranean thermohaline circulation to African monsoon intensification during sapropel S1 formation. *Quaternary Science Reviews*, 159, 139–154. https://doi.org/10.1016/j.quascirev.2017.01.020

Thunell, R. C. (1979). Pliocene - Pleistocene paleotemperature and paleosalinity history of the Mediterranean Sea: Results from DSDP Sites 125 and 132. *Marine Micropaleontology*, 4, 173-187. https://doi.org/10.1016/0377-8398(79)90013-6

Thunell, R. C., Williams, D. F., & Kennett, J. P. (1977). Late Quaternary paleoclimatology, stratigraphy and sapropel history in eastern Mediterranean deep-sea sediments. *Marine Micropaleontology*, 2, 371-388. https://doi.org/10.1016/0377-8398(77)90018-4

Triantaphyllou, M. V., Antonarakou, A., Dimiza, M., & Anagnostou, C. (2010). Calcareous nannofossil and planktonic foraminiferal distributional patterns during deposition of sapropels S6, S5 and S1 in the Libyan Sea (Eastern Mediterranean). *Geo-Marine Letters*, 30(1), 1–13. https://doi.org/10.1007/s00367-009-0145-7

Triantaphyllou, M. V. (2014). Coccolithophore assemblages during the Holocene Climatic Optimum in the NE Mediterranean (Aegean and northern Levantine Seas, Greece): Paleoceanographic and paleoclimatic implications. *Quaternary International*, 345, 56-67. https://doi.org/10.1016/j.quaint.2014.01.033

Tribovillard, N., Algeo, T. J., Lyons, T., & Riboulleau, A. (2006). Trace metals as paleoredox and paleoproductivity proxies: An update. *Chemical Geology*, 232(1–2), 12–32. https://doi.org/10.1016/j.chemgeo.2006.02.012

Woodruff, F., & Savin, S. M. (1985). $\delta^{13}C$ values of Miocene Pacific benthic foraminifera: correlations with sea level and biological productivity. *Geology,* 13(2), 119-122. https://doi.org/10.1130/0091-7613(1985)13<119:CVOMPB>2.0.CO;2

Zahn, R., Winn, K., & Sarnthein, M. (1986). Benthic foraminiferal $\delta^{13}C$ and accumulation rates of organic carbon: *Uvigerina Peregrina* group and *Cibicidoides Wuellerstorfi*. *Paleoceanography,* 1(1), 27-42. https://doi.org/10.1029/PA001i001p00027

Ziegler, M., Tuenter, E., & Lourens, L. J. (2010). The precession phase of the boreal summer monsoon as viewed from the eastern Mediterranean (ODP Site 968). *Quaternary Science Reviews,* 29(11-12), 1481-1490. https://doi.org/10.1016/j.quascirev.2010.03.011

Zonneveld, K. A. F., Versteegh, G. J. M., & de Lange, G. J. (2001). Palaeoproductivity and post-depositional aerobic organic matter decay reflected by dinoflagellate cyst assemblages of the Eastern Mediterranean S1 sapropel. *Marine Geology*, 172(3–4), 181–195. https://doi.org/10.1016/S0025-3227(00)00134-1

Chapter 2

Spatial and bathymetric reconstruction of the timescale on the most recent sapropel (S1): Implications on the operability of the database BEyOND

R. Amezcua-Buendía[1], C. Diamantini[2], G. Marino[3], D. Potena[2], A. Negri[1]

[1] *Department of Life and Environmental Sciences. Polytechnic University of Marche. Via Brecce Bianche, 60131 Ancona, Italy*

[2] *Department of Information Engineering. Polytechnic University of Marche. Via Brecce Bianche, 60131 Ancona, Italy*

[3] *Department of Marine Geosciences and Territorial Planning, Faculty of Marine Sciences, University of Vigo, 36310 Vigo, Spain.*

To be submitted

Abstract

Eastern Mediterranean sapropel S1 formed during the early to middle Holocene under pronounced climatological and oceanographic forcing that developed (at least partly) in response to (and lagged behind) the northern hemisphere summer insolation peak. Global sea-level rise, African monsoon intensification, enhanced primary production, and/or deep-water stagnation are some of the processes that can explain S1 deposition. Although, these processes have been documented in marine and terrestrial sedimentary records and/or have been simulated by numerical models, it remains ambiguous whether they resulted synchronous or diachronous deposition of organic-rich deposition across the eastern Mediterranean. Here we investigate this issue, using geochemical and micropaleontological data stored in the database Big palEo Ocean Data (*BEyOND*). We conducted the analysis by grouping data in two different ways: *(1)* the different sub-basins (Adriatic, Aegean and Levantine/Ionian); and *(2)* water depths (<600, 600-1,800 and >1,800 meters). To obtain accurate results, the cores were re-calibrated with the latest Marine13 calibration curve. The analysis of geochemical and micropaleontological data based on the core depths indicate that the age of the base and top of S1 are depth-dependent. Hence, S1 started earlier in deeper sites and, conversely, S1 ended earlier in

shallower sites and then in the deeper. The results based on sub-basins show a lag of 150 years in S1 deposition in the Adriatic Sea, which is probably related to the fact that the majority of cores in the Adriatic Sea are shallow and intermediate. Notwithstanding the slight differences in the time, these is not a statistically significant. Thus, our data suggest the sapropel S1 a synchronous event (10.1-6.5 cal. ka BP) in the whole eastern Mediterranean Sea. From these finding derives a fundamental improvement of the database *BEyOND* operability as it is allowed to correlate data based on age extending further its use to different fields of earth science.

1. Introduction

Sapropels are organic-rich layers the deposited throughout the eastern Mediterranean Sea during the last 15.4 million years, that is, since the Middle Miocene (Emeis et al., 1996; Taylforth et al., 2014). These occurred alternately to bioturbated sediments depleted in total organic carbon (TOC ≈ 0.3%) and at least 80 sapropel layers have been reported in eastern Mediterranean sediment cores from the Pliocene through the Holocene (Emeis et al., 1996). For more than 70 years, since they were first found in cores collected during the 1947-1948 Swedish Deep Sea Expedition (Kullenberg, 1952), the scientific community tried to decipher the processes that controlled sapropel deposition in the eastern Mediterranean. Consequently, a great wealth of data concerning on climate and oceanography of the Mediterranean at the time of sapropel deposition is published regarding all the different Mediterranean sub-basins (De Lange et al., 2008; Marino et al., 2009; Gallego-Torres et al., 2011; Incarbona et al., 2011; Hennekam et al., 2014, 2015; Triantaphyllou, 2014; Grimm et al., 2015; Rohling et al., 2015; Tachikawa et al., 2015; Van Helmond et al., 2015; Grant et al., 2016; Tesi et al., 2017; Zwiep et al., 2018; Filippidi & De Lange, 2019). In order to explain sapropel origin, two main mechanisms were proposed: (*1*) enhanced productivity and attendant increase in the export of organic carbon from the upper water column to the deep sea; and (*2*) surface water buoyancy gain linked to monsoon-fueled freshwater discharges along the North African margin, which promoted water column stratification, reduced deep-water ventilation, and organic matter preservation at the seafloor. According to Rohling et al. (2015), a combination of both mechanisms is suggested to be the most plausible scenario, although the contribution of each one remains under discussion.

Like older sapropels, the most recent (S1) is linked to orbital forcing, notably to a distinct minimum in the precession cycle (maximum insolation), which cause the northward migration and intensification of the North African Monsoon (Lourens et al., 1996; Rossignol-Strick, 1985; Grant et al., 2016; Ziegler et al., 2010). The enhanced runoff along the North African Margin, which occurred primarily through the Nile River (Rossignol-Strick, 1983; Emeis et al., 2000; Scrivner et al., 2004; Ducassou et al., 2009; Revel et al., 2010; Hennekam et al., 2015) with potentially complementary inputs from the northern borderlands of the Eastern Mediterranean (Rossignol-Strick, 1987; Cramp et al., 1988; Rohling & Hilgen, 1991; Kotthoff et al., 2008; Taylforth et al., 2014; Toucanne et al., 2015). Runoff reduced the density of the surface waters and increased the nutrient input, hence, enhanced primary production (De Lange & Ten Haven, 1983; Rossignol-Strick, 1985; Calvert & Fontugne, 1987; Rohling & Hilgen, 1991; Rohling, 1994; Mélières et al., 1997; Zwiep et al., 2018). Furthermore, recent studies highlight an increased exchange with the Atlantic Ocean due to global sea-level rise that preconditioned the Mediterranean Sea for the deposit of sapropel (S1) (Grimm et al., 2015; Grant et al., 2016; Cornuault et al., 2018). Thus, enhanced freshwater input led to buoyancy gain at the sea surface, thus causing water column stratification and stagnating deep-water formation, creating low-oxygen conditions that combined with (export)production and, therefore, consequent organic matter preservation (Filippidi & De Lange, 2019).

Base (ka BP)	Top (ka BP)	References
9	7	*Van Straaten (1972); Ryan (1972)*
11.7	8	*Rossignol-Strick et al., 1982*
11-12	-	*Anastasakis & Stanley 1986*
12-14		*Cramp et al., 1988*
8.7	6	*Troelstra et al., 1991*
9.2	6.4	*Perissoratis & Piper 1992*
9.3	7	*Fontugne et al., 1994*
~9	6	*Mercone et al., 2000; Rossignol-Strick, 1999*
10.8	6.1	*De Lange et al., 2008*

Table 1. Age ranges for S1 deposition

In addition to the hypothesis dealing with the mechanism triggering sapropels formation, one topic widely discussed in literature is related to the age and timing of S1 deposition. As reported in Table 1, earlier papers extrapolated age ranges from 9 to 7 ka BP (Ryan, 1972; Van Straaten, 1972), and 11.7 to 8 ka (Rossignol-Strick et al., 1982). Further age assessments were obtained by and Cramp et al. (1988) with age ranges for

the base S1 between 11-12 and 12-14 ka BP, respectively. However, these earlier ^{14}C-data were considered unreliable by Fontugne et al. (1994) due to their low resolution.

Troelstra et al. (1991) were the first to determine the age of S1 (8.7 to 6 ka BP) based on the high-resolution ^{14}C AMS dating. Nevertheless, large differences in the chronology of S1 continued in the early work: 9.2-6.4 ka (Perissoratis & Piper, 1992); 9.3-7 ka BP (Fontugne et al., 1994); and ~9-6 ka BP (Rossignol-Strick, 1999; Mercone et al., 2000). Based on the great variability in age estimates, suggesting asynchronous S1 deposition intervals (Cramp et al., 1988), different possible interpretations of the operating mechanisms were proposed. Troelstra et al. (1991), for instance, suggested that S1 deposition started earlier in the deeper parts of the Mediterranean. In contrast, Strohle & Krom (1997) argued that S1 started in intermediate water (under 500 m water depth) and moved downward reaching deeper water.

Onset and end of sapropel S1 deposition that are diachronous through the different eastern Mediterranean sub-basins were discussed in several papers. Anastasakis & Stanley (1986) postulated that S1 started in the eastern Levantine basin while a few studies on S1 from Adriatic Sea showed that the timing of sapropel deposition was asynchronous with respect to the central and eastern Mediterranean Sea (Jorissen et al., 1993; Rohling et al., 1997; Combourieu-Nebout et al., 1998; Rossignol-Strick, 1999; Giunta et al., 2003; Vigliotti et al., 2011; Rohling et al., 2015). According to these works, S1 started to deposit in the Adriatic Sea between 8.3-8.8 ka BP due to the regional setting. In particular, persistent ventilation was proposed in the Adriatic during the initial phase of sapropel which hampered the development of the oxygen-starved conditions causing a delay in the beginning of S1 deposition (Rohling et al., 1997; Mercone et al., 2000). In contrast to these, De Lange et al. (2008), based on the analysis of more than 30 cores in the eastern Mediterranean Sea, showed a synchronous S1 deposition (10.8-6.1 cal. ka BP), indicating nearly synchronous sapropel formation at all water depths. Recently, Tesi et al. (2017), after the comparison of their results with the published stratigraphic records in the Adriatic basin, concluded that the sapropel S1 deposition was synchronous in the Adriatic Sea and the eastern Mediterranean and that the apparent time lag was due to low-resolution samples or possible stratigraphic gaps. According to the last two authors, the age of S1 base and top seems, therefore, to be synchronous (considering uncertainties) at all depths and basin wide.

Recently, Amezcua-Buendía et al. (2019) developed a database (*BEyOND*[1]) to investigate the youngest sapropel (S1). The database provides a wide variety of organized and standardized paleoproxies spanning the past ~20 kyr of Mediterranean Sea paleoclimate and paleoceanographic history. The most relevant feature of *BEyOND* is the potential to use and correlate existing data also in absence of precise age assessment by means of the use of the so defined "Standardized depth" indicating 0 and 1 as the S1 top and base respectively. Although this method is successful for data correlation (see examples in Amezcua-Buendia et al., 2019), it does not allow to obtain a time frame for the events. Timing is important to extend its use to interpret data and to pinpoint paleoceanographic events.

In this study, we therefore approach this issue by exploiting the data currently published and already present in *BEyOND* with a double aim: 1) test the synchronicity of S1 across the Mediterranean; 2) introduce the "age" variable in the results obtained with the method used by Amezcua-Buendía et al. (2019).

To help clarify the different timing of S1 as said above, our approach is based on the comparison among different sub-basins (Adriatic, Aegean and, Levantine/Ionian) and water depths in order to explore if the sapropel base and top are really basin-wide synchronous.

The meaning of the results will be then discussed to obtain a univocal datum to be used for stratigraphic, paleoclimatological and palaeoceanographic reconstructions.

2. Material and Method

2.1. Sediment core

The data extracted from *BEyOND* were selected considering only those cores providing ages obtained by means of accelerator mass spectrometry (AMS) radiocarbon (^{14}C) analysis (see Table 2). To obtain accurate results, those cores (SLA-9; SL-31; PS009PC; SL123; SL148; LC-21; LC-31; and M25/4-KL11) that were not calibrated with latest Marine13 calibration curve, the radiocarbon-dated samples considered in the original reporting were calibrated using the Marine13 curve of Calib 7.10, applying the same reservoir effect (ΔR) used by the authors. All ages will be discussed as calibrated years (cal. ka BP).

[1] http://beyond.dii.univpm.it/

Core	Depth	Latitude N	Longitude E	TOC	Ba/Al	Mn/Al	Benthic	References
AMC99-1	260	45° 51.80'	14° 45.68'	x	x	x	x	*Tesi et al., 2017*
SLA-9	260	37° 31′	24° 33′		x		x	*Abu-Zied et al., 2008*
SL-31	430	38° 56′	24° 33′				x	*Abu-Zied et al., 2008*
PS009PC	552	32° 07.7'	34° 24.4'	x	x			*Hennekam et al., 2014*
SA03-1	567	41° 30.25'	17° 10.78'				x	*Tesi et al., 2017*
INVAS12-10	570	41° 30.25'	17° 10.78'	x	x	x		*Tesi et al., 2017*
SL123	728	36° 45.34'	27° 33.34'				x	*Kuhnt et al., 2007*
MP50PC	775	39° 29'	18° 31'	x	x	x		*Filippidi & De Lange, 2019*
MS21PC	1022	32° 20.70'	31° 39.00'	x	x			*Zwiep et al., 2018*
SAT04-1	1085	41° 27.46'	17° 31.05'	x	x	x	x	*Tesi et al., 2017*
SL148	1094	39° 45.23'	24° 05.75'				x	*Kuhnt et al., 2007*
MP39PC	1359	38° 49.18'	19° 6.8'	x	x	x		*Filippidi & De Lange, 2019*
LC-21	1522	35° 39.71'	26° 34.96'	x	x	x	x	*Abu-Zied et al., 2008; Casford et al., 2007*
MD04-2722	1780	33° 60'	33° 30'		x	x		*Tachikawa et al., 2015*
MP37PC	1908	38° 31.81'	19° 10.84'	x	x	x		*Filippidi & De Lange, 2019*
LC-31	2298	34° 59.76'	31° 09.81'		x		x	*Abu-Zied et al., 2008*
M25/4-KL11	3376	36° 44.75'	17° 43.03'			x		*Martinez-Ruiz et al., 2000; Emeis et al., 2000*

Table 2. Core locations in this study. The criteria used to identify the sapropel interval are TOC, Ba/Al, Mn/Al and, benthic foraminifera.

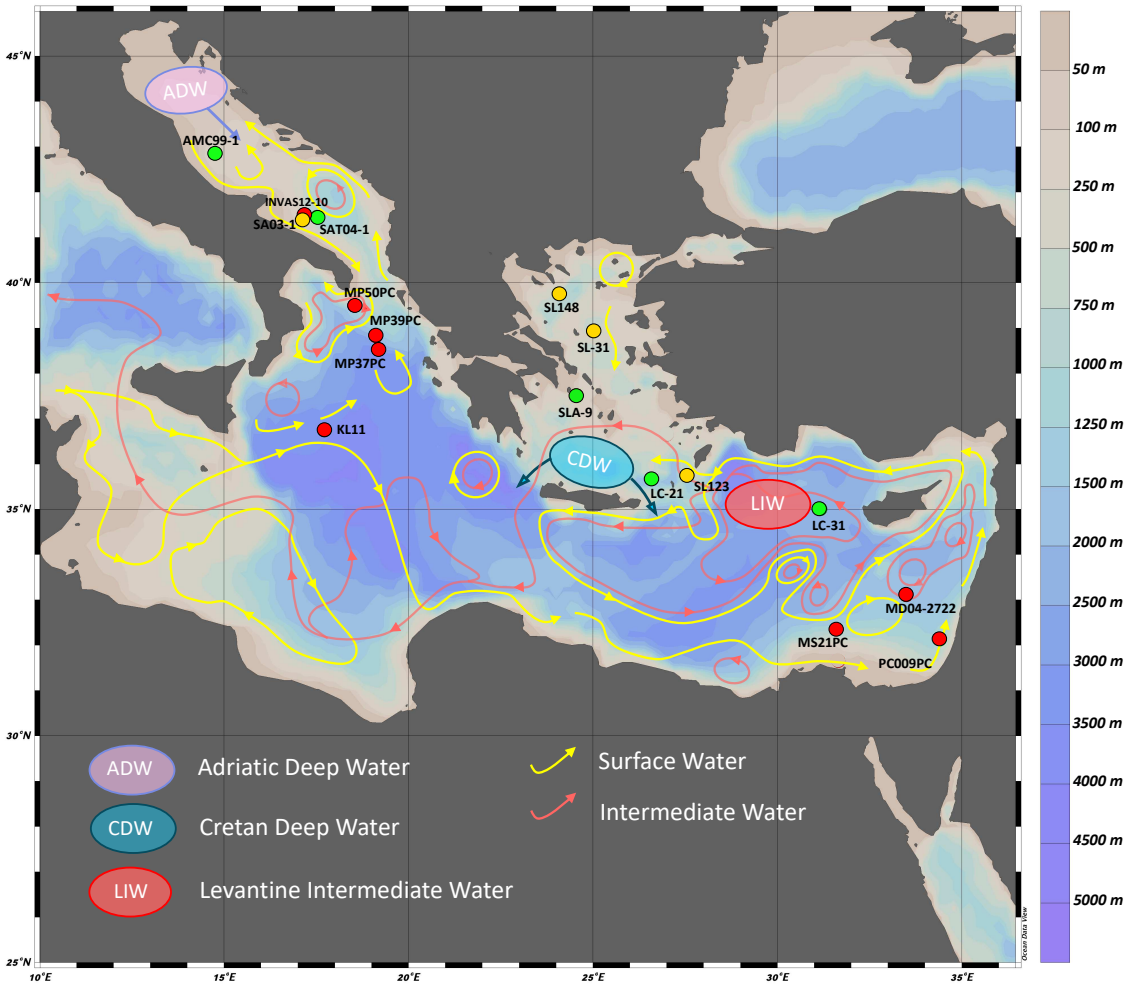

Fig. 1. Core sites in the eastern Mediterranean basin. Red dots show cores where only geochemical data are reported. Yellow dots are cores with micropaleontological data. Green dots show the cores with geochemical and micropaleontological data. The map is produced by using Ocean Data View (Schlitzer, 2020).

As a result, a total of 18 cores have been used in this study as reported in Fig. 1 and Table 2 distributed in a wide range of depth and Mediterranean sub-basins.

2.2. How the base and the top of S1 are identified

Sapropels and their boundaries are characterized by distinct geochemical signatures. For example, elevated TOC (2-30%) has been reported at the base and along the whole sapropel interval (Emeis et al., 1996, 1998; Passier et al., 1999; Nijenhuis & De Lange, 2000). TOC represents the single most important indicator of organic matter in sediments, in that it reflects the amount of organic matter exported to the seafloor that escaped degradation. On the other hand, the sedimentary Ba/Al is a key indicator of (export)production. The organic matter in the sapropels is an admixture of the marine, terrigenous, and bacterial products (Ten Haven et al., 1987), but marine organic matter is largely predominant (Calvert & Fontugne, 1987; Ten Haven et al., 1987; Buscail et al., 1992). The principal factors responsible for the accumulation of organic carbon in marine sediments are the amount of export production, the rate of deposition of organic matter at the seafloor, and the rate of degradation that is related to bottom-water conditions (i.e., oxic, dysoxic, and anoxic) (Demaison & Moore, 1980; Arthur et al., 1984; Pratt, 1984; Pratt & Ring, 1986; Arthur et al., 1987; Betts & Holland, 1991; Calvert et al., 1996; Tyson, 2001; İşler et al., 2016). During sapropel deposition, anoxic conditions at the seafloor minimize organic matter degradation and enhances its preservation. Also, enhanced primary production during the sapropels increased the rate of supply of organic matter to the seafloor (export production) and, as a result, increased the rate of deposition of the organic matter. Thus, the abrupt TOC increase is used to identify the onset of sapropel deposition. However, it cannot be considered, in some cases, as a proxy for sapropel termination because it may undergo post-depositional oxidation (burn-down) (De Lange et al., 2008). This causes an oxidation front, which is developed as consequence of the reventilation of deep waters at the end of the sapropel deposition (De Lange et al., 1989). Penetration of oxygen into the sediment oxidizes the organic matter deposited under sapropel conditions and "deepens" the sapropel top (De Lange et al., 1989, 2008; Thomson et al., 1995; Van Santvoort et al., 1996; Weldeab et al., 2003). Accordingly, other methods were proposed to recognize the real sapropel top and therefore the original thickness of the layer and the duration of sapropel deposition.

Barium (Ba) is an indicator of organic matter content in sediments and production export to the seafloor (Thomson et al., 1995). Unlike the TOC, Ba does not suffer from post-deposition mobilization, thereby allowing precise determination of the base and top of sapropels (cf., De Lange et al., 2008). Ba enrichment results from barite ($BaSO_4$) formation related with decaying organic matter while settling in the water column, thereby Ba is considered to be an excellent proxy for (export)production (Bishop, 1988; Dymond et al., 1992; Higgs et al., 1994; Thomson et al., 1995; Martinez-Ruiz et al., 2000; Nijenhuis & De Lange, 2000; De Lange et al., 2008). Other elements permit further details, such as Manganese (Mn). This element concentration is generally low within sapropels because of its mobilization under suboxic-anoxic conditions in the bottom water (Mangini et al., 2001). However, a prominent Mn peak (so-called 'Marker Bed', Mn-MB; Filippidi & De Lange, 2019) marks the top of sapropels, and indicates the penetration of oxygen in the sediment at the end of sapropel deposition (De Lange et al., 1989; Mangini et al., 1991; Pruysers et al., 1993; Thomson et al., 1995; Van Santvoort et al., 1996; Mercone et al., 2000). We therefore adopt these indicators (TOC, Barium and Marker Bed) to identify unambiguously S1 and because the Mediterranean is characterized by high detrital contribution (Martinez-Ruiz et al., 2015), we have only considered those papers using Ba and Mn values normalized to Aluminum (Ba/Al and Mn/Al).

Based on what reported above, the TOC and Ba/Al are adequate indicators for determining the sapropel onset, while the Mn/Al (Mn-MB) and Ba/Al mark the sapropel termination. In Fig. 1, are reported the 13 cores located in the different sub-basins that provided geochemical data (Table 3 and 4).

Core	Depth (m)	Region	TOC	Ba/Al	Benthic LO	Benthic HO
AMC99-1	260	Adriatic	10.07	10	-	9.96
SLA-9	260	Aegean	-	10.1	9.6	9.8
SL-31	430	Aegean	-	-	9.8	10.2
PS009PC	552	Levantine	10.06	10.06	-	-
SA03-1	567	Adriatic	-	-	9.66	10.15
INVAS12-10	570	Adriatic	10	9.93	-	-
SL123	728	Aegean	-	-	9.65	10.1
MP50PC	775	Adriatic	10.22	10.22	-	-
MS21PC	1022	Levantine	10.09	10.06	-	-
SAT04-1	1085	Adriatic	10	9.84	9.65	10.08
SL148	1094	Aegean	-	-	-	9.8
MP39PC	1359	Ionian	10.27	9.8	-	-
LC-21	1522	Aegean	10.2	10.2	9.5	10.25
MD04-2722	1780	Levantine	-	10.44	-	-
MP37PC	1908	Ionian	10.2	10.2	-	-
LC-31	2298	Levantine	-	10	9.3	9.8

Table 3. Age values considered in this study for the S1 onset. All ages are expressed in cal. ka BP.

Core	Depth (m)	Region	TOC	Ba/Al	Marker Bed	Benthic HO
AMC99-1	260	Adriatic	6.66	6.66	6.48	7
SLA-9	260	Aegean	-	6.7	-	6.8
SL-31	430	Aegean	-	-	-	6.7
PS009PC	552	Levantine	6.68	6.68	-	-
SA03-1	567	Adriatic	-	-	-	6.85
INVAS12-10	570	Adriatic	6.78	6.55	6.97	-
SL123	728	Aegean	-	-	-	6.6
MP50PC	775	Adriatic	6.75	6.75	6.25	-
MS21PC	1022	Levantine	6.16	6.16	-	-
SAT04-1	1085	Adriatic	6.7	6.7	6.88	6.75
SL148	1094	Aegean	-	-	-	6.65
MP39PC	1359	Ionian	6.67	6	5.99	-
LC-21	1522	Aegean	6.12	6.12	6.7	6.8
MD04-2722	1780	Levantine	-	6.89	6.75	-
MP37PC	1908	Ionian	7.85	6	5.91	-
LC-31	2298	Levantine	-	6	-	6.55
M25/4-KL11	3376	Ionian	7.77	6.25	6.7	-

Table 4. Age values considered in this study for the S1 top. All ages are expressed in cal. ka BP.

2.3. Use of benthic foraminifera assemblages to characterize the sapropel S1

The fluctuation in abundance of benthic foraminifera across sapropel permits to unravel the paleoenvironmental condition at the time of its sedimentation (Jorissen, 1999; Schmiedl et al., 2003; Morigi, 2009). The number and diversity of benthic foraminifera are used to characterize the environment (Kuhnt et al., 2007) and both increase with increasing organic matter flux (Herguera & Berger, 1991). However, this applicability is limited in low-oxygen environments, as well as in sapropels (Naidu & Malmgren, 1995). The vertical benthic foraminifera distribution within sediment is closely related to the amount of dissolved oxygen in bottom/pore water (Corliss, 1985; Barmawidjaja et al., 1992; Sen Gupta & Machain-Castillo, 1993; Jorissen et al., 1995; Fontanier et al., 2002; Abu-Zied et al., 2008; Melki et al., 2010). Areas with high oxygen concentrations are colonized by epifaunal (0-1 cm) and shallow-intermediate infaunal (1-4 cm), that is, species that require high oxygen (HO) concentrations as *Cibicidoides pachydermus, Gyroidinoides orbicularis, Hoeglundina elegans,* and *Planulina ariminensis*. Instead, areas with low oxygen concentrations are colonized by deep infaunal (>4 cm), species with the highest tolerance of dysoxia/intermittent anoxia, hereinafter targeted as LO, as *Chilostomella oolina, Chilostomella mediterranensis, Globobulimina affinis,* and *Evolvocassidulina bradyi* (Sen Gupta & Machain-Castillo, 1993; Rohling et al., 1997; De Stigter et al., 1998; Bernhard & Sen Gupta, 1999; Jorissen, 1999; Schmiedl et al., 2000, 2003; Mercone et al., 2001; Morigi et al., 2001; Giunta et al., 2003; Geslin et al., 2004; Fontanier et al., 2006; Abu-Zied et al., 2008). Based on this knowledge, the beginning of the dysoxic conditions is identified by the last occurrence of the HO species (hereinafter as HOD; high oxygen disappearance) while the anoxic conditions by the last presence of the LO species (hereinafter as LOD; low oxygen disappearance). Inversely, the increase in HO species (hereinafter as HOR; high oxygen recovery) close to S1 top indicate the reventilation/reoxygenation of bottom waters. Fig. 1, reports the 9 cores located in the different sub-basins that provided the micropaleontological data used for defining the extent of S1 (Table 3 and 4).

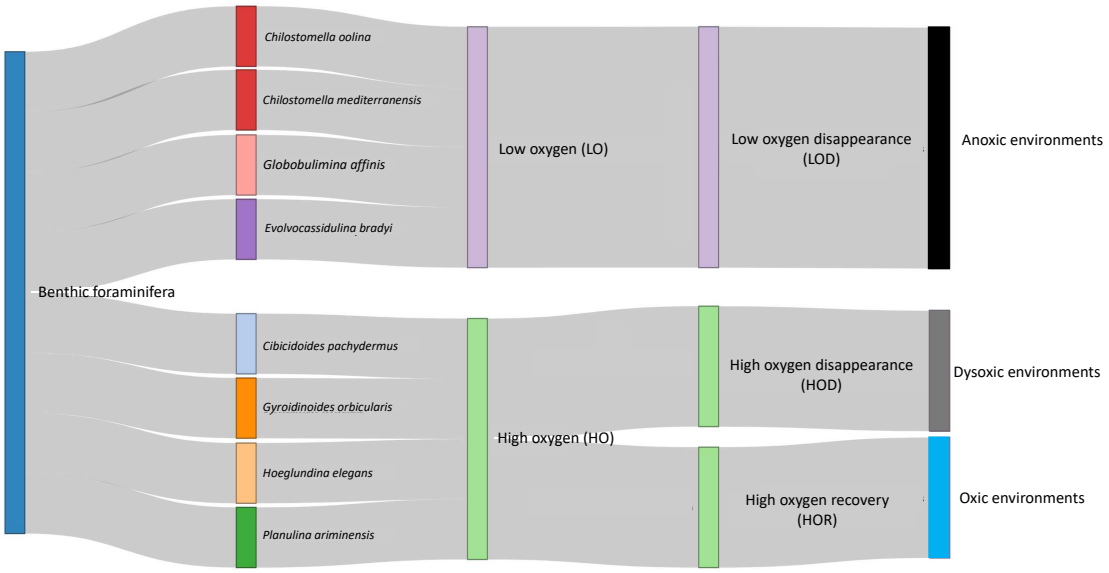

Fig. 2. Benthic foraminifera used to characterize the oxygen conditions during sapropel S1

2.4. Treatment of data

Fig. 3 and Fig. 7, show the features obtained for each indicator as result of the median value of all cores studied. First, we identify in each core the sapropel S1 interval as defined by the elements considered in Section 2.2 (TOC and Ba/Al increase on S1 base, and Ba/Al decrease and Mn-MB on S1 top) and 2.3 (HO and LO benthic signals). Then, the ages that represent the different regions or depths (see Table 5 and 6) were obtained through the median obtained from the values of the age of the single cores (see Table 3 and 4). Also, several statistical tool as ANOVA, clustering and Kernel density estimation (KDE) were used to test of similarities between data, and thus, the synchronicity of S1. The ANOVA test is obtained using the SPSS Statistic software version 25.0 (IBM Corp, 2017) while the cluster and KDE analysis using RStudio software version 1.2.5009 (RStudio, 2019).

Based on what reported above, we tested the variability of our results as follows:

i) According to water depth. Cores were divided in 0 – 600 m, considering the flow limit of the Levantine Intermediate Water (LIW) (Pinardi & Masetti, 2000); 600 – 1,800 m, considering the different characteristics obtained in previous studies (De Lange et al., 2008; Ziewp et al., 2018; Zirks et al., 2019); and >1,800 m (Zirks et al., 2019).

ii) According to the geographical location. Cores divided into three different sub-basins: the Adriatic and Aegean Seas due to their importance as deep-

water formation sites; and the Ionian, Libyan and Levantine Sea (hereafter called "Levantine/Ionian") since in the latter occurs the LIW formation, which flows along the Mediterranean Sea. The Ionian, Libyan and Levantine Sea are treated as a unique basin because although the Cretan Strait (1,800 m deep and 300 km wide) divides the Ionian and Levantine Seas, the flow between both sub-basins does not seem to be altered (Malanotte-Rizzoli and Hecht, 1988).

As said above, we used a limited number of cores (18) due to the fact that we discarded all those showing data not sufficiently resolved (cores not dated with C^{14}). This obviously produces limited data availability in some regions and/or depths like, for instance, in the Aegean basin where only two cores provided geochemical data or in the Levantine/Ionian Sea and deeper sites, where the benthic foraminifera data derived from 1 core. It is therefore evident that increasing the number of data will enhance the accuracy of the results, nonetheless, this exercise is important to monitor the variability across the basin and to test the use of the database.

3. Result

3.1. Averaged age of sapropel base and top in cores at different depth

Table 5 and Fig. 3, report the sapropel interval age variations based on cores collected at different depths. Based on the TOC and Ba/Al, the sapropel base show an age of 10.23 ± 0.12 cal. ka BP at depth > 1,800 m, 10.17 ± 0.17 cal. ka BP between 600 – 1,800 m, and finally at 10.04 ± 0.05 cal. ka BP in shallower sites (< 600 m). As for S1 top, the Mn-MB and Ba/Al decrease date at 6.69 ± 0.2 cal. ka BP in shallow sites, then at 6.56 ± 0.37 and 6.15 ± 0.35 cal. ka BP in intermediate and deep sites, respectively.

HO species disappear in intermediate sites at 10.05 ± 0.18 cal. ka BP, then in shallow sites at 10.09 ± 0.18 cal. ka BP, and finally in deep sites at 9.8 ± 0.2 cal. ka BPs. On the other hand, the LO species disappear in shallow sites at 9.66 ± 0.1 cal. ka BP and, subsequently, in intermediate and deep sites at 9.65 ± 0.08 and 9.3 ± 0.2 cal. ka BP, respectively. Conversely, the recovery of the HO species occurs at 6.77 ± 0.13 cal. ka BP in shallow sites, then in intermediate sites at 6.65 ± 0.09 cal. ka BP and deep sites at 6.55 ± 0.2 cal. ka BP.

Depth (m)	Proxies	Top	±	Bottom	±
0-600	TOC + Ba/Al	6676	0.06	10047	0.05
	Benthic HO	6775	0.13	10055	0.18
	Benthic LO	-	-	9660	0.1
	Mn/Al + Ba/Al	6698	0.2	-	-
600-1,800	TOC + Ba/Al	6550	0.34	10170	0.17
	Benthic HO	6655	0.09	10091	0.18
	Benthic LO	-	-	9650	0.08
	Mn/Al + Ba/Al	6565	0.37		
>1,800	TOC + Ba/Al	6906	0.12	10230	0.12
	Benthic HO	6550*	0.2	9800*	0.2
	Benthic LO	-	-	9300*	0.2
	Mn/Al + Ba/Al	6154	0.35	-	-

Table 5. Median calculated values grouped for different depths. *Single core value

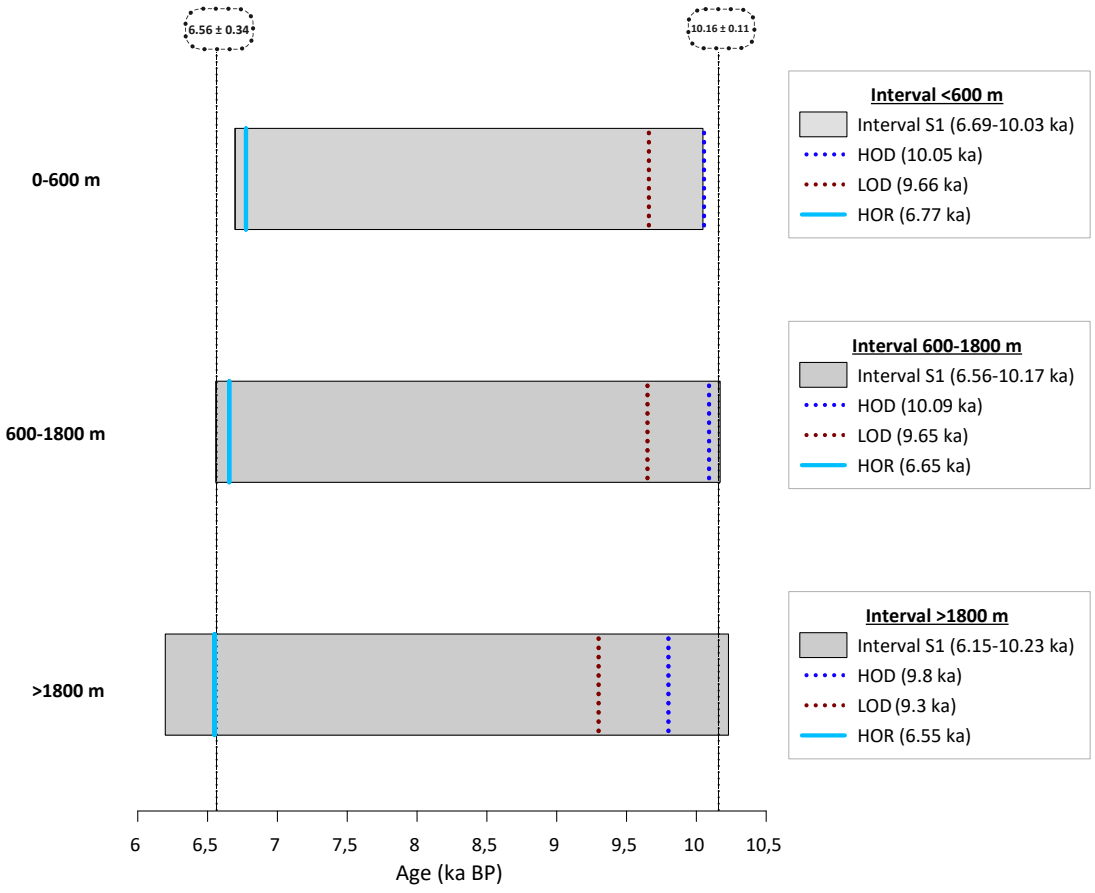

Fig. 3. Sapropel interval age variations based on the different depths. The base of sapropel is determined as the increase of TOC and Ba/Al while the decrease of Ba/Al and Mn-MB signal indicate the top of S1. The dark blue dots lines indicate the high oxygen disappearance (HOD) while the dark red dots lines indicate the low oxygen disappearance (LOD) (see Section 2.3). The blue vertical bands represent the high oxygen recovery (HOR) (see Section 2.3). The mean ages of the upper and lower boundaries (6.56 ± 0.34 and 10.16 ± 0.12 cal. ka BP) are indicated by the black vertical lines.

Descriptive Analyses

BOTTOM

DEPTH (m)	N	Median	Mean	Std. Deviation	95% Confidence Interval for Mean		Minimum	Maximum
					Lower Bound	Upper Bound		
<600	7	10047	10034	,02125	9982	10086	9.94	10.10
600-1800	11	10170	10122	,05715	9995	10250	9.80	10.44
>1800	5	10230	10208	,05851	10045	10370	10	10.32
Total	23	10165	10114	,03255	10046	10181	9.80	10.44

REGION	N	Median	Mean	Std. Deviation	95% Confidence Interval for Mean		Minimum	Maximum
					Lower Bound	Upper Bound		
Aegean	3	10175	10166	,03333	10023	10310	10.10	10.20
Levantine/Ionian	12	10151	10152	,05038	10041	10263	9.80	10.44
Adriatic	8	10003	10037	,04638	9927	10146	9.84	10.22
Total	23	10151	10113	,03255	10046	10181	9.80	10.44

ANOVA

DEPTH	Sum of Square	df	Mean Square	F	Sig
Between Groups	,089	2	,045	2,000	,162
Within Groups	,447	20	,022		
Total	,536	22			

REGION	Sum of Square	df	Mean Square	F	Sig
Between Groups	,074	2	,037	1,598	,227
Within Groups	,462	20	,023		
Total	,536	22			

Table 6. Results of the analysis of variance (One-way ANOVA) of the ages of S1 bottom based on the different sub-basins and water depths. The results showed in Descriptive Analyses and ANOVA derive from the TOC and Ba/Al data illustrated in Table 3. The one-way ANOVA test allows us to determine whether there is a significant difference in the mean distances thrown by each of the groups, in our case among the different sub-basins or water depths. When the "Sig." value (significance level) is less than 0.05, there is a significant difference between the groups with a confidence level of 95%. All statistical data analyses were performed using program SPSS version 25.0 (IBM Corp, 2017).

Table 6 shows the output of the ANOVA test where the significance value for the depth is 0.162, which is above 0.05 and, therefore, there is not a statistically significant difference between our groups means. Despite the little variations observed among the S1 base ages (Fig. 3 and Table 5), the ANOVA results showed a S1 base synchronous.

However, the results reported in Fig. 4 show little variation among the S1 base ages. In detail, the histogram and KDE results show as the data of the deeper and intermediate sites are gathered close to 10.2 cal. ka BP while that the shallower sites are gathered close to 10 cal. ka BP, in fact, this similarity is confirmed in the dendrogram result where the deeper and intermediate sites are gathered in the same cluster. Therefore, our results document that S1 deposition started slightly earlier in the deeper part of the basin (>1,800 m) and, then, it moved progressively towards the shallower sites (Fig. 3 and 4c). Noteworthy, a delay between the HO and LO species signal, in fact, HO species decrease is recorded earlier (400-500 years) than LO species at all water depths.

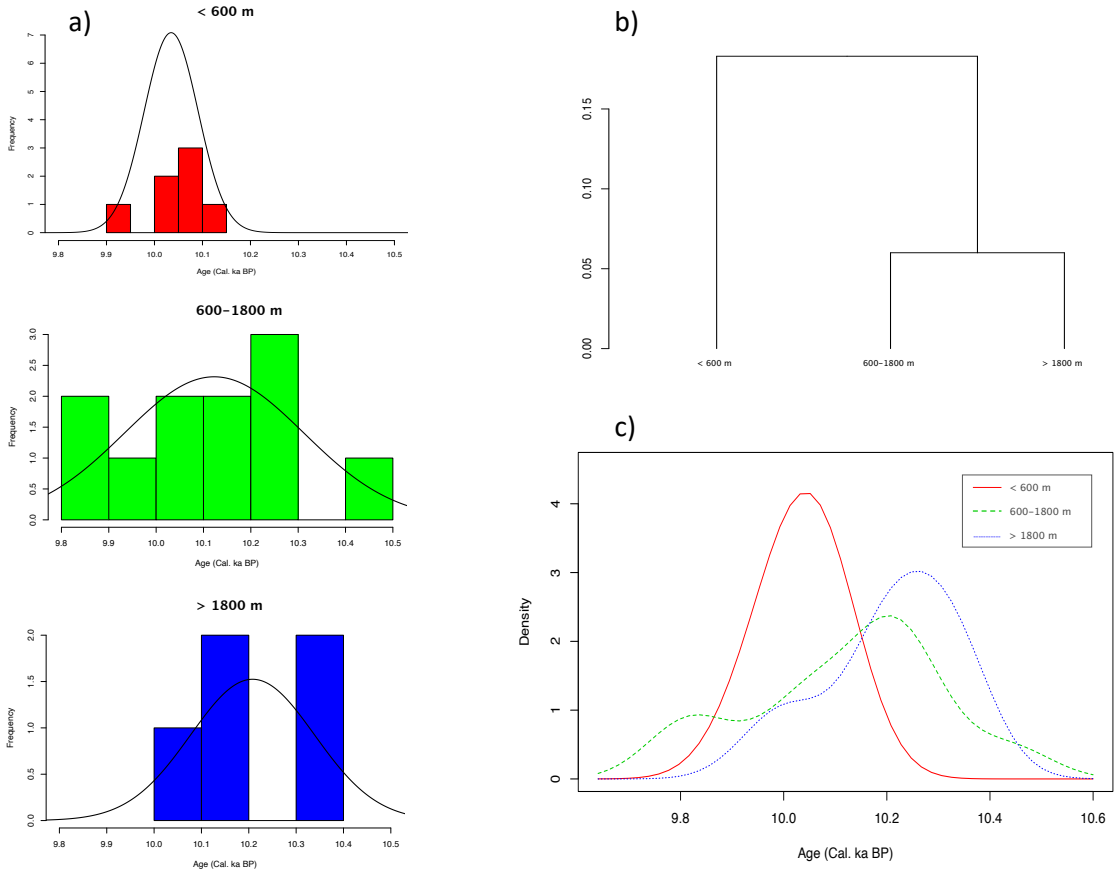

Fig. 4. Comparison of the results obtained through statistical analyses for S1 base in the different depths. The TOC and Ba/Al data showed in Table 3 were used. a) Histogram shows the distribution of the age based on the different depths. The dark solid line shows the probability density function. b) The clustering analysis assembles in the same group the ages that are more similar to each other than to those in other groups. c) In the KDE analysis, the peak of the curve shows where the data are more gathered. All graphics are obtained using RStudio software version 1.2.5009 (RStudio, 2019) and the packages "sm" (Bowman & Azzalini, 2018) and "cluster.datasets" (Novomestky, 2015).

As for the return to oxygenated conditions evidenced by the Ba/Al decrease and Mn-MB, the results obtained with the ANOVA test (Table 8) show that there is not a statistically significant difference between our groups means (Sig = 0.051, above 0.05). Nevertheless, unlike the base of S1, the clustering results show a likeness between the shallower and intermediate sites (Fig. 5b). However, this does not necessarily mean that the shallow and intermediate sites are synchronous, in fact, the results showed in Fig. 3 and Fig. 5a (see the probability density function) indicate that the S1 top occurred earlier at the shallower sites (<600 m) and, later at intermediate and deeper sites. Noteworthy, the intermediate sites show a bimodal distribution (Fig. 5c) due to influence of the different sub-basins. The recovery of the HO species predates the geochemical indicators at all water depths. This delay is almost coeval in shallow and intermediate sites (~100 years) while it is wider in deeper sites (~400 years).

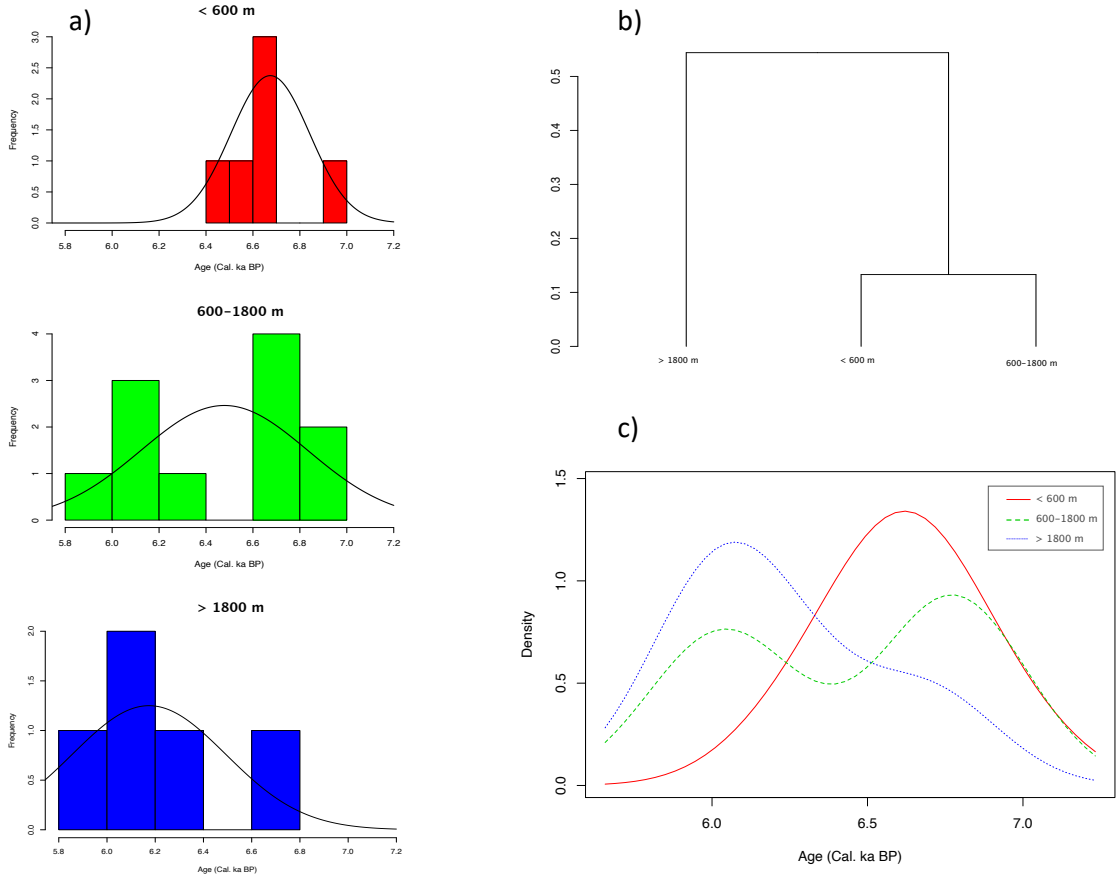

Fig. 5. Comparison of the results obtained through statistical analyses for S1 top in the different depths. The Ba/Al and Marker Bed data showed in Table 4 were used. The meaning of the graphics is given in Fig. 4.

3.2. Age of sapropel base and top in the different sub-basins

Fig. 7 and Table 7 show the ages for S1 base and top considering the cores on the different sub-basins. According to these calculations, S1 starts at 10.17 ± 0.07 cal. ka BP in the Aegean Sea, followed by the Levantine/Ionian Sea at 10.15 ± 0.16 ka BP and, finally at 10.00 ± 0.13 cal. ka BP in the Adriatic Sea (Fig. 7). A different pattern is shown by benthic foraminifera. The HO species disappear first in the Aegean Sea at 10.1 ± 0.21 cal. ka BP and, immediately following in the Adriatic Sea at 10.08 ± 0,09 cal. ka BP and, eventually, in the Levantine/Ionian Sea at 9.8 ± 0.2 cal. ka BP (Fig. 7 and Table 7). Furthermore, a similar pattern is shown by the LO species. The disappearance of these species is recorded at 9.65 ± 0,01 cal. ka BP in the Adriatic Sea, thereupon in the Aegean Sea at 9.62 ± 0.12 cal. ka BP and, finally in the Levantine/Ionian Sea at 9.3 ± 0.2 cal. ka BP.

Region	Proxies	Top	±	Bottom	±
Aegean	TOC + Ba/Al	6265	0.41	10175	0.07
	Benthic HO	6700	0.08	10100	0.21
	Benthic LO	-	-	9625	0.12
	Mn/Al + Ba/Al	6555	0.41	-	-
Levantine/Ionian	TOC + Ba/Al	6421	0.54	10151	0.16
	Benthic HO	6550*	0.2	9800*	0.2
	Benthic LO	-	-	9300*	0.2
	Mn/Al + Ba/Al	6254	0.38		
Adriatic	TOC + Ba/Al	6703	0.07	10003	0.13
	Benthic HO	6750	0.2	10082	0.09
	Benthic LO	-	-	9655	0.01
	Mn/Al + Ba/Al	6680	0.21	-	-

Table 7. Median values calculated in cores from different sub-basins regardless of depth. * Single core value.

The results obtained with the ANOVA test (Table 6) show that there is not a statistically significant difference between our groups means (Sig = 0.227, above 0.05). However, the results obtained through the clustering (Fig. 6b) and KDE analyses (Fig. 6c) show that the ages in the Levantine/Ionian and Aegean Sea were more similar than the Adriatic Sea. In detail, the KDE results (Fig. 6c) show the peak of density close to ~10.18 cal. ka BP in the Aegean Sea, at ~10.15 cal. ka BP in the Levantine/Ionian Sea and at ~10 cal. ka BP in the Adriatic Sea, in fact, the S1 base starts approximately 150 years later in the Adriatic Sea (Fig. 7 and Table 7).

TOP

Descriptive Analyses

DEPTH (m)	N	Median	Mean	Std. Deviation	95% Confidence Interval for Mean		Minimum	Maximum
					Lower Bound	Upper Bound		
<600	6	6698	6673	,06860	6497	6850	6.48	6.97
600-1800	11	6565	6473	,10935	6230	6717	6.00	6.89
>1800	5	6154	6173	,14283	5777	6570	5.92	6.70
Total	22	6565	6460	,07430	6305	6614	5.92	6.97

REGION	N	Median	Mean	Std. Deviation	95% Confidence Interval for Mean		Minimum	Maximum
					Lower Bound	Upper Bound		
Aegean	3	6555	6506	,19333	5674	7338	6.12	6.70
Levantine/Ionian	11	6254	6304	,11220	6054	6554	5.92	6.89
Adriatic	8	6680	6656	,08013	6467	6846	6.26	6.97
Total	22	6555	6640	,07430	6305	6614	5.92	6.97

ANOVA

DEPTH (m)	Sum of Square	df	Mean Square	F	Sig
Between Groups	,686	2	,343	3,495	,051
Within Groups	1,865	19	,098		
Total	2,551	21			

REGION	Sum of Square	df	Mean Square	F	Sig
Between Groups	,582	2	,291	2,808	,085
Within Groups	1,969	19	,104		
Total	2,551	21			

Table 8. Results of the analysis of variance (One-way ANOVA) of the ages of S1 top based on the different sub-basins and water depths. The results showed in Descriptive Analyses and ANOVA derive from the Ba/Al and Marker Bed data illustrated in Table 4. The one-way ANOVA test allows us to determine whether there is a significant difference in the mean distances thrown by each of the groups, in our case among the different sub-basins or water depths. When the "Sig." value (significance level) is less than 0.05, there is a significant difference between the groups with a confidence level of 95%. All statistical data analyses were performed using program SPSS version 25.0 (IBM Corp, 2017).

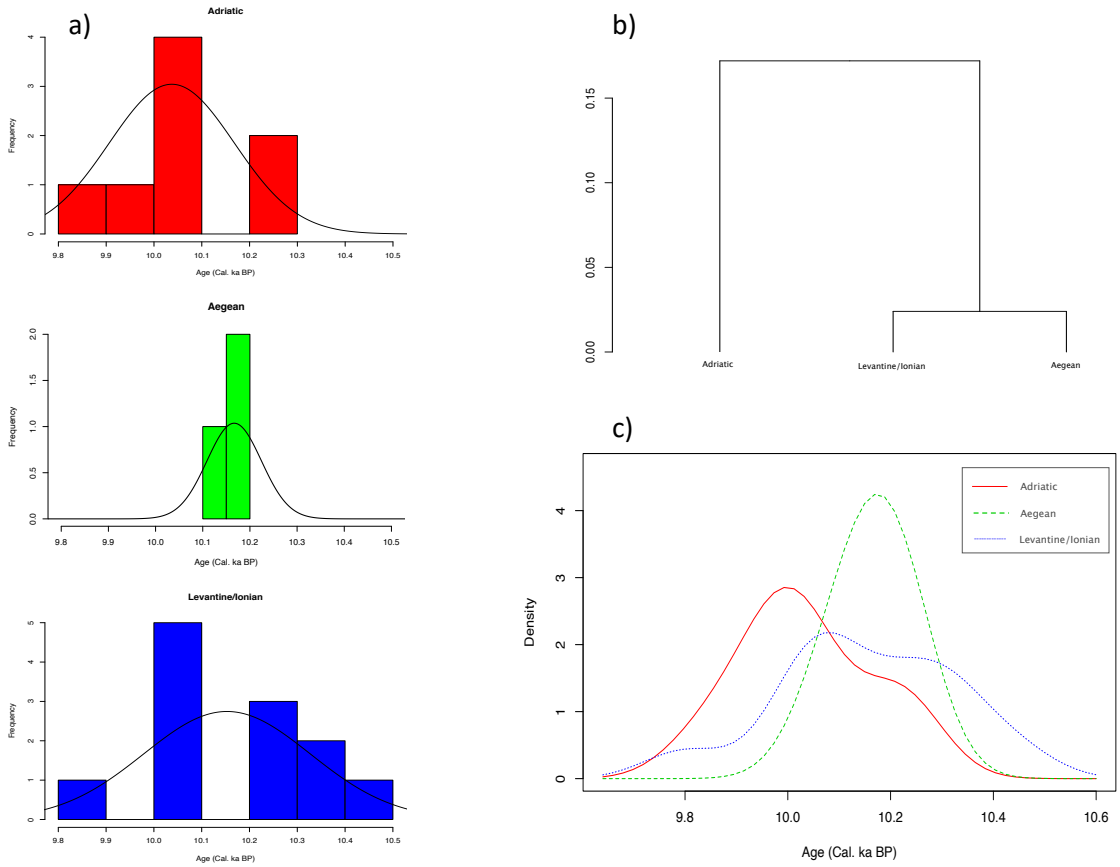

Fig. 6. Comparison of the results obtained through statistical analyses for S1 base in the different sub-regions. The TOC and Ba/Al data showed in Table 3 were used. The meaning of the graphics is given in Fig. 4.

According to my analysis, sapropel S1 ends earlier in the Adriatic Sea at 6.68 ± 0.21 cal. ka BP, followed by the Aegean Sea at 6.55 ± 0.41 cal. ka BP and the Levantine/Ionian Sea at 6.25 ± 0.38 cal. ka BP (Fig. 7 and Table 7). Moreover, an identical pattern in the HO species recolonization is observed, beginning in the Adriatic Sea at 6.75 ± 0.2 cal. ka BP, followed by Aegean Sea at 6.7 ± 0.08 cal. ka BP and, finally in the Levantine/Ionian Sea at 6.55 ± 0.2 cal. ka BP (Fig. 7 and Table 7) and, worth of note that in all cases the recovery of microfauna predates the end of sapropel.

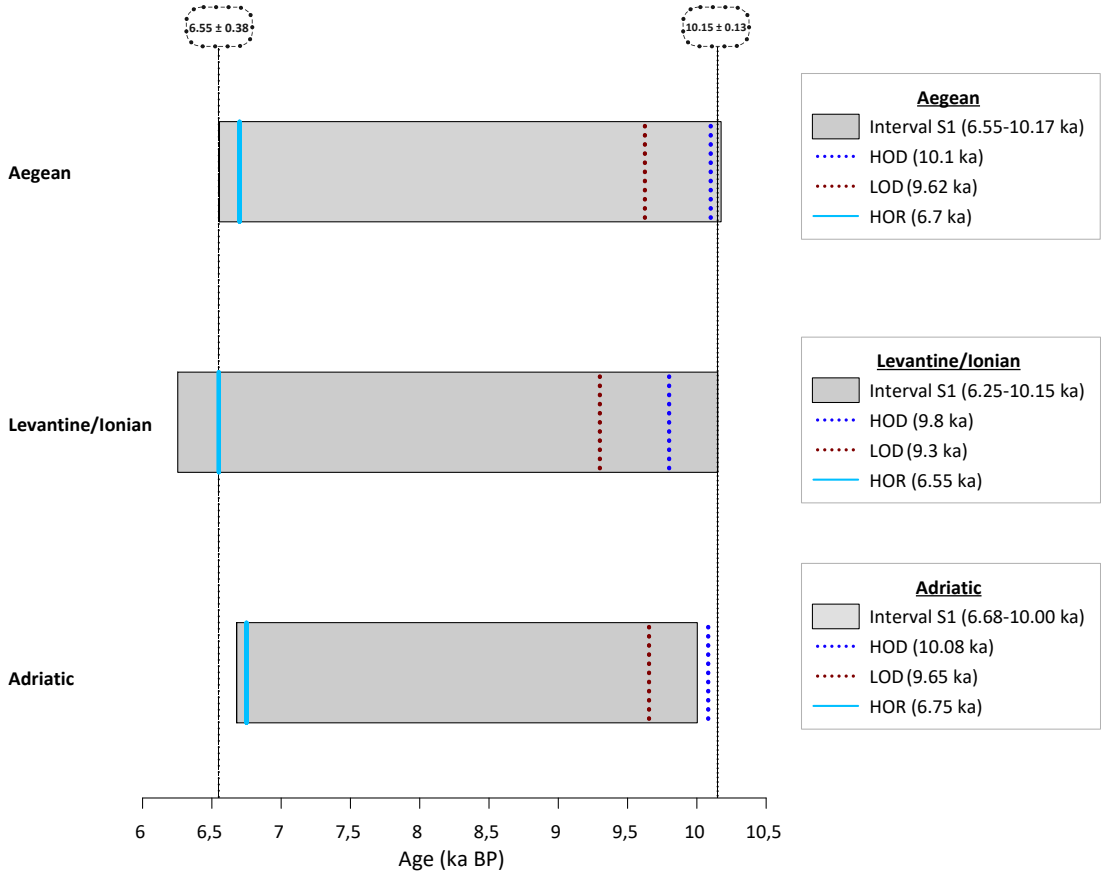

Fig. 7. Sapropel interval age variations based on the different sub-basins. For vertical bands and lines, see caption of Fig. 3. The upper and lower boundary mean calculated ages (6.55 ± 0.39 and 10.15 ± 0.13 cal. ka BP) are indicated by the black vertical lines.

As to S1 base, the ANOVA test (Table 8) show that there is not a statistically significant difference between our groups means (Sig = 0.085, above 0.05). However, the results obtained through the clustering (Fig. 8b) and KDE analyses (Fig. 8c) show that the ages in the Aegean and Adriatic Sea were more similar than in the Levantine/Ionian Sea. In particular, the KDE results show synchronous peaks close to ~6.6 cal. ka BP between the Adriatic and Aegean Sea, and at ~6 cal. ka BP in the Levantine/Ionian Sea. Noteworthy in the Levantine/Ionian as well as Aegean Sea, bimodal distributions are observed (Fig. 8c) as a result of cores at different water depths, in fact, the Aegean Sea includes shallower and intermediate sites while the Levantine Sea includes deeper and intermediate sites.

Based on the results shown in Fig. 7 and the statistical analyses (Fig. 6), it seems to be that the beginning of the S1 deposition in the Aegean and Levantine/Ionian Sea was almost coeval, while for the Adriatic Sea there was a short delay. Instead, a distinct pattern at the S1 top is observed, which ends first in the Adriatic and Aegean Sea and then in the Levantine/Ionian Sea (Fig. 7 and Fig. 8).

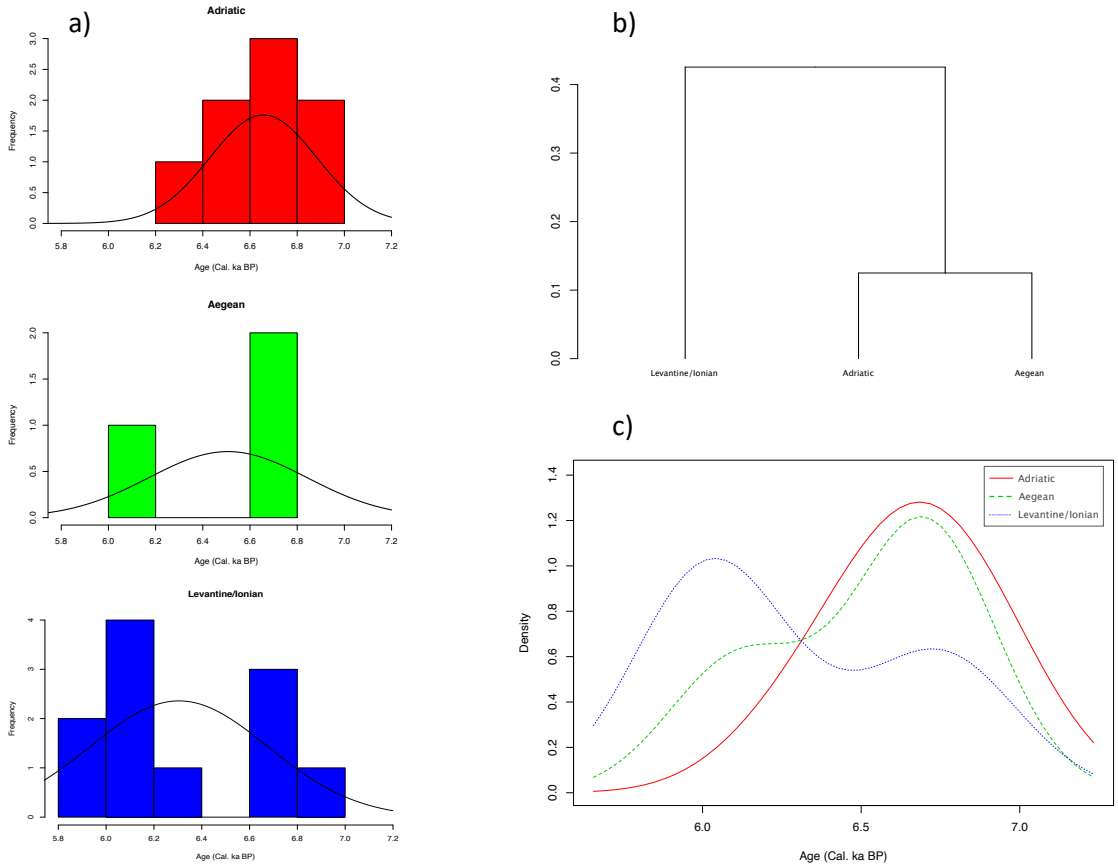

Fig. 8. Comparison of the results obtained through statistical analyses for S1 base in the different sub-regions. The Mn/Al and Ba/Al data showed in Table 4 were used. The meaning of the graphics is given in Fig. 4.

4. Discussion

4.1. Age of the sapropel (S1) onset

The analysis we made shows that if we group cores by depth or by area, we obtain slightly different results. A slightly earlier S1 deposition occurs in deep sites (>1,800 m) gradually moving at shallower depth. This is in line with Troelstra et al. (1991), however, considering that the difference of time is small, varying from 10.23 to 10.04 cal. ka BP, and taking into account uncertainties imposed by sampling and processing (~0.3 ka), and calibration and construction of the age model (±0.4) (Filippidi & De Lange, 2019), our data support De Lange et al. (2008), Schmiedl et al. (2010), Tesi et al. (2017) and Filippidi & De Lange. (2019), further suggesting that the onset of S1 was almost synchronous for all water depths.

Also, in the case of the sub-basins comparison, we found slightly different ages for the onset of S1. In fact, data suggest that the S1 deposition started almost at the same time in the Aegean and Levantine/Ionian Sea, and, only ~150 years later it started in

Adriatic Sea. This lag could be a consequence of the limited thermohaline circulation during sapropel S1. The reduced LIW formation, which is located in the Cyprus-Rhodes area (Rohling et al., 2015), would have weakened (or even ceased) the bottom water formation/ventilation causing the sapropel deposition earlier in the Aegean and Levantine/Ionian Sea due to its proximity to LIW area formation. In order to test this hypothesis, we considered the distance between the area of the LIW formation (Cyprus-Rhodes) and the Adriatic Sea and the velocity of LIW flow in the eastern Mediterranean. These velocities change along the Mediterranean Sea and oscillate between maximum velocities of 0,35 m/s in both the straits of Sicily and Rhodes (Astraldi et al., 1996; Zodiatis et al., 1993; Reeder et al., 2002; Iudicone et al., 2003) and, mean velocities of 0,08-0,1 m/s near to Tunisian coast (Sorgente et al., 2003; Ismail et al., 2012) and 0,05 m/s in the eastern Mediterranean (Menna & Poulain, 2010). However, even considering the worst scenario, with LIW flux reduced to 80% and the minimum velocity (0,05 m/s), the result cannot explain the 150 years lag our data indicate.

On the other hand, the micropaleontological data in the Adriatic and Aegean Seas show a nearly synchronous trend suggesting that the conditions in both sub-basins were similar at the beginning of S1 (Fig. 7). A slight delay is observed in the Levantine/Ionian Sea, however, this observation is based on a single core data at high depth and is scarcely indicative (Table Fig. 7 and Fig. 7). We that consider the palaeoceanographic conditions during S1 similar in the whole eastern Mediterranean Sea and the differences observed for the S1 base among different sub-basins are driven by the value of core depths. Thus, based on the geochemical and micropaleontological data, we suggest that the lag observed in the Adriatic Sea is due to cores located at depths from 1085 to 260 m, and therefore indicative of shallow and intermediate water, showing S1 base ages slightly younger than cores at greater depth. Hence, this agrees with the average ages calculated for the different classes of depths, confirming that S1 started before at greater depths and then moved at shallower sites. Noteworthy the HOD and LOD signals at the base of S1, allow us to recognize the different levels of oxygen under which S1 formed. The HOD signal evidences the beginning of the dysoxic condition while the LOD signal indicates persistent anoxia. In detail, both indicators show a depth-dependent gradient where the oxygen levels end earlier in shallow sites than in deeper. That trend can be explained by the enhanced primary production that occurred in surface waters. This process demanded a high oxygen rate, reducing thereby the oxygen concentrations in the shallow waters earlier than deep sites. Also, the disappearances of the HO and LO species suggest a time

of transition (400-500 years) between dysoxic and anoxic conditions in all depths and regions of the eastern Mediterranean Sea (Fig. 3 and Fig. 7). It seems that the beginning of S1 it produced under dysoxic conditions at least in the first 400 years before anoxic conditions settled.

The onset of S1 is the result of several processes, that is, water column stagnation and enhanced primary production (e.g., Rossignol-Strick et al., 1982; Higgs et al., 1994; Rohling, 1994; Emeis et al., 1996; Jorissen, 1999; Thomson et al., 1999; Mercone et al., 2001; Casford et al., 2003; Abu-Zied et al., 2008; Schmiedl et al., 2010). These processes occurred as result of sea-level rise (Grimm et al., 2015; Grant et al., 2016; Cornuault et al., 2018) and increased freshwater discharge from the northern borderlands (Rossignol-Strick, 1987; Rohling & Hilgen, 1991; Rohling et al., 2002b; Kotthoff et al., 2008; Toucane et al., 2015; Filippidi & De Lange, 2019) and monsoonal activity in North Africa (Rossignol-Strick, 1983, 1985; Fontugne et al., 1994; Cheddadi & Rossignol-Stick, 1995; Rohling et al., 2002a; Hennekam et al., 2014, 2015; Weldeab et al., 2014; Grant et al., 2016; Zwiep et al., 2018), which are controlled by climate dynamics (related to orbital forcing; Rossignol-Stick et al., 1982; Rossignol-Stick, 1985; Hilgen, 1991; Lourens et al., 1996) leading to abrupt climate changes on the Mediterranean region. According to this and considering the absence of physical barriers between the sub-basins during this period, we regard a synchronous onset of S1 deposition in the bathyal and abyssal basin areas at 10.16 ± 0.12 cal. ka BP.

4.2. Age of the sapropel (S1) top

Our data show that the S1 ending exhibits a depth-related and non-synchronous pattern, that is, earlier ending in shallow (< 600 m) sites (6.69 ± 0.2 cal. ka BP) than in deeper (> 1800 m) (6.15 ± 0.34 cal. ka BP). Moreover, a similar depth-dependent gradient in HOR signal at the S1 termination was observed, as it began first in shallow (6.77 ± 0.13 cal. ka BP) and intermediate sites (6.65 ± 0.09 cal. ka BP) and, finally in deep sites (6.55 ± 0.2 cal. ka BP). Additionally, S1 may have ended earlier in the Adriatic and Aegean Sea, which are considered the principal source areas for Eastern Mediterranean Deep Water (EMDW) formation (Malanotte-Rizzoli & Hecht, 1988; POEM Group, 1992; Roether et al., 1996). As for the Levantine/Ionian Sea in this study it is mostly represented by deep cores (see Table 2), and therefore this account for the later S1 termination as related to depth and not solely to the regional settings. Hence, on the basis of these

observations we might suppose that in the Adriatic and the Aegean the slightly anticipated end of S1 is related to the influence of the deep-water formation ventilating first the two basins and the reaching the farther and deeper areas of the Levantine.

The full recovery of the deep-water formation led to the vertical mixing of the water column associated with the bottom-water re-ventilation and, thereby, marked the end of S1 deposition. Hence, the establishment of well-oxygenated waters was accompanied by geochemical alterations (De Lange et al., 2008 and references therein) and the benthic foraminifera repopulation (e.g., Jorissen, 1999; Schmiedl et al., 2010; Filippidi et al., 2016; Triantaphyllou et al., 2016). According to these mechanisms, several works based on benthic foraminifera (Jorissen et al., 1993; Rohling et al., 1997; Schmiedl et al., 2010; Tesi et al., 2017) and geochemical proxies (Tachikawa et al., 2015; Filippidi & De Lange, 2019) suggested progressive oxygenation (depth-dependent). Based on our results, his depth-dependent trend in both geochemical and micropaleontological data is confirmed (Fig. 3). Furthermore, our results show that everywhere in the Mediterranean, the Mn-MB and the Ba/Al signal are found above the foraminifera recolonization (Fig. 3 and Fig. 7) suggesting that increased production continued when the bottom-water conditions were no longer anoxic but oxic or intermittently oxic (as previously observed by Filippidi et al., 2016).

In conclusion, our results show a S1 depth-related end, but considering the age uncertainties, and the fact that all ages differences are within error boundaries, we suggest that S1 end is a synchronous event at 6.56 ± 0.36 cal. ka BP. Such synchrony would explain the key role of eastern Mediterranean circulation during sapropel S1 as the recovery of the thermohaline circulation permitted the Levantine Intermediate Water (LIW) to flow along the Aegean and Adriatic Sea originating the Cretan Deep Water (CDW) and Adriatic Deep Water (ADW) that, consequently, contributed of the EMDW formation (Tsimplis et al., 1999; Pinardi et al., 2015). Considering no ADW formation can occur without the presence of LIW (Oddo & Guarnieri, 2011), only a synchronous basin-wide event can explain the thermohaline circulation restoration and thereby the synchronous end of sapropel S1.

4.3. Implications for the database BEyOND

As said in the introduction, *BEyOND* is the only open-access database for all researchers that permits archiving, extracting and, the most important skill, realizing mathematical operations in order to obtain new data through the correlation with pre-

existing dataset. In fact, *BEyOND* allows correlating the data from different regions or water depths obtaining a general trend that could be compared with other regions or water depths allowing to recognize the differences or likeness. Until now, *BEyOND* could not operate and examine the huge amount of data in term of ages lacking many such information for the proxies stored. Now, with the results obtained in this study, *BEyOND* will express all results in age (ka). This new functionality helps us to compare the different events that occurred during the S1 deposition, as the 8.2 ka event (Rohling et al., 1997; De Rijk et al., 1999; Myers & Rohling, 2000) or 7.4 ka event (Filippidi et al., 2016; Tesi et al., 2017; Filippidi & De Lange, 2019) that before with the "Standardize Depth" was difficult to observe.

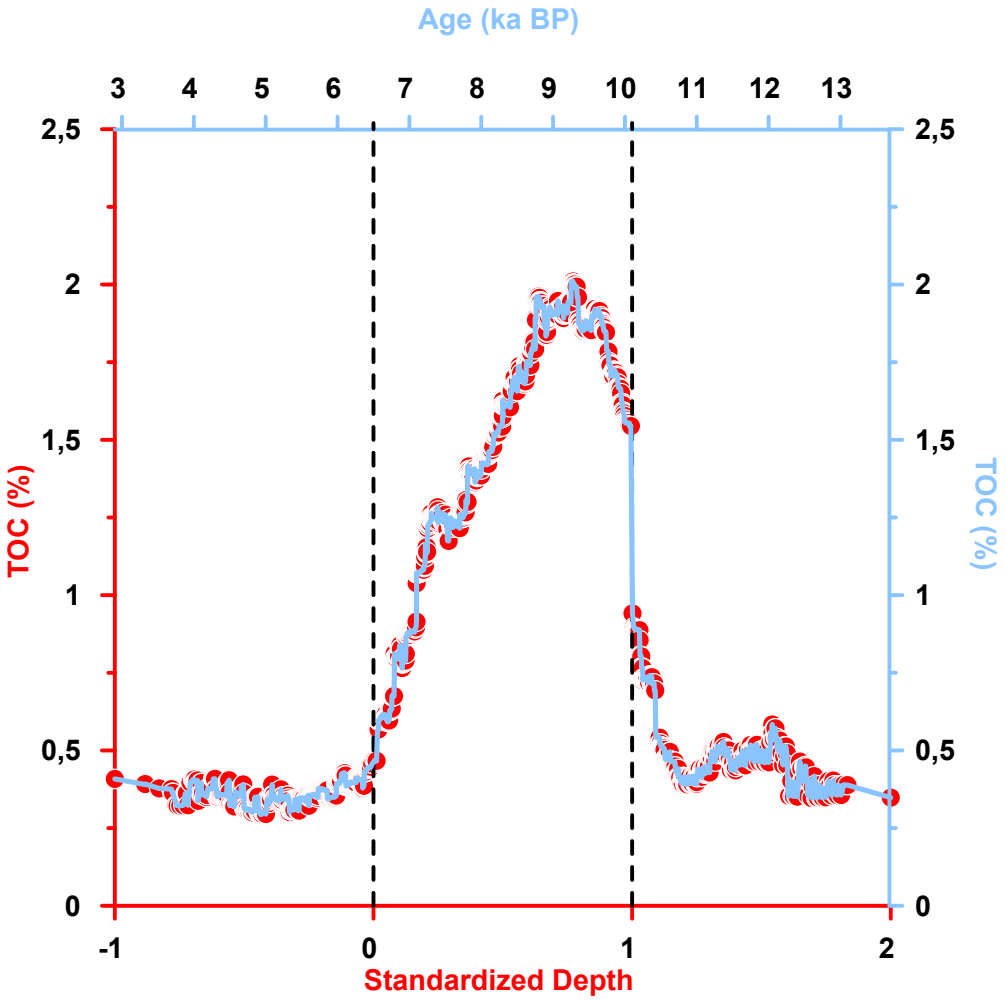

Fig. 9. TOC trend in the Eastern Mediterranean Sea obtained in Amezcua-Buendía et al. (2019). Red dots show TOC vs Standardized depth. Blue line shows TOC vs Age. Vertical dashed black lines represent sapropel interval (S1) where the beginning of sapropel is 1 (10.1 ka BP) and the top is 0 (6.5 ka BP) standardized depth.

The demonstration that the sapropel S1 is nearly synchronous across the basin permit to assign the age to all data and to correlate in term of time all the cores independently from any direct age determination. In detail, we only need to identify the base and top of the sapropel in order to realize these operations. This is shown in Fig. 9 where the TOC trend obtained by Amezcua-Buendía et al. (2019) (see Fig. 15 in Amezcua-Buendía et al., 2019), have been reconstructed and plotted versus age.

5. Conclusion

We used the database *BEyOND* to extract all the data referring to the sapropel S1 in order to test the age of the base and the top.

The 18 cores considered provided geochemical and paleontological data referred to absolute ages and we used these data to calculate average values at different water depths and located in different sub-basins in order to identify the timing of the S1 deposition.

Our analyses suggest that the most recent sapropel S1, started to deposit at ~10.1 and ended at ~6.5 cal. ka BP. Slight differences of the order of 100-130 years are observed to be depth correlated. Sapropel formation started under dysoxic conditions, and was sustained for at least 400-500 years before anoxic conditions settled. Also, our results document that benthic foraminifera recolonization occurred everywhere in the Eastern Mediterranean before the Ba/Al and MB-MN therefore supporting Filippidi et al. (2016) conclusion that productivity increase persisted also when the bottom-water conditions were no longer anoxic but oxic or intermittently oxic.

Thanks to the data obtained, the operability of *BEyOND* was improved adding absolute ages and allowing to bypass the old method that expressed the results in "Standardized Depth". Additionally, *BEyOND* can now correlate and express the results based on age even if it has not been calculated by researchers. This methodology only needs to know the depth values of S1 top and base, and through advanced analysis, we can express the results based on age.

Considering this new functionality, the database is now ready for elaborating data for paleoclimatological and paleoceanographic reconstructions and exploit the large amount of data that provide *BEyOND* to reconstruct the climate changes in the eastern Mediterranean Sea during the S1 deposition and also opening the possibility to operate expanding to older time intervals.

Finally, the exercise we performed indicates that there is a high potential for the application of the ages obtained. It is evident that in the future integration of new datasets on *BEyOND* that is an open-access database where the input of the data is possible in several formats (CVS, XML, SQL), will permit to elaborate more complex matrix and contribute to the resolution of the scientific enigma that is represented by sapropels.

References:

Abu-Zied, R.H., Rohling, E.J., Jorissen, F.J., Fontanier, C., Casford, J.S.L., Cooke, S. 2008. Benthic foraminiferal response to changes in bottom-water oxygenation and organic carbon flux in the eastern Mediterranean during LGM to Recent times. *Marine Micropaleontology*, *67*(1-2), 46-68. https://doi.org/10.1016/j.marmicro.2007.08.006

Amezcua-Buendía, R., Diamantini, C., Potena, D., Negri, A. 2019. BEyOND, a new tool for sapropel s1 studies in the Mediterranean Sea. *Alpine and Mediterranean Quaternary*, *32*(2), 167-184. https://doi.org/10.26382/AMQ.2019.11

Anastasakis, G.C., Stanley, D.J. 1986. Uppermost sapropel, eastern Mediterranean: paleoceanography and stagnation. *National Geographic Research*, 2(2), 179-197.

Arthur, M. A., Dean, W. E., & Stow, D. A. V. (1984). Models for the deposition of Mesozoic-Cenozoic fine-grained organic-carbon-rich sediment in the deep sea. Geological Society, London, Special Publications, 15(1), 527-560. https://doi.org/10.1144/GSL.SP.1984.015.01.34

Arthur, M. A., Schlanger, S. T., & Jenkyns, H. C. (1987). The Cenomanian-Turonian Oceanic Anoxic Event, II. Palaeoceanographic controls on organic-matter production and preservation. Geological Society, London, Special Publications, 26(1), 401-420. https://doi.org/10.1144/GSL.SP.1987.026.01.25

Astraldi, M., Gasparini, G. P., Sparnocchia, S., Moretti, M., Sansone, E. 1996. The characteristics of the water masses and the water transport in the Sicily Strait at long time scales. *Bulletin de l'Institut Océanographique*, 95-116.

Barmawidjaja, D.M., Jorissen, F.J., Puškarić, S., Van Der Zwaan, G.J. 1992. Microhabitat selection by benthic foraminifera in the northern Adriatic Sea. *Journal of Foraminiferal Research, 22*(4), 297. https://doi.org/10.2113/gsjfr.22.4.297

Bernhard, J.M., Sen Gupta, B.K. 1999. Foraminifera of oxygen-depleted environments. Modern Foraminifera, (pp. 201-216). Springer, Dordrecht. https://doi.org/10.1007/0-306-48104-9_12

Betts, J. N., & Holland, H. D. (1991). The oxygen content of ocean bottom waters, the burial efficiency of organic carbon, and the regulation of atmospheric oxygen. Palaeogeography, Palaeoclimatology, Palaeoecology, 97(1-2), 5-18. https://doi.org/10.1016/0031-0182(91)90178-T

Bishop, J.K.B., 1988. The barite-opal-organic carbon association in oceanic particulate matter. *Nature* 332, 341-343. https://doi.org/10.1038/332341a0

Bowman, A. W. and Azzalini, A. 2018. R package 'sm': nonparametric smoothing methods (version 2.2-5.6). http://www.stats.gla.ac.uk/~adrian/sm

Buscail, R., Cauwet, G., Murat, A., 1992. Humic substances in granulometric fractions of S1, S5, S6, S7, S8, S9 sapropels in the Eastern Mediterranean. *Proc. 6th Int. Meet. Humic Subst. Soc., Abstr.*, 253.

Calvert, S.E., Fontugne, M.R. 1987. Stable carbon isotopic evidence for the marine origin of the organic matter in the holocene black sea sapropel. *Chemical Geology: Isotope Geoscience Section*, *66*(3-4), 315-322. https://doi.org/10.1016/0168-9622(87)90051-0

Calvert, S. E., Bustin, R. M., & Ingall, E. D. (1996). Influence of water column anoxia and sediment supply on the burial and preservation of organic carbon in marine shales. Geochimica et Cosmochimica Acta, 60(9), 1577-1593. https://doi.org/10.1016/0016-7037(96)00041-5

Casford, J.S.L., Rohling, E.J., Abu-Zied, R.H., Fontanier, C., Jorissen, F.J., Leng, M.J., Schmiedl,

G., Thomson, J. 2003. A dynamic concept for eastern Mediterranean circulation and oxygenation during sapropel formation. *Palaeogeography, Palaeoclimatology, Palaeoecology*, *190*, 103-119. https://doi.org/10.1016/S0031-0182(02)00601-6

Casford, J.S.L., Abu-Zied, R., Rohling, E.J., Cooke, S., Fontainier, C., Leng, M., Millard, A., Thomson, J. 2007. A stratigraphically controlled multiproxy chronostratigraphy for the eastern Mediterranean. *Paleoceanography*, *22*(4). https://doi.org/10.1029/2007PA001422

Cheddadi, R., Rossignol-Strick, M. 1995. Eastern Mediterranean Quaternary paleoclimates from pollen and isotope records of marine cores in the Nile Cone Area. *Paleoceanography*, *10*(2), 291-300. https://doi.org/10.1029/94PA02672

Combourieu-Nebout, N., Paterne, M., Turon, J.L., Siani, G. 1998. A high-resolution record of the last deglaciation in the Central Mediterranean sea: Palaeovegetation and palaeohydrological evolution. *Quaternary Science Reviews*. https://doi.org/10.1016/S0277-3791(97)00039-5

Corliss, B.H. 1985. Microhabitats of benthic foraminifera within deep-sea sediments. *Nature, 314*, 435-438. https://doi.org/10.1038/314435a0

Cornuault, M., Tachikawa, K., Vidal, L., Guihou, A., Siani, G., Deschamps, P., Bassinot, F., Revel, M. 2018. Circulation Changes in the Eastern Mediterranean Sea Over the Past 23,000 Years Inferred From Authigenic Nd Isotopic Ratios. *Paleoceanography and Paleoclimatology*, *33*(3), 264-280. https://doi.org/10.1002/2017PA003227

Cramp, A., Collins, M., West, R. 1988. Late pleistocene-holocene sedimentation in the NW Aegean Sea: A palaeoclimatic palaeoceanographic reconstruction. *Palaeogeography, Palaeoclimatology, Palaeoecology*, *68*(1), 61-77. https://doi.org/10.1016/0031-0182(88)90017-X

Demaison, G. J., & Moore, G. T. (1980). Anoxic environments and oil source bed genesis. *AApG Bulletin*, 64(8), 1179-1209. https://doi.org/10.1306/2F91945E-16CE-11D7-8645000102C1865D

De Lange, G.J., & Ten Haven, H. 1983. Recent sapropel formation in the eastern Mediterranean. *Nature 305*, 797-798. https://doi.org/10.1038/305797a0

De Lange, G.J., Middelburg, J.J., Pruysers, P.A. 1989. Middle and Late Quaternary depositional sequences and cycles in the eastern Mediterranean. *Sedimentology*, *36*(1), 151-156. https://doi.org/10.1111/j.1365-3091.1989.tb00827.x

De Lange, G.J., Thomson, J., Reitz, A., Slomp, C.P., Principato, M.S., Erba, E., Corselli, C. 2008. Synchronous basin-wide formation and redox-controlled preservation of a Mediterranean sapropel. *Nature Geoscience*, *1*(9), 606-610. https://doi.org/10.1038/ngeo283

De Rijk, S., Hayes, A., Rohling, E.J. 1999. Eastern Mediterranean sapropel S1 interruption: An expression of the onset of climatic deterioration around 7 ka BP. *Marine Geology, 153*(1-4), 337-343. https://doi.org/10.1016/S0025-3227(98)00075-9

De Stigter, H.C., Jorissen, F.J., Van Der Zwaan, G.J. 1998. Bathymetric distribution and microhabitat partitioning of live (Rose Bengal stained) benthic foraminifera along a shelf to bathyal transect in the southern Adriatic Sea. *Journal of Foraminiferal Research, 28*(1), 40-65.

Ducassou, E., Migeon, S., Mulder, T., Murat, A., Capotondi, L., Bernasconi, S.M., Mascle, J. 2009. Evolution of the Nile deep-sea turbidite system during the late quaternary: Influence of climate change on fan sedimentation. *Sedimentology, 56*(7), 2061-2090. https://doi.org/10.1111/j.1365-3091.2009.01070.x

Dymond, J., Suess, E., Lyle, M., 1992. Barium in deep-sea sediment: a geochemical proxy for paleoproductivity. *Paleoceanography 7*(2), 163-181. https://doi.org/10.1029/92PA00181

Emeis, K.C., Party, S.S. 1996. Paleoceanography and sapropel introduction. In Proceedings of the Ocean Drilling Program, initial reports. Vol. 160, pp. 21-28.

Emeis, K.C., Schulz, H.M., Struck, U., Sakamoto, T., Doose, H., Erlenkeuser, H., Howell, M., Kroon, D., Paterne, M., 1998. Stable isotope and temperature records of sapropels from ODP Sites 964 and 967: constraining the physical environment of sapropel for- mation in the Eastern Mediterranean Sea. In: Robertson, A.H.F., Emeis, K.C., Richter, C., Camerlenghi, A. (Eds.), Proceedings of the Ocean Drilling Program. Scientific Results 160. ODP, College Station, TX, pp. 309-331.

Emeis, K.C., Struck, U., Schulz, H.M., Rosenberg, R., Bernasconi, S., Erlenkeuser, H., Sakamoto, T., Matinez-Ruiz, F. 2000. Temperature and salinity variations of Mediterranean Sea surface waters over the last 16,000 years from records of planktonic stable oxygen isotopes and alkenone unsaturation ratios. *Palaeogeography, Palaeoclimatology, Palaeoecology*, *158*(3-4), 259-280. https://doi.org/10.1016/S0031-0182(00)00053-5

Filippidi, A., & De Lange, G.J. 2019. Eastern Mediterranean Deep Water Formation During Sapropel S1: A Reconstruction Using Geochemical Records Along a Bathymetric Transect in the Adriatic Outflow Region. *Paleoceanography and Paleoclimatology*, *34*(3), 409-429. https://doi.org/10.1029/2018PA003459

Filippidi, A., Triantaphyllou, M.V., De Lange, G.J. 2016. Eastern-Mediterranean ventilation variability during sapropel S1 formation, evaluated at two sites influenced by deep-water formation from Adriatic and Aegean Seas. *Quaternary Science Reviews*, *144*, 95-106. https://doi.org/10.1016/j.quascirev.2016.05.024

Fontanier, C., Jorissen, F.J., Licari, L., Alexandre, A., Anschutz, P., Carbonel, P. 2002. Live benthic foraminiferal faunas from the Bay of Biscay: Faunal density, composition, and microhabitats. *Deep-Sea Research Part I: Oceanographic Research Papers, 49*(4), 751-785. doi: 10.1016/S0967-0637(01)00078-4. https://doi.org/10.1016/S0967-0637(01)00078-4

Fontanier, C., Jorissen, F., Anschutz, P., Chaillou, G. 2006. Seasonal variability of benthic foraminiferal faunas at 1000 m depth in the Bay of Biscay. *Journal of Foraminiferal Research, 36*(1), 61-76. https://doi.org/10.2113/36.1.61

Fontugne, M.R., Arnold, M., Labeyrie, L., Paterne, M., Calvert, S.E., Duplessy, J.C., 1994. Paleoenvironment, sapropel chronology and Nile River discharge during the last 20,000 years as indicated by deep-sea sediment records in the eastern Mediterranean. In: Bar-Yosef, O., Kra, R.S. (Eds.), Late Quaternary Chronology and Paleoclimates of the Eastern Mediterranean. Radiocarbon, Tucson, pp. 75-88.

Gallego-Torres, D., Martinez-Ruiz, F., Meyers, P.A., Paytan, A., Jimenez-Espejo, F.J., Ortega-Huertas, M. 2011. Productivity patterns and N-fixation associated with Pliocene-Holocene sapropels: Paleoceanographic and paleoecological significance. *Biogeosciences, 8*(2), 415-431. https://doi.org/10.5194/bg-8-415-2011

Geslin, E., Heinz, P., Jorissen, F., Hemleben, C. 2004. Migratory responses of deep- sea benthic foraminifera to variable oxygen conditions: Laboratory investigations. *Marine Micropaleontology, 53*(3-4), 227-243. https://doi.org/10.1016/j.marmicro.2004.05.010

Giunta, S., Negri, A., Morigi, C., Capotondi, L., Combourieu-Nebout, N., Emeis, K. C., Sangiorgi, F., Vigliotti, L. 2003. Coccolithophorid ecostratigraphy and multi-proxy paleoceanographic reconstruction in the Southern Adriatic Sea during the last deglacial time (Core AD91-17). *Palaeogeography, Palaeoclimatology, Palaeoecology, 190*, 39-59. https://doi.org/10.1016/S0031-0182(02)00598-9

Grant, K.M., Grimm, R., Mikolajewicz, U., Marino, G., Ziegler, M., Rohling, E.J. 2016. The timing of Mediterranean sapropel deposition relative to insolation, sea-level and African monsoon changes. *Quaternary Science Reviews*, *140*, 125-141. https://doi.org/10.1016/j.quascirev.2016.03.026

Grimm, R., Maier-Reimer, E., Mikolajewicz, U., Schmiedl, G., Müller-Navarra, K., Adloff, F., Grant, K.M., Ziegler, M., Lourens, L.J., Emeis, K.C. 2015. Late glacial initiation of Holocene eastern Mediterranean sapropel formation. *Nature Communications*, *6*, 7099. https://doi.org/10.1038/ncomms8099

Hennekam, R., Jilbert, T., Schnetger, B., De Lange, G.J. 2014. Solar forcing of Nile discharge and sapropel S1 formation in the early to middle Holocene eastern Mediterranean. *Paleoceanography*, *29*(5), 343-356. https://doi.org/10.1002/2013PA002553

Hennekam, R., Donders, T.H., Zwiep, K., De Lange, G.J. 2015. Integral view of Holocene precipitation and vegetation changes in the Nile catchment area as inferred from its delta sediments. *Quaternary Science Reviews*, *130*, 189-199. https://doi.org/10.1016/j.quascirev.2015.05.031

Herguera, J.C., Berger, W. 1991. Paleoproductivity from benthic foraminifera abundance: Glacial to postglacial change in the west-equatorial Pacific. *Geology, 19*(12), 1173-1176. https://doi.org/10.1130/0091-7613(1991)019<1173:PFBFAG>2.3.CO;2

Higgs, N.C., Thomson, J., Wilson, T.R.S., Croudace, I.W. 1994. Modification and complete removal of eastern Mediterranean sapropels by postdepositional oxidation. *Geology 22*(5), 423-426. https://doi.org/10.1130/0091-7613(1994)022<0423:MACROE>2.3.CO;2

Hilgen, F.J. 1991. Astronomical calibration of Gauss to Matuyama sapropels in the Mediterranean and implication for the Geomagnetic Polarity Time Scale. *Earth and Planetary Science Letters*, *104*(2–4), 226–244. https://doi.org/10.1016/0012-821X(91)90206-W

IBM Corp. 2017. IBM SPSS Statistics for Macintosh, Version 25.0. Armonk, NY: IBM Corp.

Incarbona, A., Ziveri, P., Sabatino, N., Manta, D. S., Sprovieri, M. 2011. Conflicting coccolithophore and geochemical evidence for productivity levels in the Eastern Mediterranean sapropel S1. *Marine Micropaleontology, 81*(3-4), 131-143. https://doi.org/10.1016/j.dsr.2011.12.009

İşler, E. B., Aksu, A. E., & Hiscott, R. N. (2016). Geochemistry of Aegean Sea sediments: implications for surface-and bottom-water conditions during sapropel deposition since MIS 5. Turkish Journal of Earth Sciences, 25(2), 103-125. https://doi.org/10.3906/yer-1501-35

Ismail, S.B., Sammari, C., Gasparini, G.P., Béranger, K., Brahim, M., Aleya, L. 2012. Water masses exchanged through the Channel of Sicily: Evidence for the presence of new water masses on the Tunisian side of the channel. *Deep Sea Research Part I: Oceanographic Research Papers*, *63*, 65–81. https://doi.org/10.1016/j.dsr.2011.12.009

Iudicone, D., Nardelli, B.B., Santoleri, R., Marullo, S. 2003. Distribution and mixing of intermediate water masses in the Channel of Sicily (Mediterranean Sea). *Journal of Geophysical Research C: Oceans*, *108*(9). https://doi.org/10.1029/2002jc001647

Jorissen, F.J. 1999. Benthic foraminiferal sucessions across Late Quaternary Mediterranean sapropels. *Marine Geology, 153*(1-4), 91-101. https://doi.org/10.1016/S0025-3227(98)00088-7

Jorissen, F.J., Asioli, A., Borsetti, A.M., Capotondi, L., de Visser, J.P., Hilgen, F.J., Rohling, E.J., Van der Borg, K., Vergnaud-Grazzini, C., Zachariasse, W.J. 1993. Late Quaternary central Mediterranean biochronology. *Marine Micropaleontology*, *21*(1-3), 169-189. https://doi.org/10.1016/0377-8398(93)90014-O

Jorissen, F.J., de Stigter, H.C., Widmark, J.G.V. 1995. A conceptual model explaining benthic foraminiferal microhabitats. *Marine Micropaleontology, 26*(1- 4), 3-15. https://doi.org/10.1016/0377-8398(95)00047-X

Kotthoff, U., Pross, J., Müller, U.C., Peyron, O., Schmiedl, G., Schulz, H., Bordon, A. 2008. Climate dynamics in the borderlands of the Aegean Sea during formation of sapropel S1

deduced from a marine pollen record. *Quaternary Science Reviews, 27*(7-8), 832-845. https://doi.org/10.1016/j.quascirev.2007.12.001

Kuhnt, T., Schmiedl, G., Ehrmann, W., Hamann, Y., Hemleben, C. 2007. Deep-sea ecosystem variability of the Aegean Sea during the past 22 kyr as revealed by Benthic Foraminifera. *Marine Micropaleontology, 64*(3-4), 141-162. https://doi.org/10.1016/j.marmicro.2007.04.003

Kullenberg, B. 1952. On the salinity of the water contained in marine sediments. *Medd. Oceanogr. Inst. Göteb.* 21, 221-228.

Lourens, L.J., Antonarakou, A., Hilgen, F.J., Van Hoof, A.A.M., Vergnaud-Grazzini, C., Zachariasse, W. J. 1996. Evaluation of the Plio-Pleistocene astronomical timescale. *Paleoceanography*, *11*(4), 391-413. https://doi.org/10.1029/96PA01125

Malanotte-Rizzoli, P., Hecht, A. 1988. Large-scale properties of the eastern Mediterranean: a review. *Oceanologica Acta*, *11*(4), 323-335.

Mangini, A., Eisenhauer, A., Walter, P. 1991. A spike of CO2 in the atmosphere at glacial-interglacial boundaries induced by rapid deposition of manganese in the oceans. *Tellus B, 43*(2), 97-105. https://doi.org/10.1034/j.1600-0889.1991.t01-1-00004.x

Mangini, A., Jung, M., Laukenmann, S. 2001. What do we learn from peaks of uranium and of manganese in deep sea sediments?. *Marine Geology*, *177*(1), 63-78. https://doi.org/10.1016/S0025-3227(01)00124-4

Marino, G., Rohling, E.J., Sangiorgi, F., Hayes, A., Casford, J.L., Lotter, A.F., Kucera, M., Brinkhuis, H. 2009. Early and middle Holocene in the Aegean Sea: interplay between high and low latitude climate variability. *Quaternary Science Reviews*, *28*(27–28), 3246–3262. https://doi.org/10.1016/j.quascirev.2009.08.011

Martinez-Ruiz, F., Kastner, M., Paytan, A., Ortega-Huertas, M., Bernasconi, S.M. 2000. Geochemical evidence for enhanced productivity during S1 sapropel deposition in the eastern Mediterranean. *Paleoceanography, 15*(2), 200-209. https://doi.org/10.1029/1999PA000419

Martinez-Ruiz, F., Kastner, M., Gallego-Torres, D., Rodrigo-Gámiz, M., Nieto-Moreno, V., Ortega-Huertas, M. 2015. Paleoclimate and paleoceanography over the past 20,000 yr in the Mediterranean Sea Basins as indicated by sediment elemental proxies. *Quaternary Science Reviews, 107*, 25-46. https://doi.org/10.1016/j.quascirev.2014.09.018

Mélières, M.A., Rossignol-Strick, M., Malaizé, B. 1997. Relation between low latitude insolation and $\delta^{18}O$ change of atmospheric oxygen for the last 200 kyrs, as revealed by Mediterranean sapropels. *Geophysical Research Letters*, *24*(10), 1235-1238. https://doi.org/10.1029/97GL01025

Melki, T., Kallel, N., Fontugne, M. 2010. The nature of transitions from dry to wet condition during sapropel events in the Eastern Mediterranean Sea. *Palaeogeography, Palaeoclimatology, Palaeoecology, 291*(3-4), 267-285. https://doi.org/10.1016/j.palaeo.2010.02.039

Menna, M., Poulain, P.M. 2010. Mediterranean intermediate circulation estimated from Argo data in 2003–2010. *Ocean Science*, *6*(1), 331–343. https://doi.org/10.5194/os-6-331-2010

Mercone, D., Thomson, J., Croudace, I.W., Siani, G., Paterne, M., Troelstra, S. 2000. Duration of S1, the most recent sapropel in the eastern Mediterranean Sea, as indicated by accelerator mass spectrometry radiocarbon and geochemical evidence. *Paleoceanography*, *15*(3), 336-347. https://doi.org/10.1029/1999PA000397

Mercone, D., Thomson, J., Abu-Zied, R.H., Croudace, I.W., Rohling, E.J. 2001. High-resolution geochemical and micropalaeontological profiling of the most recent eastern Mediterranean

sapropel. *Marine Geology, 177*(1-2), 25-44. https://doi.org/10.1016/S0025-3227(01)00122-0

Morigi, C. 2009. Benthic environmental changes in the Eastern Mediterranean Sea during sapropel S5 deposition. *Palaeogeography, Palaeoclimatology, Palaeoecology, 273*(3-4), 258-271. https://doi.org/10.1016/j.palaeo.2008.10.010

Morigi, C., Jorissen, F.J., Gervais, A., Guichard, S., Borsetti, A.M. 2001. Benthic foraminiferal faunas in surface sediments off NW Africa: Relationship with organic flux to the ocean floor. *Journal of Foraminiferal Research, 31*(4), 350-368. https://doi.org/10.2113/0310350

Myers, P.G., Rohling, E.J. 2000. Modeling a 200-Yr interruption of the Holocene Sapropel S1. *Quaternary Research*, *53*(1), 98-104. https://doi.org/10.1006/qres.1999.2100

Naidu, P.D., Malmgren, B.A. 1995. Do benthic foraminifer records represent a productivity index in oxygen minimum zone areas? An evaluation from the Oman Margin, Arabian Sea. *Marine Micropaleontology, 26*(1-4), 49-55. https://doi.org/10.1016/0377-8398(95)00014-3

Nijenhuis, I.A., De Lange, G.J., 2000. Geochemical constraints on Pliocene sapropel forma- tion in the eastern Mediterranean. *Marine Geology, 163*, 41-63. https://doi.org/10.1016/S0025-3227(99)00093-6

Novomestky, F. 2015. Cluster Analysis Data Sets (version 1.0-1). https://cran.r-project.org/web/packages/cluster/cluster.pdf

Oddo, P., Guarnieri, A. 2011. A study of the hydrographic conditions in the Adriatic Sea from numerical modelling and direct observations (2000-2008). *Ocean Science*, *7*(5), 549-567. https://doi.org/10.5194/os-7-549-2011

Passier, H.F., Middelburg, J.J., De Lange, G.J., Böttcher, M.E., 1999. Modes of sapropel formation in the eastern Mediterranean: some constraints based on pyrite properties. *Marine Geology*. *153*, 199-220. https://doi.org/10.1016/S0025-3227(98)00081-4

Perissoratis, C., Piper, D.J.W. 1992. Age, regional variation, and shallowest occurrence of S1 sapropel in the northern Aegean Sea. *Geo-Marine Letters*, *12*(1), 49-53. https://doi.org/10.1007/BF02092108

Pinardi, N., Masetti, E. 2000. Variability of the large scale general circulation of the Mediterranean Sea from observations and modelling: A review. *Palaeogeography, Palaeoclimatology, Palaeoecology, 158*(3-4), 153-173. https://doi.org/10.1016/S0031-0182(00)00048-1

Pinardi, N., Zavatarelli, M., Adani, M., Coppini, G., Fratianni, C., Oddo, P., ... & Bonaduce, A. (2015). Mediterranean Sea large-scale low-frequency ocean variability and water mass formation rates from 1987 to 2007: A retrospective analysis. *Progress in Oceanography*, 132, 318-332. https://doi.org/10.1016/j.pocean.2013.11.003

POEM group. 1992. General circulation of the eastern Mediterranean Sea. *Earth Sci. Rev. 32*, 285-308. https://doi.org/10.1306/AD4616E7-16F7-11D7-8645000102C1865D

Pratt, L. M. (1984). Influence of paleoenvironmental factors on preservation of organic matter in Middle Cretaceous Greenhorn Formation, Pueblo, Colorado. AAPG bulletin, 68(9), 1146-1159.

Pratt, L. M., & King, J. D. (1986). Variable marine productivity and high eolian input recorded by rhythmic black shales in Mid-Cretaceous pelagic deposits from central Italy. *Paleoceanography*, 1(4), 507-522. https://doi.org/10.1029/PA001i004p00507

Pruysers, P.A., De Lange, G.J., Middelburg, J.J., Hydes, D.J. 1993. The diagenetic formation of metal-rich layers in sapropel-containing sediments in the eastern Mediterranean. *Geochimica et Cosmochimica Acta, 57*(3), 527-536. https://doi.org/10.1016/0016-7037(93)90365-4

Reeder, M.S., Rothwell, G., Stow, D.A.V. 2002. The Sicilian gateway: anatomy of the deep-water connection between East and West Mediterranean basins. *Geological Society Memoir*, *22*(1), 171–189. https://doi.org/10.1144/GSL.MEM.2002.022.01.13

Revel, M., Ducassou, E., Grousset, F.E., Bernasconi, S.M., Migeon, S., Revillon, S., Mascle, J., Mural, A., Zaragosi, S., Bosch, D. 2010. 100,000 Years of African monsoon variability recorded in sediments of the Nile margin. *Quaternary Science Reviews*, *29*(11-12), 1342-1362. https://doi.org/10.1016/j.quascirev.2010.02.006

Roether, W., Manca, B.B., Klein, B., Bregant, D., Georgopoulos, D., Beitzel, V., Kovačević, V., Luchetta, A. 1996. Recent changes in eastern Mediterranean deep waters. *Science, 271*(5247), 333-335. https://doi.org/10.1126/science.271.5247.333

Rohling, E.J. 1994. Review and new aspects concerning the formation of eastern Mediterranean sapropels. *Marine Geology*, *122*(1-2), 1-28. https://doi.org/10.1016/0025-3227(94)90202-X

Rohling, E. J., & Hilgen, F.J. 1991. The eastern Mediterranean climate at times of sapropel formation: a review. *Geologie En Mijnbouw*, *70*(3), 253-264.

Rohling, E.J., Jorissen, F.J., De Stigter, H.C. 1997. 200 Year interruption of Holocene sapropel formation in the Adriatic Sea. *Journal of Micropalaeontology*, *16*(2), 97-108. https://doi.org/10.1144/jm.16.2.97

Rohling, E.J., Cane, T.R., Cooke, S., Sprovieri, M., Bouloubassi, I., Emeis, K.C., Schiebel, R., Kroon, D., Jorissen, F.J., Lorre, A., Kemp A.E.S. 2002a. African monsoon variability during the previous interglacial maximum. *Earth and Planetary Science Letters, 202*(1), 61-75. https://doi.org/10.1016/S0012-821X(02)00775-6

Rohling, E.J., Mayewski, P.A., Hayes, A., Abu-Zied, R.H., Casford, J.S.L. 2002b. Holocene atmosphere-ocean interactions: records from Greenland and the Aegean Sea. *Climate Dynamics, 18*(7), 587-593. https://doi.org/10.1007/s00382-001-0194-8

Rohling, E.J., Marino, G., Grant, K.M. 2015. Mediterranean climate and oceanography, and the periodic development of anoxic events (sapropels). *Earth-Science Reviews*, *143*, 62-97. https://doi.org/10.1016/j.earscirev.2015.01.008

Rossignol-Strick, M. (1983). African monsoons, an immediate climate response to orbital insolation. *Nature*. *304*(5921), 46-49. https://doi.org/10.1038/304046a0

Rossignol-Strick, M. 1985. Mediterranean Quaternary sapropels, an immediate response of the African monsoon to variation of insolation. *Palaeogeography, Palaeoclimatology, Palaeoecology*, *49*(3-4), 237-263. https://doi.org/10.1016/0031-0182(85)90056-2

Rossignol-Strick, M. 1987. Rainy periods and bottom water stagnation initiating brine accumulation and metal concentrations: 1. The Late Quaternary. *Paleoceanography*, *2*(3), 333-360. https://doi.org/10.1029/PA002i003p00333

Rossignol-Strick, M. 1999. The Holocene climatic optimum and pollen records of sapropel 1 in the eastern Mediterranean, 9000-6000 BP. *Quaternary Science Reviews*, *18*(4-5), 515-530. https://doi.org/10.1016/S0277-3791(98)00093-6

Rossignol-Strick, M., Nesteroff, W., Olive, P., Vergnaud-Grazzini, C. 1982. After the deluge: Mediterranean stagnation and sapropel formation. *Nature*, *295*(5845), 105-110. https://doi.org/10.1038/295105a0

RStudio Team. 2019. RStudio: Integrated Development for R. RStudio, Inc., Boston, MA. http://www.rstudio.com/

Ryan, W.B.F. 1972. Stratigraphy of Late Quaternary sediments in the eastern Meidterranean in: The Mediterranean Sea, ed. D.J. Stanley. In D. J. Stanley, G. Kelling, Y. Weiler (Eds.), *Dowden, Hutchinson, and Ross* (pp. 149-169).

Schlitzer, R. 2020. Ocean Data View. https://odv.awi.de/

Schmiedl, G., De Bovée, F., Buscail, R., Charrière, B., Hemleben, C., Medernach, L., Picon, P. 2000. Trophic control of benthic foraminiferal abundance and microhabitat in the bathyal Gulf of Lions, western Mediterranean Sea. *Marine Micropaleontology, 40*(3), 167-188. https://doi.org/10.1016/S0377-8398(00)00038-4

Schmiedl, G., Mitschele, A., Beck, S., Emeis, K.C., Hemleben, C., Schulz, H., Sperling, M., Weldeab, S. 2003. Benthic foraminiferal record of ecosystem variability in the eastern Mediterranean Sea during times of sapropel S5 and S6 deposition. *Palaeogeography, Palaeoclimatology, Palaeoecology, 190*, 139-164. https://doi.org/10.1016/S0031-0182(02)00603-X

Schmiedl, G., Kuhnt, T., Ehrmann, W., Emeis, K. C., Hamann, Y., Kotthoff, U., Dulski, P., Pross, J. 2010. Climatic forcing of eastern Mediterranean deep-water formation and benthic ecosystems during the past 22 000 years. *Quaternary Science Reviews*. *29*(23-24), 3006-3020. https://doi.org/10.1016/j.quascirev.2010.07.002

Scrivner, A.E., Vance, D., Rohling, E.J. 2004. New neodymium isotope data quantify Nile involvement in Mediterranean anoxic episodes. *Geology*, *32*(7), 565-568. https://doi.org/10.1130/G20419.1

Sen Gupta, B.K., Machain-Castillo, M.L. 1993. Benthic foraminifera in oxygen-poor habitats. *Marine Micropaleontology, 20*(3-4), 183-201. https://doi.org/10.1016/0377-8398(93)90032-S

Sorgente, R., Drago, A.F., Ribotti, A. 2003. Seasonal variability in the Central Mediterranean Sea circulation. *Annales Geophysicae*, *21*(1), 299–322. https://doi.org/10.5194/angeo-21-299-2003

Strohle, K., Krom, M.D. 1997. Evidence for the evolution of an oxygen minimum layer at the beginning of S-1 sapropel deposition in the eastern Mediterranean. *Marine Geology*, *140*(3), 231-236. https://doi.org/10.1016/S0025-3227(97)00058-3

Tachikawa, K., Vidal, L., Cornuault, M., Garcia, M., Pothin, A., Sonzogni, C., Bard, E., Menot, G., Revel, M. 2015. Eastern Mediterranean Sea circulation inferred from the conditions of S1 sapropel deposition. *Climate of the Past*, *11*(6), 855-867. https://doi.org/10.5194/cp-11-855-2015

Taylforth, J. E., McCay, G.A., Ellam, R., Raffi, I., Kroon, D., Robertson, A.H.F. 2014. Middle Miocene (Langhian) sapropel formation in the easternmost Mediterranean deep-water basin: Evidence from northern Cyprus. *Marine and Petroleum Geology*, *57*, 521-536. https://doi.org/10.1016/j.marpetgeo.2014.04.015

Ten Haven, H. L., Baas, M., De Leeuw, J. W., & Schenck, P. A. (1987). Late Quaternary Mediterranean sapropels, I—On the origin of organic matter in sapropel S7. *Marine geology*, 75(1-4), 137-156. https://doi.org/10.1016/0025-3227(87)90100-9

Tesi, T., Asioli, A., Minisini, D., Maselli, V., Dalla Valle, G., Gamberi, F., Langone, L., Cattaneo, A., Montagna, P., Trincardi, F. 2017. Large-scale response of the Eastern Mediterranean thermohaline circulation to African monsoon intensification during sapropel S1 formation. *Quaternary Science Reviews*, *159*, 139-154. https://doi.org/10.1016/j.quascirev.2017.01.020

Thomson, J., Higgs, N.C., Wilson, T.R.S., Croudace, I.W., De Lange, G.J., Van Santvoort, P.J.M. 1995. Redistribution and geochemical behaviour of redox-sensitive elements around S1, the most recent eastern Mediterranean sapropel. *Geochimica et Cosmochimica Acta, 59*(17), 3487-3501. https://doi.org/10.1016/0016-7037(95)00232-O

Thomson, J., Mercone, D., de Lange, G.J., van Santvoort, P.J.M., 1999. Review of recent advances in the interpretation of Eastern Mediterranean sapropel S1 from geochemical

evidence. *Marine Geology*. *153*(1-4), 77-89. https://doi.org/10.1016/S0025-3227(98)00089-9

Toucanne, S., Angue Minto'o, C.M., Fontanier, C., Bassetti, M.A., Jorry, S.J., Jouet, G. 2015. Tracking rainfall in the northern Mediterranean borderlands during sapropel deposition. *Quaternary Science Reviews*, *129*, 178-195. https://doi.org/10.1016/j.quascirev.2015.10.016

Triantaphyllou, M.V. 2014. Coccolithophore assemblages during the Holocene Climatic Optimum in the NE Mediterranean (Aegean and northern Levantine Seas, Greece): Paleoceanographic and paleoclimatic implications. *Quaternary International*, *345*, 56-67. https://doi.org/10.1016/j.quaint.2014.01.033

Triantaphyllou, M. V, Gogou, A., Dimiza, M.D., Kostopoulou, S., Parinos, C., Roussakis, G., Geraga, M., Bouloubassi, I., Fleitmann, D., Zervakis, V., Velaoras, D., Diamantopoulou, A., Sampatakaki, A., Lykousis, V. 2016. Holocene Climatic Optimum centennial-scale paleoceanography in the NE Aegean (Mediterranean Sea). *Geo-Marine Letters*, *36*(1), 51-66. https://doi.org/10.1007/s00367-015-0426-2

Troelstra, S.R., Ganssen, G.M., Van Der Borg, K., De Jong, A.F.M. 1991. A late Quaternary stratigraphic framework for eastern Mediterranean sapropel S1 based on AMS 14C dates and stable oxygen isotopes. *Radiocarbon*, *33*(1), 15-21. https://doi.org/10.1017/S0033822200013175

Tsimplis, M.N., Velegrakis, A.F., Drakopoulos, P., Theocharis, A., Collins, M.B. 1999. Cretan Deep Water outflow into the Eastern Mediterranean. *Progress in Oceanography, 44*(4), 531-551. https://doi.org/10.1016/S0079-6611(99)00042-7

Tyson, R. V. (2001). Sedimentation rate, dilution, preservation and total organic carbon: some results of a modelling study. Organic Geochemistry, 32(2), 333-339. https://doi.org/10.1016/S0146-6380(00)00161-3

Van Helmond, N.A.G.M., Hennekam, R., Donders, T.H., Bunnik, F.P.M., De Lange, G.J., Brinkhuis, H., Sangiorgi, F. 2015. Marine productivity leads organic matter preservation in sapropel S1: Palynological evidence from a core east of the Nile River outflow. *Quaternary Science Reviews*, *108*, 130-138. https://doi.org/10.1016/j.quascirev.2014.11.014

Van Santvoort, P.J.M., De Lange, G.J., Thomson, J., Cussen, H., Wilson, T.R.S., Krom, M.D., Ströhle, K. 1996. Active post-depositional oxidation of the most recent sapropel (S1) in sediments of the eastern Mediterranean Sea. *Geochimica et Cosmochimica Acta, 60*(21), 4007-4024. https://doi.org/10.1016/S0016-7037(96)00253-0

Van Straaten, L.M.J.U., 1972. Holocene stages of oxygen depletion in deep waters of the Adriatic Sea. In: D.J. Stanley (Editor), The Mediterranean Sea: a Natural Sedimentation Laboratory. Dowden, Hutchinson and Ross, Stroudsburg, Pa., pp. 631-643.

Vigliotti, L., Asioli, A., Bergami, C., Capotondi, L., Piva, A. 2011. Magnetic properties of the youngest sapropel S1 in the Ionian and Adriatic Sea: Inference for the timing and mechanism of sapropel formation. *Italian Journal of Geosciences 130*(1), 106-118. https://doi.org/10.3301/IJG.2010.29

Weldeab, S., Siebel, W., Wehausen, R., Emeis, K.C., Schmiedl, G., Hemleben, C., 2003. Late Pleistocene sedimentation in the Western Mediterranean Sea: implications for productivity changes and climatic conditions in the catchment areas. *Palaeogeography, Palaeoclimatology, Palaeoecology, 190*, 121-137. https://doi.org/10.1016/S0031-0182(02)00602-8

Weldeab, S., Menke, V., Schmiedl, G. 2014. The pace of East African monsoon evolution during the Holocene. *Geophysical Research Letters*, *41*(5), 1724-1732. https://doi.org/10.1002/2014GL059361

Ziegler, M., Tuenter, E., & Lourens, L. J. (2010). The precession phase of the boreal summer monsoon as viewed from the eastern Mediterranean (ODP Site 968). Quaternary Science Reviews, 29(11-12), 1481-1490. https://doi.org/10.1016/j.quascirev.2010.03.011

Zirks, E., Krom, M. D., Zhu, D., Schmiedl, G., Goodman-Tchernov, B.N. 2019. Evidence for the Presence of Oxygen-Depleted Sapropel Intermediate Water across the Eastern Mediterranean during Sapropel S1. *ACS Earth and Space Chemistry*, *3*(10), 2287-2297. https://doi.org/10.1021/acsearthspacechem.9b00128

Zodiatis, G. 1993. Circulation of the cretan sea-water masses (eastern mediterranean-sea). *Oceanologica Acta*, 16(2), 107-114

Zwiep, K.L., Hennekam, R., Donders, T.H., van Helmond, N.A.G.M., De Lange, G.J., Sangiorgi, F. 2018. Marine productivity, water column processes and seafloor anoxia in relation to Nile discharge during sapropels S1 and S3. *Quaternary Science Reviews*, *200*, 178-190. https://doi.org/10.1016/j.quascirev.2018.08.026

Chapter 3

Data Science approach to palaeoceanography of the eastern Mediterranean Sea during sapropel S1 deposition

R. Amezcua-Buendía[1], C. Diamantini[2], G. Marino[3], D. Potena[2], A. Negri[1]

[1] *Department of Life and Environmental Sciences. Polytechnic University of Marche. Via Brecce Bianche, 60131 Ancona, Italy*

[2] *Department of Information Engineering. Polytechnic University of Marche. Via Brecce Bianche, 60131 Ancona, Italy*

[3] *Department of Marine Geosciences and Territorial Planning, Faculty of Marine Sciences, University of Vigo, 36310 Vigo, Spain.*

To be submitted

Abstract

The sensitivity of the Mediterranean Sea to climate forcing has been matter of numerous studies. The paleoclimate changes during the early to middle Holocene were primarily modulated by changes in isolation and led to the deposition of sapropel S1 between ~10.1 and 6.5 cal. ka BP. The processes that (quasi)periodically turned the eastern Mediterranean Sea from a vigorously ventilated water column (modern) into a basin with oxygen-starved conditions (sapropel) are still a matter of debate. Here we investigate the most recent sapropel (S1) using - for the first time - a Data Analytics (DA) approach. We use specific geochemical, micropaleontological, and isotopic records from the different sub-basins (Levantine/Ionian, Adriatic, and Aegean), providing information about the different water masses. During S1 deposition, enhanced freshwater input and the water column stratification were interrupted by cold events at 9.5, 8.5 (related to 8.2 event), and 7.5 cal. ka BP, which were correlated with the Bond event in the North Atlantic. These events reactivated the intermediate/deep waters circulation in the whole eastern Mediterranean Sea (1) supplying oxygen to the (anoxic)bottom waters, and (2) modifying the intermediate and superficial waters production. These results demonstrate the close interplay between mid- (North Atlantic) and low-latitudes (North African Monsoon)

climate systems. Local forcings played a significant role increasing (export)production (sedimentary Ba/Al) in the south of the Cretan and Libyan Sea, that is however not reflected as high TOC content since low preservation affects shallow/intermediate cores. Consequently, by comparing the results in the sub-basins, we attribute the observed differences to the depth of the cores. Deeper cores located in the Levantine/Ionian Sea showed more reducing conditions and better preservation (e.g., TOC) than shallower cores in the Aegean and Adriatic Seas.

1. Introduction

The growing complexity and volume of analog and digital data (Boulton, 2018) poses unprecedented challenges and opportunities to the scientific community (Guo et al., 2017) and more widely to our society (Timmins et al., 2018). According to IBM Marketing Cloud report (2017), about 90% of the data in the world have been added in the last 2 years and it has been predicted that the worldwide data volume will increase to 175 zettabytes ($175 \bullet 10^{12}$ terabytes) in 2025 and to more than 2,100 zettabytes in 2035 (Statista, 2019). In Earth Sciences, the volume of data has grown exponentially since the first Earth observation satellite was launched half a century ago (Bugbee et al., 2019). For example, the amount of data managed by EOSDIS (Earth Observing System Data and Information System) was more than 9 Peta-Bytes in the beginning of 2018 (Huang, 2019) and is now expected to exceed 246 Peta-Bytes by 2025 (Bi, 2019).

This large amount of data and their exponential growing collectively make Big Data Analytics (BDA) a fundamental field of science that will provide ground-breaking research tools that will be instrumental to the scientific accomplishments of the next decades. BDA is the capability to study large amount of both homogeneous and heterogeneous data taken from different data sources, thereby exploring unknown patterns, unidentified correlations, and other useful information (Madhukar & Pooja, 2019). All this makes the use of BDA a challenge and at the same time a great opportunity for scientific advance.

In this framework, Amezcua-Buendía et al. (2019) developed the database *BEyOND* that through the use of Data Analytics (DA) techniques, allows us to reconstruct the dynamics behind the past climate and oceanography related changes. *BEyOND* provides a wide variety of organized and standardized paleoproxies relative to the past ~20 ka of Mediterranean Sea history, but it primarily focuses on the processes that led the

deep-water stagnation of the eastern Mediterranean Sea, and the consequent deposition of sapropel S1. By deepening our understanding of the modes of operation of the Mediterranean Sea during sapropel S1, we present a suite of complementary analyses which include micropaleontological, geochemical, and isotopic records.

The Mediterranean Sea is particularly sensitive to regional and global climate changes, and also to extreme events because of the fact it is located in a transitional climate zone (between subtropical high pressure and subpolar depression) (Andersen et al., 2018; Lionello et al., 2012; Rohling et al., 2105). For this reason, organic-rich layers, called sapropels (Cita & Grignani, 1982; Kidd et al., 1978; Mangini & Schlosser, 1986; Myers et al., 1998; Rohling, 1994) are the sedimentological expression of past environmental and climate perturbation related to Milankovitch cycles (Hilgen, 1991). Over sixty years of investigations have brought huge information about the sapropels formation; studies addressed how the whole 'sapropel mode' is related to the water masses settings and their circulation in the Eastern Mediterranean Sea (Casford et al., 2003; Emeis et al., 1996; Grimm et al., 2015; Incarbona et al., 2011; Rohling & Giesks, 1989; Rohling et al., 2015) and, fewer focused on sapropel S1 (Filippidi & De Lange, 2019; Tachikawa et al., 2015; Tesi et al., 2017; Wu et al., 2019).

Despite eastern Mediterranean sedimentary sequences spanning the Neogene have been intensively studied to unravel the causes of sapropel deposition, a model that accounts for the existing evidence remains elusive (Rohling et al., 2015). Nowadays, the well-oxygenated deep and bottom water present in the Mediterranean Sea (Tanhua et al., 2013) contrasts with the conditions inferred at the time of sapropel deposition. The enhanced production increased the export of organic carbon to deep waters, and an associated increase of the water column stratification due to excess freshwater inputs led to oxygen-starved conditions in the deeper waters, bringing the organic matter preservation and, thus, sapropel deposition (De Lange & ten Haven, 1983; De Lange et al., 2008; Möbius et al., 2010; Moodley et al., 2005; Murat & Got, 2000; Rohling et al., 2015). Indeed, the African monsoon forcing played an important role in the preconditions for sapropel deposition. Warm and humid conditions settled in the basin area, leading to increased freshwater input into the basin that contributed both to increase buoyancy of the surface layer and to injected nutrients into the photic zone (Emeis et al., 2003; Grelaud et al., 2012; Krom et al., 2002; Rohling & Gieskes, 1989; Rohling et al., 2002; Rossignol-Strick, 1985; Slomp et al., 2002).

We decided to focus on sapropel S1 because it: (*a*) is the most studied sapropel in the literature; (*b*) deposited within the range of the radiocarbon dating method, which ensures a good and independent age control for the different marine sediment cores from the eastern Mediterranean and of the contemporaneous terrestrial archives; (*c*) is the sapropel for which more (and the most diverse suite of) data are available. This implies a good coverage of the basin that is essential to characterize: (*i*) sources and foci of freshwater addition/discharge; (*ii*) intermediate- and deep-water circulation changes; (*iii*) nutrient availability and productivity changes; and (*iv*) development of deep water dysoxia/anoxia. Taken together these features make the sapropel S1 ideally suited to be investigated using a data analytics approach, which is specifically designed to highlight significative patterns from large datasets.

The present paper aims to: *(i)* contribute to identify the mechanisms leading to sapropel deposition, specifically, the more recent sapropel S1; and *(ii)* deepening our understanding of the modes of operation of the eastern Mediterranean Sea throughout S1.

The data analytics (DA) techniques allows us to explore huge volumes of data to extract novel and useful knowledge. For this reason, the *BEyOND* (http://beyond.dii.univpm.it/) database developed by Amezcua-Buendía et al. (2019) that contains data of the Mediterranean Sea past ~20 ka of history was used. *BEyOND* contains a wide variety of data (geochemical, micropaleontological, isotopic) that allows us to carry out multi-proxy studies. We have obtained trends (or stack) of different paleoproxies, during, pre- and post-sapropel deposition, with the purpose to characterize the water column in the different sub-basins of the eastern Mediterranean Sea. This would help us to understand the response of the eastern Mediterranean at different spatial scales – sub-basins and whole basin – and the associated impacts on the water mass overturning and organic carbon burial.

For this purpose, we will proceed with a review of the previous literature regarding sapropels and of all the proxies used for the paleoceanographic reconstructions in the eastern Mediterranean Sea. Then, by using the database *BEyOND* we aim to combine all the data to obtain new insights to understand the mechanisms of sapropel deposition.

2. Previous studies

2.1. Water masses and circulation

2.1.1. Modern circulation in the eastern Mediterranean Sea

The Mediterranean Sea is among the most interesting semi-enclosed basins because of numerous interactions and process which occur within it (Malanotte & Robinson, 1988). The Mediterranean Sea is constituted by two sub-basins (western and eastern Mediterranean) connected by the Strait of Sicily. All processes (e.g., rates of evaporation, salinity, runoff, precipitation...) that act in the Mediterranean Sea are controlled by the balance of the flow through the Straits of Gibraltar (Béthoux, 1979; Carter, 1956) and Sicily (Giorgi & Lionello, 2008) which spells great differences between western and eastern Mediterranean Sea. According to Robinson et al. (2001) the general circulation in the Mediterranean is composed of three principal and interacting spatial scales: basin scale, sub-basin scale (e.g., Adriatic, Levantine, Alboran) and mesoscale. Indeed, other forcing mechanisms as surface wind and thermohaline circulation play a key role in this circulation (POEM Group, 1992). Béranger (2005) draws the Mediterranean Sea as a thermodynamic system that transforms Atlantic Water (AW) into denser waters through interaction with the atmosphere because of the high evaporation rates cause convection. The thermohaline circulation of the Mediterranean Sea is the result of the density difference between the Mediterranean Sea and AW.

2.1.2. Surface water mass (SWM)

The AW flows through strait to enter in the Alboran Sea with velocities greater than 1 m s^{-1} (Béranger et al., 2005; Perkins et al., 1990) where forms the Alboran gyres (Gascard & Richez, 1985). AW with salinity above ~ 36‰ and temperature ~ 16 °C (Bryden & Kinder, 1991; Gascard & Richez, 1985; Kinder & Parilla, 1987) mixes with Mediterranean Intermediate Water (MIW), originating the Modified Atlantic Water (MAW). MAW is divided into two streams after the Almera-Oran front upon exit Alboran Sea, one going northward toward the Ibiza channel and the other flows along the Algerian current (Bryden et al., 1994). The northward flowing current feeds the Western Mid-Mediterranean Current (WMMC) which flows along the western coast of Sardinia to form the Southerly Sardinia Current (SSC) (Arnone et al., 1990). The SSC flows along the Tunisian coasts feeding the Algerian Current which will be divided into several currents (one enters the Sicily Strait and the other flows along the Tyrrhenian Sea) (Béranger et

al., 2004). The current flowing into the Tyrrhenian Sea increases its salinity (~36‰ to ~38‰), due evaporation and mixing, and temperature drop (~ 16 °C to ~ 14-15 °C) (Millot, 1999). In the Gulf of Lions, it joins northern cyclonic gyres and winter winds to induce the formation of Western Mediterranean Deep Water (WMDW) (Millot, 1999; Rohling et al., 1998; Send et al., 1999; Smith et al., 2008) (see section 2.1.4).

According to Pinardi (2015), the Tyrrhenian Sea circulation is driven by three cyclonic gyres: the South-Western Tyrrhenian Gyre (SWTG), the South-Eastern Tyrrhenian Gyre (SETG) and the Northern Tyrrhenian Gyre (NTG). The SWTG forms the called Middle Tyrrhenian Sea (MTC) that join at the SSC. The MTC, the Gulf of Lions gyre and western and eastern Alboran gyres, drive the surface western Mediterranean circulation.

The Algerian Current advances through the Strait of Sicily and it split up into two branches, the Atlantic Ionian Stream (AIS) flows along the coast of Sicily, and the Atlantic Tunisian Current (ATC) flows over the Tunisian margin (Pinardi & Masetti, 2000). Both streams feed the Mid-Mediterranean Jet along Ionian and Levantine Seas (MMJ) (POEM Group, 1992). Finally, currents arrive in the Levantine basin with salinity around 39-39.6‰ (Béranger et al., 2005; Hecht & Gertman, 2001; Malanotte-Rizzoli & Hecht, 1988; Wüst, 1961) and it heads for Cyprus and Rhodes, where it will form the Levantine Intermediate Water (LIW) (see section 2.1.3), but will also flow westward to originate the Asia Minor Current (AMC) (Theocharis, 2009).

2.1.3. Intermediate Water Circulation (IWC)

The Intermediate Water Circulation (IWC) is variable along the Mediterranean Sea. The intermediate water mass best-know is the Levantine Intermediate Water (LIW). Its formation is located in Cyprus-Rhodes area (Rohling et al., 2015) where, in winter, strong, cold and dry winds occur over the eastern Mediterranean (Özsoy, 1981). These characteristics lead the low surface temperatures and high salinities, favoring the vertical convection, and consequent, the LIW formation. Occasionally, stronger winters produce the Levantine Deep Water (Gertmann et al., 1994; Pinardi et al., 2015; Theocharis, 2009). In the Levantine basin, LIW temperature is low (15-16 °C) and the salinity very high (39.0-39.2) (Béranger et al., 2010; Malanotte-Rizzoli & Bergamasco, 1991; Painter & Tsimplis, 2003; Robinson et al., 2001; Theocharis, 2009) but when this one arrives at Strait of Sicily, its salinity (38.7-38.85) and temperature (14-14.3 °C) are reduced due to mixing with waters from the layers above and beneath them along its route (Béranger et

al., 2005; Malanotte-Rizzoli et al., 1997; Wüst, 1961). From its region of formation, the LIW flows westwards between 150-600 m, changing its salinity and temperature. A part enters in the Adriatic and Aegean Seas for contribute to precondition Eastern Mediterranean Deep Water formation (EMDW), and the major part flows along the Ionian Sea to Strait of Sicily.

LIW exits from the Strait of Sicily at a velocity of 0.2-0.3 m s^{-1} (Stansfield et al., 2003) through two passages (Tunisian and Sicilian passages). Then, the LIW turns right along the northern Sicilian coast, and follows a cyclonic path in the Tyrrhenian Sea (Millot, 1987). Flowing northward, the LIW plays an important role in the convection in the Gulf of Lions (Millot, 1987). LIW arrives at the Alboran Sea with a salinity of 38.43-38.48 and temperature of 13.1-13.2 °C, occupying depths between 200-600 m (Millot, 1987; Richez & Gascard, 1986).

Another intermediate water mass is called Cretan Intermediate Water (CIW) by Schlitzer et al. (1991). It is formed in the Cretan Sea and, is considered colder, more saline and denser than LIW (Astraldi et al., 1999; Parrilla et al., 1986).

Send et al. (1999) highlights other intermediate water masses, the Winter Intermediate Water (WIW) and Adriatic/Aegean Intermediate Water (AIW). In the Gulf of Lions, the WIW is developed during winters where the vertical mixing does not penetrate to the LIW. In addition, the WIW plays an important role in the variability of water exchanges in the Balearic channels (Pinot et al., 1998). The AIW is cooler and denser water than LIW, it is formed along the Tunisian slope owing to mixing waters formed in the Adriatic and Aegean Sea.

All these intermediate water masses flow from east to west to bring salty and warm water into the western Mediterranean Sea.

2.1.4. Deep and bottom water circulation

Deep and bottom water circulation are responsible for maintaining oxygenated the whole Mediterranean basin. The different morphologies and several straits and channel along the entire Mediterranean basin are the cause of the different deep water renewal times. The mean rate of renewal time is of 100-150 years in the Eastern Mediterranean Deep Water (EMDW) while in the Western Mediterranean Deep Water (WMDW) is 20-40 years (Roether & Schlitzer, 1991; Roether & Well, 2001; Roether et al., 1996; Stratford & Williams, 1997; Theocharis, 2009).

The Mediterranean Sea is a region with several deep-water formation sites: (*1*) the Adriatic Sea and (*2*) the Aegean Sea (during the Eastern Mediterranean Transient (EMT); Stratford et al., 1998) in which the formation of EMDW occurs (Malanotte-Rizzoli & Hecht, 1988; POEM Group, 1992; Pollak, 1951; Wüst, 1961); (*3*) the Gulf of Lions where the WMDW is formed (Béranger et al., 2005; MEDOC Group, 1970; Send et al., 1999; Wüst, 1961); occasionally, (*4*) in the Levantine basin, the LDW is produced (Gertmann et al., 1994; Pinardi et al., 2015; Rohling et al., 2015; Theocharis, 2009); (*5*) the Adriatic Sea is the source area for the Adriatic Deep Water (ADW) formation (Gacic et al., 2001; Lascaratos et al., 1999; Manca et al., 2002; Robinson et al., 2001).

The WMDW is formed following three phases: (*1*) the "preconditioning" phase expects a water column instability (loss surface and intermediate stratification waters) (Mertens & Schott, 1998) with losses of temperature because of winter cooling, dry Mistral and Tramonte continental winds (MEDOC Group, 1970; Rohling et al., 2015; Testor & Gascard, 2006; Wüst, 1961). This preconditioning phase occurs into a cyclonic surface gyre in the Gulf of Lions, that also drives the LIW toward the surface facilitating the homogenization between the surface and intermediate waters. Then, the mixing brings a density increase of surface waters allowing the deeper convection of the water column (Leaman & Schott, 1991); (*2*) a 'violent-mixing' phase takes place that eliminate the gradient between the surface and intermediate waters (Skliris & Lascaratos, 2004). During this phase, the so-called "plumes" of convective mixing originate and reach great depths in the water column (>2,000 m) (MEDOC Group, 1970; Leaman & Schott, 1991; Rohling et al., 2015; Smith et al., 2008). The mixing of deep waters with homogeneous salinity and temperature properties, as well as, a net vertical transport equal to zero, is obtained in this phase (Marshall & Schott, 1999). Finally, a "sinking and spreading" phase forms the WMDW, which flows between 1,500-3,000 m through the Balearic basin and the Tyrrhenian Sea (Marshall & Schott, 1999).

The Adriatic Sea is considered the principal source area for EMDW formation (POEM Group, 1992; Malanotte-Rizzoli & Hecht, 1988; Rohling et al., 2015; Pollak, 1951) where, in winter, the cold and dry northeasterly winds together with high rate evaporation (Bora events) bring strong cooling of the North Adriatic waters. These waters drive toward Otranto Sill along Adriatic basin where it mixes with the LIW in the road, originating the Adriatic Deep Water (ADW) (Rohling et al., 2015; Wüst, 1961). Then, the ADW exits the Strait of Otranto penetrated to the bottom water of the Ionian and

Levantine basins, contributing at the EMDW formation (Gacic et al., 2001; Lascaratos et al., 1999).

In the Aegean Sea, the Cretan basin plays a significant role as a site of formation of both intermediate and deep water masses, in particular, the Cretan Deep Water (CDW) (Tsimplis et al., 1999). These waters were considered to contribute at the EMDW formation (Lacombe & Tchernia, 1972), however, the Aegean Sea as source area of EMDW formation has been thoroughly debated (Klein et al., 1999; Lacombe et al ., 1958; Miller, 1963; Pollak, 1951; Roether et al., 1983; Wüst, 1961). Wüst (1961) observed that the Aegean Sea had a minor role but not negligible, as instead Pollak (1951) affirmed. Lacombe et al. (1958) and Miller (1963) found signals that the Aegean waters flowed into the Levantine basin through the Kasos and Karpathos straits, contributing at the EMDW formation. Nevertheless, Roether et al. (1983) used ^{3}H and ^{3}He to trace the origins and circulations of the waters. They observed as only source area for the EMDW formation the Adriatic basin. However, Roether et al. (1996) concluded with data from TV Meteor cruise M31-1 (January-February 1995) that denser Aegean waters have replaced almost 20% of the older EMDW of Adriatic origin. This event has been defined as Eastern Mediterranean Transient (EMT; Roether et al., 1996) and it confirmed the contribution of the Aegean Sea to EMDW formation and others recent changes of water mass characteristics in the Aegean basin (Roether et al., 1996; Theocharis et al., 1999).

2.2. The Sapropel Enigma

The oceanographic features described above, characterize the modern Mediterranean, but periodic perturbations of the climate and marine circulation, and ecological changes brought to the deposition of organic-rich sediment, called "sapropels" in the eastern Mediterranean Sea. These organic layers are less common in the western Mediterranean Sea, where they are known as Organic Rich Layers (ORLs) (Cramp & O'Sullivan, 1999; Emeis et al., 1991; Jimenez-Espejo et al., 2008; Meyers, 2006; Murat, 1999; Rogerson et al., 2008; Tanhua et al., 2013) and whose deposition is probably related to a different mechanism (at least for the most recent one, according to Rogerson et al., 2008).

Sapropel are characterized by color from dark grey to olive green and black and high C_{org} concentrations. C_{org} values in sapropels vary between 1-10%, but Kidd et al. (1978) considered as sapropel only those with C_{org} greater than 2%, while other authors (e.g., Martínez-Ruiz et al., 2003) estimated concentrations >1% C_{org}. Cramp and

O'Sullivan (1999) determined the term "sapropelic" for the sediment with low C_{org} content. Sapropels were described for the first time by Kullenberg (1952), during the Swedish Deep-Sea Expedition, and later, by Olausson (1960), who examined similar sediments and called them "sapropelitic layer". Since that time, these characteristic layers have become known as "sapropels" (Murat & Got, 2000).

Several mechanisms have been proposed that might have led to the deposition of sapropels, but until now, we do not know the precise process of it. The first hypothesis was by Bradley (1938), where he theorized about the "varved" sediment moderately rich in organic matter because of lowering sea-level rise. Kullenberg (1952) and Olausson (1961) linked the sapropel formation to lower surface salinities and bottom water stagnation leading to the accumulation of organic matter. Ryan (1972) related sapropel deposition with the input of meltwater from northern European ice and, Troelstra et al. (1991) proposed glacial meltwater as a key factor for the preconditioning of the Mediterranean Sea for sapropel formation. Another way to explain input the freshwater in the Mediterranean Sea was suggested by Rossignol-Strick et al. (1982). They noted an increased rainfall in equatorial Africa region that it translated in runoff into the Mediterranean Sea through the Nile River. Rossignol-Strick (1983) linked the increased rainfall with African monsoon, which is controlled by orbital forcing, especially minimum precession/maximun insolation. Periods of minimum precession/maximum insolation are represented by northward migration and increased African monsoonal activity. This freshwater input into the eastern Mediterranean Sea caused the reduction of thermohaline circulation (Calvert, 1983; De Lange et al., 2008; Emeis et al., 2000; Meyer & Kump, 2008; Rossignol-Strick, 1985), lowered surface water salinity and led to subsequent stagnation of the water column (Bar-Matthews et al., 2000, 2003; Emeis et al., 2003; Rohling, 1994; Rohling & Hilgen, 1991). Another possible freshwater source active at the time of sapropel deposition were probably the rivers from the Tibesti Mountains (Bar-Matthews, 2014; Osborne et al., 2008; Rohling et al., 2002), and rainfall in the whole Mediterranean Sea (Kallel et al., 1997; Rohling et al., 2002).

De Lange & Ten Haven (1983) suggested that the stagnation of the deep water was not the only factor for the sapropel deposition, but also to a higher productivity in the surface water. The continuous input of freshwater into the Mediterranean Sea brought an increase of nutrient and consequently, higher productivity. As a consequence, the increased productivity led to oxygen depletion (hence anoxia), which is a prerequisite for

deposition and preservation of organic matter (Bar-Matthews et al., 2000; De Lange et al., 2008; Möbius et al., 2010; Moodley et al., 2005; Murat & Got, 2000).

The relatively low density of the Mediterranean Intermediate Water (MIW) and the interruption of the Eastern Mediterranean Deep Water (EMDW) formation due to increased river runoff and temperature surface water was then proposed by Rohling & Gieskes (1989) to explain the stagnation of the Mediterranean Sea and, consequently, sapropel deposition. The stratification favored the failure of deep-water formation and the shoaling of the MIW consequently shoaling both the nutricline and pycnocline within the lower photic zone (Ariztegui et al., 2000; Principato et al., 2003; Rohling, 1991; Rohling & Gieskes, 1989; Sachs & Repeta, 1999). The failure of deep-water formation contributed then to the preservation of the organic matter (Castradori, 1993; Cramp & O'Sullivan, 1999; Rohling, 1994).

Despite the numerous multi-proxy studies (Casford et al., 2007; Ducassou et al., 2007; Giunta et al., 2003; Hennekam et al., 2014, 2015; Incarbona et al., 2011; Marino et al., 2009; Meier et al., 2004; Principato et al., 2003; Reed et al., 2011; Tachikawa et al., 2015; Tesi et al., 2017; Van Helmond et al., 2015; Versteegh et al., 2010; Wu et al., 2017; Ziegler et al., 2010; Zonneveld et al., 2001; Zwiep et al., 2018), the precise mechanism leading to sapropel deposition is still debated. Two main mechanisms are invoked to explain the sapropel formation (see Rohling et al. (2015)): (*1*) increased surface water buoyancy because of increased Nile freshwater input related to the intensification of the North African Monsoon and also of the freshwater discharge from the northern Mediterranean borderlands. The reduced density of the surface waters triggered thermohaline circulation reduction, reduced deep-water ventilation, and as a result, enhanced organic matter preservation. In this regard, a recent study based in simulation with a 3-dimensional ocean circulation model (Grimm et al., 2015) included the sea-level rise and sea surface warming as cause of the deep-water anoxia prior to S1 deposition; (*2*) enhanced marine production due to nutrient injection into the photic zone, by runoff (e.g., Nile River), shoaling of the nutricline and pycnocline within the lower photic zone, and brought to increased export of organic carbon to deep waters.

However, recently there is growing consensus on a combination of enhanced production, preconditioning from sea-level rise, and reduced deep-water ventilation as the main factors that caused sapropel deposition, although the respective contribution of each mechanism remains unknown (e.g., Filippidi & De Lange, 2019; Grant et al., 2016; Rohling et al., 2015).

3. Paleoclimate and paleoceanography proxy

Fig. 1 summarize all the proxies generally used in paleoceanography, that are reviewed in the following lines.

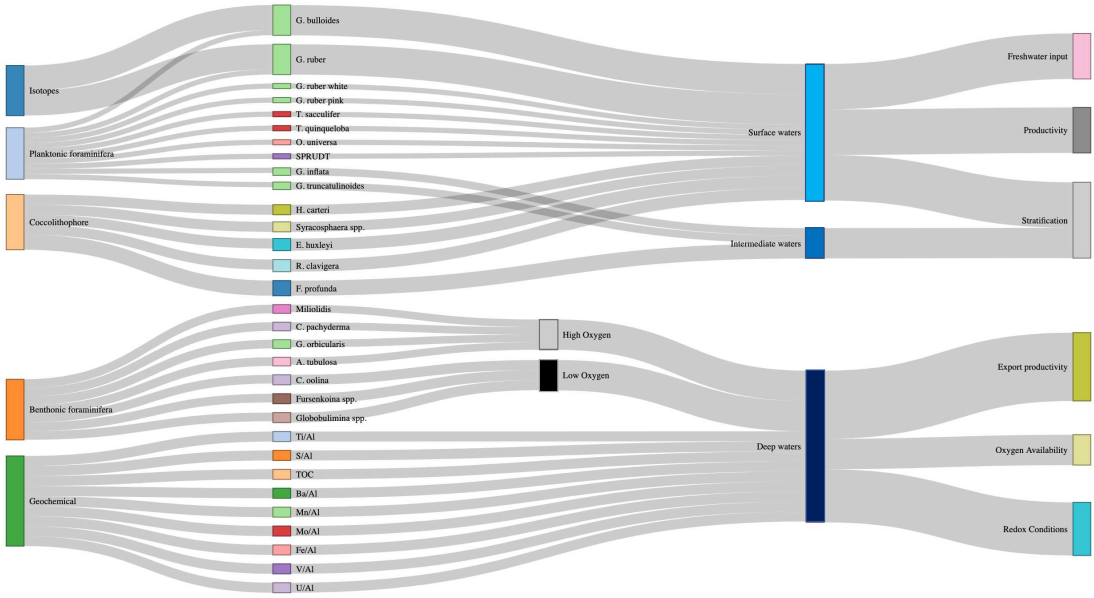

Fig. 1. Proxies used in paleoceanography and in this study.

3.1. Freshwater fluctuation and stratification of the water column in the Mediterranean Sea

Several studies recognized the input of freshwater into the Mediterranean Sea as a key factor for sapropel deposition (Filippidi & De Lange, 2019; Grimm et al., 2015; Hennekam et al., 2014, 2015; Rohling, 1994; Rohling et al., 2015; Rossignol-Strick, 1985; Rossignol-Strick et al., 1982; Zwiep et al., 2018). In literature, several proxies are related to enhanced freshwater input and, as a result, the stratification of the water column: (*i*) planktonic foraminifera as *Trilobatus sacculifer, Globoconella inflata, Globorotalia truncatulinoides,* and *Orbulina universa* (Kontakiotis, 2016; Mojtahid et al., 2015; Principato et al., 2003; Rohling et al., 1997); (*ii*) several coccolithophores as *Helicosphaera carteri, Syracosphaera spp.,* and *Rhabdosphaera clavigera* (Colmenero-Hidalgo et al., 2004; Flores et al., 1997; Grelaud et al., 2012; Incarbona et al., 2011; Negri & Giunta, 2001; Principato et al., 2003; Triantaphyllou, 2014; Triantaphyllou et al., 2009, 2010; Young, 1994); (*iii*) major elements as Ti/Al (Filippidi & De Lange, 2019; Frigola et al., 2007; Hennekam et al., 2014; Jimenez-Espejo et al., 2007; Tachikawa et al., 2015; Wehausen & Brumsack, 1999); and (*iv*) stable isotopes from planktic foraminifera as *Globigerinoides ruber* and *Globigerina bulloides* (Hennekam et al., 2014, 2015; Jimenez-Espejo et al., 2007, 2008; Marino et al., 2007, 2009).

The freshwater addition to the basin increases surface buoyancy and leads to water column stratification, interrupting the deep-water production and, as a result, the reduction deep-water ventilation. The reduced surface buoyancy loss is thought to trigger shoaling of intermediate water into the lower photic zone (i.e., the preferred habitat of the coccolithophore *Florisphaera profunda*), facilitating nutrient advection from below and so triggering the development of a deep chlorophyll maximum (DCM), consequently (Castradori, 1993; Corselli et al., 2002; Grelaud et al., 2012; Kemp et al., 1999; Myers, 2002; Myers et al., 1998; Rohling, 1994; Rohling & Gieskes, 1989). Therefore, high values of *F. profunda* are related to water column stratification (Corselli et al., 2002; Incarbona et al., 2011, 2019; Meier et al., 2004; Negri & Giunta, 2001; Principato et al., 2003; Triantaphyllou, 2014). Besides, the coccoliths as *Florisphaera profunda* and *Rhabdosphaera clavigera* and deep-dwelling planktonic species as *Globorotalia inflata* and *Globorotalia truncatulinoides* are largely influenced by water column stratification (Ariztegui et al., 2000; Casford et al., 2002; Capotondi et al., 2006; Mojtahid et al., 2015; Principato et al., 2003, 2006).

3.2. Surface productivity and export productivity

Planktonic foraminifera as *Globigerina bulloides* and *Turborotalita quinqueloba* (Kontakiotis, 2016; Mallo et al., 2017; Mojtahid et al., 2015; Rohling et al., 1997) or coccolithophore as *Emiliania huxleyi* (Broerse et al., 2000; Incarbona et al., 2011; López-Otálvaro et al., 2008; Triantaphyllou, 2014; Young, 1994) are considered as paleoproductivity proxies. Indeed, enhanced primary production is reflected as (export)production in deep water, in fact, the Ba/Al and TOC are the main indicators of this (export)production (Azrieli-Tal et al., 2014; Bishop, 1988; De Lange, 1986; Dymond et al., 1992; Eagle et al., 2003; Filippidi & De Lange, 2019; Hennekam et al., 2014; Jilbert et al., 2010; Martinez-Ruiz et al., 2000; Mercone et al., 2000; Tachikawa et al., 2015; Thomson et al., 1995; Van Os et al., 1991; Van Santvoort et al., 1997; Wehausen & Brumsack, 1999; Zwiep et al., 2018). However, barium is a better indicator than TOC because of it not affected by post-depositional processes (Calvert & Fontugne, 2001; De Lange et al., 2008; Thomson et al., 1995, 1999; Van Santvoort et al., 1996; Weldeab et al., 2003).

3.3. Redox and anoxic conditions

Several major and trace elements are considered redox-sensitive elements that provide us essential information that characterize the redox conditions of deep-waters and the sediments, as well as chemical and hydrographic properties of paleomarine systems. Elements as vanadium (V), iron (Fe), uranium (U), sulfur (S) and molybdenum (Mo) are enriched in sediment deposited under reducing conditions, as in the sapropel (Algeo, 2004; Algeo & Rowe, 2012; Filippidi & De Lange, 2019; Gallego-Torres et al., 2010; Jilbert et al., 2010; Jimenez-Espejo et al., 2007; Martinez-Ruiz et al., 2000, 2015; McKay & Pedersen, 2014; Nijenhuis et al., 1999; Thomson et al., 1995; Tribovillard et al., 2006; Warning & Brumsack, 2000; Zwiep et al., 2018). The redox-sensitive elements used respond at different pathways of precipitation depending on the different redox conditions. In detail, Uranium (U) enrichment process occurred around the Fe-reduction boundary (Algeo & Tribovillard, 2009; Tribovillard et al., 2012) and therefore starts to accumulate in the sediment under suboxic conditions (Zwiep et al., 2018). Vanadium (V) and Molybdenum (Mo) are usually enriched under suboxic-anoxic conditions at the sediment/water interface (Calvert & Pedersen, 1993; Filippidi & De Lange, 2019; Filippidi et al., 2016; Hennekam et al., 2015; Jilbert et al., 2010; Tribovillard et al., 2006; Zirks et al., 2018). In addition, Sulphur (S) and Iron (Fe) enrichments before/during sapropel is attributed to pyrite formation and incorporation into sediments which points to suboxic conditions at the sediment/water interface (Anderson & Raiswell, 2004; Lyons & Severmann, 2006; Passier et al., 1996, 1997; Reed et al., 2011; Thomson et al., 1995).

Nevertheless, when using these redox proxies, it must be taken into account that the dissolution/precipitation of these can be altered through post-depositional oxidation (burn-down) after reventilation of the water column (Thomson et al., 1995). Besides, manganese (Mn) enrichment and the presence of benthic foraminifera offer information about oxic/anoxic conditions in the deep-water. The Mn is generally low within sapropels because of its mobilization under suboxic-anoxic conditions in the bottom water (Mangini et al., 2001), however, a prominent Mn peak (so-called 'Marker Bed', Mn-MB; Filippidi & De Lange, 2019) marks the top of sapropels, and indicates the penetration of oxygen in the sediment at the end of sapropel deposition (De Lange et al., 1989; Mangini et al., 1991; Pruysers et al., 1993; Thomson et al., 1995; Van Santvoort et al., 1996; Mercone et al., 2000).

On the other hand, the vertical benthic foraminifera distribution at and/or below the sediment-water interface is closely related to the amount of dissolved oxygen in

bottom/pore water, and to organic carbon flux coming from surface-water productivity (Abu-Zied et al., 2008; Barmawidjaja et al., 1992; Corliss, 1985; Fontanier et al., 2002; Herguera & Berger, 1991; Jorissen, 1988; Jorissen et al., 1995; Linke & Lutze, 1993; Melki et al., 2010; Sen Gupta & Machain-Castillo, 1993). The oligotrophic areas, where there are food limitations but high dissolved oxygen concentrations, are colonized by epifaunal and shallow infaunal benthic foraminifera while in eutrophic areas, with high food available and reduced oxygen condition from dysoxic to anoxic, deep infaunal prevails. The zone of nitrate reduction is characterized by intermediate infaunal because of epifaunal and shallow infaunal species are not competitive anymore (Abu-Zied et al., 2008; Jorissen, 1999; Jorissen et al., 1995). According to this knowledge, the Oxygen Index (OI) (Schmiedl et al., 2003) was used to illustrate the changes in oxygen contents. This index was obtained as (HO/(HO+LO)Div)*0.5), where HO=relative abundances of high oxygen indicators (Miliolidis, *Articulina tubulosa*, *Gyroidina orbicularis* and *Cibicidoides pachyderma*), LO= relative abundances of low oxygen indicators (*Fursenkoina spp., Chilostomella oolina, Globobulimina spp.*), and Div=normalized benthic foraminiferal diversity H(S). The term was multiplied by 0.5 to distinguish between anoxic (minimum value=0) and oxic (maximum value=1) conditions (Schmiedl et al., 2003, 2010).

3.4. Paleotemperature proxies

In the eastern Mediterranean Sea, the planktonic foraminifera as *G. ruber pink* and *white*, and SPRUDTS-group (Rohling et al. (1993): clustered *Globigerinella siphonifera*, *Hastigerina pelagica*, *Globoturborotalita rubescens*, *Orbulina universa*, *Globigerina digitata*, *Globoturborotalita tenella*, and *Trilobatus sacculifer*) are indicative of warm (subtropical) waters (Reynolds & Thunell, 1989; Rohling et al. 1993; Tolderlund & Bé, 1972). According to Rodríguez-Sanz et al. (2017), the $\delta^{18}O$ signal in *G. ruber* recorded across sapropels may also reflect anomalous warming of the surface-water layer where they inhabited.

4. Materials & methods

The data presented in this study are stored in the database *BEyOND* (Amezcua-Buendía et al., 2019). For our purpose, a suitable selection of the cores is required in order to efficiently use the DA techniques. A minimum of 5 sediment samples within the

sapropel interval was required for each core, and because of these requirements a total of 10 cores (<5 sediment samples) was discarded. In detail, 102 cores were used (Fig. 2), which cover the Adriatic Sea (18 cores), the Aegean Sea (13 cores) and the Levantine, Ionian and Libyan Seas (71 cores). The Levantine, Ionian and Libyan Seas (hereafter called "Levantine/Ionian") are treated as a unique basin, because although the Cretan Strait (1,800 m deep and 300 km wide) divides the Ionian and Levantine Seas, the flow between both sub-basins does not seem to be altered (Malanotte-Rizzoli & Hecht, 1988).

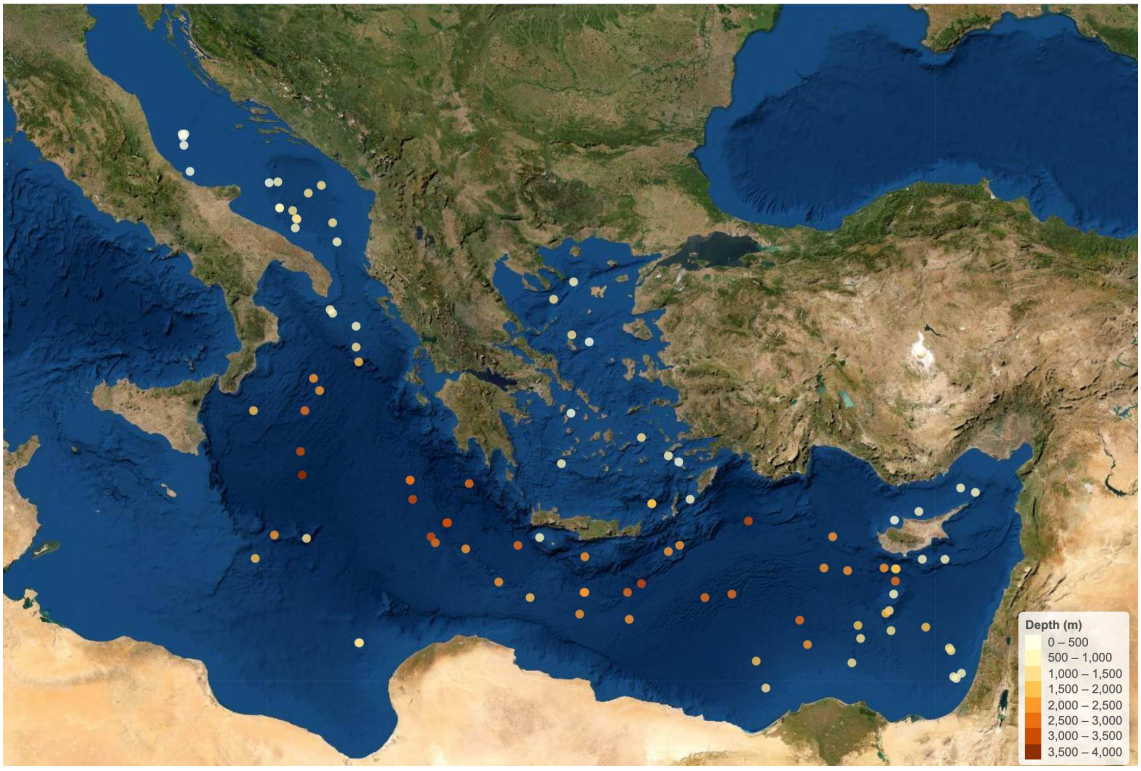

Fig. 2. Map of Mediterranean Sea with locations and depths of cores used in study.

Name	Latitude	Longitude	Sea	Depth (m)
IN68-23	42.19	14.93	Adriatic	64
PRAD1-2	42.6763	14.7704	Adriatic	185
IN68-21	42.89	14.79	Adriatic	252
CM92-43	42.8867	14.7325	Adriatic	252
AMC99-1	42.8502	14.7502	Adriatic	260
SLA-9	37.5167	24.55	Aegean	260
SH1972-13	35.33	32.72	Levantine	388
IN 68-28	41.99	16.92	Adriatic	396
SL-31	38.9333	25	Aegean	430
NS-18	36.5256	27.2708	Aegean	496
NS-14	36.6486	27.0078	Aegean	505
PS009PC	32.1283	34.4067	Levantine	552
SA03-1	41.5042	17.1797	Adriatic	567
INVAS12-10	41.5042	17.1797	Adriatic	570
GeoB 11185-1	39.5552	18.4556	Ionian	612
SH1972-3	34.53	33.41	Levantine	657
T87/2/20G	34.97	23.75	Levantine	707
IN 68-38	41.13	17.58	Adriatic	716
GeoTü SL123	35.7555	27.5557	Aegean	728
SH1972-2	35.91	34.77	Levantine	730
MD84-629	32.04	34.21	Levantine	745
MP50PC	39.4931	18.5233	Adriatic	775
80KB11	36.5	24.3	Aegean	795
IN 68-29	42	17.14	Adriatic	797
AP01.1	39.2275	19.1217	Ionian	811
190	36	34.38	Levantine	832
AD91-17	40.87	18.6375	Adriatic	844
SH1972-17	35.51	33.33	Levantine	850
9509	32.0167	34.2667	Levantine	884
160-966B	33.7997	32.7025	Levantine	926
M51/3 (SL152)	40.0865	24.6108	Aegean	978
9501	34.5333	33.9833	Levantine	980
SK-1	39.0667	24.5667	Aegean	1000
MD90-917	41.2978	17.613	Adriatic	1010
MS21PC	32.345	31.6501	Levantine	1022
IN 68-5	41.23	18.53	Adriatic	1030
NS-40	37.0167	26.3167	Aegean	1078
ST04-1	41.4577	17.5175	Adriatic	1085
GeoTü SL148	39.7538	24.0963	Aegean	1094
KET82-16	41.31	17.59	Adriatic	1166
IN 68-7	41.93	18.24	Adriatic	1225
IN 68-9	41.79	17.91	Adriatic	1234
M51/3 (569-3)	33.453	32.5752	Levantine	1294
MP39PC	38.8198	19.1147	Ionian	1359
UM42	34.9564	17.8625	Ionian	1375
MD84-641	33.0333	32.6333	Levantine	1375
MS27PT	31.8083	29.4694	Levantine	1389
M31/3 (562-5)	32.7742	19.191	Ionian	1391
GeoTü SL96	32.7775	19.1978	Libyan	1399
GeoTü KL83	32.6087	34.1389	Levantine	1433
M51/3 (GeoTü SL110)	32.6492	34.1037	Levantine	1437
MD84-637	32.856	31.8603	Levantine	1450
CP10/11	34.5353	16.5667	Ionian	1501
MD 81-LC-21	35.6667	26.5833	Aegean	1522
SL60	35.6692	26.5942	Aegean	1522
CHN119-12PG	32.38	29.225	Levantine	1581
SL29	33.3931	32.505	Levantine	1587
MD84-648	33.1333	31.7944	Levantine	1660
KET82-22	37.56	16.53	Ionian	1691

MD04-2722	33.1	33.5	Levantine	1780
M51/3 (563-5)	33.718	23.5012	Ionian	1881
MP37PC	38.5303	19.1808	Ionian	1908
160-968	34.3192	32.75	Levantine	1960
160-968C	34.3328	32.7536	Levantine	1964
SH1972-7	34.35	32.45	Levantine	2000
P6508-36B	32.733	30.517	Levantine	2000
MD84-658	35.0333	17.05	Ionian	2020
M40/4 (SL67)	34.8142	27.296	Levantine	2157
BC3	33.3808	24.7667	Ionian	2180
160-969A	33.84	24.8845	Ionian	2200
160-969E	33.8411	24.8831	Ionian	2201
HCM2/22	34.5769	24.9047	Aegean	2211
75KS50	34.69	27	Levantine	2290
MD 81 (LC-31)	35	31.1667	Levantine	2298
SL9	34.2881	31.5267	Levantine	2302
RC09-191	38.2	18.033	Ionian	2345
CHN119-6PG	33.2633	26.015	Levantine	2372
TR171-24	34.05	22.7167	Libyan	2380
ADE3-23	34.75	21.88	Libyan	2459
M25/4-KL12	37.9663	18.184	Ionian	2468
CHN119-18PC	34.3467	30.93	Ionian	2484
CHN119-16PG	33.2467	30.3317	Levantine	2523
M25/4-KL13	37.5535	17.824	Ionian	2533
BC06	34.875	21.1189	Ionian	2539
160-967D	34.0742	32.7314	Levantine	2550
RC09-178	33.733	27.917	Levantine	2628
TR171-27	33.83	25.98	Levantine	2680
TTR-GL94	36.0875	21.9675	Ionian	2687
BC19	33.7917	28.6139	Levantine	2750
M40/4 (GeoTü SL71)	34.8112	23.1942	Ionian	2788
10103-1B	36.16	20.48	Ionian	2880
10103-8K	36.16	20.48	Ionian	2895
BC07	35.7597	20.5444	Ionian	3022
75KS52	34.01	26.32	Levantine	3118
TR172-22	35.32	29.02	Levantine	3150
UM15	35.2844	21.4022	Ionian	3308
BC02	35.2858	21.4153	Ionian	3349
6SL	35	21	Ionian	3350
SL114	35.29	21.4144	Ionian	3390
160-964A	36.2603	17.7497	Ionian	3658
160-964B	36.2603	17.7525	Ionian	3658
M25/4-KL11	36.7458	17.7175	Ionian	3776

Table 1. Sediment cores description.

We investigated the eastern Mediterranean based on the different water masses:

1. Surface water masses (SWM); provide information about the impact of the atmospheric and/or continental processes on surface water properties (e.g., salinity, nutrients, productivity, circulation). We address this by looking at three geographic areas: (*i*) Levantine+Ionian+libyan; (*ii*) Adriatic; and (*iii*) Aegean Seas. This will allow identifying the developments of the SWM in response to local forcing.

2. Intermediate Water (IW); their circulation, productivity and carbon cycling along with the surface properties addressed above provide information about stratification of the upper water column.
3. Deep-water (DW); their geochemistry and (benthic) assemblages provide information on the oxygen availability and organic carbon burial in response to deep, intermediate, and surface processes.

The methodology adopted in this study is based on the use of the database *BEyOND* and DA techniques. We use the Amezcua-Buendía et al. 2019 methodology to correlate the data, and then we introduce the age values obtained in Chapter 2 (10.1 and 6.5 cal. ka BP). This latter is obtained through three equations where: S_t and S_b are the age for sapropel top (6.5 cal. ka BP) and bottom (10.1 cal. ka BP), and d_1 and d_2 are the top and bottom depths measured for each sample.

$$S_{1i} = S_t + (S_b - S_t) * d_1$$

$$S_{2i} = S_t + (S_b - S_t) * d_2$$

$$S_k = average\ \{S_{1i}, S_{2i}\}$$

The S_{1i} and S_{2i} are the ages obtained for the top and bottom of the sample while S_k is the final age of the sample. The results shown in Section 5 were obtained through SQL queries realized on *BEyOND*. In detail, (*1*) we correlated the cores based on the sub-basins; (2) using the depth values for each core, we obtained a "single virtual core" with a "Standardized depth" and the mean values stack for every proxy examined; (*3*) we then changed the "Standardized depth" with the age values (obtained in Chapter 2) as described above. The eastern Mediterranean Sea was divided into three sub-basins where up to five categories of proxies (isotopes, planktonic and benthic foraminifera, coccolithophore and geochemical) were analyzed.

5. Results

5.1. Geochemistry

The geochemical data are represented by 33 cores in the eastern Mediterranean Sea, 25 cores from the Levantine/Ionian Sea report all the proxies, 5 cores in the Adriatic Sea, and only 3 cores in the Aegean Sea.

Fig. 3 reports the data in the different sub-basins. A sedimentary interruption is evident in the Aegean and Adriatic Seas around 8.8 – 8 cal. ka BP splitting the sapropel S1 into, respectively, "S1a" (from 10.1 to 8.5 cal. ka BP) and "S1b" (from 8 to 6.5 cal. ka BP) intervals (cf. De Rijk et al., 1999). The S1 interval shows high values for TOC, Ba/Al, V/Al, Mo/Al, S/Al, Fe/Al, and U/Al, whereas Ti/Al show low concentrations. The sapropel is characterized by very low values of Mn/Al except for a clear increase close to the top. The TOC, Ba/Al, Mn/Al, V/Al, S/Al, and Fe/Al are higher in Levantine/Ionian Sea than Aegean and Adriatic Seas. The maximum values of these proxies are reached through S1a.

As expected, TOC concentrations increase in all sub-basins during the sapropel interval, in fact, at the base and the top values are very low (0.2%) whereas in the sapropel these values range between 0.4 and 2.4% (Fig. 3a). In detail, the TOC ranges between 0.5 and 2.4% in the Levantine/Ionian Sea, 0.5 and 1.6% in the Aegean Sea and, 0.3 and 1% in the Adriatic Sea during S1. In the Levantine/Ionian Sea, higher concentrations are presented in S1a (>1.5%) than S1b (<1.5%) with a continuously decrease interval of TOC since 8.7 cal. ka BP until the base of S1 (2.1 to 0.4%). The Aegean Sea shows high concentrations in S1a (1.6 – 1.2%) and S1b (1.4 – 1%), which are divided by lower concentrations (<1%) during the interruption. A similar pattern is followed in the Adriatic Sea with high concentrations in S1a (>0.8%) and S1b (>0.6%) and lower during the interruption (0.6%).

Ba/Al values show large differences between sapropel (0.0042 – 0.003) and non-sapropel layers (0.003 – 0.0025) in all sub-basins (Fig. 3b). During S1, the Ba/Al ranges between 0.016 and 0006 in the Levantine/Ionian Sea, 0.014 and 0.008 in the Aegean Sea and, 0.0042 and 0.003 in the Adriatic Sea. In the Levantine/Ionian Sea, the Ba/Al values follow a bell-shaped curve where its maximum values are reached during the interruption (~8.2 cal. ka BP). About Ba/Al in Aegean and Adriatic Seas, high values are shown in S1a (0.13 – 0.01 and 0.0042 – 0.0036, respectively) and S1b (0.012 – 0.009 and 0.0039

– 0.0027, respectively) separated by lower values (~0.008 and ~0.0035) during the interruption.

Regarding Mn/Al, a prominent enrichment is found close to the top of S1 in all sub-basins (Fig. 3c). In detail, the Mn/Al values start to increase at 7.45 cal. ka BP reaching their maximum values of 0.81 around 7.2 cal. ka BP in the Levantine/Ionian Sea. High values (0.76 – 0.52) continue until 6.8 cal. ka BP where decrease down to its minimum value of 0.12 at the base of S1. In the Adriatic Sea, Mn/Al values increase from 0.014 to 0.12 at 7.4 cal. ka BP and start to decrease at 7.2 cal. ka BP reaching its minimum values of 0.016 around 6.9 cal. ka BP. In the Aegean Sea, the increase in the Mn/Al values starts between 7.85 and 7.6 cal. ka BP showing a pronounced peak at 6.91 cal. ka BP (0.18). Then, the Mn/Al values continue to decrease above the S1 top.

V/Al values show higher values during sapropel than non-sapropel layers in all sub-basins (Fig. 3d). The V/Al values in S1 oscillate between 0.0032 and 0.0018 in the Levantine/Ionian Sea, 0.0066 and 0.002 in Aegean Sea and, 0.002 and 0.0012 in Adriatic Sea. Both Aegean and Adriatic Seas, two prominent peaks at the base of S1 (0.0066 and 0.002, respectively) and above of the interruption (0.005 and 0.0016, respectively) are noted. In the Levantine/Ionian Sea, V/Al values rapidly increase at the base of S1 reaching its maximum value (0.0066) and then it decreases and reaches its minimum value of 0.0018 close to the S1 top.

As for Mo/Al in the sub-basins, high values are seen throughout sapropel interval, in particular in S1a for Levantine/Ionian and Aegean Sea, whereas low values are recorded in non-sapropel intervals (Fig. 3e). In detail, in the Levantine/Ionian Sea, the Mo/Al values rapidly increase at the base of S1 reaching 0.00033 from <0.0001, and then, two slight peaks at 9.0 cal. ka BP (0.00028) and on the top of S1 (0.00013) are noted. The Mo/Al values show similar patterns in the Aegean Sea since it increases at the base of S1, showing two peaks at 10.1 (0.00043) and 9.55 cal. ka BP (0.00037). A slight increase (from 0.000041 to 0.00024) occurs above of interruption and continues along S1b. The Mo/Al values in the Adriatic Sea show three prominent peaks at 9.6 (0.000084), 8.1 (0.000083), and 6.47 cal. ka BP (0.0000544).

The U/Al values are similar in S1a and higher than the values observed in S1b for all sub-basins (Fig. 3h). In the Levantine/Ionian and Aegean Seas, the U/Al values remain more or less stable (0.0002 – 0.00015) during S1a, with the exception the minimum values of 0.00015 at ~9.3, at ~8.7, and at ~8.3 cal. ka BP in the Levantine/Ionian Sea, and 0.00014 at 8.7 cal. ka BP in the Aegean Sea. The U/Al values in the Adriatic Sea show

three peaks at ~9.7 (0.00006), ~9.2 (0.000064), and ~8.7 (0.000064) cal. ka BP whereas lower values (0.000045 – 0.000023) are showed in S1b.

Regarding S/Al, a prominent enrichment is found below to the sapropel in all sub-basins (Fig. 3f). In detail, the S/Al values start to increase at 10.66 cal. ka BP and reach its maximum value of 0.1 around 10 cal. ka BP in the Levantine/Ionian Sea. Then, S/Al values continuously decrease to reach the minimum value of 0.019 at 7.4 cal. ka BP, with the exception of the two enrichment intervals around 9.1 and 8.7 cal. ka BP. A similar pattern is found in the Adriatic Sea where shows its maximum values of 0.09 between 9.99 and 9.6 cal. ka BP. Then, lower values (0.06 – 0.02) during S1 are showed with the exception of two slight peaks of 0.058 and 0.057 at 9.1 and 8.5 cal. ka BP. In the Aegean Sea, a prominent peak (0.0016) of S/Al is observed at 10.3 cal. ka BP after which S/Al values decrease. Also, there are two slight peaks of S/Al at 8 and 6.9 cal. ka BP (0.00064 and 0.00048, respectively).

Different Fe/Al values oscillations are shown in Fig. 3g. In the Levantine/Ionian Sea, the Fe/Al values start to increase at 11.1 cal. ka BP reaching the maximum values of 0.82 around 9.1 cal. ka BP; they decrease continuously toward the top of the sapropel. An enrichment of Fe/Al occurs at the base of the sapropel in the Adriatic Sea (from 0.48 to 0.54), and then a marked drop (from 0.50 to 0.43) around 9.2 cal. ka BP occurs. Fe/Al values range between 0.46 and 0.5 during the rest of S1, with the exception of slight enrichment (0.52) close to the S1 top. In the Aegean Sea, the Fe/Al values start to increase at 11.3 cal. ka BP and reach its maximum value of 0.84 around 10.3 cal. ka BP. Then, Fe/Al values decrease at the base of S1 and oscillate between 0.74 and 0.64 along S1. There are two slight peaks of 0.7 at 7.8 and 6.9 cal. ka BP

Ti/Al values decrease during S1 with regard to the non-sapropel layer in Levantine/Ionian and Adriatic Seas (Fig. 3i). In particular, values (0.06) remain low during S1, with the exception of the interruption where the values are higher (0.069) in the Levantine/Ionian Sea. In the Adriatic Sea, Ti/Al values start to decrease at the base of S1 reaching its minimum value of 0.039 around 9.2 cal. ka BP, and then slowly increase at higher values (0.047) during S1b, with the exception of two intervals with low values (0.045) at ~8 and ~7.2 cal. ka BP.

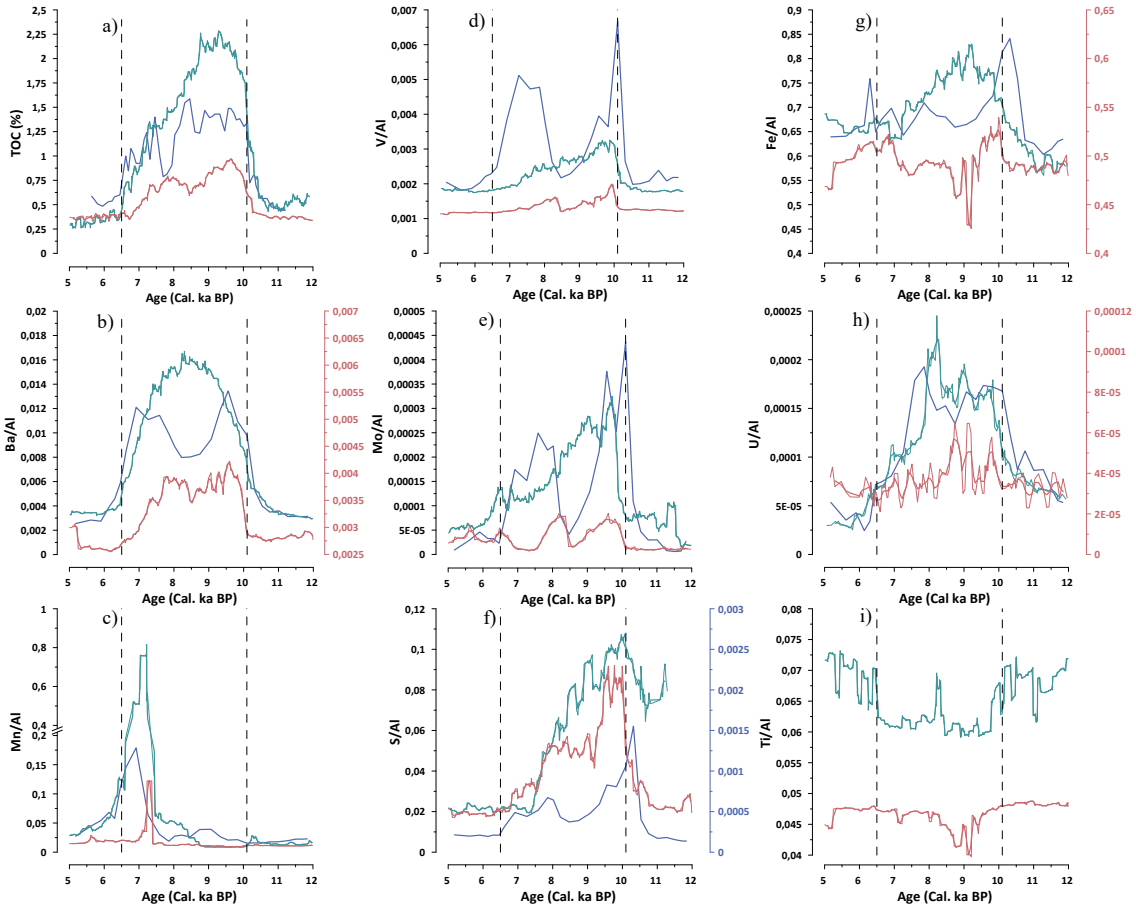

Fig. 3. Sediment geochemistry plotted vs age. (a) TOC (b) Ba/Al (c) Mn/Al (d) V/Al (e) Mo/Al (f) S/Al (g) Fe/Al (h) U/Al (i) Ti/Al. The color lines represent the different sub-basins: Levantine/Ionian Sea (green); Aegean Sea (blue); Adriatic Sea (red). Vertical dashed black lines show the S1 interval (10.1 – 6.5 cal. ka BP).

5.2. Planktonic foraminifera and Oxygen Index

The planktonic species observed in Fig. 4 are obtained from 27 cores, where 14 core derive from the Adriatic Sea, 10 cores from Levantine/Ionian Sea, and 3 cores from the Aegean Sea. In the eastern Mediterranean Sea, the planktonic foraminifera as *T. sacculifer*, *T. quinqueloba*, *G. ruber pink* and *white*, *O. universa*, the SPRUDTS-group (Rohling et al., 1993) and *G. bulloides* are abundant during S1 interval, while *G. inflata*, and *G. truncatulinoides* tend to decrease (Fig. 4).

The occurrences of *T. sacculifer* increase in the three study regions during S1 but showing great differences between them (Fig. 4a). In the Aegean Sea, higher abundances of *T. sacculifer* are found at 9.5 cal. ka BP (17%) and between 8.2 and 7 cal. ka BP (10 – 26%) than within the interval 9.4 – 8.4 cal. ka BP and the top of S1 where the abundances decrease to a level of 5%. In the Levantine/Ionian Sea, a rise of the *T. sacculifer* (from 2.3 to 9.7%) at the base of S1 is observed remaining steady at ~9.5% during S1, with the

exception of the two notable peaks between 8.8 and 8.3 (13%), and 7.3 and 6.9 cal. ka BP (13%). In the Adriatic Sea, it is not very abundant, in fact, it varies between 0 – 1.8% during S1, with several peaks at 9.7 (0.58%), 8.5 (0.67%), ~7.4 (1.8%) and 6.9 cal. ka BP (1.6%).

T. quinqueloba shows a greater abundance in the Adriatic Sea than the Aegean and Levantine/Ionian Seas (Fig. 4b). In detail, in the Aegean Sea, *T. quinqueloba* increases before the S1 deposition reaching the maximum value at 10.34 cal. ka BP (31%). After that, it decreases to disappear at 9.6 cal. ka BP and remains absent until 9.1 cal. ka BP. Then, two peaks at 8.6 (20%) and 6.6 cal. ka BP are observed. In the Levantine/Ionian Sea, *T. quinqueloba* is absent during S1, with the exception of two peaks at 9.1 (9%) and ~7 cal. ka BP (5%). *T. quinqueloba* rises at the base of S1 reaching the maximum value at 9.4 cal. ka BP (26%) in the Adriatic Sea. Then, decrease to a level of 16% at 9.1 cal. ka BP and increases again until the interruption interval (29%) where at 7.6 – 7.3 cal. ka BP drop to a level of 17%. A slight increase (from 17 to 24%) occurs at ~7.2 cal. ka BP until to S1 top.

The two morphotypes of *G. ruber* show higher presence during sapropel than non-sapropel layers throughout eastern Mediterranean Sea (Fig. 4c). *G. ruber pink* starts to increase early of the S1 in the Aegean and Levantine/Ionian Seas, and at the base of S1 in the Adriatic Sea showing higher value in S1a than S1b (Fig. 4c). In the Aegean Sea, *G. ruber pink* increases slightly from 11 to 10.2 cal. ka BP where rises notably reaching a maximum at 9.5 cal. ka BP (25%). Then, it oscillates between 21 – 8% until 8.5 cal. ka BP, where an increasing trend (8 – 21%) is noted. After 7.2 cal. ka BP, *G. ruber pink* drops to a level of 5% close to the S1 top. In the Levantine/Ionian Sea, *G. ruber pink* starts to increase at 10.7 cal. ka BP reaching a maximum at 9.1 cal. ka BP (8%). Then, a decreasing trend is observed until the base of S1 (from 8 to 3%). In the Adriatic Sea, *G. ruber pink* increases at the base of S1 showing two prominent peaks at 9.1 and 7.9 cal. ka BP (11 and 9%, respectively). During S1, low abundances of *G. ruber pink* are observed at 9.5 cal. ka BP (1%) and during the interruption (~8.2 cal. ka BP, 2%). This specie disappears at ~6.5 cal. ka BP in the Adriatic Sea. On the other hand, *G. ruber white* is particularly abundant earlier of S1 and during S1a in all sub-basins (Fig. 4d). In detail, *G. ruber white* starts to increase at ~11.2 cal. ka BP (15%) and rises up to 38% at 10.3 cal. ka BP in the Aegean Sea. Also, three increasing trends are observed at 9.3, 7.8 cal. ka BP, and on the base of S1. In contrast, the abundances of *G. ruber white* drop significantly to values of 10% at 9.5 and 5% at 7.8 cal. ka BP. In the Levantine Sea, *G. ruber white*

increases at 11.3 cal. ka BP and reaches its maximum in abundances at 10 cal. ka BP (54%). Then, a continuously decreasing trend of *G. ruber white* is observed throughout S1 (54 to 30%) in the Levantine/Ionian Sea. In the Adriatic Sea, *G. ruber white* gradually increases at 10.7 cal. ka BP and reaches the maximum value (39%) in the upper part of the sapropel at 9.6 cal. ka BP. Low abundances are observed between 9.2 and 8 cal. ka BP, with a minimum of 3% at 8.3 cal. ka BP. After the interruption, *G. ruber white* shows an increasing trend between 7.7 and 7.2 cal. ka BP whereas the base of S1 is characterized by lower abundances (>10%).

G. truncatulinoides disappears in the lower part of the sapropel (Fig. 4e). In the Levantine/Ionian and Aegean Seas, *G. truncatulinoides* is absent throughout S1, although in the Levantine/Ionian Sea a slight increase (0.3%) between 9.5 and 8.7 cal. ka BP is worth noting. In the Adriatic Sea, *G. truncatulinoides* shows a peak within S1 centered around 9.9 cal. ka BP and, then, it decreases to a minimum of <1% until completely disappear at 8.7 cal. ka BP. Also, *G. truncatulinoides* temporary reappears with a slight increase (<1%) at 8.2 and 7.2 cal. ka BP in the Adriatic Sea.

O. universa increases in abundance during S1 in the Levantine/Ionian and Aegean Seas, in contrast with the Adriatic Sea (Fig. 4f). In the Aegean Sea, *O. universa* increases abruptly at the base of S1 reaching a maximum of 16% at 9.9 cal. ka BP and, then, it continuously decreases up to 8.5 cal. ka BP. After the interruption interval (~8 cal. ka BP), *O. universa* again increase between 7.9 and 7.2 cal. ka BP (6 – 10%) and it shows low abundances (<3%) in the top part of S1. Similar trend is followed in Levantine/Ionian Sea, in fact, two increasing trends are showed between 9.9 – 9.2 and 8 – 7 cal. ka BP, with an average value of 3.5%. In contrast, lower abundances of *O. universa* are noted in the sapropel than in pre-sapropel layers in the Adriatic Sea. Several fluctuations between 4 – 2% are noted throughout S1 although in this interval a clear positive fluctuation with maximum (6%) located at 9.6 and 9.2 cal. ka BP is worth noting.

The planktonic foraminifera that form the SPRUDT-group increase during S1 in all sub-basins (Fig. 4g). In the Aegean Sea, SPRUDT-group increases abruptly at the base of S1 with several fluctuations (4.5 – 2.5%) and reaches a maximum value of 5% at 8.5 cal. ka BP. Then, low values (< 3%) are showed during 8.3 – 7.8 cal. ka BP followed by three intervals with higher abundances (> 3%) at 7.7, 7.1, and 6.7 cal. ka BP. In the Levantine/Ionian Sea, SPRUDT-group shows higher abundances during S1b than S1a, in fact, at the base of S1 theses increase from 0.9 to 3.7%, while during S1b reaching a maximum of 5% at 7.1 cal. ka BP. In the Adriatic Sea, SPRUDT-group is most present

on S1a than S1b, showing a slight increase at the base of S1 (2 to 3.5%) and higher abundances between 9.4 and 8.2 cal. ka BP (5 – 9%). Low values (2%) throughout S1b are observed.

G. inflata shows lower abundances in sapropel than non-sapropel layers in the three sub-basins (Fig. 4h). In the Aegean Sea, lower values are observed during S1 with the exception of two peaks at 9.6 (2%) and between 9.1 – 8.8 cal. ka BP (6%). *G. inflata* increase abruptly at the top of S1 (11%) in the Adriatic Sea. In the Levantine/Ionian Sea, *G. inflata* shows a trend with abundances between 3 and 4%. Also, several negative excursions (< 2%) are observed at 10, 8.2, and ~7.4 cal. ka BP. *G. inflata* increases close to S1 top (7 cal. ka BP) reaching a maximum value of 5.6% at 6.3 cal. ka BP. In the Adriatic Sea, *G. inflata* drop abruptly at the base of S1 reaching the minimum value of 1% at 9.6 cal. ka BP. Two intervals with a slight increase of *G. inflata* are observed between 9.5 – 8.7 and 8 – 7.5 cal. ka BP, with a peak at 8.25 cal. ka BP. As in the Aegean and Levantine/Ionian Seas, *G. inflata* increase close to S1 top (7.1 cal. ka BP) reaching a maximum value of 7.3% at 6.2 cal. ka BP.

G. bulloides shows different trends in each sub-basins (Fig. 4i). In the Aegean Sea, a decreasing trend (42 – 17%) of *G. bulloides* is observed from 11.3 until 9.7 cal. ka BP. Then, it increases to a level of 35% at 8.9 cal. ka BP with a slight excursion (23%) at ~8.6 and it increases again until the interruption interval (39%) where at 8.2 – 7.9 cal. ka BP drop to a level of 28%. Two peaks (40%) are observed at 7.8 and 6.8 divided by low values (30 – 25%) between 7.8 and 6.9 cal. ka BP. The lower abundances of *G. bulloides* are observed at the S1 top (15%). In the Levantine Sea, *G. bulloides* starts to decrease from 11.3 cal. ka BP (13%) reaching a minimum of 2.5% at 9.4 cal. ka BP. During S1, *G. bulloides* oscillates between 2 and 4%, with the exception at 8.6 cal. ka BP where a peak is observed (> 4%). High abundances (> 4%) are observed at S1 top. In contrast, higher abundances are observed at the base of S1 in the Adriatic Sea reaching a maximum of 37% at 9.6 cal. ka BP. Then, a decreasing trend is observed until 8.2 cal. ka BP (from 37 to 24%), with a peak at 8.6 cal. ka BP (28%). Two intervals with higher abundances are observed between 8.2 – 7.6 and 7.5 – 6.5 cal. ka BP (26 and 30%, respectively). Lower abundances are observed at S1 top (24%) in the Adriatic Sea.

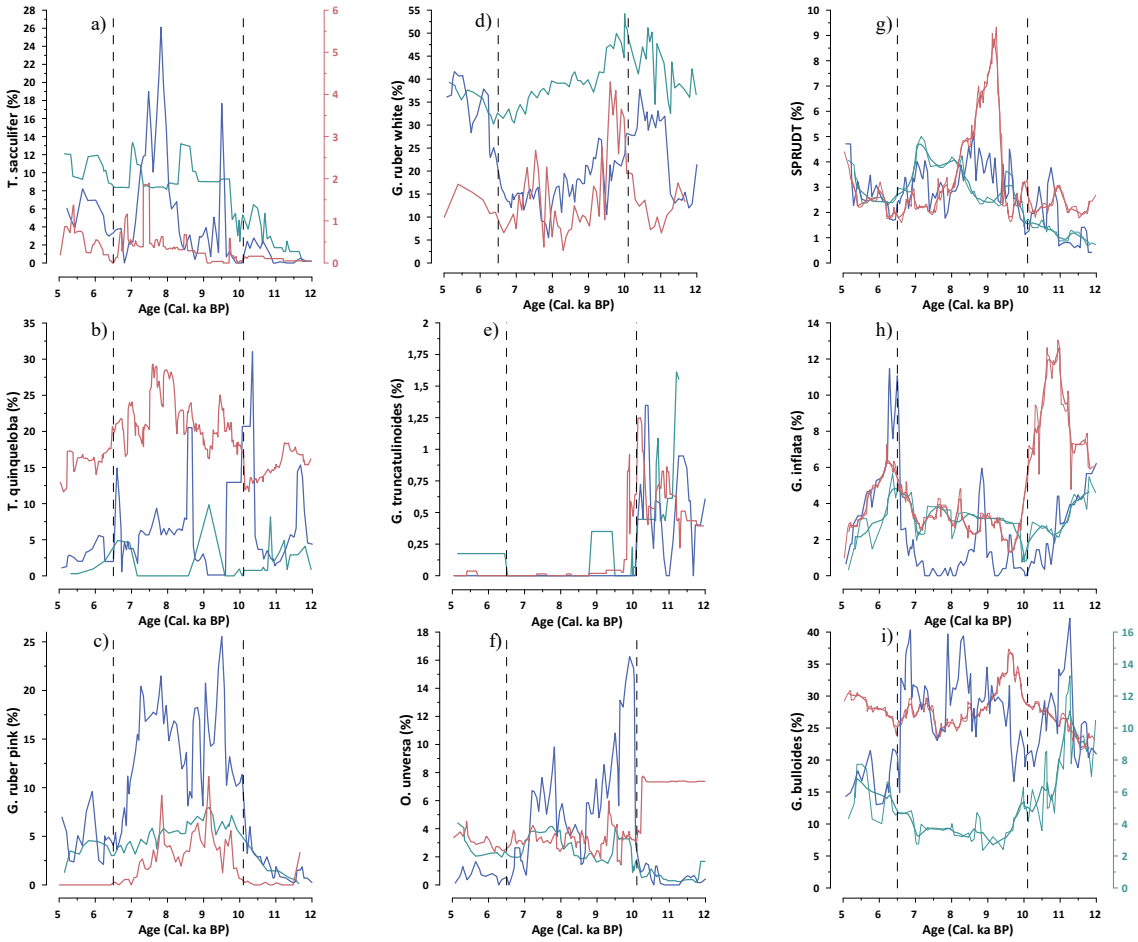

Fig. 4. Planktonic foraminifera fluctuations plotted vs age. Relative abundances of (a) *Trilobatus sacculifer*, (b) *Turborotalita quinqueloba*, (c) *Globigerinoides ruber pink*, (d) *Globigerinoides ruber white*, (e) *Globorotalia truncatulinoides*, (f) *Orbulina universa*, (g) SPRUDT-group, (h) *Globoconella inflata*, and (i) *Globigerina bulloides*. The color lines represent the different sub-basins: Levantine/Ionian Sea (green); Aegean Sea (blue); Adriatic Sea (red). Vertical dashed black lines show the S1 interval (10.1 – 6.5 cal. ka BP).

As for the oxygen index calculated for all sub-basins, a total of 11 cores are used from the eastern Mediterranean Sea, which derive 5 cores from the Aegean Sea, 3 cores from the Adriatic Sea, and 3 cores from the Levantine/Ionian Sea. Slight differences are observed among sub-basins (Fig. 5), where clear anoxic conditions are observed in the Levantine/Ionian Sea between 9.2 – 8.8 and 7.8 – 7.5 cal. ka BP. Two shorter anoxic intervals at 8.7 and 8 cal. ka BP are also observed. During the interruption interval, between ~8.5 and 8 cal. ka BP, and later of 7.5 cal. ka BP, values around 0.5 indicate more dysoxic conditions. Unlike S1 base where fully oxygenated conditions were observed, S1 top and post-S1 were not oxygenated. In the Aegean Sea, environments depleted in oxygen are observed during the whole S1a and part of the S1b (between 7.3 and 6.5 cal. ka BP). Waters partially oxygenated are observed between 8.5 – 8 and 7.8 –

7.4 cal. ka BP. In contrast to the Levantine/Ionian and Aegean Seas, the Adriatic Sea presented more oxygenated conditions, in fact, waters depleted in oxygen only are observed between 9.9 – 9.3 and 7.9 – 7.6 cal. ka BP.

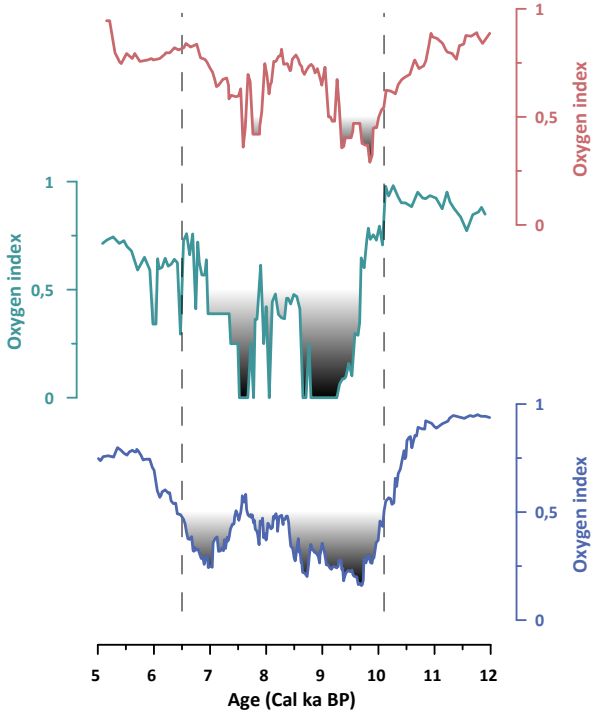

Fig. 5. Foraminifera-based oxygen index (OI, (Schmiedl et al., 2010) plotted vs age. Value of 1 refers to fully oxygenated conditions while 0 represents anoxic environment. The color lines represent the different sub-basins: Levantine/Ionian Sea (green); Aegean Sea (blue); Adriatic Sea (red). Vertical dashed black lines show the S1 interval (10.1 – 6.5 cal. ka BP).

5.3. Coccolithophore

The coccolith data are represented by 22 cores in the eastern Mediterranean Sea, where 16 cores come from the Levantine/Ionian Sea, 5 cores from the Aegean Sea, and 1 from the Adriatic Sea. In Fig. 6, the S1 interval shows high abundances of *F. profunda*, *H. carteri*, and *R. clavigera* during S1 interval. In contrast, lower abundances are shown for *E. huxleyi* and *Syracosphaera spp*.

F. profunda increases in the whole Mediterranean Sea, but its presence seems to be higher in the Aegean and Levantine/Ionian Seas than the Adriatic Sea (Fig. 6a). In Aegean Sea, *F. profunda* rises from 55 to 73% at the base of the sapropel. Then, it remains constant between 70 – 60% during S1a and S1b, with the exception of several negative excursions at 8.2 and 7.9 cal. ka BP reaching a minimum of 57% and lower abundances (< 55%) between 7.3 – 7 cal. ka BP and close to S1 top (43%). In the Levantine/Ionian Sea, *F. profunda* increases before S1, in fact, it rises from 20 to 37% at 10.7 cal. ka BP

reaching a maximum of 42% within S1 (9.7 cal. ka BP). After that, it decreases constantly until the end of S1, with the exception of pronounced negative excursions at 9.5 (35%), 8.8 (30%), 7.4 cal. ka BP (19%), and at the end of S1 (18%). In the Adriatic Sea, *F. profunda* starts to increase before S1 (10.3 cal. ka BP) with one pronounced peak (5%) at 9.6 cal. ka BP, and soon after it decreases and fluctuate between 2 and 3% throughout S1.

H. carteri increases before S1 in the whole Mediterranean Sea showing abundances within sapropel layer between 1 – 5% (Fig. 6b). In particular, *H. carteri* rises abruptly at 11 cal. ka BP in the Aegean Sea showing an increasing trend between 11 and 9.7 cal. ka BP, but values widely fluctuate (1 – 2%). During S1 the abundances oscillate between 0.5 – 1.5 % with several negative excursions (< 1%) at 9.3, 8.2, 7.6, 7 cal. ka BP, and at the end of S1. In the Levantine/Ionian Sea, *H. carteri* starts to increase at 10.7 cal. ka BP, but it decreases slightly at the base of S1 before increasing again to 9.8 cal. ka BP (2.2%). Then, *H. carteri* oscillates between 1.5 and 2% until 7 cal. ka BP where it drops to minimum values (1 %). In the Adriatic Sea, *H. carteri* increases shortly before S1 deposition showing several peaks (5%) at 9.8, 8.1, and 7 cal. ka BP. During S1 interval, *H. carteri* oscillates between 2 and 4% with the lower abundances at the S1 top.

R. clavigera increases slightly in the Levantine/Ionian and Aegean Seas during S1 showing higher values in S1a than S1b (Fig. 6c)(no data available for the Adriatic Sea). In particular, *R. clavigera* shows abundances between 2.7 and 0.7% in S1a while lower values (2 – 0.3%) are observed during S1b in the Aegean Sea. In the Levantine/Ionian Sea, *R. clavigera* starts to increase at 11 cal. ka BP reaching a maximum of 2% at 9.3 cal. ka BP and during this interval, two negative excursions (< 0.5%) at 10 and 9.5 cal. ka BP are observed. Throughout S1a, *R. clavigera* oscillates between 1.5 and 0.6% while during S1b lower abundances (< 1%) are shown.

E. huxleyi shows lower abundances in the sapropel than non-sapropel layers in the whole Mediterranean Sea (Fig. 6d). Also, large differences are observed among the sub-basins, where values range between 90 and 80% in the Adriatic Sea, and 40 and 20% in the Levantine/Ionian and Aegean Seas. In detail, *E. huxleyi* decreases at the base of S1 from 40 to 22%, and soon after it increases up to 35% (9.5 cal. ka BP) and remaining around this value until 8.2 cal. ka BP in Aegean Sea. Then, a slight increase is observed during the interruption (from 27 to 39%). During S1b, *E. huxleyi* shows two increasing trends between 7.2 and 7, and at the sapropel top, with maximum values of 45 and 53% respectively. In the Levantine/Ionian Sea, *E. huxleyi* starts to decrease at 11 cal. ka BP reaching a minimum value of 33% at 9.9 cal. ka BP. It oscillates between 37 and 33%

throughout S1a while higher values are observed during S1b (35 – 43%). Before the S1 layer, *E. huxleyi* shows high abundances that oscillate between 88 and 92% in the Adriatic Sea. At the base of S1, it decreases from 92 to 83% and exhibit fluctuations of 5 – 6% on average throughout S1a. Lower abundances of 83% occur during the interruption at 8.2 cal. ka BP, after which there is an increase located between 7.9 – 7.1 cal. ka BP. Close to S1 top, *E. huxleyi* fluctuates between 88 and 85%.

Syracosphaera spp. shows lower abundances during sapropel than non-sapropel layers in the Levantine/Ionian and Aegean Seas (not data in the Adriatic Sea) (Fig. 6e). In the Aegean Sea, *Syracosphaera spp.* drops abruptly at 10.4 cal. ka BP (from 8 to 3%). It shows low values (3%) throughout S1, with the exception of two negative excursions at 9.3 – 8.8 and 7.4 – 6.8 cal. ka BP. In the Levantine/Ionian Sea, a negative trend is observed for *Syracosphaera spp.*, during S1a (from 4 to 1.5%) while a continuous increase occurs during S1b (from 1.5 to 4%).

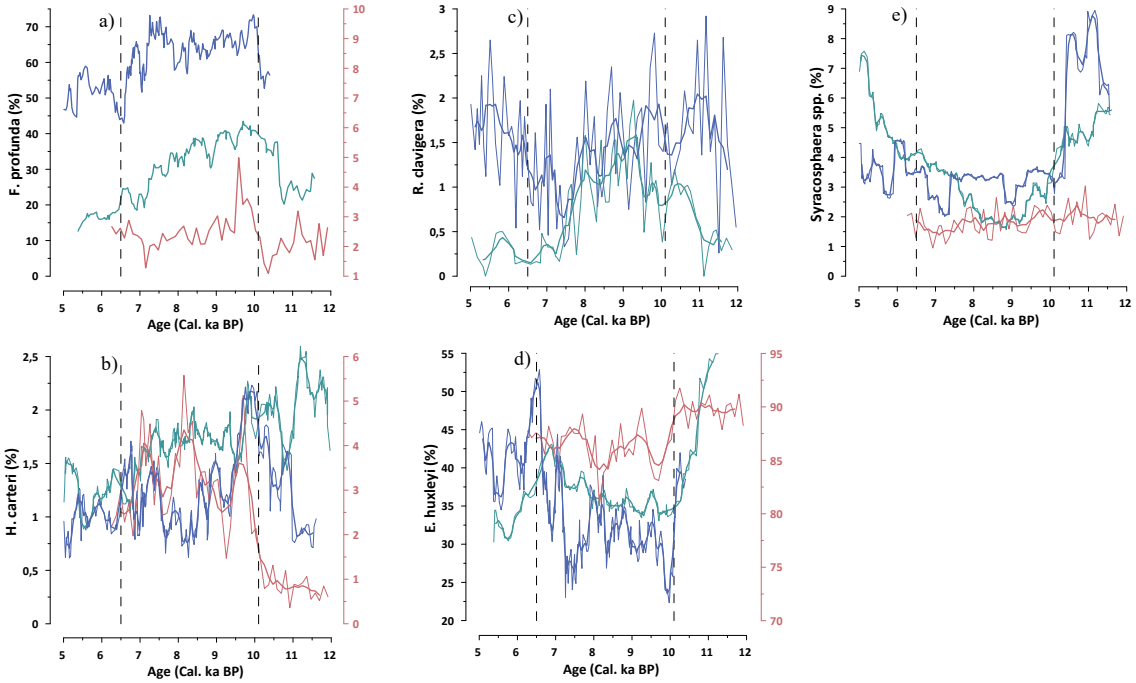

Fig. 6. Variations of selected coccolith plotted vs age. Relative abundances of (a) *Florisphaera profunda*, (b) *Helicosphaera carteri*, (c) *Rhabdosphaera clavigera*, (d) *Emiliania huxleyi*, and (e) *Syracosphaera spp.* The color lines represent the different sub-basins: Levantine/Ionian Sea (green); Aegean Sea (blue); Adriatic Sea (red). Vertical dashed black lines show the S1 interval (10.1 – 6.5 cal. ka BP).

5.4. Stable Isotopes

The isotopic signals are obtained from planktonic foraminifera *Globigerinoides ruber* and *Globigerina bulloides* (Fig. 7). The isotopic records are represented by 52 cores in the eastern Mediterranean Sea, 40 cores from the Levantine/Ionian Sea, 8 cores from the Adriatic Sea, and 4 cores from the Aegean Sea. The stable oxygen and carbon isotope signals show a similar trend with higher values in pre-sapropel layers and lighter values during the sapropel S1 (Fig. 7a-f).

A rapid decrease of $\delta^{18}O_{bulloides}$ is observed in Levantine/Ionian and Adriatic Seas (Fig. 7c). In particular, between 11.5 and 9.6 cal. ka BP an abrupt decrease of 1.5‰ in Adriatic and Levantine/Ionian Seas is noted. From about 9.6 until 8 cal. ka BP (Fig. 7c), the $\delta^{18}O_{bulloides}$ oscillates around a mean of 1.28‰ with a minimum of 1.05‰ centered on 9.5 cal. ka BP in the Adriatic Sea. In contrast, lighter values of $\delta^{18}O_{bulloides}$ are observed in the Levantine/Ionian Sea, which oscillates around 1.01‰. Between 8 and 6.8 cal. ka BP in the Adriatic Sea, the $\delta^{18}O_{bulloides}$ are lighter reaching a minimum of 1.01‰, followed by a gradual increase until the S1 top (~0.4 ‰). In the Levantine/Ionian Sea, from 8 cal. ka BP until the top of S1, a continuous increase of $\delta^{18}O_{bulloides}$ is observed (~0.4 ‰).

Before the onset of S1, $\delta^{18}O_{ruber}$ a negative shift of ~1.8‰ in the whole Mediterranean Sea (Fig. 7a). In detail, $\delta^{18}O_{ruber}$ values are heavier in the Adriatic Sea than Levantine/Ionian and Aegean Seas, even if low fluctuations are observed in all sub-basins during S1. In the Adriatic Sea, $\delta^{18}O_{ruber}$ shows fluctuations around 0.5 ‰ during S1 with two negative shifts at 9.4 (-0.26‰) and 7.3 cal. ka BP (-0.4‰). These, close to the top of S1, show heavier values (0.6‰). Between 9.6 and 7.2 cal. ka BP, the $\delta^{18}O_{ruber}$ values fluctuate with an average of -0.44‰ in the Levantine/Ionian Sea, followed by a gradual increase (0.7‰) towards heavier values close to S1 end. Noteworthy, two abrupt increase (~0.4) of $\delta^{18}O_{ruber}$ values are noted between 8.5 – 8.1 and 7.4 – 7.2 cal. ka BP. In the Aegean Sea, $\delta^{18}O_{ruber}$ shifts back to lighter values through the onset of S1, which then decrease of 0.6‰ at 9.4 cal. ka BP. From 9.4 cal. ka BP onwards, the $\delta^{18}O_{ruber}$ values show an average of ~0.2‰ with the exception of negative $\delta^{18}O_{rube}$ shift towards lighter values between 8.5 – 8 and 7.4 – 7.1 cal. ka BP, and close to S1 end.

In the Adriatic and Levantine/Ionian Seas, $\delta^{18}O_{ruber}$ is lighter within S1 than in pre-sapropel sections (Fig. 7b). In contrast, lighter $\delta^{18}O_{ruber}$ values are observed before S1 than within S1 in the Aegean Sea. In detail, between 11.5 and 9.6 cal. ka BP, $\delta^{18}O_{ruber}$ increases of 0.6‰ in the Aegean Sea, which is followed by a jump to values as low as -0.53‰ at ~8.2 cal. ka BP. From 8 cal. ka BP onwards, the $\delta^{18}O_{ruber}$ continuously increases also

above the S1 top. In the Adriatic Sea, between 10.5 and 8.5 cal. ka BP, $\delta^{18}O_{ruber}$ reveals an abrupt negative shift of 0.8‰, which then increases (0.2‰) between 8.5 and 8 cal. ka BP. From 8 cal. ka BP up to the S1 top, $\delta^{18}O_{ruber}$ values oscillate around -0.1‰. In the Levantine/Ionian Sea, before the onset of S1, the $\delta^{18}O_{ruber}$ shifts to lighter values (0.77 to -0.2‰) than terminates within S1. Then, $\delta^{18}O_{ruber}$ oscillates between -0.1 and 0.04‰ throughout S1 with two intervals that show the lighter $\delta^{18}O_{ruber}$ values between 8.8 – 8.2 and 7.4 – 7.2 cal. ka BP. Noteworthy, an abrupt increase of $\delta^{18}O_{ruber}$ occurs to S1 top.

The $\delta^{13}C_{ruber}$ records show a shift from enriched values (0.75‰) in pre-sapropel layers to more depleted values (-0.25 in the Levantine/Ionian and -0.65 in the Aegean Seas) during S1 (Fig. 7d). In detail, between 11 and 10.1 cal. ka BP the Aegean Sea is characterized by 1‰ decrease in $\delta^{13}C_{ruber}$ followed by a lighter increase of 0.5‰ between 10.1 and 9.4 cal. ka BP and shifts back to lighter values (-0.64‰) at ~8.8 cal. ka BP. From 8.7 cal. ka BP onwards, the $\delta^{13}C_{ruber}$ values continuously increase, with the exception of two intervals at 8.4 – 8 and 7.6 – 7 cal. ka BP, which are characterized by lighter values. In the Levantine/Ionian Sea, the $\delta^{13}C_{ruber}$ values show a gradual decrease of 0.4‰ between 10.8 and 10.1, which remains around 0.6‰ until 9.3 cal. ka BP. The lighter values of $\delta^{13}C_{ruber}$ are noted between 9.3 and 8.6 cal. ka BP, with a minimum of 0.36‰ centered on 8.7 cal. ka BP. From 8.6 cal. ka BP onwards, the $\delta^{13}C_{ruber}$ values continuously increase up to the S1 top.

In the Levantine/Ionian Sea, the $\delta^{13}C_{ruber}$ shifts to lighter values (0.61 to 0.3‰) between 11 and 10.1 cal. ka BP, which then remains with a mean of 0.35‰ until about 9.1 cal. ka BP (Fig. 7e). The lighter values (0.30-0.14‰) of $\delta^{13}C_{ruber}$ are noted between 9.1 and 8 cal. ka BP, which are interrupted by an increase towards heavier values at 8.4 cal. ka BP. From 8 cal. ka BP onwards, the $\delta^{13}C_{ruber}$ values continuously increase until 7.7 cal. ka BP, where the values oscillate between 0.55 and 0.45‰ until the sapropel end.

Before the onset of S1, the $\delta^{13}C_{bulloides}$ records shifts to lighter values (-0.44 to -1.91‰) than terminates within S1 (Fig. 7f). Then, from 9.6 cal. ka BP onwards, the $\delta^{13}C_{bulloides}$ values show an average of about -1.65‰ with un light increase of 0.15‰ at 9 cal. ka BP. Close to S1 top, the $\delta^{13}C_{bulloides}$ values increase towards reaching a minimum of -1‰ at 5.7 cal. ka BP.

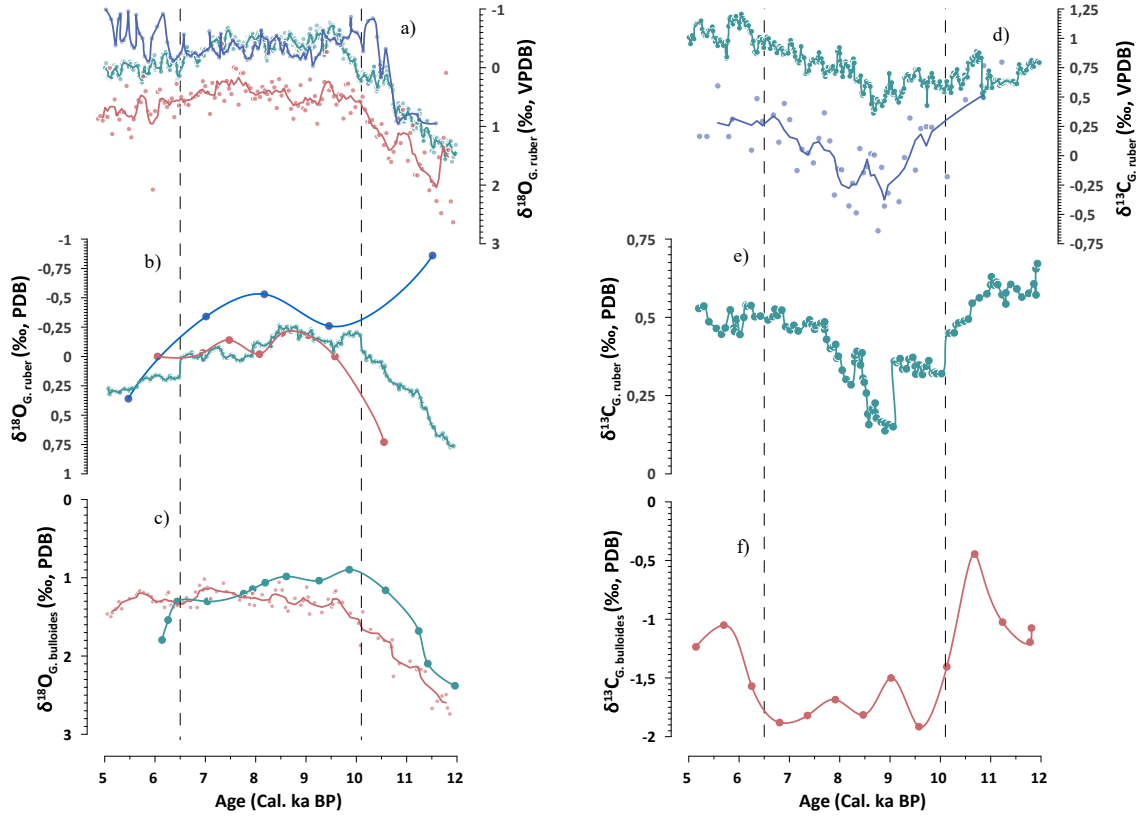

Fig. 7. Stable oxygen and carbon isotope records plotted vs age. (a) $\delta^{18}O_{ruber}$ in ‰ VPDB. (b) $\delta^{18}O_{ruber}$ in ‰ PDB. (c) $\delta^{18}O_{bulloides}$ in ‰ PDB. (d) $\delta^{13}C_{ruber}$ in ‰ VPDB. (e) $\delta^{13}C_{ruber}$ in ‰ PDB. (f) $\delta^{13}C_{bulloides}$ in ‰ PDB. The color lines represent the different sub-basins: Levantine/Ionian Sea (green); Aegean Sea (blue); Adriatic Sea (red). Vertical dashed black lines show the S1 interval (10.1 – 6.5 cal. ka BP).

6. Discussion

6.1. Eastern Mediterranean Sea at the time of sapropel S1 deposition: stratification

Our data show clear trends in the proxies that allow us to recognize several recurrent features characterizing the sapropel S1. Among them, the increased inflow of depleted-$\delta^{18}O/\delta^{13}C$ water is clearly recorded before/during sapropel S1 throughout the eastern Mediterranean Sea (Fig. 8a-b). Also, the indicators associated with changes in the water surface salinity (*O. universa*, *T. sacculifer*, and *Syracosphaera spp.*) and humidity (Ti/Al) suggest increased freshwater input to the Mediterranean Sea (Fig. 8c). In addition, a significant increase of *H. carteri*, *R. clavigera*, and *L. granifera*, and the absence/reduction of planktonic foraminifera as *G. inflata* and *G. truncatulinoides* (Fig. 8) evidenced the freshwater input in the eastern Mediterranean Sea that led to buoyancy gain at the sea surface, thus causing water column stratification. Worth of note is the scarcity of *T. sacculifer* and *O. universa* in the Adriatic Sea (Fig. 8e-f), indicating a lesser freshwater input in this sub-basins.

It is known that the sapropel deposition is linked to orbital forcing, notably to minimum precession/maximum insolation, which are related to humid climate conditions that resulted in enhanced runoff into the Mediterranean Sea and, as a consequence, enhanced water column stratification (Emeis et al., 2000; Grant et al., 2016; Marino et al., 2009; Rohling et al., 2015; Rossignol-Strick, 1985). Although the principal sources for surface-water freshening in the eastern Mediterranean Sea are still disputed, the most important sources are (*1*) the runoff along the North African Margin (produced by the intensification of the North African Monsoon) through the Nile River (Rossignol-Strick, 1983; Emeis et al., 2000; Scrivner et al., 2004; Ducassou et al., 2009; Revel et al., 2010; Hennekam et al., 2015) and Saharan wadi systems (Rohling et al., 2002; Scrivner et al., 2004; Osborne et al., 2008; Wu et al 2016, 2017), (*2*) the enhanced precipitation in Northern Mediterranean Borderlands (NMB) (Bosmans et al., 2015; Desprat et al., 2003; Filippidi & De Lange, 2019; Kallel et al., 1997; Kotthoff et al., 2008b; Rohling & Hilgen, 1991; Toucanne et al., 2015) and, (*3*) ice-volume/sea-level changes that led the inflow of less saline Atlantic waters into the Mediterranean Sea (Cornuault et al., 2018; Grant et al., 2016; Grimm et al., 2105; Rohling et al., 2015; Zwiep et al., 2018).

Consequent to the stratification, a DCM development is evidenced by *F. profunda* and *N. pachyderma* right cooling + *N. incompta* increase during S1 deposition (Fig. 8g-h), however, little variations are observed among the sub-basins. According to Rossignol-Strick (1985) and Kemp et al. (1999), the input of freshwater contributed to enhanced nutrients supply to the system, enhancing primary production as a result of the well-developed DCM (Castradori, 1993; Kemp et al., 1999; Meier, 2004; Rohling & Gieskes, 1989; Weldeab et al., 2003). Earlier studies (Castradori, 1993; Negri & Giunta, 2001; Corselli et al., 2002; Principato et al., 2003) suggested the presence of a DCM only at the beginning of sapropel deposition while Meier et al. (2004) supported its existence throughout S1.

Our results show a DCM throughout the whole S1 but with little variations that are evident at 9.5, 8.5, and 7.5 cal. ka BP. These events are governed by cold phases compatible with millennial-scale Bond cycles (Bond et al., 1997, 2001) in the Levantine/Ionian and Aegean Seas (Fig. 11; see Section 6.3). These cold events decreased the freshwater input to the eastern Mediterranean Sea (observed by lower abundances of *T. sacculifer* and *O. universa*; Fig. 8e-f), that in turn, reduced the water column stratification (observed by lower abundances of *R. clavigera*, *H. carteri*, and *L. granifera*;

Fig. 8i-k), and reactivated the intermediate/deep water formation. This pattern could explain the observed fluctuations of the DCM (Fig. 8g-h and Fig. 11).

Instead, in the Adriatic Sea, a peak of *F. profunda* at the beginning of S1, suggests the occurrence of a DCM (Castradori, 1993) but, at the same time, the absence of *N. pachyderma* right cooling (+ *N. incompta*) suggests, according to Rohling & Gieskes (1989), that the DCM was not so strong (Fig. 8g-h, Panel III). Thus, the short or even absent DCM in the Adriatic Sea is suggestive of a lesser freshwater input than in the Levantine/Ionian and Aegean Seas. This is consistent with the low abundances of *T. sacculifer* and *O. universa* observed in the Adriatic Sea (Fig. 8e-f, Panel III) that confirm the lesser freshwater input in this sub-basin. If we consider the freshwater input, due to the NMB precipitation (Bard et al., 2002; Kallel et al., 1997, 2000; Toucanne et al., 2015; Zanchetta et al., 2007) and the sea-level rise due to the Atlantic waters entering the Mediterranean (Grant et al., 2016; Grimm et al., 2015; Cornuault et al., 2018), we may expect a similar influence in all the sub-basins, instead the North African Monsoon (Nile River) would have had a lesser influence over the Adriatic Sea.

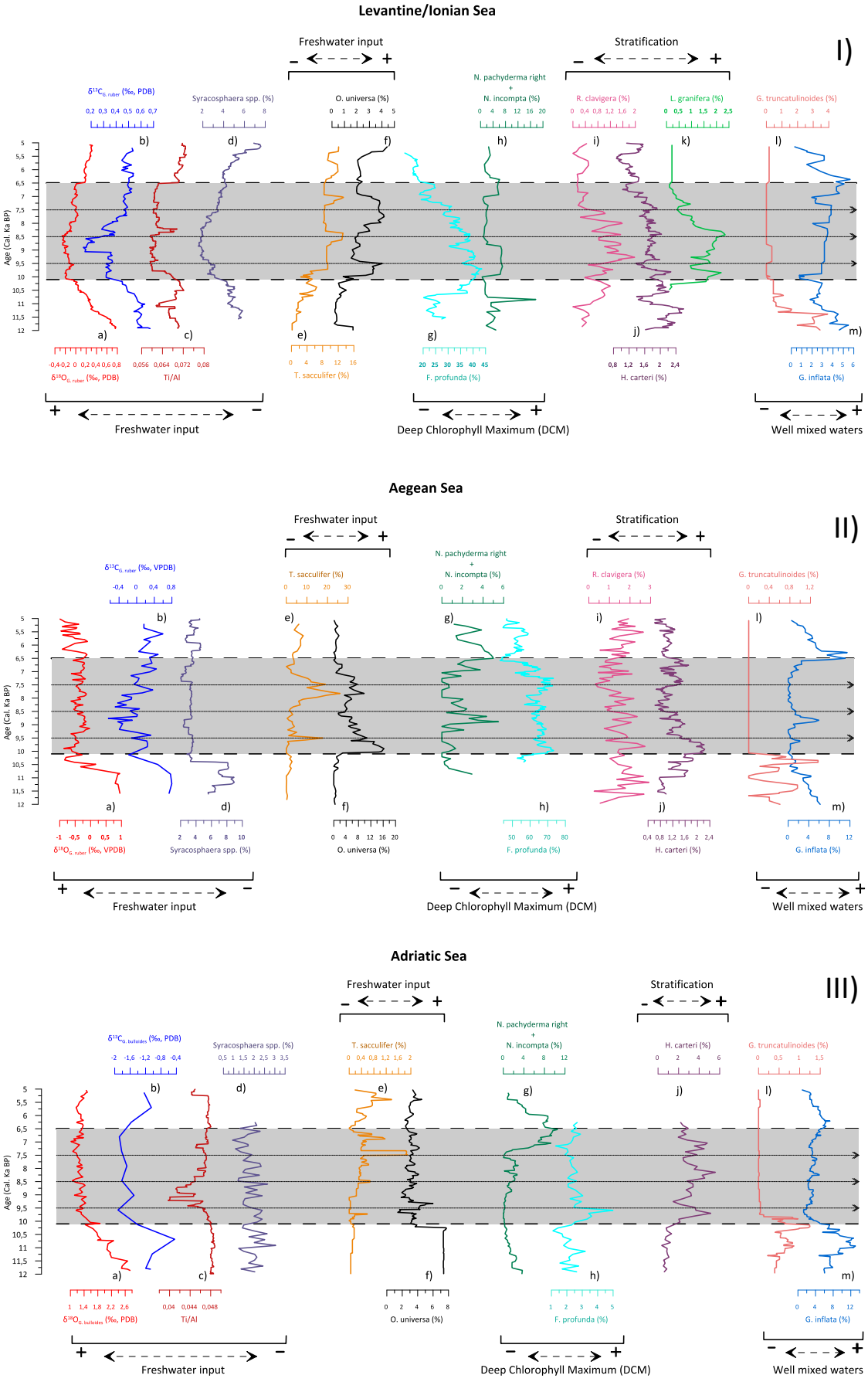
Levantine/Ionian Sea
I)
Freshwater input
Stratification
Age (Cal. Ka BP)
Freshwater input
Deep Chlorophyll Maximum (DCM)
Well mixed waters
Aegean Sea
II)
Freshwater input
Stratification
Freshwater input
Deep Chlorophyll Maximum (DCM)
Well mixed waters
Adriatic Sea
III)
Freshwater input
Stratification
Freshwater input
Deep Chlorophyll Maximum (DCM)
Well mixed waters

Fig. 8 (left). Overview of selected planktonic foraminifera, coccolithophore, geochemical and isotopic data from Levantine/Ionian (Panel I), Aegean (Panel II), and Adriatic (Panel III) Seas plotted against age. a) Stable oxygen and b) carbon records; c) Ti/Al; relative abundances of d) *Syracosphaera spp.*, e) *Trilobatus sacculifer,* f) *Orbulina universa,* g) *Neogloboquadrina pachyderma + Neogloboquadrina incompta,* h) *Florisphaera profunda,* i) *Rhabdosphaera clavigera,* j) *Helicosphaera carteri,* k) *Leonella granifera* (related to stratification waters (Meier, 2004; Vink, 2004)), l), and m) *Globorotalia truncatulinoides*. The gray band indicates the extent of S1 (10.1 – 6.5 cal. ka BP). The horizontal lines mark the Bond events 6 (~9.5 ka BP) and 5 (~8.5 – 8.2 ka BP) and the 7.5 – 7.4 ka BP event (Filippidi et al., 2016).

6.2. Eastern Mediterranean Sea at the time of the sapropel S1 deposition: redox condition and oxygen availability

The sapropels layers present distinct geochemical compositions that provided information about the bottom/pore water conditions, which are key controls on organic matter preservation. To describe the different redox-conditions, we followed the definitions used by Filippidi et al. (2016): 'Anoxic' conditions exhibit the complete lack of dissolved oxygen and sulphide waters. 'Suboxic' conditions consider reducing conditions without the complete lack of dissolved oxygen but require the presence of additional electron acceptors (Fe(III)), and 'oxic' conditions means the complete oxygenation of the bottom waters.

Our results (Fig. 9) show the enrichments of redox-sensitive elements (U, V, and Mo), S, and Fe during sapropel deposition on the eastern Mediterranean Sea indicating that suboxic/anoxic conditions were established at the sediment/water interface. In addition, a phase of preconditioning of the eastern Mediterranean Sea is observed between ~11 cal. ka BP and the onset of S1. This phase is characterized by suboxic conditions where we observed the uptake redox-sensitive elements into the sediment accompanied by the pyrite formation (S/Al and Fe/Al enrichments; Fig. 9) while a gradual deterioration of the oxygen conditions is described by the oxygen index (OI; Fig. 9a). These results are in line with previous studies (Filippidi & De Lange, 2019; Schmiedl et al., 2010; Tachikawa et al., 2015; Tesi et al., 2017) and confirmed that the deterioration of the eastern Mediterranean Sea circulation begun almost 1 thousand years before S1 formation started, and it was key for the sapropel deposition (Grimm et al., 2015). During the S1 interval, anoxic conditions were settled only in the Levantine/Ionian Sea considering the OI values (Fig. 9a), however, these results could be influenced by the depth of the cores. Thus, considering that the whole eastern Mediterranean basin has been predominantly oxygen-free below ~1,800 m (De Lange et al., 2008) and that the OI

results are obtained from cores between 1,400 – 2,300 m in the Levantine/Ionian, 260 – 1,500 m in the Aegean Sea, and 260 – 1,085 m in the Adriatic Sea, exclusively the Levantine/Ionian bottom waters were anoxic while the Aegean and Adriatic were low oxygenated.

Based on the results shown in Fig. 9, it seems that the reducing conditions during S1b (8 – 6.5 cal. ka BP) were not as severe as during S1a (10.1 – 8.5 cal. ka BP). These differences affected the organic matter preservation and underline as the suboxic/anoxic conditions are key controls on sapropel deposition. This is consistent with the differences (geochemical) observed among the sub-basins (Fig. 3, Section 5.1), where higher organic matter preservation is observed in the Levantine/Ionian Sea (anoxic conditions) than Aegean and Adriatic Seas (suboxic conditions).

Previous studies (De Lange et al., 2008; Reitz et al., 2006; Thomson et al., 1995; Van Santvoort et al., 1996) demonstrated that sapropels could suffer syngenetic processes as pyrite formation that occurs before S1, but besides that, postdepositional processes as oxidation front (burn-down) that occurs at the top of S1 may also affect the primary composition of the sediments. The latter occurred after the penetration of oxygen into the sediment, which produced the consequent oxidation of the organic matter and pyrite (De Lange et al., 1989; Filippidi & De Lange, 2019; Pruysers et al., 1991; Reitz et al., 2006). Upon oxygenation, high levels of dissolved manganese precipitate into the sediment originating a distinct Mn-peak called 'Marker Bed'(Ariztegui et al., 2000; Cita et al., 1989; De Lange et al., 1989, 2008; Thomson et al., 1995; Van Santvoort et al., 1996). According to Filippidi & De Lange (2019), the oxidations front is recognizable between the Marker Bed and the preceding Mn/Al peak below the Marker Bed that unfortunately was not recorded in all the cores studied. As our data are the result of the mean data obtained from different cores, this caused the Marker Bed not being positioned exactly at the top of S1 due to the differences between the two peaks. Thus, looking at the Mn/Al peak (Fig. 9b) and the low values of TOC, Fe/Al, and S/Al during S1 (Fig. 10a and 9e-f), an oxidation front is evident in all sub-basins, although it was not possible to detail its extension.

Despite this limitation it is possible to pinpoint the recovery of the deep-water formation, which was fairly synchronous at ~6.5 cal. ka BP in the whole eastern basin (Chapter 2). However, the OI show progressive oxygenation started around ~7.5 cal. ka BP in the shallow cores of the Adriatic and Levantine/Ionian Sea, and at ~7 cal. ka BP in

the intermediate cores of the Aegean Sea (Fig. 9a). According to results shown in Chapter 2 and previous studies (Schmiedl et al., 2010; Tesi et al., 2017), this progressive oxygenation follows a bathymetric gradient, starting at shallow sites and gradually extended to greater water depths.

Our data also show that during the S1 interval, suboxic conditions (sulphide waters + low oxygen; Fig. 9) occur in the Aegean and Adriatic Seas while anoxic conditions (sulphide waters + depleted oxygen; Fig. 9) are observed in the Levantine/Ionian Sea. Noteworthy this latter basin is characterized by high depth in the Levantine/Ionian Sea (Fig. 14), and we hypothesize that depth is responsible for lower oxygen concentration and therefore the main driver for anoxic conditions

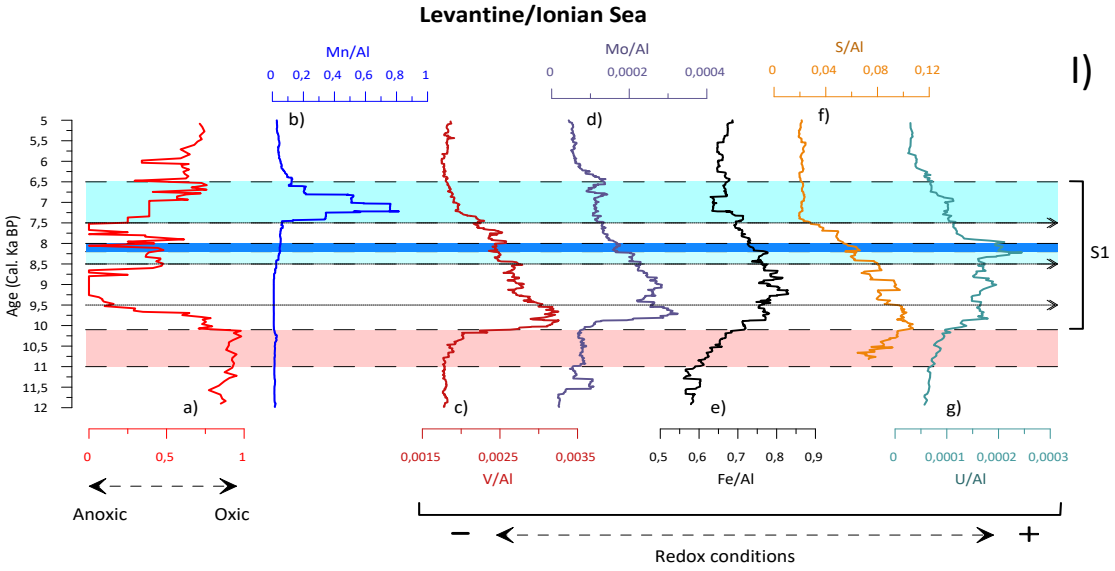
Levantine/Ionian Sea
I)
Mn/Al
0 0,2 0,4 0,6 0,8 1
Mo/Al
0 0,0002 0,0004
S/Al
0 0,04 0,08 0,12
b)
d)
f)
Age (Cal. Ka BP)
5 5,5 6 6,5 7 7,5 8 8,5 9 9,5 10 10,5 11 11,5 12
S1
a)
c)
e)
g)
0 0,5 1
Anoxic
Oxic
0,0015 0,0025 0,0035
V/Al
0,5 0,6 0,7 0,8 0,9
Fe/Al
0 0,0001 0,0002 0,0003
U/Al
−
+
Redox conditions

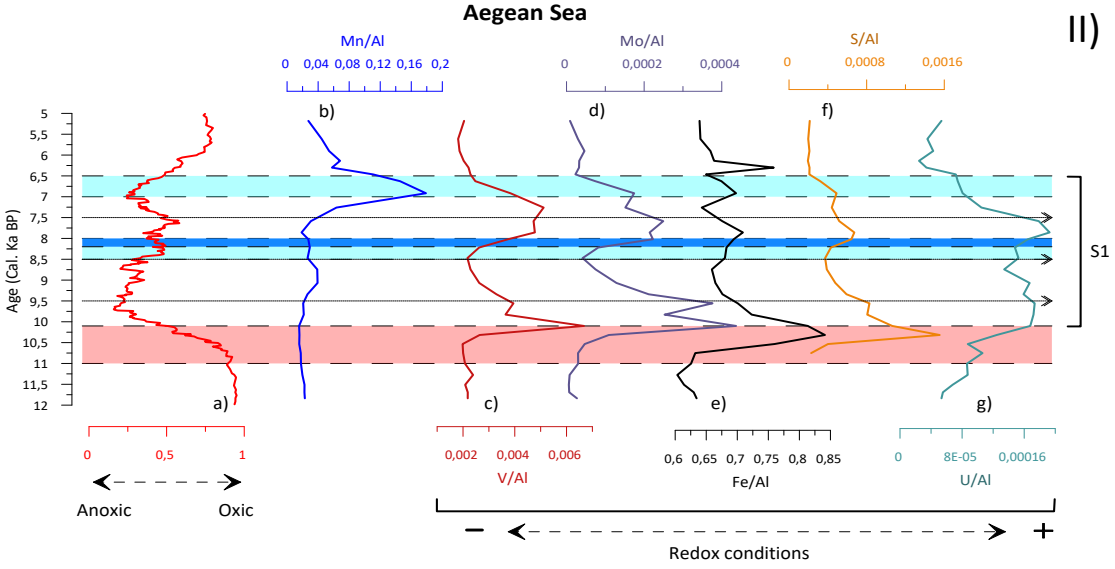
Aegean Sea
II)
Mn/Al
0 0,04 0,08 0,12 0,16 0,2
Mo/Al
0 0,0002 0,0004
S/Al
0 0,0008 0,0016
b)
d)
f)
Age (Cal. Ka BP)
5 5,5 6 6,5 7 7,5 8 8,5 9 9,5 10 10,5 11 11,5 12
S1
a)
c)
e)
g)
0 0,5 1
Anoxic
Oxic
0,002 0,004 0,006
V/Al
0,6 0,65 0,7 0,75 0,8 0,85
Fe/Al
0 8E-05 0,00016
U/Al
−
+
Redox conditions

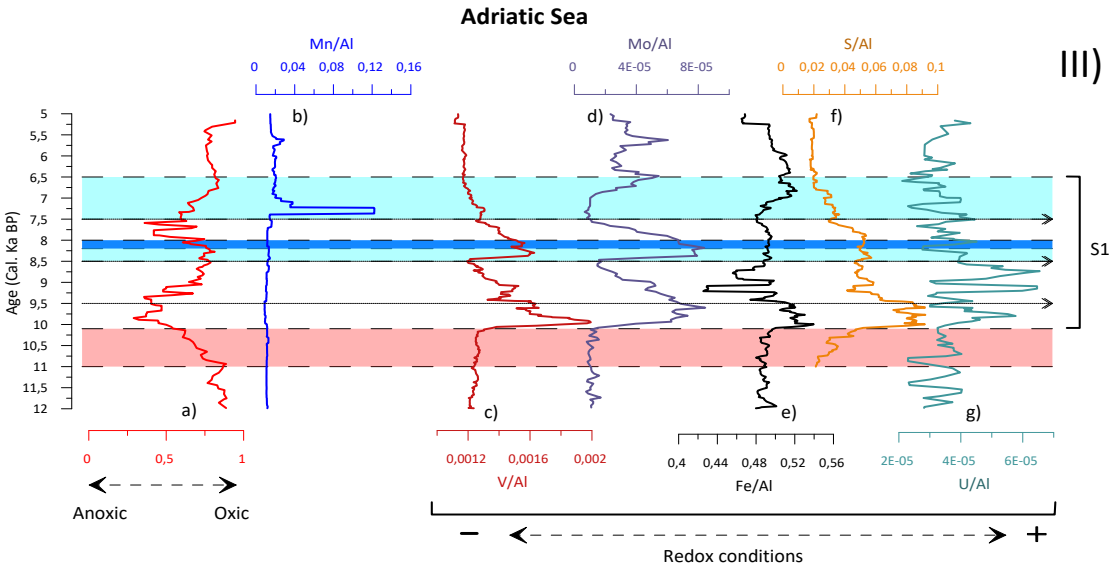
Adriatic Sea
III)
Mn/Al
0 0,04 0,08 0,12 0,16
Mo/Al
0 4E-05 8E-05
S/Al
0 0,02 0,04 0,06 0,08 0,1
b)
d)
f)
Age (Cal. Ka BP)
5 5,5 6 6,5 7 7,5 8 8,5 9 9,5 10 10,5 11 11,5 12
S1
a)
c)
e)
g)
0 0,5 1
Anoxic
Oxic
0,0012 0,0016 0,002
V/Al
0,4 0,44 0,48 0,52 0,56
Fe/Al
2E-05 4E-05 6E-05
U/Al
−
+
Redox conditions

Fig. 9 (left). Oxygen content and reducing conditions during S1 in the Levantine/Ionian (Panel I), Aegean (Panel II), and Adriatic (Panel III) Seas. a) Foraminifera-based oxygen index (OI, (Schmiedl et al., 2010), and distribution of geochemistry proxies b) Mn/Al, c) V/Al, d) Mo/Al, e) Fe/Al, f) S/Al, and U/Al plotted against age. The red band indicates the onset of the suboxic condition. The blue bands mark the reoxygenation event observed while the dark blue band mark the event 8.2 (Casford et al., 2003). The horizontal lines mark the Bond events 6 (~9.5 ka BP) and 5 (~8.5 – 8.2 ka BP) and the 7.5 – 7.4 ka BP event (Filippidi et al., 2016).

6.3. Eastern Mediterranean Sea at the time of the sapropel S1 deposition: Primary production and export production

Our results show significant enrichment in TOC and Ba/Al (export-production) during S1 as the result of enhanced primary production (Fig. 10). Significant differences are however observed in both TOC and Ba/Al indicators among the sub-basins (Fig. 3a-b and Fig. 10), where the highest values are observed in the Levantine/Ionian Sea (deep cores; see Fig. 14) than in the Aegean and Adriatic Seas (shallow and intermediate cores; see Fig. 14). It is therefore evident that the deeper cores (characterized by severe reducing conditions) show enhanced preservation (see Section 6.2) of TOC and Ba/Al, which explains the differences observed among the sub-basins.

On the other hand, the higher export production recorded in the sediment is the result of enhanced primary production in the intermediate (DCM development) and surface waters. Ba/Al results indicate enhanced primary production (Fig. 10), but the coccolithophore record show alternating fluctuations of superficial (*E. huxleyi*) and intermediate waters (*F. profunda*) (Fig. 11). In detail, the distribution pattern of the species related to DCM development (*F. profunda* and *N. pachyderma* + *N. incompta*) and surface water production (*E. huxleyi*, *G. bulloides,* and *T. quinqueloba*) show that the pycnocline/nutricline depth changed with high-frequency pacing that may be compatible with millennial-scale Bond events (Bond et al., 1997, 2001). In fact, Fig. 11 shows that these fluctuations occurred approximately every 1 ka, that is exactly the periodicity that characterizes the cooling phases related to the final steps of the deglaciation (IRD events) in the North Atlantic. These are in turn associated with a decrease in solar activity (Bond et al., 1997, 2001) or changes in ocean circulation (Broecker et al., 2001; Debret et al., 2007; McManus et al., 1999). These short-lived events were noted in several publications (Desprat et al., 2013, Incarbona & Di Stefano, 2019; Kotthoff et al., 2008a; Marino et al., 2009) showing that such changes affected the Mediterranean Sea and borderlands. According to Brayshaw et al. (2010), the winter Mediterranean hydroclimate depends on the Mediterranean storm activity, which is influenced by the position and intensity of the

North Atlantic storm. Thus, these cold events may have contributed to reduce winter precipitations hence causing lesser freshwater discharge into the Mediterranean Sea during the sapropel S1 deposition (Bosmans et al., 2015; Simon et al., 2017; Toucane et al., 2015). This possibly led to a reduction of the water column stratification and the reactivation of LIW/deep-water formation. At the same time, enhanced surface water production due to absence/reduction of DCM characterized these cold events favouring the increase of *E. huxleyi* evidenced in our data. (Fig. 11).

Fig. 10 (right). The surface, intermediate, and (export)production during S1 in the Levantine/Ionian (Panel I), Aegean (Panel II), and Adriatic (Panel III) Seas. Geochemical data and relative abundances of planktonic foraminifera and coccolithophore plotted against age. a) TOC (%), b) Ba/Al, c) *Florisphaera profunda*, d) *Neogloboquadrina pachyderma* + *Neogloboquadrina incompta,* e) *Emiliania huxleyi,* f) *Globigerina bulloides*, and g) *Turborotalita quinqueloba*. The gray band indicates the extent of S1 (10.1 – 6.5 cal. ka BP). The horizontal lines mark the Bond events 6 (~9.5 ka BP) and 5 (~8.5 – 8.2 ka BP) and the 7.5 – 7.4 ka BP event (Filippidi et al., 2016).

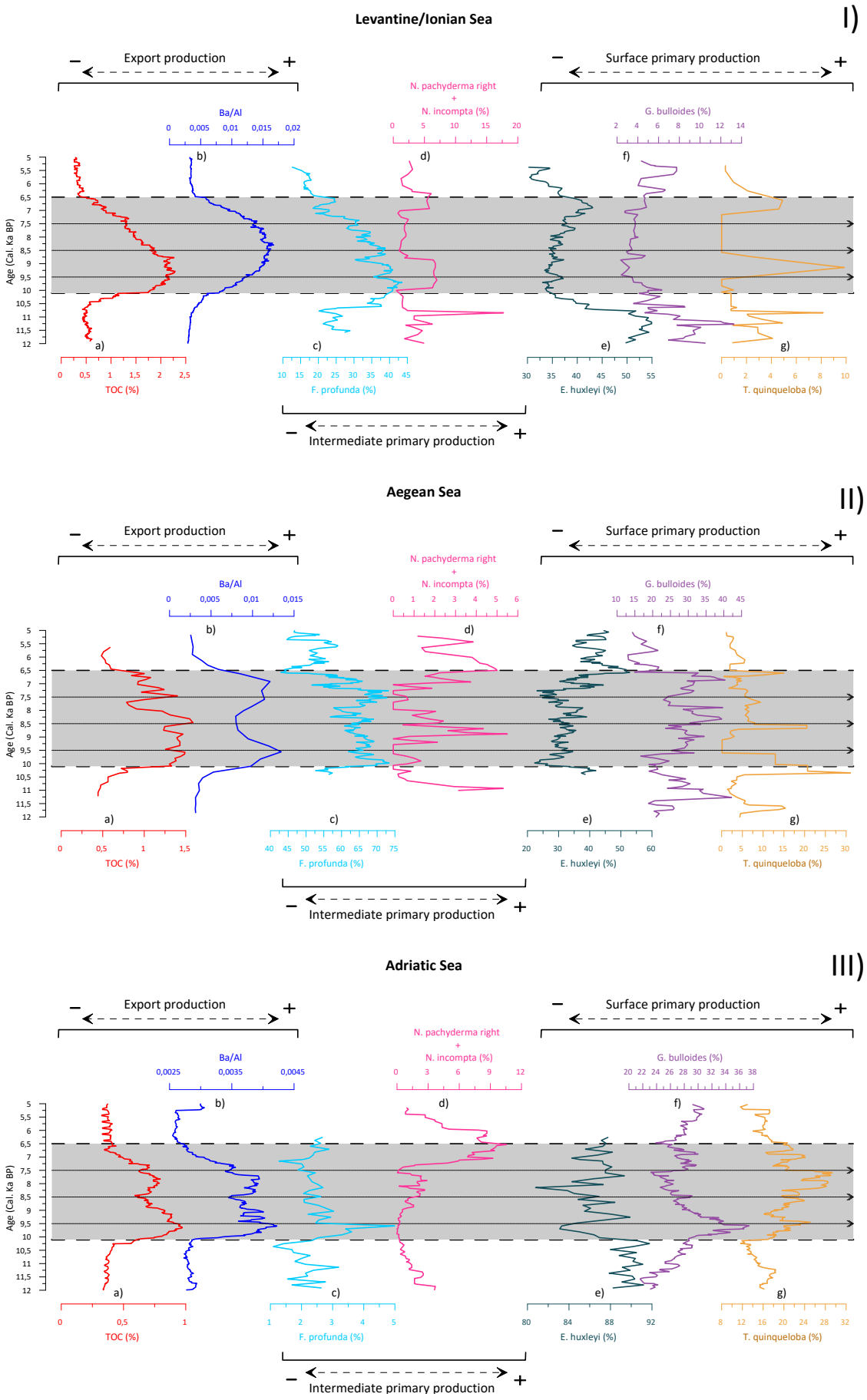
I)
Levantine/Ionian Sea
Export production
Surface primary production
Ba/Al
N. pachyderma right + N. incompta (%)
G. bulloides (%)
Age (Cal. Ka BP)
TOC (%)
F. profunda (%)
E. huxleyi (%)
T. quinqueloba (%)
Intermediate primary production
II)
Aegean Sea
Export production
Surface primary production
Ba/Al
N. pachyderma right + N. incompta (%)
G. bulloides (%)
Age (Cal. Ka BP)
TOC (%)
F. profunda (%)
E. huxleyi (%)
T. quinqueloba (%)
Intermediate primary production
III)
Adriatic Sea
Export production
Surface primary production
Ba/Al
N. pachyderma right + N. incompta (%)
G. bulloides (%)
Age (Cal. Ka BP)
TOC (%)
F. profunda (%)
E. huxleyi (%)
T. quinqueloba (%)
Intermediate primary production

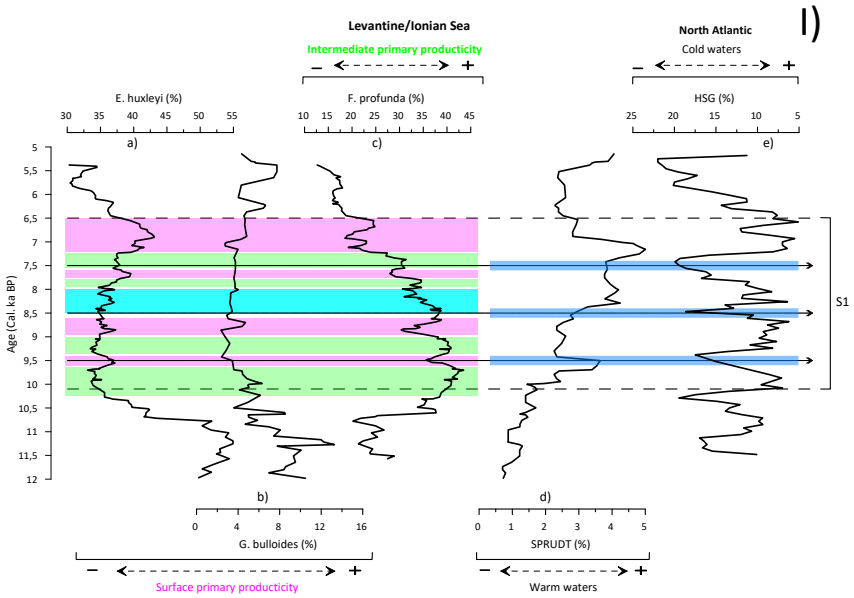
I)
Levantine/Ionian Sea
Intermediate primary productivity
North Atlantic
Cold waters
E. huxleyi (%)
F. profunda (%)
HSG (%)
a)
c)
e)
Age (Cal. ka BP)
S1
b)
d)
G. bulloides (%)
SPRUDT (%)
Surface primary productivity
Warm waters

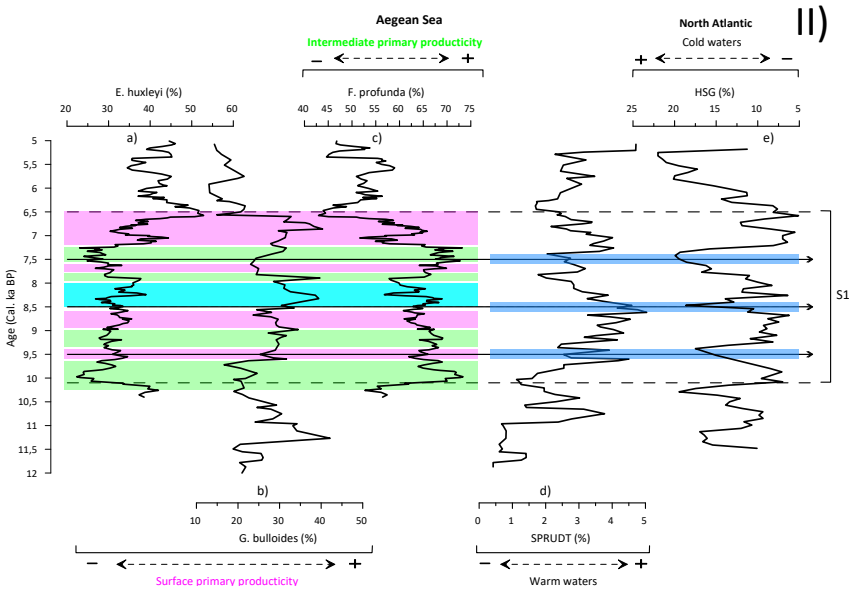
II)
Aegean Sea
Intermediate primary productivity
North Atlantic
Cold waters
E. huxleyi (%)
F. profunda (%)
HSG (%)
a)
c)
e)
Age (Cal. ka BP)
S1
b)
d)
G. bulloides (%)
SPRUDT (%)
Surface primary productivity
Warm waters

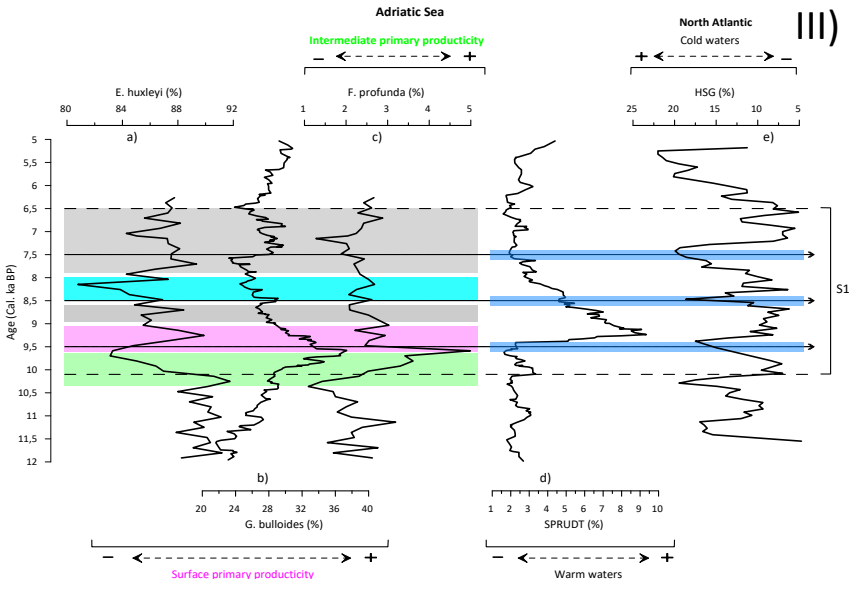
III)
Adriatic Sea
Intermediate primary productivity
North Atlantic
Cold waters
E. huxleyi (%)
F. profunda (%)
HSG (%)
a)
c)
e)
Age (Cal. ka BP)
S1
b)
d)
G. bulloides (%)
SPRUDT (%)
Surface primary productivity
Warm waters

Fig. 11 (left). The surface/intermediate primary production and cold events during S1 in the Levantine/Ionian (Panel I), Aegean (Panel II), and Adriatic (Panel III) Seas. Relative abundances of a) *Emiliania huxleyi*, b) *Globigerina bulloides*, c) *Florisphaera profunda*, d) SPRUDT-group (Rohling et al. (1993): *Globigerinella siphonifera*, *Hastigerina pelagica*, *Globoturborotalita rubescens*, *Orbulina universa*, *Globigerina digitata*, *Globoturborotalita tenella*, and *Trilobatus sacculifer*) that characterize warm waters, in contrast with the cold waters indicate by e) stacked Hematite Stained Grains (HSG %) from North Atlantic records (Bond et al., 2001). The green bands mark the intervals with intermediate primary production while the pink bands indicate surface primary production. The blue band marks the reoxygenation interval (~8.5 – 8 cal. ka BP). The intervals where the information is not clearly recorded, it is indicated with a grey band. The horizontal blue lines mark the Bond events 6 (~9.5 ka BP) and 5 (~8.5 – 8.2 ka BP) and the 7.5 – 7.4 ka BP event (Filippidi et al., 2016).

The cold events observed at 8.5 and 7.5 cal. ka BP (Fig. 11) are probably associated with well-known 8.2 and 7.4 ka events (Ariztegui et al., 2000; Filippidi et al., 2016, 2019; Rohling et al., 1997; Tesi et al., 2017; Triantaphyllou et al., 2016). These events caused the temporary resumption of the deep-water formation, causing the interruption of the sapropel deposition (Bar-Matthews et al., 1999; De Rijk et al., 1999; Kotthoff et al., 2008a; Marino et al., 2009; Rohling et al., 1997). Our data show a similar event at 9.5 cal. ka BP that resulted in little variations of the (export)production (Fig. 10a-b) and moderate redox conditions (Fig. 9c-g), with the possible improvement of bottom-water oxygenation (Fig. 9a).

6.4. Primary production or organic matter preservation?

An old and still unresolved debate characterizing sapropel studies deals with the question productivity or preservation (Cheddadi et al., 1991; Cramp & O'Sullivan, 1999; Demaison & Moore, 1980; Emeis & Weissert, 2009; Howell & Thunell, 1992; Murat & Got, 2000; Rohling, 1994; Strohle & Krom, 1997). In this section, we will try to address this issue by analyzing the total organic carbon (TOC), which represents the single largest constituent of organic matter, and the Ba/Al in order to understand why our results show the Levantine/Ionian Sea more anoxic and productive than Aegean and Adriatic Seas. The questions which arise are: 1) Were the records observed in the Levantine/Ionian Sea influenced by local forcing or there were other factors? 2) Was then increased productivity or, was better preservation?

The principal factors responsible for the accumulation and preservation of the organic matter are related to (*1*) the rate of deposition; (*2*) the amount of export production, and (*3*) the rate of degradation, which is related to the bottom-waters

conditions (i.e., oxic, dysoxic, and anoxic) and the water depths. A number of different studies have reported a positive correlation between the sedimentation rate and TOC under oxic bottom-waters in both modern and ancient marine sediments (e.g., Betts & Holland, 1991; Calvert, 1987; Canfield, 1989; Müller & Suess, 1979; Tyson, 2005). However, according to numerous studies (Algeo & Heckel, 2008; Betts & Holland, 1991; Brumsack, 1980; Jones, 1983; Mercone et al., 2000; Tyson, 1995, 2001, 2005), an inverse o neutral correlation between TOC and sedimentation rate in anoxic/suboxic conditions was observed. Considering the results shown in Fig. 12, where the TOC exhibited values ranging from 1.2 and 3.2 % within sedimentation rates between 4 and 6 cm/ka, we suggest that the sedimentation rate was not a crucial factor to explain the higher organic matter values observed in S1.

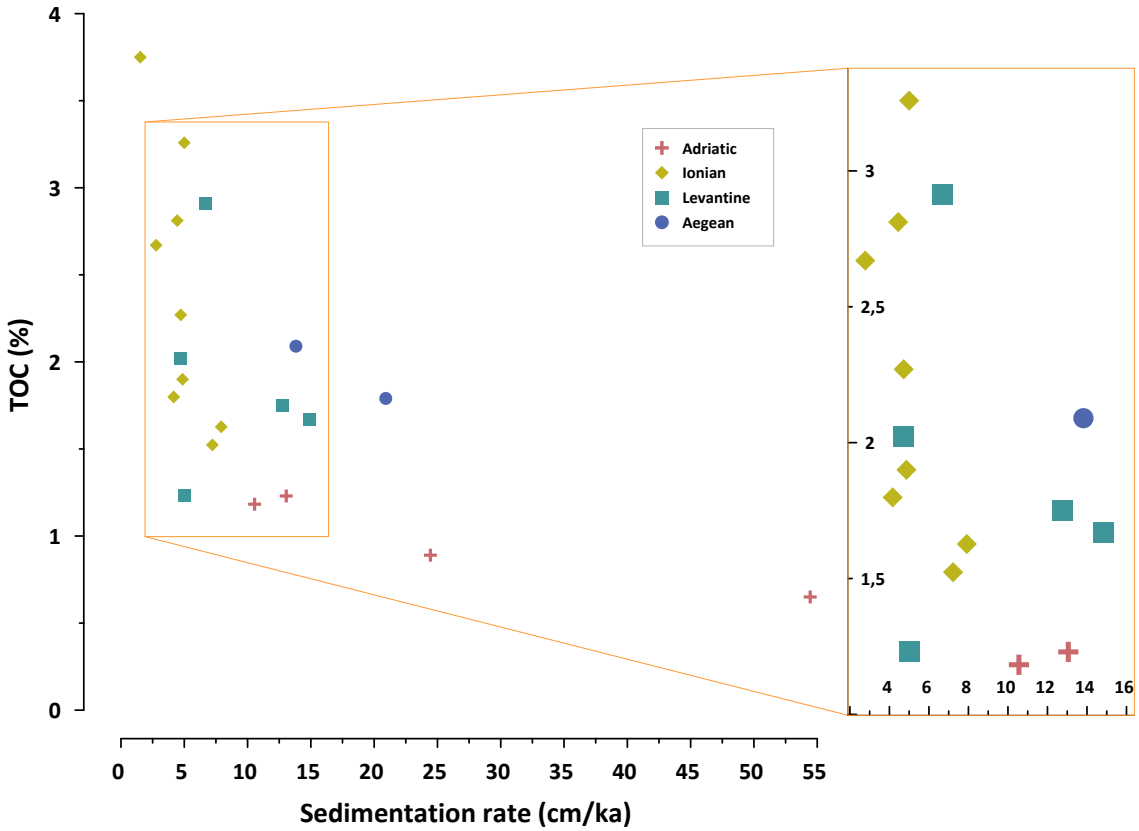

Fig. 12. Maximum organic carbon in S1 versus the sedimentation rate. The thicknesses of cores were calculated based on the interval of Barium enrichment during S1, avoiding false thicknesses due to post-depositional processes.

Previous studies (Anastasakis & Stanley, 1984; Anastasakis, 1988; De Lange et al., 2008; Murat, 1991; Murat & Got, 2000; Rohling, 1994) observed a clear relationship between TOC and water depth. Our results are therefore in line with these studies since we observe an increase of TOC with depth (Fig. 13). Considering the low relation

between TOC and sedimentation rate, two (main) factors can be responsible in the TOC concentrations: (*1*) variations in degradation processes of organic matter in the water column and at the sediment-water interface (related to water conditions); and (*2*) increase of the (export)production.

The sapropel deposition occurs under reducing conditions (anoxic/suboxic) that allowed enhanced organic matter preservation. Previous studies (De Lange et al., 2008; Filippidi & De Lange., 2019; Tesi et al., 2017) observed more severe reducing conditions in deeper than shallow cores. According to the Fig. 14, we observed that the deeper cores are located mainly in the Levantine/Ionian Sea, and this is consistent with the results shown in Fig. 9 and Fig. 10, where the indicators related to redox conditions and (export)production show higher values in the Levantine/Ionian Sea than Aegean and Adriatic Seas. Accordingly, the higher TOC values located in the Levantine/Ionian Sea are associated with deeper cores, characterized by severe reducing conditions that enhanced the organic matter preservation.

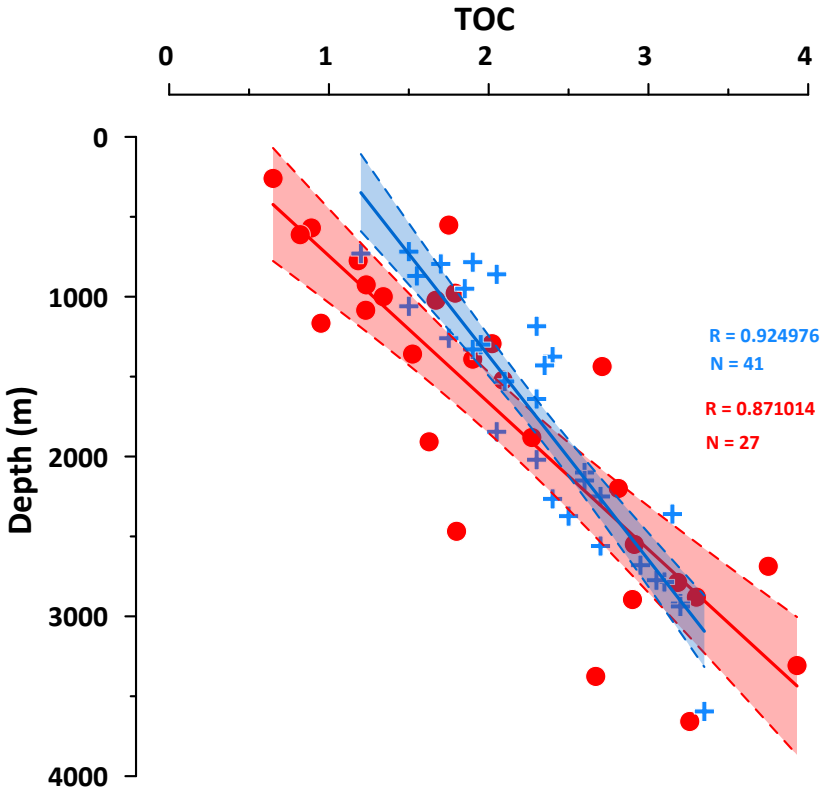

Fig. 13. Maximum total organic carbon of S1 versus water depth. The blue dots represent TOC (wt%) from Murat & Got (2000). The red dots represent TOC (% and wt%) obtained from *BEyOND* database (Amezcua-Buendía et al., 2019). Dashed blue and red lines represent the 1σ confidence bounds of the linear regressions (solid blue and red line). In order to avoid misunderstandings with the postdepositional processes (oxidation of the organic carbon), the maximum values of TOC are used.

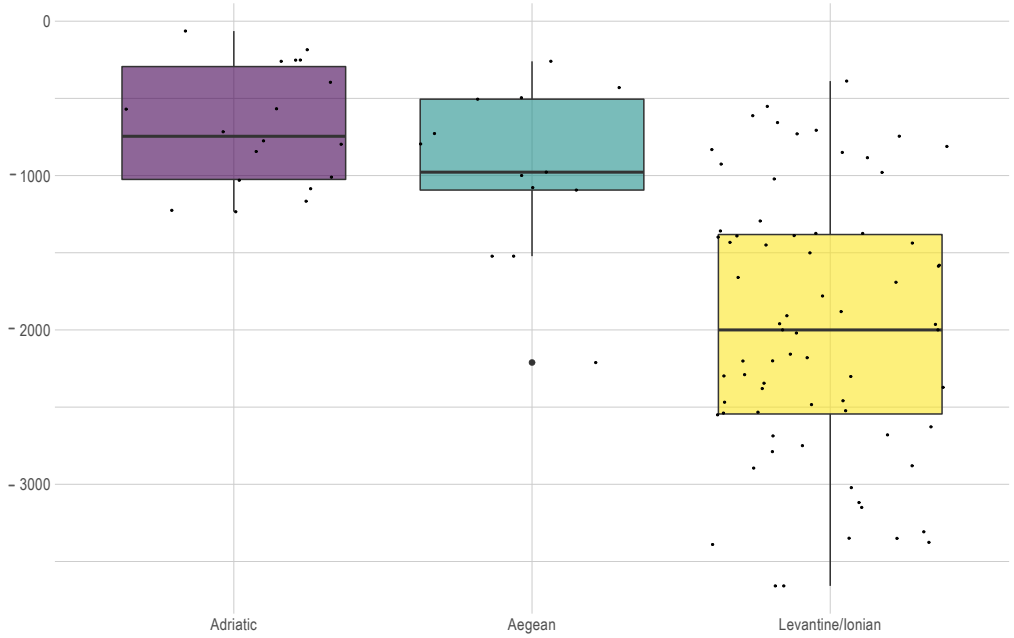

Fig. 14. Boxplots for the depth of the cores according to the different sub-basins. The cores used are described in Table 1.

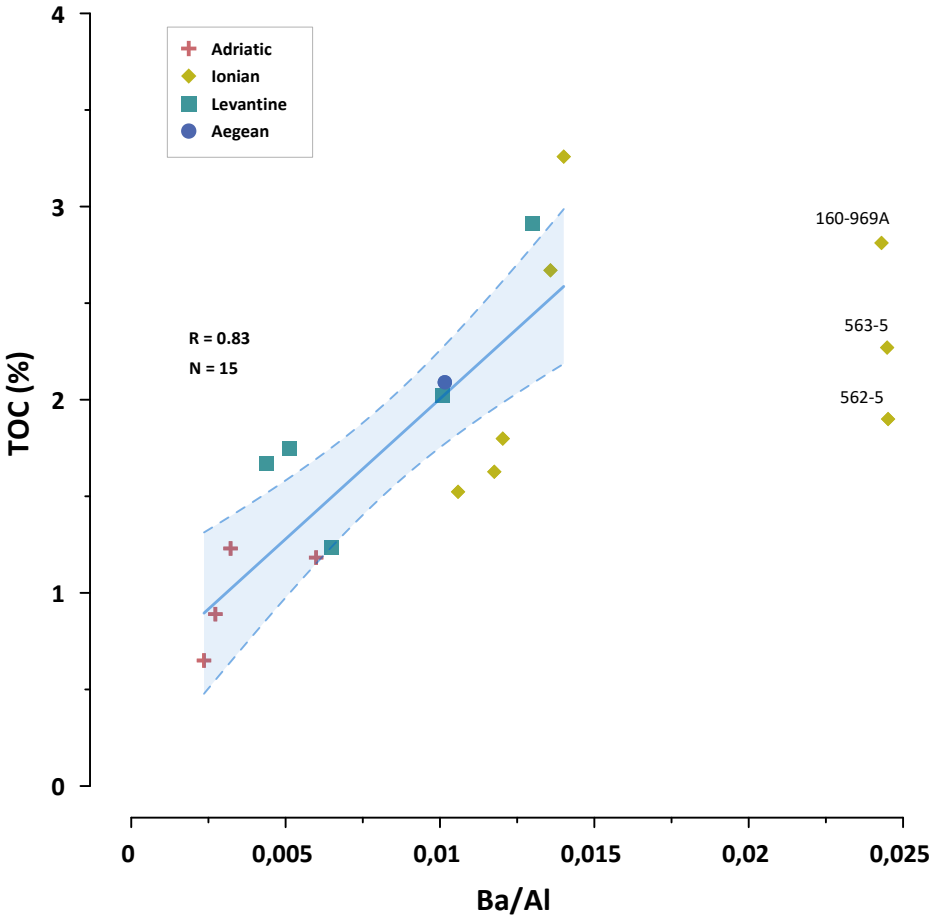

Fig. 15. Correlation between TOC and Ba/Al in the different sub-basins.

During the sapropel deposition, the increase of primary production resulted in enhanced (export)production (TOC and Ba/Al) (Fig. 10). In Fig. 15, both TOC and Ba/Al show a positive correlation except for three cores located in the Ionian Sea (562-5; 160-969A; and 563-5; more details in Table 1). By examining the reasons for this difference, we observed that the three cores were affected by postdepositional processes (burn-down), which oxidized the original organic matter. These differences are also observed in Fig. 16, where high concentrations of TOC (Fig. 16a) are observed in the northeastern Ionian Sea and south of Crete and Cyprus, while high values of Ba/Al (Fig. 16b) are located in central/south of Ionian and the Libyan Sea.

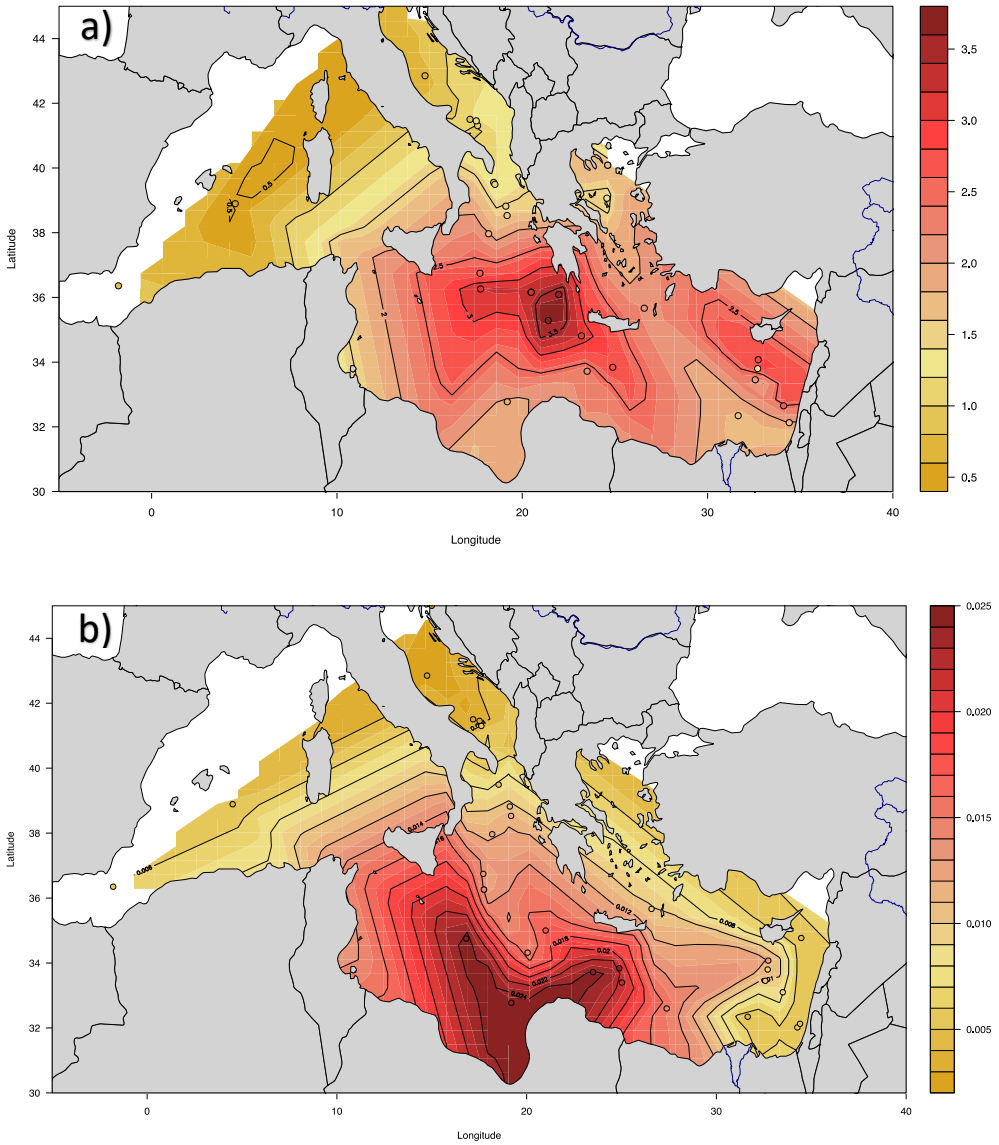

Fig. 16. a) Isoline map of the maximum value of TOC during S1 deposition. b) Isoline map of the average values of Ba/Al during S1 deposition. The maps are obtained using RStudio software version 1.2.5009 (RStudio, 2019) and the packages "Akima" (Akima et al., 2016), "mapdata" (Deckmyn, 2018), and "maps" (Deckmyn, 2018).

To understand whether these differences between TOC and Ba/Al in these three cores are associated with enhanced primary production (based on local forcing) or deficient preservation, we recalculated the original organic carbon oxidized. The organic carbon was calculated according to Müller & Suess (1977) based on (R) primary productivity from the equation:

$$\% \text{ Org. C} = \frac{0.003 \cdot R \cdot S^{0.30}}{P_S\,(1-\Phi)} \tag{1}$$

The data of (S) sedimentation rate, (P_s) dry bulk sediment, and (Φ) porosity for the cores 160-969A were obtained from Gallego-Torres et al., 2011. For the cores 562-5 and 563-5, the sedimentation rates were obtained from Meier et al. (2004), while that dry bulk sediments and porosity data were estimated values from Emeis et al. (1996) and Anastasakis & Stanley (1986) in the eastern Mediterranean Sea.

The primary productivity was calculated from the new production (6), and this from the Ba fluxes (5). In order to evaluate the Ba fluxes (F_{Ba}), it was necessary to calculate the biogenic barium (Ba_{bio}) and the accumulation rates of biogenic barium (AR Ba_{bio}), respectively. Ba_{bio} was calculated by subtracting the concentration of terrigenous Ba from the total Ba concentration analyzed (Ba_{tot}):

$$Ba_{bio} = Ba_{tot} - (Al \cdot Ba/Al_{Aluminosilicate}) \tag{2}$$

In sediment where the conditions were variable, it was necessary to calculate the AR Ba_{bio}:

$$AR\ Ba_{bio} = Ba_{bio} \cdot MAR/1000 \tag{3}$$

where the mass accumulation rates (MAR g/cm^2/ka) are the result of the sedimentation rate (S; cm/ka) and dry bulk density (g/cm^3)

$$MAR = S \cdot P_S \tag{4}$$

Pfeifer et al. (2001) presented an equation which used the equations (3) and (4):

$$F_{Ba} = \frac{AR\ Ba_{bio}}{0.209} \cdot \log(\text{MAR}) - 0.213 \tag{5}$$

Based on Ba flux (5), Francois et al. (1995) calculated the new production (P_{new}):

$$P_{new} = 1.95(F_{Ba})^{1.41} \tag{6}$$

Primary productivity (R) was calculated according to equation from Eppley & Peterson (1979) based on P_{new}:

$$R = 20(P_{new})^{0.5}$$

The new TOC values (Fig. 17) show a better correlation (R=0.88) between TOC and Ba/Al than those observed in Fig. 15 (R=0.83).

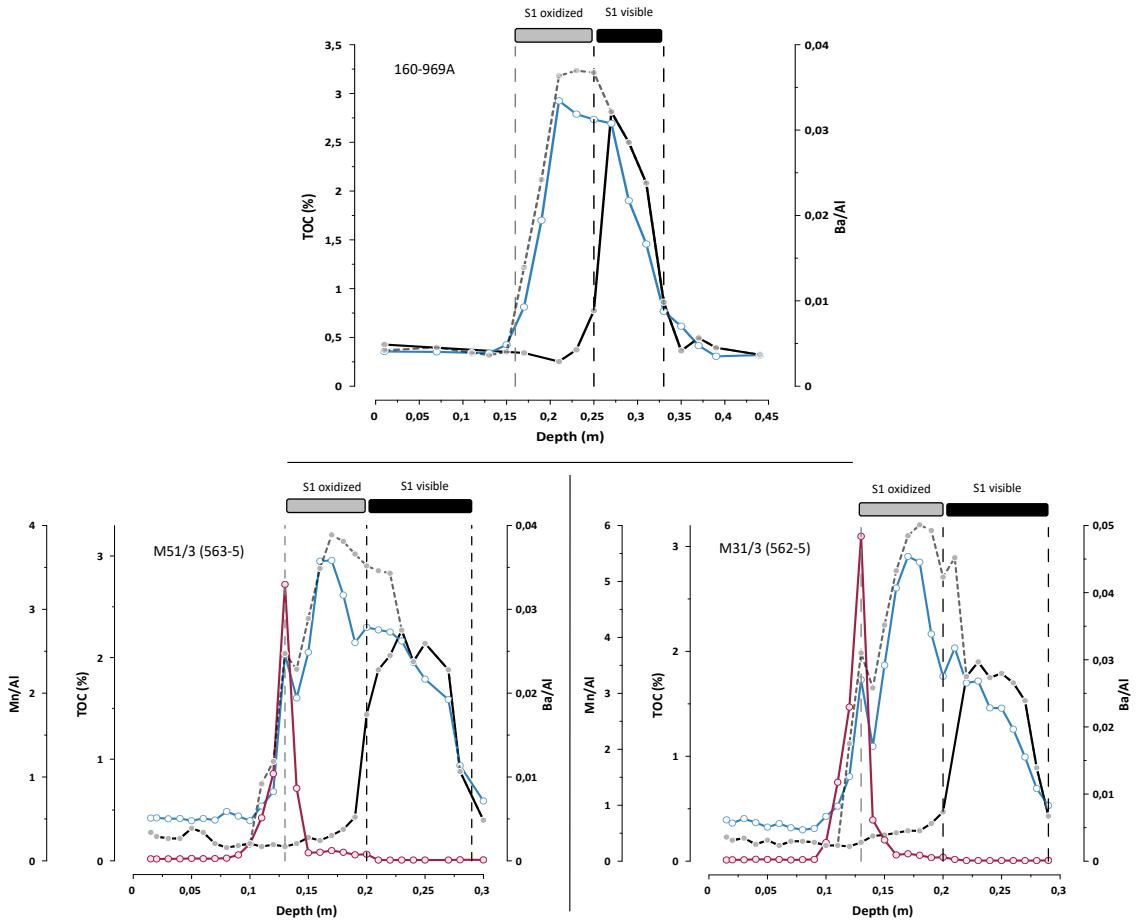

Fig. 17. Elemental profiles: TOC (%; black line), Ba/Al (blue line) and Mn/Al (red lines) for the cores 563-5, 562-5, and 160-969A. The dashed grey lines show the TOC values recalculated (oxidized organic matter).

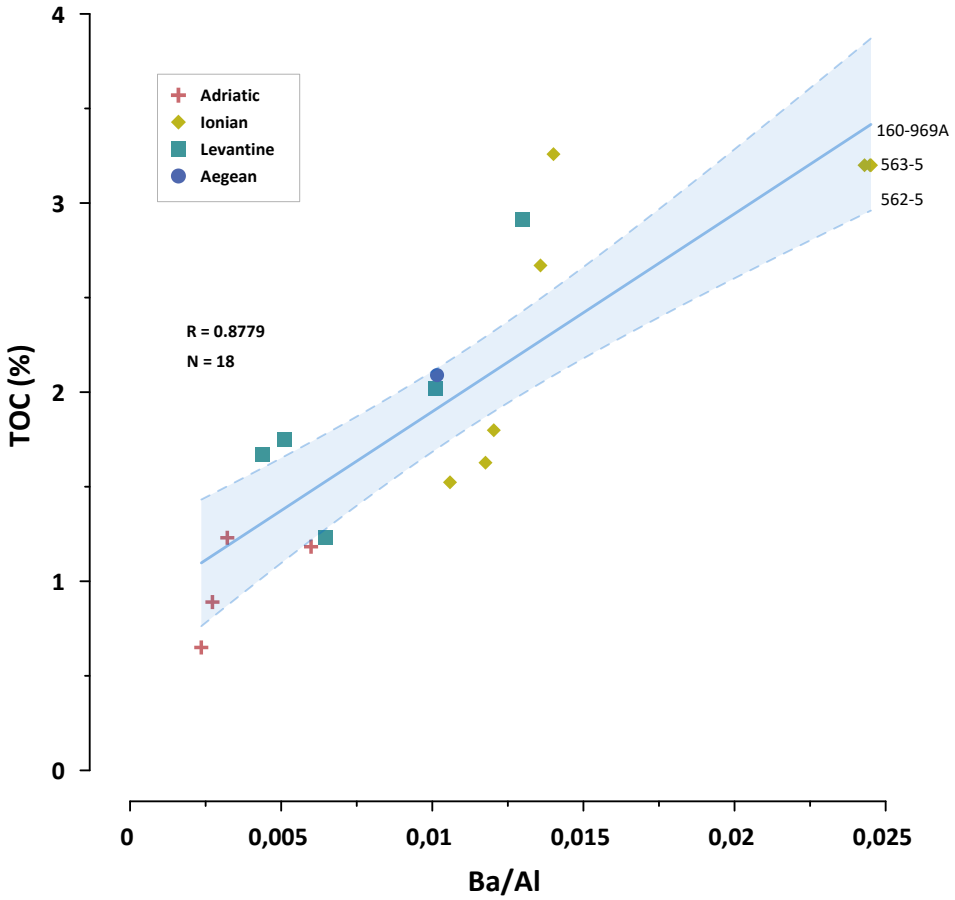

Fig. 18. Correlation between TOC values recalculated and Ba/Al in the different sub-basins.

Also, the maps shown in Fig. 19 were modified with the new TOC values. Now, we can see that the high Ba/Al values observed in the Ionian and Libyan Seas (included south of Crete and Cyprus) are related to high TOC values in these areas. These results suggest higher (export)production (related to primary production) in the Ionian and Libyan Seas (including south Cretan and Cyprus), as was suggested recently by Incarbona et al. (2019). However, the high Ba/Al (~0.025) values obtained in the three cores (Fig. 18), showed similar TOC contents (~3%) that cores with lower Ba/Al values (~0,014). These differences could be related to water depths, which affected organic matter preservation. Also, the Ba/Al increase with the water depth as a result of the longer residence time of sinking organic matter in the water column and thus more time for barite formation (Dymond et al., 1992; von Breymann et al., 1992; Weldeab et al., 2003). This is consistent with the results observed in Fig. 20. Nevertheless, we also find that the higher Ba/Al values (e.g., core 562-5, 563-5, or 160-969A) were not seen in the deeper waters. This pattern could be explained by the influence of local forcing as the presence of cyclonic and anticyclonic gyres in the Libyan Sea (anticyclone in the Gulf of Sirte) and

south of Crete (Crete cyclone and Ierapetra anticyclone), which further increased productivity in these areas. Thus, we can explain the differences observed between TOC and Ba/Al contents in the cores 562-5 (1391 m), 563-5 (1881 m), and 160-969A (2200 m) as a result of the organic matter preservation. Despite the high productivity observed in these areas, the bottom water anoxia was less severe due to the depths of the cores, causing lower preservation of the organic matter.

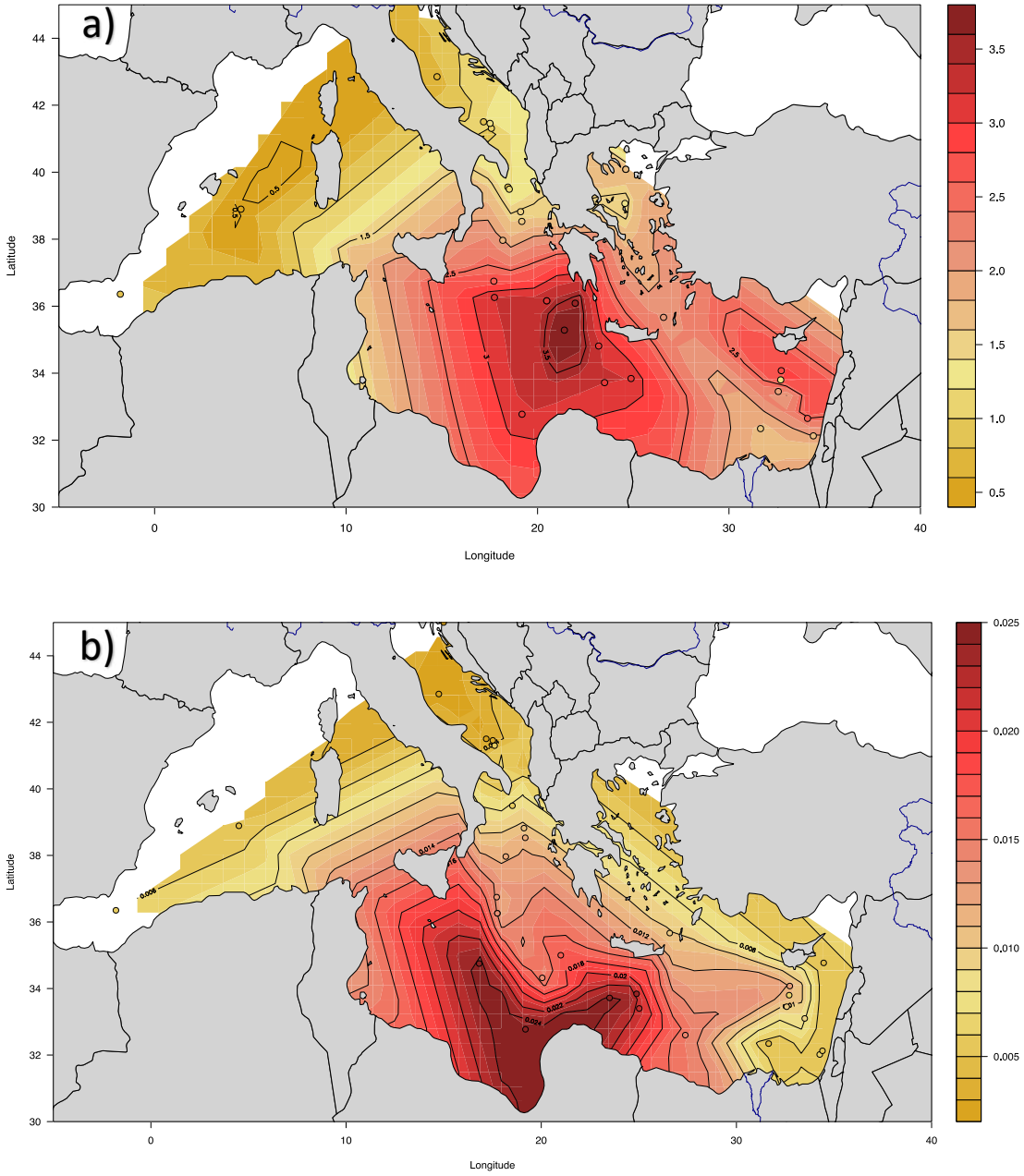

Fig. 19. a) Isoline map of the (recalculated) maximum value of TOC during S1 deposition. b) Isoline map of the average values of Ba/Al during S1 deposition. The maps are obtained using RStudio software version 1.2.5009 (RStudio, 2019) and the packages "Akima" (Akima et al., 2016), "mapdata" (Deckmyn, 2018), and "maps" (Deckmyn, 2018).

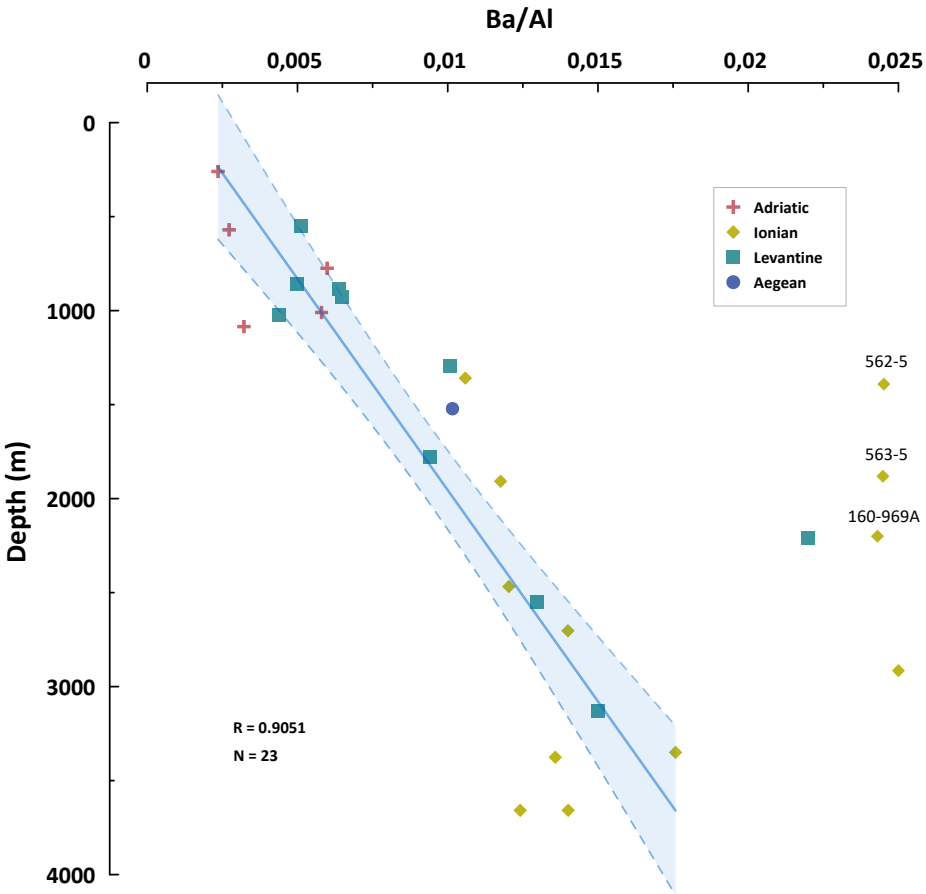

Fig. 20. Average of Ba/Al values during S1 versus water depth.

7. Conclusion

We use a novel approach for the study of sapropel S1 based on the integration of a large amount of data by Data Analytics techniques. The results show a large input of freshwater in the whole eastern Mediterranean Sea that caused enhanced production (and export-production) and increase the water column stratification as a result of increased surface water buoyancy. These conditions reduced the intermediate/deep water formation that led to oxygen-starved conditions and organic matter preservation.

The S1 deposition is preceded by a phase of preconditioning that appeared at least 1 ka before in the whole eastern Mediterranean Sea, which shows a gradual deterioration of the deep-water ventilation. Also, the hydrographic changes contributed to DCM development, which varied with high-frequency pacing that may be compatible with millennial-scale Bond cycles. These periodic oscillations (~ 1 ka) are related to cold events at 9.5, 8.5 (related to 8.2 event), and 7.5 cal. ka BP that triggered the restart of intermediate waters, and consequently deep-water formation, which caused improvement of oxygen conditions in the deep water. Thus, our results confirm the close interplay

between mid- (North Atlantic) and low-latitudes (monsoon) climate systems during the S1 deposition.

During the S1 deposition, increased productivity was widespread in the whole eastern Mediterranean Sea, furthermore, the primary production could be further increased by local forcings as was observed in the Libyan Sea and south of Crete. However, this additional production (and export-production) was not reflected in higher organic matter content into the sediment as a result of low preservation. Thus, the organic matter content in S1 is more a result of organic matter preservation, which increases with the depth, than organic matter supply (production and export-production). This is consistent with the results obtained in the Levantine/Ionian Sea, which is characterized by deeper cores. The high organic matter content obtained in the Levantine/Ionian Sea is linked to higher preservation as a result of more severe redox conditions established in deeper waters.

Overall, the Mediterranean seawater circulation and climate were strongly related to local and global forcings, which influenced to S1 deposition. Our results show that the differences among the sub-basins are related to the depth of the cores that had a significant effect on organic matter preservation.

References:

Abu-Zied, R. H., Rohling, E. J., Jorissen, F. J., Fontanier, C., Casford, J. S. L., & Cooke, S. (2008). Benthic foraminiferal response to changes in bottom-water oxygenation and organic carbon flux in the eastern Mediterranean during LGM to Recent times. *Marine Micropaleontology*, 67(1–2), 46–68. https://doi.org/10.1016/j.marmicro.2007.08.006

Akima, H., Gebhardt, A., Petzold, T., & Maechler, M. (2016). Package 'akima'. Available in : https://cran.r-project.org/web/packages/akima/index.html

Algeo, T. J., & Heckel, P. H. (2008). The Late Pennsylvanian midcontinent sea of North America: a review. *Palaeogeography, Palaeoclimatology, Palaeoecology,* 268(3-4), 205-221. https://doi.org/10.1016/j.palaeo.2008.03.049

Algeo, T. J., & Rowe, H. (2012). Paleoceanographic applications of trace-metal concentration data. *Chemical Geology*, 324, 6-18. https://doi.org/10.1016/j.chemgeo.2011.09.002

Algeo, T. J., & Tribovillard, N. (2009). Environmental analysis of paleoceanographic systems based on molybdenum–uranium covariation. *Chemical Geology*, 268(3-4), 211-225. https://doi.org/10.1016/j.chemgeo.2009.09.001

Algeo, T. J. (2004). Can marine anoxic events draw down the trace element inventory of seawater?. *Geology*, 32(12), 1057-1060. https://doi.org/10.1130/G20896.1

Amezcua-Buendía, R., Diamantini, C., Potena, D., & Negri, A. (2019). BEyOND, a new tool for sapropel S1 studies in the Mediterranean Sea. *Alpine and Mediterranean Quaternary*, 32 (2), 167-184. https://doi.org/10.26382/AMQ.2019.11

Anastasakis, G.C., 1988. Uppermost limit of sapropel (-lic) deposition in the Aegean and North Levantine Seas. In: G.C. Anastasakis (Editor), National Centre for Marine Research 1945 1965 1985. *Natl. Cent. Mar. Res.*, Athens, pp. 19 20

Anastasakis, G. C., & Stanley, D. J. (1986). Uppermost Sapropel, Eastern Mediterranean-Paleoceanography and Stagnation. *National Geographic Research*, 2(2), 179-197.

Anastasakis, G. C., & Stanley, D. J. (1984). Sapropels and organic-rich variants in the Mediterranean: sequence development and classification. *Geological Society, London, Special Publications*, 15(1), 497-510. https://doi.org/10.1144/GSL.SP.1984.015.01.32

Andersen, M. B., Matthews, A., Vance, D., Bar-Matthews, M., Archer, C., & de Souza, G. F. (2018). A 10-fold decline in the deep Eastern Mediterranean thermohaline overturning circulation during the last interglacial period. *Earth and Planetary Science Letters*, 503, 58–67. https://doi.org/10.1016/j.epsl.2018.09.013

Anderson, T. F., & Raiswell, R. (2004). Sources and mechanisms for the enrichment of highly reactive iron in euxinic Black Sea sediments. *American Journal of Science*, 304(3), 203-233. https://doi.org/10.2475/ajs.304.3.203

Ariztegui, D., Asioli, A., Lowe, J. J., Trincardi, F., Vigliotti, L., Tamburini, F., ... & Van der Kaars, S. (2000). Palaeoclimate and the formation of sapropel S1: inferences from Late Quaternary lacustrine and marine sequences in the central Mediterranean region. *Palaeogeography, Palaeoclimatology, Palaeoecology*, 158(3–4), 215–240. https://doi.org/10.1016/S0031-0182(00)00051-1

Arnone, R. A., Wiesenburg, D. A., & Saunders, K. D. (1990). The origin and characteristics of the Algerian Current. *Journal of Geophysical Research*, 95(C2), 1587. https://doi.org/10.1029/jc095ic02p01587

Astraldi, M., Balopoulos, S., Candela, J., Font, J., Gacic, M., Gasparini, G. P., ... & Tintoré, J. (1999). The role of straits and channels in understanding the characteristics of Mediterranean

circulation. *Progress in Oceanography* 44(1-3), 65–108. https://doi.org/10.1016/S0079-6611(99)00021-X

Azrieli-Tal, I., Matthews, A., Bar-Matthews, M., Almogi-Labin, A., Vance, D., Archer, C., & Teutsch, N. (2014). Evidence from molybdenum and iron isotopes and molybdenum-uranium covariation for sulphidic bottom waters during Eastern Mediterranean sapropel S1 formation. *Earth and Planetary Science Letters*, 393, 231-242. https://doi.org/10.1016/j.epsl.2014.02.054

Bar-Matthews, M. (2014). History of Water in the Middle East and North Africa. *Treatise on Geochemistry (Second Editions)*, 14, 109–128. https://doi.org/10.1016/B978-0-08-095975-7.01210-9

Bar-Matthews, M., Ayalon, A., Gilmour, M., Matthews, A., & Hawkesworth, C. J. (2003). Sea–land oxygen isotopic relationships from planktonic foraminifera and speleothems in the Eastern Mediterranean region and their implication for paleorainfall during interglacial intervals. *Geochimica et Cosmochimica Acta*, 67(17), 3181–3199. https://doi.org/10.1016/S0016-7037(02)01031-1

Bar-Matthews, M., Ayalon, A., & Kaufman, A. (2000). Timing and hydrological conditions of Sapropel events in the Eastern Mediterranean, as evident from speleothems, Soreq cave, Israel. *Chemical Geology*, 169(1–2), 145–156. https://doi.org/10.1016/S0009-2541(99)00232-6

Bar-Matthews, M., Ayalon, A., Kaufman, A., & Wasserburg, G. J. (1999). The Eastern Mediterranean paleoclimate as a reflection of regional events: Soreq cave, Israel. *Earth and Planetary Science Letters*, 166(1-2), 85-95. https://doi.org/10.1016/S0012-821X(98)00275-1

Bard, E., Delaygue, G., Rostek, F., Antonioli, F., Silenzi, S., & Schrag, D. P. (2002). Hydrological conditions over the western Mediterranean basin during the deposition of the cold Sapropel 6 (ca. 175 kyr BP). *Earth and Planetary Science Letters*, 202(2), 481-494. https://doi.org/10.1016/S0012-821X(02)00788-4

Barmawidjaja, D. M., Jorissen, F. J., Puškarić, S., & Van Der Zwaan, G. J. (1992). Microhabitat selection by benthic foraminifera in the northern Adriatic Sea. *Journal of Foraminiferal Research*, 22(4), 297. https://doi.org/10.2113/gsjfr.22.4.297

Béranger, K., Drillet, Y., Houssais, M. N., Testor, P., Bourdallé-Badie, R., Alhammoud, B., ... & Crépon, M. (2010). Impact of the spatial distribution of the atmospheric forcing on water mass formation in the Mediterranean Sea. *Journal of Geophysical Research: Oceans*, 115(C12). https://doi.org/10.1029/2009JC005648

Béranger, K., Mortier, L., & Crépon, M. (2005). Seasonal variability of water transport through the Straits of Gibraltar, Sicily and Corsica, derived from a high-resolution model of the Mediterranean circulation. *Progress in Oceanography*, 66(2–4), 341–364. https://doi.org/10.1016/j.pocean.2004.07.013

Béranger, K., Mortier, L., Gasparini, G. P., Gervasio, L., Astraldi, M., & Crépon, M. (2004). The dynamics of the Sicily Strait: A comprehensive study from observations and models. *Deep-Sea Research Part II: Topical Studies in Oceanography*, 51(4-5), 411-440. https://doi.org/10.1016/j.dsr2.2003.08.004

Béthoux, J.P. (1979). Budgets of the Mediterranean Sea. Their dependence on the local climate and on the characteristics of the Atlantic waters. *Oceanol. Acta*, 2(2), 157-163.

Bethoux, J. P. (1989). Oxygen consumption, new production, vertical advection and environmental evolution in the Mediterranean Sea. *Deep Sea Research Part A. Oceanographic Research Papers*, 36(5), 769-781. https://doi.org/10.1016/0198-0149(89)90150-7

Betts, J. N., & Holland, H. D. (1991). The oxygen content of ocean bottom waters, the burial efficiency of organic carbon, and the regulation of atmospheric oxygen. *Palaeogeography, Palaeoclimatology, Palaeoecology,* 97(1-2), 5-18. https://doi.org/10.1016/0031-0182(91)90178-T

Bi, H., Xue, Y., Merritt, P., Windmill, C., & Davis, B. (2019). A Heterogeneous and Interactive Big Earth Data Framework. *Proceedings of the 2019 International Conference on Big Data Engineering (BDE 2019).* ACM, New York, NY, USA, 85-91. https://doi.org/10.1145/3341620.3341628.

Bishop, J. K. (1988). The barite-opal-organic carbon association in oceanic particulate matter. *Nature,* 332(6162), 341. https://doi.org/10.1038/332341a0

Bond, G., Kromer, B., Beer, J., Muscheler, R., Evans, M. N., Showers, W., ... & Bonani, G. (2001). Persistent solar influence on North Atlantic climate during the Holocene. *Science*, 294(5549), 2130-2136. https://doi.org/10.1126/science.1065680

Bond, G., Showers, W., Cheseby, M., Lotti, R., Almasi, P., DeMenocal, P., ... & Bonani, G. (1997). A pervasive millennial-scale cycle in North Atlantic Holocene and glacial climates. *Science*, 278(5341), 1257-1266. https://doi.org/10.1126/science.278.5341.1257

Bosmans, J. H. C., Drijfhout, S. S., Tuenter, E., Hilgen, F. J., Lourens, L. J., & Rohling, E. J. (2015). Precession and obliquity forcing of the freshwater budget over the Mediterranean. *Quaternary Science Reviews*, 123, 16-30. https://doi.org/10.1016/j.quascirev.2015.06.008

Boulton, G. (2018). The challenges of a big data earth. Big Earth Data, 2(1), 1-7. https://doi.org/10.1080/20964471.2017.1397411

Bradley W. H. (1938). Mediterranean sediments and Pleistocene sea levels. *Science*, 88, 376-379

Brayshaw, D. J., Hoskins, B., & Black, E. (2010). Some physical drivers of changes in the winter storm tracks over the North Atlantic and Mediterranean during the Holocene. *Philosophical Transactions of the Royal Society A: Mathematical, Physical and Engineering Sciences*, 368(1931), 5185-5223. https://doi.org/10.1098/rsta.2010.0180

Broecker, W. S., Sutherland, S., & Peng, T. H. (1999). A possible 20th-century slowdown of Southern Ocean deep water formation. *Science*, 286(5442), 1132-1135. Https://doi.org/10.1126/science.286.5442.1132

Debret, M., Bout-Roumazeilles, V., Grousset, F., Desmet, M., McManus, J. F., Massei, N., ... & Trentesaux, A. (2007). The origin of the 1500-year climate cycles in Holocene North-Atlantic records. *Climate of the Past Discussions, European Geosciences Union (EGU), 2007*, 3 (2), pp.679-692.

Broerse, A. T., Ziveri, P., Van Hinte, J. E., & Honjo, S. (2000). Coccolithophore export production, species composition, and coccolith-CaCO3 fluxes in the NE Atlantic (34 °N 21 °W and 48 °N 21 °W). *Deep-Sea Research Part II: Topical Studies in Oceanography*, 47(9-11), 1877-1905. https://doi.org/10.1016/S0967-0645(00)00010-2

Brumsack, H. J. (1980). Geochemistry of Cretaceous black shales from the Atlantic Pcean (DSDP Legs 11, 14, 36 and 41). *Chemical Geology*, 31, 1-25. https://doi.org/10.1016/0009-2541(80)90064-9

Bryden, H. L., Candela, J., & Kinder, T. H. (1994). Exchange through the Strait of Gibraltar. *Progress in Oceanography*, 33(3), 201-248. https://doi.org/10.1016/0079-6611(94)90028-0

Bryden, H.L., Kinder, T.H., 1991. Steady two-layer exchange through the Strait of Gibraltar. *Deep Sea Research Part A. Oceanographic Research Papers*, 38, S445–S463. https://doi.org/10.1016/S0198-0149(12)80020-3

Bugbee, K., Griffin, R., Freitag, B., Miller, J., Ramachandran, R., & Zhang, J. (2019). Alternative Earth Science Datasets For Identifying Patterns and Events.

Calvert, S. (1983). Geochemistry of Pleistocene sapropels and associated sediments from the Eastern Mediterranean. *Oceanologica Acta*, 6(3), 255–267.

Calvert, S. E. (1987). Oceanographic controls on the accumulation of organic matter in marine sediments. *Geological Society, London, Special Publications*, 26(1), 137-151. https://doi.org/10.1144/GSL.SP.1987.026.01.08

Calvert, S. E., & Fontugne, M. R. (2001). On the late Pleistocene-Holocene sapropel record of climatic and oceanographic variability in the Eastern Mediterranean. *Paleoceanography*, 6(1), 78-94. https://doi.org/10.1029/1999PA000488.

Calvert, S. E., & Pedersen, T. F. (2007). Chapter Fourteen Elemental Proxies for Palaeoclimatic and Palaeoceanographic Variability in Marine Sediments: Interpretation and Application. *Developments in Marine Geology*, 1, 567–644. https://doi.org/10.1016/S1572-5480(07)01019-6

Canfield, D. E. (1989). Sulfate reduction and oxic respiration in marine sediments: implications for organic carbon preservation in euxinic environments. *Deep Sea Research Part A. Oceanographic Research Papers*, 36(1), 121-138.

Capotondi, L., Principato, M. S., Morigi, C., Sangiorgi, F., Maffioli, P., Giunta, S., ... & Corselli, C. (2006). Foraminiferal variations and stratigraphic implications to the deposition of sapropel S5 in the eastern Mediterranean. *Palaeogeography, Palaeoclimatology, Palaeoecology*, 235(1-3), 48-65. https://doi.org/10.1016/j.palaeo.2005.09.023

Carter, D. B. (1956). The water balance of the Mediterranean and Black Seas. Centerton, N.J: Drexel Institute of Technology, Laboratory of Climatology. 9, 127-174

Casford, J. S. L., Abu-Zied, R., Rohling, E. J., Cooke, S., Fontanier, C., Leng, M., ... & Thomson, J. (2007). A stratigraphically controlled multiproxy chronostratigraphy for the eastern Mediterranean. *Paleoceanography*, 22(4). https://doi.org/10.1029/2007PA001422

Casford, J. S. L., Rohling, E. J., Abu-Zied, R., Cooke, S., Fontanier, C., Leng, M., & Lykousis, V. (2002). Circulation changes and nutrient concentrations in the late Quaternary Aegean Sea: a nonsteady state concept for sapropel formation. *Paleoceanography*, 17(2), 14-1. https://doi.org/10.1029/2000PA000601

Casford, J. S. L., Rohling, E. J., Abu-Zied, R. H., Fontanier, C., Jorissen, F. J., Leng, M. J., ... & Thomson, J. (2003). A dynamic concept for eastern Mediterranean circulation and oxygenation during sapropel formation. *Palaeogeography, Palaeoclimatology, Palaeoecology*, 190,103-119. https://doi.org/10.1016/S0031-0182(02)00601-6

Castradori, D. (1993). Calcareous nannofossils and the origin of eastern Mediterranean sapropels. *Paleoceanography*, 8(4), 459-471. https://doi.org/10.1029/93PA00756

Cheddadi, R., Rossignol-Strick, M., & Fontugne, M. (1991). Eastern Mediterranean palaeoclimates from 26 to 5 ka BP documented by pollen and isotopic analysis of a core in the anoxic Bannock Basin. *Marine Geology*, 100(1-4), 53-66. https://doi.org/10.1016/0025-3227(91)90224-R

Cita, M. B., & Grignani, D. (1982). Nature and origin of Late Neogene Mediterranean sapropels. In Nature and origin of Cretaceous carbon-rich facies. Symposium (pp. 165-196).

Cita, M. B., Camerlenghi, A., Erba, E., McCoy, F. W., Castradori, D., Cazzani, A., & Violenti, D. (1989). Discovery of mud diapirism in the Mediterranean Ridge. A preliminary report. *Bollettino della Società geologica italiana*, 108, 537–543.

Colmenero-Hidalgo, E., Flores, J. A., Sierro, F. J., Bárcena, M. Á., Löwemark, L., Schönfeld, J., & Grimalt, J. O. (2004). Ocean surface water response to short-term climate changes revealed by coccolithophores from the Gulf of Cadiz (NE Atlantic) and Alboran Sea (W Mediterranean). *Palaeogeography, Palaeoclimatology, Palaeoecology*, 205(3–4), 317–336. https://doi.org/10.1016/j.palaeo.2003.12.014

Corliss, B. H. (1985). Microhabitats of benthic foraminifera within deep-sea sediments. *Nature*, 314, 435-438, 435–438. https://doi.org/10.1038/314435a0

Cornuault, M., Tachikawa, K., Vidal, L., Guihou, A., Siani, G., Deschamps, P., ... & Revel, M. (2018). Circulation changes in the Eastern Mediterranean Sea over the past 23,000 years inferred from authigenic Nd isotopic ratios. *Paleoceanography and Paleoclimatology*, 33(3), 264-280. https://doi.org/10.1002/2017PA003227

Corselli, C., Principato, M. S., Maffioli, P., & Crudeli, D. (2002). Changes in planktonic assemblages during sapropel S5 deposition: Evidence from Urania Basin area, eastern Mediterranean. *Paleoceanography*, 17(3), 1-1. https://doi.org/10.1029/2000PA000536

Cramp, A., & O'Sullivan, G. (1999). Neogene sapropels in the Mediterranean: a review. *Marine Geology*, 153(1–4), 11–28. https://doi.org/10.1016/S0025-3227(98)00092-9

De Lange, G. J. (1986). Early diagenetic reactions in interbedded pelagic and turbiditic sediments in the Nares Abyssal Plain (western North Atlantic): Consequences for the composition of sediment and interstitial water. *Geochimica et Cosmochimica Acta*, 50(12), 2543–2561. http://doi.org/10.1016/0016-7037(86)90209-7

De Lange, G. J., & Ten Haven, H. L. (1983). Recent sapropel formation in the eastern Mediterranean. *Nature*, 305(5937), 797–798. https://doi.org/10.1038/305797a0

De Lange, G. J., Middelburg, J. J., & Pruysers, P. A. (1989). Middle and Late Quaternary depositional sequences and cycles in the eastern Mediterranean. *Sedimentology*, 36(1), 151-156. https://doi.org/10.1111/j.1365-3091.1989.tb00827.x

De Lange, G. J., Thomson, J., Reitz, A., Slomp, C. P., Speranza Principato, M., Erba, E., & Corselli, C. (2008). Synchronous basin-wide formation and redox-controlled preservation of a Mediterranean sapropel. *Nature Geoscience*, (9), 606. https://doi.org/10.1038/ngeo283

De Rijk, S., Hayes, A., & Rohling, E. J. (1999). Eastern Mediterranean sapropel S1 interruption: an expression of the onset of climatic deterioration around 7 ka BP. *Marine Geology*, 153(1-4), 337-343. https://doi.org/10.1016/S0025-3227(98)00075-9

Debret, M., Bout-Roumazeilles, V., Grousset, F., Desmet, M., McManus, J. F., Massei, N., ... & Trentesaux, A. (2007). The origin of the 1500-year climate cycles in Holocene North-Atlantic records. *Climate of the Past Discussions, European Geosciences Union (EGU), 2007*, 3 (2), pp.679-692.

Deckmyn, 2018: Deckmyn, M. A. (2018). Package 'mapdata'. Available in: https://cran.rstudio.com/web/packages/mapdata/index.html

Deckmyn, 2018: Deckmyn, M. A. (2018). Package 'maps'. Available in: https://cran.r-project.org/web/packages/maps/index.html

Demaison, G. J., & Moore, G. T. (1980). Anoxic environments and oil source bed genesis. *AApG Bulletin*, 64(8), 1179-1209.

Desprat, S., Combourieu-Nebout, N., Essallami, L., Sicre, M. A., Dormoy, I., Peyron, O., ... & Turon, J. L. (2013). Deglacial and Holocene vegetation and climatic changes in the southern Central Mediterranean from a direct land–sea correlation. *Climate of the Past, European Geosciences Union (EGU), 2013*, 9 (2), pp.767-787

Desprat, S., Goñi, M. F. S., & Loutre, M. F. (2003). Revealing climatic variability of the last three millennia in northwestern Iberia using pollen influx data. *Earth and Planetary Science Letters*, 213(1-2), 63-78. https://doi.org/10.1016/S0012-821X(03)00292-9

Ducassou, E., Capotondi, L., Murat, A., Bernasconi, S. M., Mulder, T., Gonthier, E., ... & Mascle, J. (2007). Multiproxy Late Quaternary stratigraphy of the Nile deep-sea turbidite system - Towards a chronology of deep-sea terrigeneous systems. *Sedimentary Geology*, 200(1-2), 1-13. https://doi.org/10.1016/j.sedgeo.2007.01.023

Ducassou, E., Migeon, S., Mulder, T., Murat, A., Capotondi, L., Bernasconi, S. M., & Mascle, J. (2009). Evolution of the Nile deep-sea turbidite system during the Late Quaternary: influence of climate change on fan sedimentation. *Sedimentology*, 56(7), 2061-2090. https://doi.org/10.1111/j.1365-3091.2009.01070.x

Dymond, J., Suess, E., & Lyle, M. (1992). Barium in Deep-Sea Sediment: A Geochemical Proxy for Paleoproductivity. *Paleoceanography*, 7(2), 163-181. https://doi.org/10.1029/92PA00181

Eagle, M., Paytan, A., Arrigo, K. R., van Dijken, G., & Murray, R. W. (2003). A comparison between excess barium and barite as indicators of carbon export. *Paleoceanography*, 18(1). https://doi.org/10.1029/2003PA000922

Emeis, K. C., & Party, S. S. (1996). Paleoceanography and sapropel introduction. In Emeis, K. C., Robertson, A. H. F., Richter, C. (Eds.), *Proceedings of the Ocean Drilling Program, initial reports*, 160, 21-28.

Emeis, K. C., & Weissert, H. (2009). Tethyan–Mediterranean organic carbon-rich sediments from Mesozoic black shales to sapropels. *Sedimentology*, 56(1), 247-266.

Emeis, K. C., Camerlenghi, A., McKenzie, J. A., Rio, D., & Sprovieri, R. (1991). The occurrence and significance of Pleistocene and Upper Pliocene sapropels in the Tyrrhenian Sea. *Marine Geology*, 100(1–4), 155–182. https://doi.org/10.1016/0025-3227(91)90231-R

Emeis, K. C., Sakamoto, T., Wehausen, R., & Brumsack, H. J. (2000). The sapropel record of the eastern Mediterranean Sea — results of Ocean Drilling Program Leg 160. *Palaeogeography, Palaeoclimatology, Palaeoecology*, 158(3–4), 371–395. https://doi.org/10.1016/S0031-0182(00)00059-6

Emeis, K. C., Schulz, H., Struck, U., Rossignol-Strick, M., Erlenkeuser, H., Howell, M. W., ... & Sakamoto, T. (2003). Eastern Mediterranean surface water temperatures and $\delta^{18}O$ composition during deposition of sapropels in the late Quaternary. *Paleoceanography*, 18(1). https://doi.org/10.1029/2000PA000617

Eppley, R. W., & Peterson, B. J. (1979). Particulate organic matter flux and planktonic new production in the deep ocean. *Nature*, 282(5740), 677-680. https://doi.org/10.1038/282677a0

Filippidi, A., & De Lange, G. J. (2019). Eastern Mediterranean Deep Water Formation During Sapropel S1: A Reconstruction Using Geochemical Records Along a Bathymetric Transect in the Adriatic Outflow Region. *Paleoceanography and Paleoclimatology,* 34(3), 409-429. https://doi.org/10.1029/2018PA003459

Filippidi, A., Triantaphyllou, M. V., & De Lange, G. J. (2016). Eastern-Mediterranean ventilation variability during sapropel S1 formation, evaluated at two sites influenced by deep-water formation from Adriatic and Aegean Seas. *Quaternary Science Reviews*, 144, 95-106. https://doi.org/10.1016/j.quascirev.2016.05.024

Flores, J. A., Sierro, F. J., Francés, G., Vázquez, A., & Zamarreño, I. (1997). The last 100,000 years in the western Mediterranean: sea surface water and frontal dynamics as revealed by

coccolithophores. *Marine Micropaleontology*, 29(3–4), 351–366. https://doi.org/10.1016/S0377-8398(96)00029-1

Fontanier, C., Jorissen, F. J., Licari, L., Alexandre, A., Anschutz, P., & Carbonel, P. (2002). Live benthic foraminiferal faunas from the Bay of Biscay: Faunal density, composition, and microhabitats. *Deep-Sea Research Part I: Oceanographic Research Papers*, 49(4), 751-785. https://doi.org/10.1016/S0967-0637(01)00078-4

Francois, R., Honjo, S., Manganini, S. J., & Ravizza, G. E. (1995). Biogenic barium fluxes to the deep sea: Implications for paleoproductivity reconstruction. *Global Biogeochemical Cycles*, 9(2), 289-303. https://doi.org/10.1029/95GB00021

Frigola, J., Moreno, A., Cacho, I., Canals, M., Sierro, F. J., Flores, J. A., ... & Curtis, J. H. (2007). Holocene climate variability in the western Mediterranean region from a deepwater sediment record. *Paleoceanography,* 22(2). https://doi.org/10.1029/2006PA001307

Gačić, M., Lascaratos, A., Manca, B., & Mantziafou, A. (2001). Adriatic Deep Water and Interaction with the Eastern Mediterranean Sea. In: Cushman-Roisin, B., Gačić, M., Poulain, P. M., Artegiani, A. (eds) *Physical Oceanography of the Adriatic Sea*. Springer, Dordrecht (pp. 111–142). https://doi.org/10.1007/978-94-015-9819-4_4

Gallego-Torres, D., Martinez-Ruiz, F., De Lange, G. J., Jimenez-Espejo, F. J., & Ortega-Huertas, M. (2010). Trace-elemental derived paleoceanographic and paleoclimatic conditions for Pleistocene Eastern Mediterranean sapropels. *Palaeogeography, Palaeoclimatology, Palaeoecology,* 293(1-2), 76-89. https://doi.org/10.1016/j.palaeo.2010.05.001

Gallego-Torres, D., Martinez-Ruiz, F., Meyers, P. A., Paytan, A., Jimenez-Espejo, F. J., & Ortega-Huertas, M. (2011). Productivity patterns and N-fixation associated with Pliocene-Holocene sapropels: Paleoceanographic and paleoecological significance. *Biogeosciences*, 8(2), 415–431. https://doi.org/10.5194/bg-8-415-2011

Gascard, J. C., & Richez, C. (1985). Water masses and circulation in the Western Alboran Sea and in the Straits of Gibraltar. *Progress in Oceanography*, 15(3), 157-216. https://doi.org/10.1016/0079-6611(85)90031-X

Gertmann, I. F., Ovchinnikov, I. M., & Popv, Y. I. (1994). Deep convection in the eastern basin of the Mediterranean Sea. *Oceanology*, 34(1), 19-25.

Giorgi, F., & Lionello, P. (2008a). Climate change projections for the Mediterranean region. *Global and Planetary Change*, 63(2), 90–104. https://doi.org/10.1016/j.gloplacha.2007.09.005

Giunta, S., Negri, A., Morigi, C., Capotondi, L., Combourieu-Nebout, N., Emeis, K. C., ... & Vigliotti, L. (2003). Coccolithophorid ecostratigraphy and multi-proxy paleoceanographic reconstruction in the Southern Adriatic Sea during the last deglacial time (Core AD91-17). *Palaeogeography, Palaeoclimatology, Palaeoecology*. https://doi.org/10.1016/S0031-0182(02)00598

Grant, K. M., Grimm, R., Mikolajewicz, U., Marino, G., Ziegler, M., & Rohling, E. J. (2016). The timing of Mediterranean sapropel deposition relative to insolation, sea-level and African monsoon changes. *Quaternary Science Reviews*, 140, 125–141. https://doi.org/10.1016/j.quascirev.2016.03.026

Grelaud, M., Marino, G., Ziveri, P., & Rohling, E. J. (2012). Abrupt shoaling of the nutricline in response to massive freshwater flooding at the onset of the last interglacial sapropel event. *Paleoceanography*, 27(3). https://doi.org/10.1029/2012PA002288

Grimm, R., Maier-Reimer, E., Mikolajewicz, U., Schmiedl, G., Müller-Navarra, K., Adloff, F., ... & Emeis, K. C. (2015). Late glacial initiation of Holocene eastern Mediterranean sapropel formation. *Nature Communications*, 6, 7099. https://doi.org/10.1038/ncomms8099

Guo, H., Liu, Z., Jiang, H., Wang, C., Liu, J., & Liang, D. (2017). Big Earth Data: A new challenge and opportunity for Digital Earth's development. *International Journal of Digital Earth*, 10(1), 1-12. https://doi.org/10.1080/17538947.2016.1264490

Hilgen, F. J., (1991). Astronomical calibration of Gauss to Matuyama sapropels in the Mediterranean and implication for the geomagnetic polarity time scale. *Earth and planetary science letters,* 104, 226–244. https://doi.org/10.1016/0012-821X(91)90206-W

Hecht, A., & Gertman, I. (2001). Physical features of the eastern Mediterranean resulting from the integration of POEM data with Russian Mediterranean cruises. *Deep-Sea Research Part I: Oceanographic Research Papers*, 48(8), 1847–1876. https://doi.org/10.1016/S0967-0637(00)00113-8

Hennekam, R., Jilbert, T., Schnetger, B., & de Lange, G. J. (2014). Solar forcing of Nile discharge and sapropel S1 formation in the early to middle Holocene eastern Mediterranean. *Paleoceanography*, 29(5), 343-356. https://doi.org/10.1002/2013PA002553

Hennekam, R., Donders, T. H., Zwiep, K., & de Lange, G. J. (2015). Integral view of Holocene precipitation and vegetation changes in the Nile catchment area as inferred from its delta sediments. *Quaternary Science Reviews*, 130, 189–199. https://doi.org/10.1016/j.quascirev.2015.05.031

Herguera, J. C., & Berger, W. H. (1991). Paleoproductivity from benthic foraminifera abundance: glacial to postglacial change in the west-equatorial Pacific. *Geology*, 19(12), 1173-1176. https://doi.org/10.1130/0091-7613(1991)019<1173:PFBFAG>2.3.CO;2

Howell, M. W., & Thunell, R. C. (1992). Organic carbon accumulation in Bannock Basin: evaluating the role of productivity in the formation of eastern Mediterranean sapropels. *Marine Geology*, 103(1-3), 461-471. https://doi.org/10.1016/0025-3227(92)90032-D

Huang, Z. (2019). An On-Demand Processing Framework for Faster Remote Sensing Big Data Analysis. *IOP Conference Series: Earth and Environmental Science*, 234(1), 012060. https://doi.org/10.1088/1755-1315/234/1/012060

IBM Marketing Cloud (2017). 10 Key Marketing Trends for 2017 and Ideas for exceeding customer expectations. Available at: https://www-01.ibm.com/common/ssi/cgibin/ssialias?htmlfid=WRL12345USEN

Incarbona, A., & Di Stefano, E. (2019). Calcareous nannofossil palaeoenvironmental reconstruction and preservation in sapropel S1 at the Eratosthenes Seamount (Eastern Mediterranean). *Deep Sea Research Part II: Topical Studies in Oceanography*, 164, 206-215. https://doi.org/10.1016/j.dsr2.2018.10.004

Incarbona, A., Abu-Zied, R. H., Rohling, E. J., & Ziveri, P. (2019). Reventilation episodes during the sapropel S1 deposition in the eastern Mediterranean based on holococcolith preservation. *Paleoceanography and Paleoclimatology*, 34(10), 1597-1609. https://doi.org/10.1029/2019PA003626

Incarbona, A., Ziveri, P., Sabatino, N., Manta, D. S., & Sprovieri, M. (2011). Conflicting coccolithophore and geochemical evidence for productivity levels in the Eastern Mediterranean sapropel S1. *Marine Micropaleontology,* 81(3-4), 131-143. https://doi.org/10.1016/j.marmicro.2011.09.003

Jilbert, T., Reichart, G. J., Mason, P., & de Lange, G. J. (2010). Short-time-scale variability in ventilation and export productivity during the formation of Mediterranean sapropel S1. *Paleoceanography*, 25(4). https://doi.org/10.1029/2010PA001955

Jimenez-Espejo, F. J., Martinez-Ruiz, F., Rogerson, M., González-Donoso, J. M., Romero, O. E., Linares, D., ... & Perez Claros, J. A. (2008). Detrital input, productivity fluctuations, and water mass circulation in the westernmost Mediterranean Sea since the Last Glacial

Maximum. Geochemistry, *Geophysics, Geosystems*, 9(11). https://doi.org/10.1029/2008GC002096

Jimenez-Espejo, Francisco J., Martinez-Ruiz, F., Sakamoto, T., Iijima, K., Gallego-Torres, D., & Harada, N. (2007). Paleoenvironmental changes in the western Mediterranean since the last glacial maximum: High resolution multiproxy record from the Algero-Balearic basin. *Palaeogeography, Palaeoclimatology, Palaeoecology*, 246(2–4), 292–306. https://doi.org/10.1016/j.palaeo.2006.10.005

Jones, R. W. (1983). Organic matter characteristics near the shelf-slope boundary.

Jorissen, F. J. (1988). Benthic foraminifera from the Adriatic Sea: principles of phenotypic variation (Doctoral dissertation, Utrecht University).

Jorissen, F. J. (1999). Benthic foraminiferal microhabitats below the sediment-water interface. *Modern Foraminifera (pp. 161-179). Springer, Dordrecht*. https://doi.org/10.1007/0-306-48104-9_10

Jorissen, F. J., de Stigter, H. C., & Widmark, J. G. V. (1995). A conceptual model explaining benthic foraminiferal microhabitats. *Marine Micropaleontology*, 26(1-4), 3-15. https://doi.org/10.1016/0377-8398(95)00047-X

Kallel, N., Duplessy, J. C., Labeyrie, L., Fontugne, M., Paterne, M., & Montacer, M. (2000). Mediterranean pluvial periods and sapropel formation over the last 200 000 years. Palaeogeography, Palaeoclimatology, Palaeoecology, 157(1-2), 45-58. https://doi.org/10.1016/S0031-0182(99)00149-2

Kallel, N., Paterne, M., Duplessy, J. C., Vergnaudgrazzini, C., Pujol, C., Labeyrie, L., ... & Pierre, C. (1997). Enhanced rainfall in the Mediterranean region during the last sapropel event. *Oceanolica Acta*, 20(5), 697–712.

Kemp, A. E. S., Pearce, R. B., Koizumi, I., Pike, J., & Rance, S. J. (1999). The role of mat-forming diatoms in the formation of Mediterranean sapropels. *Nature*, 398(6722), 57. https://doi.org/10.1038/18001

Kidd, R. B., Cita, M. B., & Ryan, W. B. F. (1978). Stratigraphy of eastern Mediterranean sapropel sequences recovered during DSDP Leg 42A and their paleoenvironmental significance. *Initial Reports of the Deep Sea Drilling Project*, 42 (Pt. 1). https://doi.org/10.2973/dsdp.proc.42-1.113-1.1978

Kinder, T., & Parilla, G. (1987). Yes, some of the Mediterranean outflow does come from great depth. *Journal of Geophysical Research: Oceans*, 92(C3), 2901–2906. https://doi.org/10.1029/JC092iC03p02901

Klein, B., Roether, W., Manca, B. B., Bregant, D., Beitzel, V., Kovacevic, V., & Luchetta, A. (1999). The large deep water transient in the Eastern Mediterranean. *Deep-Sea Research Part I: Oceanographic Research Papers*, 46(3), 371-414. https://doi.org/10.1016/S0967-0637(98)00075-2

Kontakiotis, G. (2016). Late Quaternary paleoenvironmental reconstruction and paleoclimatic implications of the Aegean Sea (eastern Mediterranean) based on paleoceanographic indexes and stable isotopes. *Quaternary International*, 401, 28–42. https://doi.org/10.1016/j.quaint.2015.07.039

Kotthoff, U., Müller, U. C., Pross, J., Schmiedl, G., Lawson, I. T., van de Schootbrugge, B., & Schulz, H. (2008a). Lateglacial and Holocene vegetation dynamics in the Aegean region: an integrated view based on pollen data from marine and terrestrial archives. *The Holocene*, 18(7), 1019-1032. https://doi.org/10.1177/0959683608095573

Kotthoff, U., Pross, J., Müller, U. C., Peyron, O., Schmiedl, G., Schulz, H., & Bordon, A. (2008b). Climate dynamics in the borderlands of the Aegean Sea during formation of sapropel S1

deduced from a marine pollen record. *Quaternary Science Reviews*, 27(7–8), 832–845. https://doi.org/10.1016/j.quascirev.2007.12.001

Krom, M. D., Stanley, J. D., Cliff, R. A., & Woodward, J. C. (2002). Nile River sediment fluctuations over the past 7000 yr and their key role in sapropel development. *Geology*, 30(1), 71-74. https://doi.org/10.1130/0091-7613(2002)030<0071:NRSFOT>2.0.CO;2

Krom, M. D., Groom, S., & Zohary, T. (2003). The Eastern Mediterranean. *The Biogeochemistry of Marine Systems*, 91-122.

Kullenberg, B. (1952). On the salinity of the water contained in marine sediments. *Medd. Oceanogr. Inst. Göteb.* 21, 1–38.

Lacombe, H., & Tchernia, P. (1972). Caractères hydrologiques et circulation des eaux en Méditerranée, The Mediterranean Sea DJ Stanley, 25–36.

Lacombe, H., Tchernia, P., & Benoist, G. (1958). Contribution a l'etude hydrologique de la mer Egee en periode d'ete. Bull. Inf., COEC, 8, 454-468.

Lascaratos, A., Roether, W., Nittis, K., & Klein, B. (1999). Recent changes in deep water formation and spreading in the eastern Mediterranean Sea: a review. *Progress in Oceanography*, 44(1–3), 5–36. https://doi.org/10.1016/S0079-6611(99)00019-1

Leaman, K. D., & Schott, F. A. (1991). Hydrographic Structure of the Convection Regime in the Gulf of Lions: Winter 1987. *Journal of Physical Oceanography,* 21(4), 575-598. https://doi.org/10.1175/1520-0485(1991)021<0575:hsotcr>2.0.co;2

Linke, P., & Lutze, G. F. (1993). Microhabitat preferences of benthic foraminifera—a static concept or a dynamic adaptation to optimize food acquisition?. *Marine Micropaleontology*, 20(3–4), 215–234. https://doi.org/10.1016/0377-8398(93)90034-U

Lionello, P. (Ed.). (2012). The climate of the Mediterranean region: From the past to the future. *Elsevier*.

López-Otálvaro, G. E., Sierro, F. J., & Cacho, I. (2008). Variations in coccolithophorid production in the Eastern Equatorial Pacific at ODP Site 1240 over the last seven glacial–interglacial cycles. *Marine Micropaleontology*, 69(1), 52–69. https://doi.org/10.1016/J.MARMICRO.2007.11.009

Lyons, T. W., & Severmann, S. (2006). A critical look at iron paleoredox proxies: New insights from modern euxinic marine basins. *Geochimica et Cosmochimica Acta*, 70(23), 5698-5722. https://doi.org/10.1016/j.gca.2006.08.021

Madhukar M., & Pooja. (2019). Earth Science [Big] Data Analytics. In: Dey N., Bhatt C., Ashour A. (eds) *Big Data for Remote Sensing: Visualization, Analysis and Interpretation*. *Springer*, Cham. https://doi.org/10.1007/978-3-319-89923-7_4

Malanotte-Rizzoli, P., & Bergamasco, A. (1991). The wind and thermally driven circulation of the eastern Mediterranean Sea. Part II: the Baroclinic case. *Dynamics of Atmospheres and Oceans*, 15(3-5), 355-419. https://doi.org/10.1016/0377-0265(91)90026-C

Malanotte-Rizzoli P., & Hecht, A. (1988). Large-scale properties of the Eastern Mediterranean: A review. *Oceanol Acta*, 11(4), 323-335.

Malanotte-Rizzoli, P., & Robinson, A. R. (1988). POEM: physical oceanography of the eastern Miditerranean. Eos, *Transactions American Geophysical Union*, 69(14), 194-203.

Malanotte-Rizzoli, P., Manca, B. B., d'Alcalà, M. R., Theocharis, A., Bergamasco, A., Bregant, D., ... & Sansone, E. (1997). A synthesis of the Ionian Sea hydrography, circulation and water mass pathways during POEM-phase I. *Progress in Oceanography*, 39(3), 153-204. https://doi.org/10.1016/S0079-6611(97)00013-X

Mallo, M., Ziveri, P., Graham Mortyn, P., Schiebel, R., & Grelaud, M. (2017). Low planktic foraminiferal diversity and abundance observed in a spring 2013 west-east Mediterranean Sea plankton tow transect. *Biogeosciences*, 14(9). https://doi.org/10.5194/bg-14-2245-2017

Manca, B. B., Kovaĉević, V., Gaĉić, M., & Viezzoli, D. (2002). Dense water formation in the Southern Adriatic Sea and spreading into the Ionian Sea in the period 1997-1999. *Journal of Marine Systems*, 33–34, 133–154. https://doi.org/10.1016/S0924-7963(02)00056-8

Mangini, A., & Schlosser, P. (1986). The formation of eastern Mediterranean sapropels. *Marine Geology*, 72(1-2), 115-124. https://doi.org/10.1016/0025-3227(86)90102-7

Mangini, A., Eisenhauer, A., & Walter, P. (1991). A spike of CO2 in the atmosphere at glacial-interglacial boundaries induced by rapid deposition of manganese in the oceans. *Tellus B*, 43(2), 97-105. https://doi.org/10.1034/j.1600-0889.1991.t01-1-00004.x

Mangini, A., Jung, M., & Laukenmann, S. (2001). What do we learn from peaks of uranium and of manganese in deep sea sediments?. *Marine Geology*, 177(1-2), 63-78. https://doi.org/10.1016/S0025-3227(01)00124-4

Marino, G., Rohling, E. J., Rijpstra, W. I. C., Sangiorgi, F., Schouten, S., & Sinninghe Damsté, J. S. (2007). Aegean sea as driver of hydrographic and ecological changes in the eastern Mediterranean. *Geology,* 35(8), 675-678. https://doi.org/10.1130/G23831A.1

Marino, G., Rohling, E. J., Sangiorgi, F., Hayes, A., Casford, J. L., Lotter, A. F., ... & Brinkhuis, H. (2009). Early and middle Holocene in the Aegean Sea: interplay between high and low latitude climate variability. *Quaternary Science Reviews*, 28(27–28), 3246–3262. https://doi.org/10.1016/j.quascirev.2009.08.011

Marshall, J., & Schott, F. (1999). Open-ocean convection: Observations, theory, and models. *Reviews of Geophysics*, 37(1), 1-64. https://doi.org/10.1029/98RG02739

Martinez-Ruiz, F., Kastner, M., Paytan, A., Ortega-Huertas, M., & Bernasconi, S. M. (2000). Geochemical evidence for enhanced productivity during S1 sapropel deposition in the eastern Mediterranean. *Paleoceanography*, 15(2), 200–209. https://doi.org/10.1029/1999PA000419

Martinez-Ruiz, F., Kastner, M., Gallego-Torres, D., Rodrigo-Gámiz, M., Nieto-Moreno, V., & Ortega-Huertas, M. (2015). Paleoclimate and paleoceanography over the past 20,000yr in the Mediterranean Sea Basins as indicated by sediment elemental proxies. *Quaternary Science Reviews*, 107, 25–46. https://doi.org/10.1016/j.quascirev.2014.09.018

Martínez-Ruiz, F., Paytan, A., Kastner, M., González-Donoso, J. M., Linares, D., Bernasconi, S. M., & Jimenez-Espejo, F. J. (2003). A comparative study of the geochemical and mineralogical characteristics of the S1 sapropel in the western and eastern Mediterranean. *Palaeogeography, Palaeoclimatology, Palaeoecology*, 190, 23–37. https://doi.org/10.1016/S0031-0182(02)00597-7

McKay, J. L., & Pedersen, T. F. (2014). Geochemical response to pulsed sedimentation: Implications for the use of Mo as a paleo-proxy. *Chemical Geology*, 382, 83–94. https://doi.org/10.1016/j.chemgeo.2014.05.009

McManus, J. F., Oppo, D. W., & Cullen, J. L. (1999). A 0.5-million-year record of millennial-scale climate variability in the North Atlantic. *Science*, 283(5404), 971-975. https://doi.org/10.1126/science.283.5404.971

MEDOC Group. (1970). Observation of formation of deep water in the Mediterranean Sea, 1969. *Nature*, 227(5262), 1037–1040. https://doi.org/10.1038/2271037a0

Meier, K. J. S., Zonneveld, K. A. F., Kasten, S., & Willems, H. (2004). Different nutrient sources forcing increased productivity during eastern Mediterranean S1 sapropel formation as reflected by calcareous dinoflagellate cysts. *Paleoceanography*, 19(1), 1–12. https://doi.org/10.1029/2003PA000895

Melki, T., Kallel, N., & Fontugne, M. (2010). The nature of transitions from dry to wet condition during sapropel events in the Eastern Mediterranean Sea. *Palaeogeography, Palaeoclimatology, Palaeoecology*, 291(3-4), 267-285. https://doi.org/10.1016/j.palaeo.2010.02.039

Mercone, D., Thomson, J., Croudace, I. W., Siani, G., Paterne, M., & Troelstra, S. (2000). Duration of S1, the most recent sapropel in the eastern Mediterranean Sea, as indicated by accelerator mass spectrometry radiocarbon and geochemical evidence. *Paleoceanography*, 15(3), 336-347. https://doi.org/10.1029/1999PA000397

Mertens, C., & Schott, F. (1998). Interannual variability of deep-water formation in the northwestern Mediterranean. *Journal of physical oceanography*, 28(7), 1410-1424. https://doi.org/10.1175/1520-0485(1998)028<1410:IVODWF>2.0.CO;2

Meyer, K. M., & Kump, L. R. (2008). Oceanic Euxinia in Earth History: Causes and Consequences. *Annual Review of Earth and Planetary Sciences*, 36, 251-288. https://doi.org/10.1146/annurev.earth.36.031207.124256

Meyers, P. A., & Doose, H. (1999). Sources, preservation, and thermal maturity of organic matter in Pliocene-Pleistocene organic-carbon-rich sediments of the western Mediterranean Sea. *Proceedings of the Ocean Drilling Program: Scientific Results,* 161, 383-390

Meyers, Philip A. (2006). Paleoceanographic and paleoclimatic similarities between Mediterranean sapropels and Cretaceous black shales. *Palaeogeography, Palaeoclimatology, Palaeoecology*, 235(1–3), 305-320. https://doi.org/10.1016/j.palaeo.2005.10.025

Miller, A. R. (1963). Physical oceanography of the Mediterranean Sea: A discourse. *Rapp. Comm. Int. Mer Medit.*, 17, 857–871

Millot, C. (1987). Circulation in the Hydrodynamics General circulation Mediterranean Sea Mesoscale phenomena. *Oceanologica Acta*, 10(2), 143–149

Millot, C. (1999). Circulation in the Western Mediterranean Sea. *Journal of Marine Systems*, 20(1–4), 423–442. https://doi.org/10.1016/S0924-7963(98)00078-5

Möbius, J., Lahajnar, N., & Emeis, K. C. (2010). Diagenetic control of nitrogen isotope ratios in Holocene sapropels and recent sediments from the Eastern Mediterranean Sea. *Biogeosciences*, 7(11), 3901–3914. https://doi.org/10.5194/bg-7-3901-2010

Mojtahid, M., Manceau, R., Schiebel, R., Hennekam, R., & de Lange, G. J. (2015). Thirteen thousand years of southeastern Mediterranean climate variability inferred from an integrative planktic foraminiferal-based approach. *Paleoceanography*, 30(4), 402-422. https://doi.org/10.1002/2014PA002705

Moodley, L., Middelburg, J. J., Herman, P. M. J., Soetaert, K., & de Lange, G. J. (2005). Oxygenation and organic-matter preservation in marine sediments: Direct experimental evidence from ancient organic carbon-rich deposits. *Geology, 33(11), 889-892*. https://doi.org/10.1130/G21731.1

Müller, P. J., & Suess, E. (1979). Productivity, sedimentation rate, and sedimentary organic matter in the oceans—I. Organic carbon preservation. *Deep Sea Research Part A. Oceanographic Research Papers*, 26(12), 1347-1362. https://doi.org/10.1016/0198-0149(79)90003-7

Murat, A. (1991). Enregistrement sédimentaire des paléoenvironnements quaternaires en Méditerranée orientale (Doctoral dissertation, Perpignan).

Murat, A. (1999). Pliocene-Pleistocene occurrence of sapropels in the Western Mediterranean Sea and their relation to eastern Mediterranean sapropels. In *Proceedings of the Ocean Drilling Program: Scientific Results*, 161, 519-527

Murat, A., & Got, H. (2000). Organic carbon variations of the eastern Mediterranean Holocene sapropel: a key for understanding formation processes. *Palaeogeography, Palaeoclimatology, Palaeoecology*, 158(3–4), 241–257. https://doi.org/10.1016/S0031-0182(00)00052-3

Myers, P. G. (2002). Flux-forced simulations of the paleocirculation of the Mediterranean. *Paleoceanography*, 17(1), 9-1. https://doi.org/10.1029/2000PA000613

Myers, P. G., Haines, K., & Rohling, E. J. (1998). Modeling the paleocirculation of the Mediterranean: The last glacial maximum and the Holocene with emphasis on the formation of sapropel S1. *Paleoceanography*, 13(6), 586-606. https://doi.org/10.1029/98PA02736

Negri, A., & Giunta, S. (2001). Calcareous nannofossil paleoecology in the sapropel S1 of the Eastern Ionian sea: Paleoceanographic implications. *Palaeogeography, Palaeoclimatology, Palaeoecology*, 169(1–2), 101–112. https://doi.org/10.1016/S0031-0182(01)00219-X

Nijenhuis, I. A., Bosch, H. J., Damsté, J. S., Brumsack, H. J., & de Lange, G. J. (1999). Organic matter and trace element rich sapropels and black shales: A geochemical comparison. *Earth and Planetary Science Letters*, 169(3-4), 277-290. https://doi.org/10.1016/S0012-821X(99)00083-7

Olausson, E. (1960). Description of sediment from the Mediterranean and the Red Sea. Rep. *Swedish Deep-Sea Exped*., 1947-1948. 8 (3), 287.

Olausson, E. (1961). Studies of deep sea cores. *Rep, swed. Deep Sea Exped*., 1947-1948, 8 (4), 353-391.

Osborne, A. H., Vance, D., Rohling, E. J., Barton, N., Rogerson, M., & Fello, N. (2008). A humid corridor across the Sahara for the migration of early modern humans out of Africa 120,000 years ago. *Proceedings of the National Academy of Sciences of the United States of America*, 105(43), 16444-16447. https://doi.org/10.1073/pnas.0804472105

Özsoy, E. (1981). On the atmospheric factors affecting the Levantine Sea (No. 25). European Centre for Medium Range Weather Forecasts.

Painter, S. C., & Tsimplis, M. N. (2003). Temperature and salinity trends in the upper waters of the Mediterranean Sea as determined from the MEDATLAS dataset. *Continental Shelf Research,* 23(16), 1507-1522. https://doi.org/10.1016/j.csr.2003.08.008

Parrilla, G., Kinder, T. H., & Preller, R. H. (1986). Deep and intermediate mediterranean water in the western Alboran Sea. *Deep Sea Research Part A, Oceanographic Research Papers*, 33(1), 55–88. https://doi.org/10.1016/0198-0149(86)90108-1

Passier, H. F., Middelburg, J. J., de Lange, G. J., & Böttcher, M. E. (1997). Pyrite contents, microtextures, and sulfur isotopes in relation to formation of the youngest eastern Mediterranean sapropel. *Geology*, 25(6), 519-522. https://doi.org/10.1130/0091-7613(1997)025<0519:PCMASI>2.3.CO;2

Passier, H. F., Middelburg, J. J., Van Os, B. J., & De Lange, G. J. (1996). Diagenetic pyritisation under eastern Mediterranean sapropels caused by downward sulphide diffusion. Geochimica et Cosmochimica Acta, 60(5), 751-764.

Perkins, H., Kinder, T., & Violette, P.L., (1990). The Atlantic inflow in the Western Alboran Sea. *Journal of Physical Oceanography*, 20, 242–263, https://doi.org/10.1175/1520-0485(1990)020<0242:TAIITW>2.0.CO;2

Pfeifer, K., Kasten, S., Hensen, C., & Schulz, H. D. (2001). Reconstruction of primary productivity from the barium contents in surface sediments of the South Atlantic Ocean. *Marine Geology*, 177(1-2), 13-24. https://doi.org/10.1016/S0025-3227(01)00121-9

Pinardi, N., & Masetti, E. (2000). Variability of the large scale general circulation of the Mediterranean Sea from observations and modelling: A review. *Palaeogeography, Palaeoclimatology, Palaeoecology*, 158(3–4), 153–173. https://doi.org/10.1016/S0031-0182(00)00048-1

Pinardi, N., Zavatarelli, M., Adani, M., Coppini, G., Fratianni, C., Oddo, P., ... & Bonaduce, A. (2015). Mediterranean Sea large-scale low-frequency ocean variability and water mass formation rates from 1987 to 2007: A retrospective analysis. *Progress in Oceanography*, 132, 318–332. https://doi.org/10.1016/j.pocean.2013.11.003.

Pinot, J. M., López-Jurado, J. L., Riera, M., Jansa, J., Font, J., & Tintoré, J. (1998). Time flow variability in the Balearic channels and its relevance to the western Mediterranean circulation. *Rapport des Reunions du Commission International de la Mer Mediterranee*, 35, 188-189.

POEM group. (1992). General circulation of the eastern Mediterranean Sea. *Earth Sci. Rev.* 32, 285–308.

Pollak, M. J. (1951). The sources of the deep water of the eastern Mediterranean Sea. *Journal of Marine Research*, 10(1), 128-152.

Principato, M. S., Giunta, S., Corselli, C., & Negri, A. (2003). Late Pleistocene-Holocene planktonic assemblages in three box-cores from the Mediterranean Ridge area (west-southwest of Crete): Palaeoecological and palaeoceanographic reconstruction of sapropel S1 interval. *Palaeogeography, Palaeoclimatology, Palaeoecology*, 190, 61–77. https://doi.org/10.1016/S0031-0182(02)00599-0

Principato, M. S., Crudeli, D., Ziveri, P., Slomp, C. P., Corselli, C., Erba, E., & De Lange, G. J. (2006). Phyto_ and zooplankton paleofluxes during the deposition of sapropel S1 (eastern Mediterranean): Biogenic carbonate preservation and paleoecological implications. *Palaeogeography, Palaeoclimatology, Palaeoecology*, 235(1-3), 8-27. https://doi.org/10.1016/j.palaeo.2005.09.021

Pruysers, P. A., de Lange, G. J., & Middelburg, J. J. (1991). Geochemistry of eastern Mediterranean sediments: Primary sediment composition and diagenetic alterations. *Marine Geology*, 100(1-4), 137-154. https://doi.org/10.1016/0025-3227(91)90230-2

Pruysers, P. A., de Lange, G. J., Middelburg, J. J., & Hydes, D. J. (1993). The diagenetic formation of metal-rich layers in sapropel-containing sediments in the eastern Mediterranean. *Geochimica et Cosmochimica Acta*, 57(3), 527-536. https://doi.org/10.1016/0016-7037(93)90365-4

Reed, D. C., Slomp, C. P., & de Lange, G. J. (2011). A quantitative reconstruction of organic matter and nutrient diagenesis in Mediterranean Sea sediments over the Holocene. *Geochimica et Cosmochimica Acta*, 75(19), 5540–5558. https://doi.org/10.1016/J.GCA.2011.07.002

Reitz, A., Thomson, J., de Lange, G. J., & Hensen, C. (2006). Source and development of large manganese enrichments above eastern Mediterranean sapropel S1. *Paleoceanography*, 21(3). https://doi.org/10.1029/2005PA001169

Revel, M., Ducassou, E., Grousset, F. E., Bernasconi, S. M., Migeon, S., Révillon, S., ... & Bosch, D. (2010). 100,000 years of African monsoon variability recorded in sediments of the Nile margin. *Quaternary Science Reviews*, 29(11-12), 1342-1362. https://doi.org/10.1016/j.quascirev.2010.02.006

Richez, C., & Gascard, J. C. (1986). Meditteranean water flows when approaching the Straits of Gibraltar. *Deep Sea Research Part A, Oceanographic Research Papers*, 33(1), 135-137. https://doi.org/10.1016/0198-0149(86)90112-3

Robinson, A. R., Leslie, W. G., Theocharis, A., & Lascaratos, A. (2001). Mediterranean Sea Circulation. *Encyclopedia of Ocean Sciences(Second Edition)* (pp. 710–725) . https://doi.org/10.1016/B978-012374473-9.00376-3

Rodríguez-Sanz, L., Bernasconi, S. M., Marino, G., Heslop, D., Mueller, I. A., Fernandez, A., ... & Rohling, E. J. (2017). Penultimate deglacial warming across the Mediterranean Sea revealed by clumped isotopes in foraminifera. *Scientific reports*, 7(1), 1-11. https://doi.org/10.1038/s41598-017-16528-6

Roether, W., & Schlitzer, R. (1991). Eastern Mediterranean deep water renewal on the basis of chlorofluoromethane and tritium data. *Dynamics of Atmospheres and Oceans*, 15(3–5), 333–354. https://doi.org/10.1016/0377-0265(91)90025-B

Roether, W., & Well, R. (2001). Oxygen consumption in the Eastern Mediterranean. *Deep-Sea Research Part I: Oceanographic Research Papers*, 48(6), 1535-1551. https://doi.org/10.1016/S0967-0637(00)00102-3.

Roether, W., Manca, B. B., Klein, B., Bregant, D., Georgopoulos, D., Beitzel, V., ... & Luchetta, A. (1996). Recent changes in eastern Mediterranean deep waters. *Science*, 271(5247), 333-335. https://doi.org/10.1126/science.271.5247.333

Roether, W., Schlosser, P., Kuntz, R. & Weiss, W. (1983). Transient tracer studies of the thermohaline circulation of the Mediterranean. *Reports in Meteorology and Oceanography*, 41, 291-317.

Rogerson, M., Cacho, I., Jimenez-Espejo, F., Reguera, M. I., Sierro, F. J., Martinez-Ruiz, F., ... & Canals, M. (2008). A dynamic explanation for the origin of the western Mediterranean organic-rich layers. *Geochemistry, Geophysics, Geosystems*, 9(7). https://doi.org/10.1029/2007GC001936

Rohling, E. J. (1991). Shoaling of the Eastern Mediterranean Pycnocline due to reduction of excess evaporation: Implications for sapropel formation. *Paleoceanography*, 6(6), 747-753. https://doi.org/10.1029/91PA02455

Rohling, E. J. (1994). Review and new aspects concerning the formation of eastern Mediterranean sapropels. *Marine Geology*, 122(1–2), 1–28. https://doi.org/10.1016/0025-3227(94)90202-X

Rohling, E. J., & Gieskes, W. W. (1989). Late Quaternary changes in Mediterranean intermediate water density and formation rate. *Paleoceanography*, 4(5), 531–545. https://doi.org/10.1029/PA004i005p00531

Rohling, E. J., & Hilgen, F. J. (1991). The eastern Mediterranean climate at times of sapropel formation: a review. *Journal of Geosciences/Geologie en Mijnbouw*.

Rohling, E. J., Cane, T. R., Cooke, S., Sprovieri, M., Bouloubassi, I., Emeis, K. C., ... & Kemp, A. E. S. (2002). African monsoon variability during the previous interglacial maximum. *Earth and Planetary Science Letters*, 202(1), 61-75. https://doi.org/10.1016/S0012-821X(02)00775-6

Rohling, E. J., Hayes, A., De Rijk, S., Kroon, D., Zachariasse, W. J., & Eisma, D. (1998). Abrupt cold spells in the northwest Mediterranean. *Paleoceanography*, 13(4), 316–322. https://doi.org/10.1029/98PA00671

Rohling, E. J., Jorissen, F. J., & De Stigter, H. C. (1997). 200 year interruption of Holocene sapropel formation in the Adriatic Sea. *Journal of Micropalaeontology*, 16(2), 97-108. https://doi.org/10.1144/jm.16.2.97

Rohling, E. J., Jorissen, F. J., Grazzini, C. V., & Zachariasse, W. J. (1993). Northern Levantine and Adriatic Quaternary planktic foraminifera; reconstruction of paleoenvironmental gradients. *Marine Micropaleontology*, 21(1-3), 191-218. https://doi.org/10.1016/0377-8398(93)90015-P

Rohling, E. J., Marino, G., & Grant, K. M. (2015). Mediterranean climate and oceanography, and the periodic development of anoxic events (sapropels). *Earth-Science Reviews*, 143, 62-97. https://doi.org/10.1016/j.earscirev.2015.01.008

Rossignol-Strick, M. (1983). African monsoons, an immediate climate response to orbital insolation. *Nature*, 304(5921), 46. https://doi.org/10.1038/304046a0

Rossignol-Strick, M. (1985). Mediterranean Quaternary sapropels, an immediate response of the African monsoon to variation of insolation. *Palaeogeography, Palaeoclimatology, Palaeoecology*, 49(3–4), 237–263. https://doi.org/10.1016/0031-0182(85)90056-2

Rossignol-Strick, M., Nesteroff, W., Olive, P., & Vergnaud-Grazzini, C. (1982). After the deluge: Mediterranean stagnation and sapropel formation. *Nature*, 295(5845), 105–110. https://doi.org/10.1038/295105a0

RStudio Team. 2019. RStudio: Integrated Development for R. RStudio, Inc., Boston, MA. http://www.rstudio.com/

Ryan, W. B. F. (1972). Stratigraphy of Late Quaternary sediments in the eastern Mediterranean. D.J. Stanley (Ed.), The Mediterranean Sea: a Natural Sedimentation Laboratory, pp. 149-169 (Stroudsburg, Pennsylvania, Dowden, Hutchinson and Ross).

Sachs, J. P., & Repeta, D. J. (1999). Oligotrophy and nitrogen fixation during eastern Mediterranean sapropel events. *Science*, 286(5449), 2485-2488. https://doi.org/10.1126/science.286.5449.2485

Schlitzer, R., Roether, W., Oster, H., Junghans, H. G., Hausmann, M., Johannsen, H., & Michelato, A. (1991). Chlorofluoromethane and oxygen in the Eastern Mediterranean. *Deep Sea Research Part A. Oceanographic Research Papers*, 38(12), 1531-1551. https://doi.org/10.1016/0198-0149(91)90088-W

Schmiedl, G., Kuhnt, T., Ehrmann, W., Emeis, K. C., Hamann, Y., Kotthoff, U., ... & Pross, J. (2010). Climatic forcing of eastern Mediterranean deep-water formation and benthic ecosystems during the past 22 000 years. *Quaternary Science Reviews*, 29(23-24), 3006-3020. https://doi.org/10.1016/j.quascirev.2010.07.002

Schmiedl, G., Mitschele, A., Beck, S., Emeis, K. C., Hemleben, C., Schulz, H., ... & Weldeab, S. (2003). Benthic foraminiferal record of ecosystem variability in the eastern Mediterranean Sea during times of sapropel S5 and S6 deposition. *Palaeogeography, Palaeoclimatology, Palaeoecology*, 190, 139–164. https://doi.org/10.1016/S0031-0182(02)00603-X

Scrivner, A. E., Vance, D., & Rohling, E. J. (2004). New neodymium isotope data quantify Nile involvement in Mediterranean anoxic episodes. *Geology*, 32(7), 565-568. https://doi.org/10.1130/G20419.1

Sen Gupta, B. K., & Machain-Castillo, M. L. (1993). Benthic foraminifera in oxygen-poor habitats. *Marine Micropaleontology*, 20(3-4), 183-201. https://doi.org/10.1016/0377-8398(93)90032-S

Send, U., Font, J., Krahmann, G., Millot, C., Rhein, M., & Tintoré, J. (1999). Recent advances in observing the physical oceanography of the Western Mediterranean Sea. *Progress in Oceanography* 44(1-3), 37-64. https://doi.org/10.1016/S0079-6611(99)00020-8

Simon, D., Marzocchi, A., Flecker, R., Lunt, D. J., Hilgen, F. J., & Meijer, P. T. (2017). Quantifying the Mediterranean freshwater budget throughout the late Miocene: New implications for sapropel formation and the Messinian Salinity Crisis. *Earth and Planetary Science Letters*, 472, 25-37. https://doi.org/10.1016/j.epsl.2017.05.013

Skliris, N., & Lascaratos, A. (2004). Impacts of the. Nile River damming on the thermohaline circulation and water mass characteristics of the Mediterranean Sea. *Journal of Marine Systems,* 52(1-4), 121-143. https://doi.org/10.1016/j.jmarsys.2004.02.005

Slomp, C. P., Thomson, J., & de Lange, G. J. (2002). Enhanced regeneration of phosphorus during formation of the most recent eastern Mediterranean sapropel (S1). *Geochimica et Cosmochimica Acta*, 66(7), 1171-1184. https://doi.org/10.1016/S0016-7037(01)00848-1

Smith, R.O., Bryden, H.L., Stansfield, K. (2008). Observations of new western Mediterranean deep water formation using Argo floats 2004–2006. *Ocean Science*. 4, 133–149.

Sournia A. (1973). La production primaire planctonique en Méditerranée, Newsletter of the cooperative investigations in the Mediterranean, special issue No. 5, *Monaco*, 128 p.

Stansfield, K., Gasparini, G. P., & Smeed, D. A. (2003). High-resolution observations of the path of the overflow from the Sicily Strait. *Deep-Sea Research Part I: Oceanographic Research Papers*, 50(9), 1129-1149. https://doi.org/10.1016/S0967-0637(03)00099-2

Statista (2019). Digital Economy Compass. Available at: https://cdn.statcdn.com/download/pdf/DigitalEconomyCompass2019.pdf

Stratford, K., & Williams, R. G. (1997). A tracer study of the formation, dispersal, and renewal of Levantine Intermediate Water. *Journal of Geophysical Research: Oceans*, 1 02(C6), 12539-12549. https://doi.org/10.1029/97JC00019

Stratford, K., Williams, R. G., & Drakopoulos, P. G. (1998). Estimating climatological age from a model-derived oxygen-age relationship in the Mediterranean. *Journal of Marine Systems*, 18(1-3), 215-226. https://doi.org/10.1016/S0924-7963(98)00013-X

Strohle, K., & Krom, M. D. (1997). Evidence for the evolution of an oxygen minimum layer at the beginning of S-1 sapropel deposition in the eastern Mediterranean. *Marine Geology*, 140(3-4), 231-236. https://doi.org/10.1016/S0025-3227(97)00058-3

Tachikawa, K., Vidal, L. A., Cornuault, M., Garcia, M., Pothin, A., Sonzogni, C., ... & Revel, M. (2015). Eastern Mediterranean Sea circulation inferred from the conditions of S1 sapropel deposition. *Climate of the Past*, 11(6), 855–867. https://doi.org/10.5194/cp-11-855-2015

Tanhua, T., Hainbucher, D., Schroeder, K., Cardin, V., Álvarez, M., & Civitarese, G. (2013). The Mediterranean Sea system: A review and an introduction to the special issue. *Ocean Science*, 9(5), 789-803. https://doi.org/10.5194/os-9-789-2013

Tesi, T., Asioli, A., Minisini, D., Maselli, V., Dalla Valle, G., Gamberi, F., ... & Trincardi, F. (2017). Large-scale response of the Eastern Mediterranean thermohaline circulation to African monsoon intensification during sapropel S1 formation. *Quaternary Science Reviews*, 159, 139–154. https://doi.org/10.1016/j.quascirev.2017.01.020

Testor, P., & Gascard, J. C. (2006). Post-convection spreading phase in the Northwestern Mediterranean Sea. *Deep Sea Research Part I: Oceanographic Research Papers*, 53(5), 869–893. https://doi.org/10.1016/J.DSR.2006.02.004

Theocharis, A. (2009). Variability of the thermohaline properties in the Eastern Mediterranean during the post-EMT period (1995-2008) and SST changes in the Aegean (1985-2008). *CIESM Workshop Monographs*, 38, 35–40

Theocharis, A., Nittis, K., Kontoyiannis, H., Papageorgiou, E., & Balopoulos, E. (1999). Climatic changes in the Aegean Sea influence the Eastern Mediterranean thermohaline circulation (1986-1997). *Geophysical Research Letters*, 26(11), 1617-1620. https://doi.org/10.1029/1999GL900320

Thomson, J., Mercone, D., De Lange, G. J., & Van Santvoort, P. J. M. (1999). Review of recent advances in the interpretation of eastern Mediterranean sapropel S1 from geochemical evidence. *Marine Geology,* 153(1-4), 77-89. https://doi.org/10.1016/S0025-3227(98)00089-9

Thomson, J., Higgs, N. C., Wilson, T. R. S., Croudace, I. W., De Lange, G. J., & Van Santvoort, P. J. M. (1995). Redistribution and geochemical behaviour of redox-sensitive elements around S1, the most recent eastern Mediterranean sapropel. *Geochimica et Cosmochimica Acta*, 59(17), 3487-3501. https://doi.org/10.1016/0016-7037(95)00232-O

Timmins, K. A., Green, M. A., Radley, D., Morris, M. A., & Pearce, J. (2018). How has big data contributed to obesity research? A review of the literature. *International Journal of Obesity*, 42(12), 1951-1962. https://doi.org/10.1038/s41366-018-0153-7

Toucanne, S., Minto'o, C. M. A., Fontanier, C., Bassetti, M. A., Jorry, S. J., & Jouet, G. (2015). Tracking rainfall in the northern Mediterranean borderlands during sapropel deposition. *Quaternary Science Reviews*, 129, 178-195. https://doi.org/10.1016/j.quascirev.2015.10.016

Triantaphyllou, M. V. (2014). Coccolithophore assemblages during the Holocene Climatic Optimum in the NE Mediterranean (Aegean and northern Levantine Seas, Greece): Paleoceanographic and paleoclimatic implications. *Quaternary International*, 345, 56-67. https://doi.org/10.1016/j.quaint.2014.01.033

Triantaphyllou, M. V., Antonarakou, A., Dimiza, M., & Anagnostou, C. (2010). Calcareous nannofossil and planktonic foraminiferal distributional patterns during deposition of sapropels S6, S5 and S1 in the Libyan Sea (Eastern Mediterranean). *Geo-Marine Letters*, 30(1), 1–13. https://doi.org/10.1007/s00367-009-0145-7

Triantaphyllou, M. V., Antonarakou, A., Kouli, K., Dimiza, M., Kontakiotis, G., Papanikolaou, M. D., ... & Dermitzakis, M. D. (2009). Late Glacial-Holocene ecostratigraphy of the south-eastern Aegean Sea, based on plankton and pollen assemblages. *Geo-Marine Letters*, 29(4), 249-267. https://doi.org/10.1007/s00367-009-0139-5

Triantaphyllou, M. V., Gogou, A., Dimiza, M. D., Kostopoulou, S., Parinos, C., Roussakis, G., ... & Velaoras, D. (2016). Holocene climatic optimum centennial-scale paleoceanography in the NE Aegean (Mediterranean Sea). *Geo-Marine Letters*, 36(1), 51-66. https://doi.org10.1007/s00367-015-0426-2

Tribovillard, N., Algeo, T. J., Lyons, T., & Riboulleau, A. (2006). Trace metals as paleoredox and paleoproductivity proxies: An update. *Chemical Geology*, 232(1–2), 12–32. https://doi.org/10.1016/j.chemgeo.2006.02.012

Tribovillard, N., Algeo, T. J., Baudin, F., & Riboulleau, A. (2012). Analysis of marine environmental conditions based onmolybdenum–uranium covariation—Applications to Mesozoic paleoceanography. *Chemical Geology*, 324, 46-58. https://doi.org/10.1016/j.chemgeo.2011.09.009

Troelstra, S., Ganssen, G., Van der Borg, K., & De Jong, A. (1991). A Late Quaternary Stratigraphic Framework for Eastern Mediterranean Sapropel S1 based on AMS ^{14}C Dates and Stable Oxygen Isotopes. *Radiocarbon*, 33(1), 15-21. https://doi.org/10.1017/S0033822200013175

Tsimplis, M. N., Velegrakis, A. F., Drakopoulos, P., Theocharis, A., & Collins, M. B. (1999). Cretan deep water outflow into the Eastern Mediterranean. *Progress in oceanography*, 44(4), 531-551. https://doi.org/10.1016/S0079-6611(99)00042-7

Turley, C. M., Bianchi, M., Christaki, U., Conan, P., Harris, J. R. W., Psarra, S., ... & Van Wambeke, F. (2000). Relationship between primary producers and bacteria in an oligotrophic sea--the Mediterranean and biogeochemical implications. *Marine Ecology Progress Series*, 193, 11-18. https://doi.org/10.3354/meps193011

Tyson, R. V. (1995). Abundance of organic matter in sediments: TOC, hydrodynamic equivalence, dilution and flux effects. *Sedimentary organic matter* (pp. 81-118). Springer, Dordrecht. https://doi.org/10.1007/978-94-011-0739-6_5

Tyson, R. V. (2001). Sedimentation rate, dilution, preservation and total organic carbon: some results of a modelling study. *Organic Geochemistry*, 32(2), 333-339. https://doi.org/10.1016/S0146-6380(00)00161-3

Tyson, R. V. (2005). The "productivity versus preservation" controversy: cause, flaws, and resolution. *Special Publication-SEPM*, 82, 17. https://doi.org/10.2110/pec.05.82.0017

Van Helmond, N. A., Hennekam, R., Donders, T. H., Bunnik, F. P., de Lange, G. J., Brinkhuis, H., & Sangiorgi, F. (2015). Marine productivity leads organic matter preservation in sapropel S1: palynological evidence from a core east of the Nile River outflow. *Quaternary Science Reviews*, 108, 130-138. https://doi.org/10.1016/j.quascirev.2015.05.031

Van Os, B. J. H., Middelburg, J. J., & de Lange, G. J. (1991). Possible diagenetic mobilization of barium in sapropelic sediment from the eastern Mediterranean. *Marine Geology*, 100(1–4), 125–136. https://doi.org/10.1016/0025-3227(91)90229-W

Van Santvoort, P. J. M., de Lange, G. J., Thomson, J., Cussen, H., Wilson, T. R. S., Krom, M. D., & Ströhle, K. (1996). Active post-depositional oxidation of the most recent sapropel (S1) in sediments of the eastern Mediterranean Sea. *Geochimica et Cosmochimica Acta*, 60(21), 4007-4024. https://doi.org/10.1016/S0016-7037(96)00253-0

Van Santvoort, P. J. M., de Lange, G. J., Langereis, C. G., Dekkers, M. J., & Paterne, M. (1997). Geochemical and paleomagnetic evidence for the occurrence of "missing" sapropels in eastern Mediterranean sediments. *Paleoceanography*, 12(6), 773-786. https://doi.org/10.1029/97PA01351

Versteegh, G. J. M., Zonneveld, K. A. F., & de Lange, G. J. (2010). Selective aerobic and anaerobic degradation of lipids and palynomorphs in the Eastern Mediterranean since the onset of sapropel S1 deposition. *Marine Geology*, 278(1-4), 177-192. https://doi.org/10.1016/j.margeo.2010.10.007.

Vink, A. (2004). Calcareous dinoflagellate cysts in South and equatorial Atlantic surface sediments: diversity, distribution, ecology and potential for palaeoenvironmental reconstruction. *Marine Micropaleontology*, 50(1-2), 43–88. https://doi.org/10.1016/S0377-8398(03)00067-7

Von Breymann, M. T., Emeis, K. C., & Suess, E. (1992). Water depth and diagenetic constraints on the use of barium as a palaeoproductivity indicator. *Geological Society, London, Special Publications*, 64(1), 273-284. https://doi.org/10.1144/GSL.SP.1992.064.01.18

Wehausen, R., & Brumsack, H. J. (1999). Cyclic variations in the chemical composition of eastern Mediterranean Pliocene sediments: a key for understanding sapropel formation. *Marine Geology*, 153(1-4), 161-176. https://doi.org/10.1016/S0025-3227(98)00083-8

Warning, B., & Brumsack, H. J. (2000). Trace metal signatures of eastern Mediterranean sapropels. *Palaeogeography, Palaeoclimatology, Palaeoecology* 158(3-4), 293-309. https://doi.org/10.1016/S0031-0182(00)00055-9

Weldeab, S., Menke, V., & Schmiedl, G. (2014). The pace of East African monsoon evolution during the Holocene. *Geophysical Research Letters*, 41(5), 1724-1732. https://doi.org/10.1002/2014GL059361

Weldeab, S., Siebel, W., Wehausen, R., Emeis, K.-C., Schmiedl, G., & Hemleben, C. (2003). Late Pleistocene sedimentation in the Western Mediterranean Sea: implications for productivity changes and climatic conditions in the catchment areas. *Palaeogeography, Palaeoclimatology, Palaeoecology*, 190, 121–137. https://doi.org/10.1016/S0031-0182(02)00602-8

Wu, J., Böning, P., Pahnke, K., Tachikawa, K., & de Lange, G. J. (2016). Unraveling North-African riverine and eolian contributions to central Mediterranean sediments during Holocene sapropel S1 formation. *Quaternary Science Reviews*, 152, 31-48. https://doi.org/10.1016/j.quascirev.2016.09.029

Wu, J., Liu, Z., Stuut, J. B. W., Zhao, Y., Schirone, A., & de Lange, G. J. (2017). North-African paleodrainage discharges to the central Mediterranean during the last 18,000 years: A multiproxy characterization. *Quaternary Science Reviews*, 163, 95-113. https://doi.org/10.1016/j.quascirev.2017.03.015.

Wu, J., Pahnke, K., Böning, P., Wu, L., Michard, A., & de Lange, G. J. (2019). Divergent Mediterranean seawater circulation during Holocene sapropel formation–Reconstructed using Nd isotopes in fish debris and foraminifera. *Earth and Planetary Science Letters,* 511, 141-153. https://doi.org/10.1016/j.epsl.2019.01.036

Wüst, G. (1961). On the vertical circulation of the Mediterranean Sea. *Journal of Geophysical Research*, 66(10), 3261–3271. https://doi.org/10.1029/jz066i010p03261

Young, J. R. (1994). Functions of coccoliths. A. Winter, W.G. Siesser (Eds.), *Coccolithophores*, Cambridge University Press, Cambridge (1994), pp. 63-82.

Zanchetta, G., Drysdale, R. N., Hellstrom, J. C., Fallick, A. E., Isola, I., Gagan, M. K., & Pareschi, M. T. (2007). Enhanced rainfall in the Western Mediterranean during deposition of sapropel S1: stalagmite evidence from Corchia cave (Central Italy). *Quaternary Science Reviews*, 26(3-4), 279-286. https://doi.org/10.1016/j.quascirev.2006.12.003

Ziegler, M., Tuenter, E., & Lourens, L. J. (2010). The precession phase of the boreal summer monsoon as viewed from the eastern Mediterranean (ODP Site 968). *Quaternary Science Reviews,* 29(11-12), 1481-1490. https://doi.org/10.1016/j.quascirev.2010.03.011

Zirks, E., Krom, M. D., Zhu, D., Schmiedl, G., & Goodman-Tchernov, B. N. (2019). Evidence for the Presence of Oxygen-Depleted Sapropel Intermediate Water across the Eastern Mediterranean during Sapropel S1. ACS Earth and Space Chemistry, 3(10), 2287-2297. https://doi.org/10.1021/acsearthspacechem.9b00128

Zonneveld, K. A. F., Versteegh, G. J. M., & de Lange, G. J. (2001). Palaeoproductivity and post-depositional aerobic organic matter decay reflected by dinoflagellate cyst assemblages of the Eastern Mediterranean S1 sapropel. *Marine Geology*, 172(3–4), 181–195. https://doi.org/10.1016/S0025-3227(00)00134-1

Zwiep, K. L., Hennekam, R., Donders, T. H., van Helmond, N. A. G. M., de Lange, G. J., & Sangiorgi, F. (2018). Marine productivity, water column processes and seafloor anoxia in relation to Nile discharge during sapropels S1 and S3. *Quaternary Science Reviews,* 200, 178-190. https://doi.org/10.1016/j.quascirev.2018.08.02

General conclusions and future perspective related to sapropel studies

For the first time, the sapropel (S1) has been studied through a novel method based on data analytics techniques (Chapter 3). Several steps were followed to obtain, organize, and relation the data in order to test the usefulness of these novel techniques in sapropel (Chapter 1), as the detailed evaluation of the timing of sapropel (S1) formation (Chapter 2).

The great wealth of Mediterranean paleoclimatic and palaeoceanographic data at the time of sapropel deposition was used in the design of the database model of *BEyOND*, which highlighted the need for data standardization as the main issue when working with a huge data volumes. The revaluation of the precise sapropel timing followed in Chapter 2 shows a synchronous S1 deposition in the whole eastern Mediterranean Sea between 10.1 and 6.5 cal. ka BP with slight differences of the order of 100-130 years, showing a depth-dependent deposition.

The combination of geochemical, micropaleontological, and isotopes records analyzed in Chapter 3 highlighted the local and global forcings driving the sapropel S1 deposition. The large input of freshwater in the whole eastern Mediterranean Sea together with the cold events observed at 9.5, 8.5 (related to 8.2 ka event), and 7.5 cal. ka BP, confirm a close interplay between mid- (North Atlantic) and low-latitudes (North African Monsoon) climate systems. These cold events associated with the Bond cycles (Bond et al., 1997, 2001) caused activation of the intermediate waters circulation and the subsequent resumption of deep-water formation that improved the oxygen availability at the sea bottom. In addition, the S1 onset did not occur under anoxic waters, as these were settled 400-500 years after S1 onset (Chapter 2), in line with the progressive deterioration of deep water ventilation (preconditioning phase; Filippidi & De Lange, 2019; Schmiedl et al., 2010; Tachikawa et al., 2015; Tesi et al., 2017).

Furthermore, the severe redox conditions and high TOC contents observed in the Levantine/Ionian sea are related to presence of deeper cores. Thus, the different geochemical signatures observed in the sub-basins are not representative of the local forcings but correlate to different water depths.

Future perspective in this field have to consider an increasing role of the DA in the study of the entire Quaternary sedimentary record. This work put the base for this approach to be extended to the Quaternary sapropel record, to investigate if other events that although share the same astronomical mechanism (precession minima, and insolation

maxima) were deposited under different conditions (e.g. warm sapropel S1/S5 vs cold sapropel S6/S8), underwent the same process. In order to explore the teleconnection with the Atlantic ocean and the palaeoceanographic role that these play in the Mediterranean, new data in *BEyOND* will be a fundamental achievement to explore the sedimentary response to these processes.

References:

Bond, G., Kromer, B., Beer, J., Muscheler, R., Evans, M. N., Showers, W., ... & Bonani, G. (2001). Persistent solar influence on North Atlantic climate during the Holocene. *Science*, 294(5549), 2130-2136. https://doi.org/10.1126/science.1065680

Bond, G., Showers, W., Cheseby, M., Lotti, R., Almasi, P., DeMenocal, P., ... & Bonani, G. (1997). A pervasive millennial-scale cycle in North Atlantic Holocene and glacial climates. *Science*, 278(5341), 1257-1266. https://doi.org/10.1126/science.278.5341.1257

Filippidi, A., & De Lange, G. J. (2019). Eastern Mediterranean Deep Water Formation During Sapropel S1: A Reconstruction Using Geochemical Records Along a Bathymetric Transect in the Adriatic Outflow Region. *Paleoceanography and Paleoclimatology*, 34(3), 409-429. https://doi.org/10.1029/2018PA003459

Schmiedl, G., Kuhnt, T., Ehrmann, W., Emeis, K. C., Hamann, Y., Kotthoff, U., ... & Pross, J. (2010). Climatic forcing of eastern Mediterranean deep-water formation and benthic ecosystems during the past 22 000 years. *Quaternary Science Reviews*, 29(23-24), 3006-3020. https://doi.org/10.1016/j.quascirev.2010.07.002

Tachikawa, K., Vidal, L., Cornuault, M., Garcia, M., Pothin, A., Sonzogni, C., ... & Revel, M. (2015). Eastern Mediterranean Sea circulation inferred from the conditions of S1 sapropel deposition. *Climate of the Past Discussions*, 11, 855–867. https://doi.org/10.5194/cp-11-855-2015

Tesi, T., Asioli, A., Minisini, D., Maselli, V., Dalla Valle, G., Gamberi, F., ... & Trincardi, F. (2017). Large-scale response of the Eastern Mediterranean thermohaline circulation to African monsoon intensification during sapropel S1 formation. *Quaternary Science Reviews*, 159, 139–154. https://doi.org/10.1016/j.quascirev.2017.01.020

Acknowledgements

First of all, I'd like to express my gratitude to UNIVPM for financially supporting my studies in Italy.

I would like to thank my supervisor, Prof. Alessandra Negri, for giving me the opportunity to enrichment my academic career. I am grateful for the support and patience during these years. Thanks for inviting me to seminars, congresses, and workshops, and for sending me to Flagstaff and Vigo to improve my computer knowledge and paleoceanography. I really appreciate all this help and dedication.

Further, I would like to thank my co-supervisors Prof. Claudia Diamantini, Prof. Domenico Potena, and Dr. Gianluca Marino for supervising my work and stimulate me in this multidisciplinary project. Special thanks go to Claudia for sharing his experience in databases and data mining; to Domenico for helping me with the innumerable "query" in the database; and to Gianluca for his continuous support and guidance.

Thanks to Prof. Nicholas McKay for your help and hospitality during my stage at Northern Arizona University.

I warmly thanks to Prof. Anna Sabbatini and my colleagues of the PaleoLab for scientific and social support.